The Occurrence and Origins of Streamlined Forms in Central British Columbia

by

Jerry Donald McClenagan
B.A., Rice University, 1981
M.S., West Texas A&M University, 1995

A Dissertation Submitted in Partial Fulfillment of the
Requirements for the Degree of

DOCTOR OF PHILOSOPHY

in the Department of Earth and Ocean Science

Supervisors: Dr. Victor Levson and Dr. Eileen van der Flier – Keller

ABSTRACT

The purpose of this research is to gain understanding of the occurrence and origin of streamlined forms in central British Columbia. More than 50,000 landforms, primarily drumlins and crag-and-tail ridges, were digitally mapped over an area covering five 1:250,000 NTS map sheets. Visual Basic programs were written to statistically analyze the streamlined forms database and to simulate site-scale, two-dimensional glacial erosion. Results show three principal ice and/or meltwater flow directions: southeast flows probably originating in the Skeena Mountains, northeast flows from the Coast Mountains and Quanchas Range, and west flows originating east of the Babine and Telkwa Ranges. Rat-tails and striae occur up to 1680 m elevation and record uphill flow to the west in these ranges.

Streamlined forms were investigated at outcrop scale (*e.g.* rat-tails), landform scale (*e.g.* drumlins) and landscape scale (as defined by closed contours). On bedrock outcrops, cross-cutting striae are common and they both parallel and cross-cut rat-tails. Small rat-tails occur on, and parallel to, larger rat-tails but they do not cross-cut, suggesting a different origin than striae. Rat-tails are interpreted as being formed by subglacial meltwater flows, an interpretation supported by the glacial erosion model. Lowland streamlined forms (*e.g.* drumlins and crag-and-tails) are interpreted as either glacially-formed ridges subsequently shaped by meltwater floods or as being formed entirely by meltwater floods. This interpretation is largely based on the common

occurrence of interconnecting hairpin furrows around these streamlined forms and on the demonstrated association of hairpin furrows with fluvial erosion.

The results of topographic analysis indicate that an interconnecting system of valleys separates uplands that can be objectively defined by single (closed) contours. The aspect ratios of the uplands are highly correlated (L/W = 2.38, R^2 = 0.89) with values that are similar to those reported for braid bars and erosional residuals thought to have been formed by glacial outburst floods. This upland/lowland landform assemblage may, in places, represent streamlined erosional residuals within braided channel networks formed, at least in part, by subglacial or glacial outburst floods.

Supervisors: Dr. V. Levson, (Department of Earth and Ocean Science)

Dr. E. van der Flier – Keller, (Department of Earth and Ocean Science)

TABLE OF CONTENTS

ABSTRACT ..... **ii**

TABLE OF CONTENTS ..... **iv**

LIST OF FIGURES ..... **ix**

LIST OF TABLES ..... **xv**

ACKNOWLEDGEMENTS ..... **xvi**

DEDICATION ..... **xvii**

1. INTRODUCTION, TERMINOLOGY AND BACKGROUND **1**

1.1. INTRODUCTION 1
1.1.1. Objectives 2
1.1.2. Summary of contributions 3
1.1.3. Overview of thesis methods 5
1.1.4. Study area 6
1.1.4.1. Previous work 6
1.1.4.2. Ice flow history 11
1.1.4.3. Physiography 12
1.1.4.4. Surficial geology 15
1.1.4.5. Bedrock geology 17
1.2. STREAMLINED FORM DESCRIPTION AND CLASSIFICATION 20
1.2.1. Defining streamlined forms 20
1.2.2. Streamlined forms classification 23
1.2.2.1. Drumlins 25
1.2.2.2. Flutings 29
1.2.2.3. Other streamlined forms and more general terms 31
1.2.2.4. Streamlined erosional marks in bedrock 31
1.2.3. Terms used in this dissertation 35
1.3. ORIGIN OF DRUMLINS AND STREAMLINED BEDROCK FORMS 35
1.3.1. Drumlins formed by glacial ice 36
1.3.2. Drumlins formed by moderate subglacial meltwater flows with or without the contribution of ice 41
1.3.3. Drumlins formed by catastrophic subglacial meltwater floods 41
1.3.4. Streamlined bedrock form origins 46

2. STREAMLINED FORMS MAPPING **52**

2.1. INTRODUCTION 52
2.2. PREVIOUS WORK 52
2.3. METHODS 54

2.4. RESULTS 57
2.4.1. Streamlined forms map 57
2.4.1.1. Comparison of thesis map with other streamlined forms maps 57
2.4.2. Flow directions 68
2.4.3. Streamlined forms occurrence and flow patterns 78
2.4.3.1. Relationship of valleys to paths of streamlined forms 78
2.4.3.2. Valleys and gaps in streamlined forms occurrence 79
2.4.3.3. Streamlined forms density 83
2.4.3.4. Flow out of cirques 86
2.5. DISCUSSION 86
2.5.1. Principle flow directions 86
2.5.2. Source areas based on principle flow directions 88
2.5.3. Causes of low streamlined forms densities in valleys and lowlands 90
2.5.4. Orientations of valleys and streamlined forms 93
2.5.5. Streamlined forms and cirques 99

3. STATISTICAL ANALYSES 101

3.1. INTRODUCTION 101
3.2. PREVIOUS STREAMLINED FORMS NUMERICAL ANALYSES 103
3.3. METHODS 104
3.3.1. Geographic areas for different analyses 108
3.3.2. Quality control of database and analyses 110
3.4. RESULTS AND DISCUSSION 112
3.4.1. Average topographic elevation by map sheet 112
3.4.2. Streamlined forms distribution by elevation 115
3.4.3. Streamlined forms density 118
3.4.4. Elevation effects 120
3.4.4.1. Elevation and streamlined form length 120
3.4.4.2. Discussion of elevation and streamlined form length 124
3.4.4.3. Elevation and bearing deviation 125
3.4.4.4. Discussion of elevation and bearing deviation 126
3.4.5. Slope effects 127
3.4.5.1. Slope and streamlined form frequency 127
3.4.5.2. Slope and streamlined form length 128
3.4.5.3. Discussion of slope and streamlined form length and frequency 130
3.4.5.4. Slope and bearing deviation 132
3.5. SUMMARY 135
3.5.1. Timing of valley and streamlined forms formation 135
3.5.2. Level slopes and streamlined form length 136
3.5.3. Scale of SF forming flow 137

4. INCREMENTAL GLACIAL EROSION ANALYSIS 139

4.1. INTRODUCTION 139
4.2. PREVIOUS WORK 141
4.3. METHODS 142
4.3.1. Shear stress derivation 142

4.3.2. Reverse shear and longitudinal shear stresses....144
4.3.3. Analysis tool design and use....146
4.3.3.1. Platform and output....146
4.3.3.2. Parameters....147
4.3.3.3. Erosional processing....149
4.3.3.4. Analysis tool use....151
4.3.4. Assumptions....152
4.4. Results And Discussion....154
4.4.1. Flat rock with resistant core erosion....154
4.4.2. Rock drumlin erosion....166
4.5. Summary and Discussion....173
4.5.1. Discussion of analysis assumptions....173
4.5.2. Asymmetric forms and inclined planes....175
4.5.3. Simulated rock peneplains and propagating ridges....176
4.5.4. Hypotheses....176
4.5.5. Application to reality....177
4.5.6. Comparison to a similar analysis....178
4.5.7. Field observations related to analysis results....180

5. FIELD STUDIES....182

5.1. Introduction....182
5.2. Previous Work....183
5.2.1. Previous work pertaining to streamlined forms composition....183
5.2.2. Previous work pertaining to streamlined bedrock forms....184
5.3. Methods....185
5.4. Results....187
5.4.1. Lowland streamlined forms....187
5.4.2. Alpine streamlined forms....191
5.4.3. Rat-tails....196
5.4.3.1. Spatial and size relationships....198
5.4.3.2. Flow response to surface irregularity....198
5.4.3.3. Rat-tail length-to-width ratios....214
5.4.4. Striae at rat-tail sites....217
5.4.5. Cavettos....217
5.5. Discussion....220
5.5.1. Summary of streamlined forms observations....220
5.5.1.1. Composition of streamlined forms....220
5.5.1.2. Morphology of streamlined forms....221
5.5.1.3. Uphill and westward flow....221
5.5.1.4. Flow behaviour....222
5.5.2. Interpretations....222
5.5.2.1. Uphill flow....222
5.5.2.2. Parallel flows in valleys and uplands....224
5.5.2.3. Uniform streamlined bedrock form directions....224
5.5.2.4. Similar shapes at all scales....225
5.5.2.5. Erosional versus constructional mechanism....226

5.5.2.6. Parallel rat-tails and striae and cross-cutting striae 229
5.5.2.7. Converging rat-tails in a rock cavity....230
5.5.2.8. Relationship of rat-tail length to width 230
5.5.3. Origins of streamlined forms 231
5.5.3.1. Summary of findings and interpretations....232
5.5.3.2. Application to the origin problem....233

6. TOPOGRAPHIC ANALYSIS AND CLOSED CONTOURS 237

6.1. INTRODUCTION 237
6.2. PREVIOUS WORK....238
6.3. METHODS 242
6.3.1. Topographic analysis....242
6.3.2. Shape analysis 247
6.4. RESULTS....247
6.4.1. Fault maps and closed contour boundaries 248
6.4.2. Shape analysis 255
6.5. DISCUSSION 264
6.5.1. Similarity of closed contour shapes to erosional residuals 265
6.5.2. Spatial arrangement of closed contours....268
6.5.3. Orientations of streamlined forms and closed contour long axes 272
6.5.4. Interpretation....273
6.5.4.1. Shape analysis 273
6.5.4.2. Closed contour long axes 275
6.5.4.3. Requirements of a meltwater origin hypothesis 275
6.5.4.4. Alternate explanation of closed contour morphology....277
6.5.4.5. Aspect ratio correlation....280

7. SUMMARY AND CONCLUSIONS 284

7.1. SUMMARY 285
7.1.1. Study area and streamlined form origin theories 285
7.1.2. Streamlined forms map....286
7.1.3. Statistical analyses....288
7.1.4. Glacial erosion analysis 289
7.1.5. Field studies 291
7.1.6. Topographic analysis and closed contours 294
7.2. CONCLUSIONS....294
7.2.1. Origins of streamlined forms 294
7.2.1.1. Findings supporting a water origin 295
7.2.1.2. Alternative interpretations of findings for water....296
7.2.1.3. Findings supporting an ice origin 297
7.2.1.4. Alternative interpretations of findings for ice 298
7.2.2. Conclusions....299
7.2.3. Implications of meltwater floods....300
7.2.4. Future work....302

REFERENCES 304

APPENDIX A. STREAMLINED FORMS ON SHADED RELIEF IMAGES.....327

APPENDIX B. LOCATIONS OF STREAMLINED FORMS COMPOSED PRIMARILY OF DIAMICTON 348

APPENDIX C. STREAMLINED BEDROCK FORMS.....349

APPENDIX D. CLOSED CONTOURS LESS THAN 100 KM^2 WITH LENGTH AND WIDTH AXES 351

LIST OF FIGURES

Figure 1. Study area location, major physiographic boundaries from Holland (1964). The lighter dashed line represents the boundary between the Nechako Plateau and the rest of the Interior Plateau. 7
Figure 2. Topography of study area showing centers of NTS 93E, 93F, 93K, 93L, and 93M. Shaded elevation contours are from 0 m (dark grey) to 2600 m (white) above sea level.... 8
Figure 3. Mountain ranges, plateaus, and basins of the study area..... 14
Figure 4. Generalized surficial geology of the study area. Produced from digital data, GSC Map 1880A, Fulton (1995). 16
Figure 5. Bedrock geology of the study area. Most bedrock is covered by glacial sediments and outcrop limits are often inferred. Compiled from Massey *et al.* (2003a) and Massey *et al.* (2003b). 19
Figure 6. Study area faults, digital data from MacIntyre (1996). Note the lack of fault traces in the eastern part of the study area, due partially to the extensive Quaternary sediment cover. 21
Figure 7. Streamlined shapes 22
Figure 8. Stereo pair of drumlins (flutings) on Hazelton Mountain. Flow is downhill and towards the bottom right of the photos. Some of the stoss (up flow) ends of the drumlins are truncated by cliff faces (A). Stoss-end crescentic furrows are visible that merge with lateral furrows separating the drumlins, producing U-shaped furrows (B). Note the curvilinear drumlins and furrows towards the top of the photo (C). Province of British Columbia air photo 30BCC 94080 No. 55 and 56. 24
Figure 9. Long sections and plan views of streamlined landforms..... 26
Figure 10. Rat-tail at Dome Mountain Mine, inferred flow direction indicated by arrow. Clast is about 3 cm across. 33
Figure 11. Drumlin formation by subglacial sediment deformation, from Boulton (1987). Reproduced from 'A theory of drumlin formation by subglacial sediment deformation by G.S. Boulton from Drumlin Symposium, eds. J. Menzies and J. Rose, www.tandf.no/boreas, 1987, pp. 25-80, by permission of Taylor & Francis AS. 38
Figure 12. Drumlins formed by infilling of subglacial cavities, re-drawn after Fisher and Shaw (1992) 42
Figure 13. Erosion of hairpin scour by horseshoe vortex. Longitudinal vortex from an upstream hairpin furrow merges into the next horseshoe vortex such that hairpin scours do not cross-cut one another. Reprinted from Sedimentary Geology, v 91, J. Shaw, Hairpin erosional marks, horseshoe vortices and subglacial erosion, pp 269-283, 1994, with permission from Elsevier. 44
Figure 14. Remnant ridge left by water or wind flowing around an obstacle. Area immediately down flow of the obstacle is a zone of low shear stress (Allen, 1982)..... 50
Figure 15. Streamlined landforms in Central British Columbia ..... in map pocket
Figure 16. Comparison of streamlined forms distribution for NTS 93K. Contours represent percent total streamlined forms per four square kilometre area. 59
Figure 17. Distribution by strike of streamlined forms in NTS 93K. Strike is given as an azimuth. A somewhat higher percentage of SF bearing southeast and bearing between 60 - 70° are depicted on Figure 15 than are shown on Plouffe's map. 61
Figure 18. Drumlins, flutings, and crag-and-tails near the east reach of Ootsa Lake, modified from Levson and Mate (2002). The lack of SF in the lowland area from Ootsa Lake to Cheslatta Lake is noted both here and on Figure 15..... 67

Figure 19. View from above of simple hairpin furrow. Flow is to the right. Shaded area represents negative relief troughs. 70
Figure 20. Stylized interconnected hairpin furrows. Flow is to the right. 70
Figure 21. SPOT satellite image of traced hairpin furrows around drumlins in NTS 93M 051. Figure 22 is the same view without tracings. Flow was to the southeast. Scale bar = 500 m. North is at the top of the figure. 71
Figure 22. SPOT satellite image of part of NTS 93M 051. Hairpin furrows are shown traced in Figure 21. Scale bar = 500 m. North is at the top of the figure. 71
Figure 23. DEM image of the Hazelton drumlin field. Tapered SF and hairpin furrows are visible. Flow was towards the southwest. Figure 24 shows the same image with hairpin furrows traced. 72
Figure 24. Furrows traced on a DEM image of the Hazelton drumlin field. Figure 23 is the same DEM image without traced furrows. Flow was to the southwest. 73
Figure 25. DEM image of southeast part of NTS 93M, the Babine River valley. Flow is interpreted as being towards the south-southeast based on tapering forms and hairpin furrows. Scale bar is approximately 4 km long and north is towards the top of the photo. 74
Figure 26. Landsat satellite images of SF in the SE part of NTS 93F (bottom) and NE corner of 93K (top). Flow is interpreted as being towards the NE and ENE, respectively. The white scale bar is approximately 2 km long. Note the tapered SF shown in the lake (arrow). North is toward the top of the figure. 75
Figure 27. Flow directions from streamlined forms mapping. 77
Figure 28. East-northeast trending SF crossing valleys oblique to flow in east Ootsa. Scale bar = 10 km. 80
Figure 29. Northeast-trending SF parallel the bend around the western reach of Ootsa Lake, and then continue obliquely to the eastern reach of Ootsa. A few SF run southeast and parallel the eastern reach of Ootsa. Streamlined forms to the south of Ootsa's eastern reach bear ENE, oblique to Ootsa Lake in this location (see also Figure 28). Scale bar = 10 km. 81
Figure 30. Two maps showing the relationship between glaciolacustrine (purple), glaciofluvial (orange), alluvial (yellow), and bedrock\colluvium (brown) deposits and SF occurrence in NTS 93K. Some areas of low SF density (left map) coincide with glaciolacustrine, glaciofluvial, and alluvial sediments (right map). Surficial geology units from Plouffe (2000). Scale bar = 10 km. 82
Figure 31. Valleys with low SF densities in NTS 93M. Valleys 1 and 2 are parallel to southeast flow. Location 3 is subparallel and location 4 is a cross valley. Note the westward oriented SF path along the Suskwa River that crosses the north end of the Bulkley Valley and leads into the Skeena River valley. Scale bar = 10 km. 84
Figure 32. Valleys / lowlands with low SF densities near Francois Lake. Five lowland areas (labelled 1-5) trend approximately SE and are cross valleys to ENE flow. Relatively few ENE SF occur in the valleys. Four NE- or ENE-trending lowlands with low SF density are labelled a-d. Scale bar = 10 km. 85
Figure 33. Northeast trending SF emanating from cirques (circled). Top map shows SF in the Hogem Ranges. Left bottom map shows SF in the Telkwa Range. Scale bars = 10 km. 87
Figure 34. Streamlined forms (black lines) and surficial geology in NTS 93K. Streamlined forms density is less in the southern half of the map. Glaciofluvial (orange) and fluvial (yellow) deposits are greater in the southern half of the map. Till is pale green and glaciolacustrine sediments are purple. Surficial geology from Plouffe (2000). Scale bar is 10 km long. 92
Figure 35. Shaded relief image of NTS 93K. Note prevalent northeast and southeast trending valleys and lakes in northern two-thirds of the map sheet, corresponding to two of the dominant flow directions in study area. Contour intervals = 50 m. 96

Figure 36. Streamlined forms in northern part of NTS 93K. ENE-trending forms cross-cut SE-trending SF at loction 1. Scale bar = 10 km. Red cross is located at about 125°W and 55°N. 97
Figure 37. Streamlined forms emanating from cirque valleys in NTS 93K (top) and NTS 93L (bottom). Locations of SF paths emanating from cirques are indicated by numbers 1-3. Scale bar = 10 km. 100
Figure 38. Derivation of rectangle used for computing local terrain slope for a SF. 107
Figure 39. Average and maximum elevations by NTS sheet from DEM grid files. Average values are in normal, larger font; maximum values are in italics. 113
Figure 40. Distribution of point values for recalculated DEM grids for NTS map areas 93E, F, K, L, and M. DEM grids were recalculated using a Surfer grid function to reduce grid sizes to one percent of initial size. 114
Figure 41. Number of SF within elevation intervals in the study area. Each bar represents the number of SF found between the next lower elevation and the bar's elevation. 114
Figure 42. Comparison of SF frequency by elevation and topographic elevation frequency. SF frequency follows same general trend as topographic elevation frequency, but shows a greater percentage of SF between about 850 m and 1250 m elevation than would be expected if SF were randomly distributed across elevation. 117
Figure 43. Study area SF density as number of SF per square kilometre. Shaded areas represent SF density values and lines represent elevation contours (see legend). 119
Figure 44. Streamlined form frequency by slope, NTS 93F and NTS 93K. 129
Figure 45. Average lengths of SF by slope intervals, NTS 93F and NTS 93K. 129
Figure 46. Graph of bearing deviation for four slope bins, data from Table 7. Square sizes are indicated in legend. 134
Figure 47. Derivation of total shear stress acting along a land surface due to the weight of an ice sheet. 143
Figure 48. Starting surfaces for simulated erosion, rock drumlin (top) and flat surface with resistant core (bottom). 149
Figure 49. Flat erosion, difference in erosion patterns due to hardness factor variation. Iterations range from 0 to 1200 (see Table 9). All axes values in this and subsequent figures are in metres. Dark rectangle on x-axis represent location of resistant core. Flow direction is left to right. 156
Figure 50. "Run-away" erosion on down-ice side of resistant core. Hardness factor = 4. Dark rectangle on x-axis represents approximate location of resistant core. Flow direction is left to right. 157
Figure 51. Flat surface erosion with erosion bit = 0.001. Only the beginning surface and iterations 200, 600, and 1200 are shown. 159
Figure 52. Extended flat surface erosion with erosion bit = 0.001. Iterations from 3,000 to 12,000, in increments of 1,000, are shown. 159
Figure 53. Flat surface erosion patterns with 0.02 erosion bit at 0° dip. Compare with Figure 49 bottom, in which parameters are the same as here except for the erosion bit. Iterations shown: 100, 200, 400, 600, 800, 1000, and 1200. 160
Figure 54. Flat surface erosion on uphill slopes. Dips = -20° (top) and –5° (bottom). Flow is to the right. Resistant core located between 4.5 and 5 on the x-axis. Iterations shown: 0, 100, 200, 400, 600, 800, 1000, and 1200. 162
Figure 55. Flat surface erosion on downhill slopes. Dips = 5° (top) and 20° (bottom). Flow is to the right. Resistant core located between 4.5 and 5 on the x-axis. Iterations shown: 0, 100, 200, 400, 600, 800, 1000, and 1200. 163
Figure 56. Inclination differences between erosion surfaces of resistant core and adjacent rock. 165

Figure 57. Rock drumlin erosion using ebit = 0.001. 167
Figure 58. Edge effect of rock drumlin erosion. Drumlin shape is planed down in its original location, but modified shape is propagated up-ice. Flow is left to right. Iterations shown in the bottom figure are from 0 to 800 in increments of 100 iterations. 167
Figure 59. Rock drumlin erosion using ebit = 0.01 on uphill slope, dip = -20°. Iterations shown: 0, 100, 200, 400, 600, 800, 1000, 1200. 169
Figure 60. Rock drumlin erosion using ebit = 0.01 on downhill slope, dip = 5°. Iterations shown: 0, 100, 200, 400, 600, 800, 1000, 1200. 170
Figure 61. Rock drumlin erosion using ebit = 0.02 on level slope. Iterations shown: 0, 100, 200, 400, 600, 800, 1000, 1200. 171
Figure 62. Rock drumlin erosion, -20° (left) and 20° (right) dips, ebit = 0.02 172
Figure 63. Air photo pair of Microwave Ridge. Streamlined forms at the site were produced by flow towards the west. Bedding planes on the ridge strike generally north-south and dip to the west. British Columbia Government air photos, SAS30C996133 – 459 and 460. 181
Figure 64. Streamlined forms field study sites. Contours are from 1000 m to 2500 m in 500 m intervals. 186
Figure 65. Stoss ends of streamlined forms on Hazelton Peak. Flow was from right to left and downhill. 193
Figure 66. Lateral furrow between two streamlined forms on Hazelton Peak. Furrow bifurcates at stoss end of another SF. Flow was away from the viewer. 193
Figure 67. Composite photograph of SF on Nine Mile Mountain. View is to the east. Flow was from left to right and uphill. 194
Figure 68. Stereo pair of streamlined forms on Evelyn mountain north of Hudson Bay Mountain. Composition is interpreted as primarily bedrock. North is at the top of the photo, and flow was to the west. British Columbia Government air photos, SAS30C996133 – 84 and 85. North-south lineations at top of photos mark steep, unvegetated scarp extending down from a sharp ridge 195
Figure 69. Lateral furrow along streamlined form flank on north side of Hudson Bay Mountain. Flow was towards the viewer. 195
Figure 70. Streamlined forms on Microwave ridge; flow is from right to left. 197
Figure 71. Typical weathered bedrock SF on Dome Mountain. Flow was away from the viewer. The exposed bedrock ridge is about 12 m long and 2 m wide. 197
Figure 72. Rat-tail swarm at site 112. Pen is 15 cm long and points downstream (uphill). Each rat-tail appears to be initiated by a clast in the bedrock. 199
Figure 73. Small rat-tail (circled) in rat-tail swarm at site 115. Note how even smaller streamlined features are located on the sides of the larger rat-tail. Flow was to the upper right. 200
Figure 74. Very small- and small-scale rat-tails at site 152f. The clear part of the pen head (lower left) is about 1 cm long and points to a small rat-tail upon the tail of which are a number of parallel, very small rat-tails. Fine grains in the bedrock initiated the very small rat-tails. Flow was to the upper right. 201
Figure 75. Large, 50-cm long rat-tail with superimposed smaller rat-tail that formed along its side (see arrow), site 152j. The pen at the top of the photo is about 15 cm long. 202
Figure 76. A) Small rat-tails on the right side (looking down flow) of a medium SBF at site 125. The smaller rat-tails follow the streamlines around and over the SBF. Flow was away from the viewer. B) Photo of approximate area enclosed by rectangle on photo A. 203
Figure 77. Swarm of very small rat-tails on stoss end of small SBF at site 128. Clear head of pen is about 1 cm long. Flow was toward the top right. The estimated dip of the rat-tail-covered surface is ~40° NE. Dominant flow at the site is to the west. 204

Figure 78. A) Very small rat-tails at site 162. Flow was to the right. The black rectangle indicates the area represented by photo B. B) Magnification of miniature rat-tails showing proximal hairpin scours, indicated by arrows. Scale bar equals approximately 2 cm.....205
Figure 79. Dome Mountain Mine site. Flow was to the right and uphill. The orientations of rat-tails at this site are generally parallel to the flow axes of the medium-scale SBF shown in the photograph.....206
Figure 80. Looking down at rat-tails and striae descending into angular joint cavity at site 131. The cavity is on the tail of the medium-scale SF shown in Figure 71. Pen is 15 cm long and points down flow. Traces on left depict rat-tail and striae orientations relative to the cavity wall.....208
Figure 81. Curving rat-tail trail at site 152o. The line diagram on the left shows representative rat-tail traces. The curving path (open-head arrows) is following a furrow around a rock SF located to the left of the photo area. Flow that is oblique to and appears to converge with the curving path (closed-head arrow) is parallel to the main flow direction at the site. Representative rat-tail orientations are given on the line drawing.....209
Figure 82. Medium-small-scale SF at site 152k. Solid line indicates curved path of small SF along the larger SF flank. Dashed line outlines proximal scour of larger SF. Arrows define ends of undercut SF base.....210
Figure 83. Streamlined rock face that modified flow direction at site 118. There is a continuum of orientation change of small rat-tails from bearings that are subparallel to the strike of the face, to the main flow direction on the upper surface of the outcrop. Flow was toward the top of the photo. The same changes in flow direction are noted in striae / grooves...211
Figure 84. Rat-tails curving out of a joint that strikes nearly normal to flow, site 126. The initial rat-tail bearings appear to be inherited from the joint strike, and the final bearings parallel the main flow direction. Flow is away from the viewer.....212
Figure 85. Small rat-tails on vertical face at site 124. Flow was away from the viewer. GPS is about 15 cm long.....213
Figure 86. Arrow points to rat-tails on a near vertical rock face at site 123. The small increments on the field book are 1 cm. Flow was toward the top right of the photo.....213
Figure 87. Rat-tails in curving furrow. Arrow points to plucked part of rat-tail clast. Flow was toward the top right of the photo.....215
Figure 88. Power curve for lengths and widths of 115 rat-tails in the study area (see Table 14). There is a strong correlation, $R^2 = 0.89$, between length and width.....216
Figure 89. Striae and rat-tails in furrow at site 152p. Note parallelism of rat-tails with other rat-tails and with some striae; striae cross-cut other striae and rat-tails.....218
Figure 90. Straight cavetto at Dome Mountain Mine site. Flow was towards upper right. Rat-tails near cavetto overhang are those shown on Figure 89.....219
Figure 91. Cavetto at site 111 on Microwave ridge. Pencil is about 15 cm long. Flow is toward the upper left.....219
Figure 92. Cavetto at site 97, Microwave ridge. Pencil is about 15 cm long. Flow was towards the upper left.....220
Figure 93. Lemniscate loop. Shape is generated by equation 1. Shape factor *k* is defined by equation 2. The Xm length is used in streamlined form analyses.....239
Figure 94. Contour maps of the north half of NTS 93F, 100 m contour interval. The top map is using a full-size TRIM1 DEM, and the bottom map uses the same grid recalculated to 10% of the number of nodes in the full-size grid. Upper right corner of contour maps are at about 124.01° W longitude and 54.04° N latitude.....243
Figure 95. Contour maps at maximum zoom of contouring software. Scale bar = 5 km. Top map is using full-size grid. Bottom map uses recalculated grid. Contour interval = 100 m. ...244
Figure 96. Closed contours interpreted as streamined erosional residuals.....in map pocket

Figure 97. Small-scale duplicate of Figure 96, the main closed contour map found in the map pocket. See Figure 96 for complete legend. X shows an area lacking large landforms. Direction of increasing size of CC is indicated by the arrow at Y. 249
Figure 98. Erosional residuals in glacial outburst flood channels in Minnesota (bottom) and in area of anastomosed channels near Minot, North Dakota (top). Residuals are formed in sediment although bedrock is exposed between residuals in the Minnesota spillway. Flow directions are towards the east. Maps from Kehew and Lord, 1986, with permission from the Geological Society of America. 250
Figure 99. Erosional residuals of the Channelled Scabland in Washington, products of the Lake Missoula outburst flood(s) (Baker, 1973; Baker *et al.*, 1987). Flow is generally towards the southwest. North is towards the top of the figure, and scale bar represents approximately 30 km. From Baker *et al.*, 1987; reprinted with permission from the Geological Society of America. 251
Figure 100. "The Labyrinth", interpreted as a subglacial meltwater channel system at Dry Valleys, Antarctica (Sugden *et al.*, 1991; Benn and Evans, 1998). Oblique aerial photograph from the cover of December 1983 issue of Geology (Denton, 1983). Reprinted with permission from George H. Denton. The distance across the channel in the vicinity of the butte in the background is about 600 m. 252
Figure 101. Faults over closed contours, north half of study area. Only closed contours greater than 10 km^2 are shown. 253
Figure 102. Faults over closed contours, south half of study area. Only closed contours greater than 10 km^2 are shown. 254
Figure 103. First order closed contours showing length and width axes. Only closed contours with areas greater than 100 km^2 are shown. 257
Figure 104. Second order closed contours showing length and width axes. Closed contour areas are greater than 100 km^2. Second order forms are at higher elevations than first order forms (see Figure 96, map pocket). 258
Figure 105. Third order closed contours showing length and width axes. Closed contour areas are greater than 100 km^2. Third order forms are at higher elevations than first and second order forms (see Figure 96, map pocket). 259
Figure 106. Streamlined erosional residuals formed in glacial lake spillways, taken from Kehew and Lord (1986). Upper figure is derived from Minot spillway residuals in North Dakota; lower figure is from Minnesota spillway. Scale bars are 1 km long. Length and width axes used by Kehew and Lord in numerical shape analysis are shown. Reprinted by permission of Geological Society of America. 260
Figure 107. Plot of width versus length for study area closed contours. 263
Figure 108. "Statistical braid bar", re-drawn from Rachoki (1981). Flow is towards the right. The distal angle is represented by x. 269
Figure 109. Long axes of closed contours greater than 100 km^2 in area. 270
Figure 110. Long axes of closed contours less than 100 km^2 in area. 271
Figure 111. Frequency histograms of streamlined landforms (drumlins, crag-and-tails, etc.) and closed contour strikes. 273
Figure 112. A few large-scale closed contours in more isolated locations that have possibly more lemniscate shapes (see numbered locations). 276

LIST OF TABLES

Table 1. Streamlined forms counts, lengths, and elevations by NTS sheet 113
Table 2. Effect of elevation on SF length; moving square sampling and ANOVA, $P < 0.05$ .. 122
Table 3. Effect of elevation on SF length; moving square, lower 2/8 fraction sampling, and ANOVA, $P < 0.05$ 124
Table 4. Elevation effect on bearing deviation, NTS 93F. Bold values are significant results at $P < 0.05$. 126
Table 5. Slope effect on SF length, NTS 93F and NTS 93K, $P < 0.05$; top two average lengths per square size are in bold. 130
Table 6. Slope effect on bearing deviation, 93F, two slope bins, $P < 0.05$. Greatest deviation in bold 133
Table 7. Slope effect on bearing deviation, 93F, four slope bins, $P < 0.05$. No significant effect. 134
Table 8. Parameters used for incremental glacial erosion analysis 148
Table 9. Parameter values for simulated erosion 154
Table 10. Composition of lowland streamlined forms 188
Table 11. Lateral variation in streamlined form composition, Hazelton streamlined forms field 189
Table 12. Vertical variations in streamlined form composition, Hazelton drumlin field. Top sample is 1 m below SF crest; bottom sample is 2-3 m below SF crest 190
Table 13. Streamlined forms in alpine areas 192
Table 14. Rat-tail length and width statistics 215
Table 15. Streamlined forms origins indicated by field study findings 234
Table 16. Descriptive statistics of the area (km^2) of closed contours 248
Table 17. Length, width, and aspect ratio (L/W) of study area closed contours < 2.5 km^2 in area 261
Table 18. Aspect ratios for different size ranges of study area closed contours 261
Table 19. Shape statistics for erosional residuals 262
Table 20. Regression equations for closed contours, erosional residuals, and river islands 264

ACKNOWLEDGEMENTS

Special thanks to Dr. Victor Levson for encouragement, insight, careful reviews, fairness, and humour.

I also acknowledge and thank my co-supervisor, Dr. Eileen van der Flier-Keller, and the members of my committee, Dr. Dan Smith and Dr. Andrew Weaver. Also thanks to Dr. Alain Plouffe for serving as an external examiner. All were helpful.

I thank Golden Software of Golden, Colorado for their gift of Surfer and Didger GIS mapping programs. The programs were the primary software tool used in dissertation mapping projects. They worked well.

Acknowledgement for the use of Landsat 7 data, indicated in the dissertation as "Landsat images":

> These data are distributed by EROS Data Center Distributed Active Archive Center (EDC-DAAC) located at the U.S. Geological Survey's EROS Data Center in Sioux Falls, South Dakota, U.S.A..

Acknowledgement for the use of SPOT data, indicated in the dissertation as "SPOT images":

> SPOT data used within this dissertation provided by the Skeena Region, Ministry of Sustainable Resource Management, Government of British Columbia.
>
> SPOT data © CNES 2001. Received by the Canada Centre for Remote Sensing (CCRS). Processed and distributed by RADARSAT International under license from CCRS.

Acknowledgement for digital data used for topographic and shaded relief maps:

> Digital base map from British Columbia Ministry of Environment, Land, and Parks. Modified from 1:20,000 TRIM I data.

DEDICATION

Thank you to my wife, Pamela, and my children Duncan, Eliza, and Rory for their continual support in what has turned out to be a long undertaking. What will life "after PhD" be like?

"...the same day were all the fountains of the great deep broken up, and the floodgates of heaven were opened."

- Genesis 7:11

"The waters are hid as with a stone, and the face of the deep is frozen."

- Job38:30

"When all other contingencies fail, whatever remains, however improbable, must be the truth."

--Sherlock Holmes

1. INTRODUCTION, TERMINOLOGY AND BACKGROUND

1.1. INTRODUCTION

This dissertation presents data and discussion about the occurrence and origin of streamlined forms in central British Columbia. Streamlined forms include landforms (*e.g.* drumlins), and streamlined bedrock forms (*e.g.* rat-tails). Theories about the origins of streamlined forms in glaciated terrain are currently in dispute.

The contention mainly concerns whether drumlins were formed by subglacial ice (*e.g.*, Smalley and Unwin, 1968; Shaw and Freshauf, 1973; Boulton, 1987; Boyce and Eyles, 1991; Boulton, 1996; Hattestrand *et al.*, 1999; Clark, 2002; Rattas and Piotrowski, 2003), by meltwater floods (*e.g.*, Shaw, 1983; Shaw and Kvill, 1984; Shaw and Sharpe, 1987; Shaw, 1996; Shaw, 2002), or by both types of flow (Dardis and McCabe, 1987; Mate, 2000; Knight, 2002). Whether streamlined bedrock forms such as rat-tails and rock drumlins were formed by water or ice is also disputed (Boulton, 1974; Kor *et al.* 1991).

The purpose of this dissertation is to provide a better understanding of the occurrence and origins of streamlined forms (SF) in central British Columbia. Some of the main contributions of this work include: provision of a regionally extensive digital map of SF in the study area, development of computer methods for statistical analyses of large databases, development of a computer model simulating glacial erosion, development of a method for objective landform recognition using topographic analysis, and description of large-scale landform patterns not previously described. A more detailed summary of major contributions is given in Section 1.1.2.

The study area is of particular interest for two main reasons. First, the area spans a boundary between mountainous regions and the Interior Plateau. Fraser Glaciation flow emanated from the Coast and Stikine mountains onto the Nechako Plateau at times, and flow also is evident from the plateau to the mountains. The area, therefore, is important in that at least three major flow directions are represented. Second, a comprehensive study of streamlined forms across the entire study area had not been conducted prior to this work. One of the main practical applications of the latter is in the field of mineral exploration (*e.g.* determining source areas for mineralized erratics and soil anomalies). This research also has applications for the study of SF in other regions and has direct geological implications for areas outside the study, especially in the down flow direction of major SF fields.

1.1.1. Objectives

The main research objectives are as follows:

1. Develop a methodology to digitally produce a regional-scale map of streamlined landforms in the study area using digital elevation models and satellite images, produce the map, and analyze streamlined landform occurrence. The streamlined forms map is intended to provide a comprehensive record of streamlining flow including direction, location, elevation range, and response to topography. The objective is to provide an extensive digitally captured database of streamlined form size, orientation, and location.

2. Statistically test whether SF length and orientation are affected by location, elevation, and/or topographic variation. Results will be related to flow characteristics expected from ice and water.
3. Observe and describe streamlined bedrock forms and SF composed of sediment in the study area and relate those observations to SF origins. Field study data will be used to make inferences regarding whether SF in the study area are primarily erosional or depositional forms. Inferences about the erosive mechanism will be made using observations of shapes, sizes, and spatial arrangements of streamlined bedrock forms.
4. Simulate bedrock erosion beneath a glacier or ice sheet using a two-dimensional computer model. The purpose is to test whether a streamlined form persists beneath an ice sheet and/or whether a resistant clast in a rock surface results in a streamlined form as the surface is progressively eroded.
5. Analyze topography by mapping kilometre-scale "closed contours" using digital elevation models, and statistically test the correlation of closed contour length to width. Results of the test will be compared to similar results from numerical analysis of fluvial landform shapes available in the literature. The purpose is to determine if some landforms can be interpreted as fluvial features based on their shapes.

1.1.2. Summary of contributions

The completion of these objectives has resulted in significant contributions to the knowledge of streamlined forms in central British Columbia. The study includes

development of a comprehensive, regional-scale database of more than 50,000 SF mapped as georeferenced lineations with length, orientation, and slope attributes. No comparable database has previously been produced for any area in the Canadian Cordillera. Analyses of this database allowed for the observation of relationships between landscape attributes and SF characteristics, and permitted inferences to be made about SF-forming flow. The database is also useful for glacial flow path studies.

This thesis research includes the development of a computer program that models surface erosion over time due to shear stresses at the base of an ice sheet or glacier. The model allows comparison of results that arise from modification of single or multiple parameters. Three types of surfaces are "eroded" using the model: a planar surface with variable resistance to erosion, a planar surface of homogeneous resistance, and a "typical" drumlin long section.

Computer methods for statistically analyzing georeferenced lineations were developed during the thesis research. The methods include the capability to divide a large geographic area into smaller areas (or bins) that can be analyzed separately. This allows the detection of statistical differences at a local scale, which may be different from statistical differences calculated on the larger, regional scale database. The size of these sample bins can be varied programmatically.

A method for computer analysis of digital topographic data is developed. A correlation between lengths and widths of closed contours is found. These results possibly indicate the signature of a meltwater formative process for some landforms.

1.1.3. Overview of thesis methods

Several different approaches are used to accomplish the thesis objectives. Detailed descriptions of methods are provided at the beginning of the following chapters and are summarized here.

Streamlined forms mapping is accomplished using GIS software and digital images. The locations and lengths of SF recognized on shaded relief digital elevation model (DEM) images or on satellite images are digitized as lines. The georeferenced coordinates of these lines are stored in text files. The resulting map is visually analyzed for relationships between topography and drumlin occurrence, bearing, and length. Quality control is conducted by comparing the thesis map with previous drumlin mapping that overlaps the study area.

Numerical analysis of SF lineations is accomplished using computer spreadsheet data handling and by writing custom task-specific programs. The elevations of SF coordinates are obtained using DEMs. Streamlined form length, orientation, and midpoint location are obtained by calculation from measured data. Statistical and numerical analyses of relationships between topography and drumlin properties are accomplished using the drumlin database and DEM grids.

The incremental glacial erosion model was built using Microsoft® Excel and Visual Basic for Applications (VBA). The model permits parameter adjustments in an Excel worksheet, and shows the incremental erosion on screen as an Excel chart depicting the long section of an eroding surface.

Field work consisted of detailed study of several streamlined bedrock form sites and of reconnaissance-scale investigation of drumlins at several locations across the

study area. Streamlined bedrock forms were measured, photographed, and described. Streamlined forms sections are described.

Mapping of study area closed contours is accomplished using topographic maps generated from DEM grids and DEM shaded relief images. Numerical shape analysis of the mapped landforms is conducted using digitizing software, Excel, and VBA.

1.1.4. Study area

The study area is in central British Columbia (Figure 1), and it covers about 67,000 km^2 in area. It is located between 53° and 56° latitude, between 124° and 128° west longitude, and includes National Topographic System (NTS) grids 93E, 93F, 93K, 93L and 93M (Figure 2). Forestry is the dominant land use. Mining and agriculture are also important. Highway 16, connecting Prince George in the interior and Prince Rupert on the coast, bisects the area from east to west. Logging roads and secondary gravel roads provide access to more remote locations. Smithers is the principle population center, and is serviced by a controlled airport with daily passenger service.

1.1.4.1. Previous work

Kerr (1934) suggested that four glaciation styles are apparent in northern British Columbia. He suggested that the early part of a glacial period is marked by topographically controlled alpine glaciation. As ice sheets expand, topographic control on ice flow direction progressively lessens, culminating in cover by a continental ice sheet. Extensive drumlinization in north central British Columbia was described by Armstrong and Tipper (1948). Drumlins and other geomorphic features were used to

construct a model of Pleistocene history (Tipper, 1971a) and multiple glaciation (Tipper, 1971b) in central British Columbia.

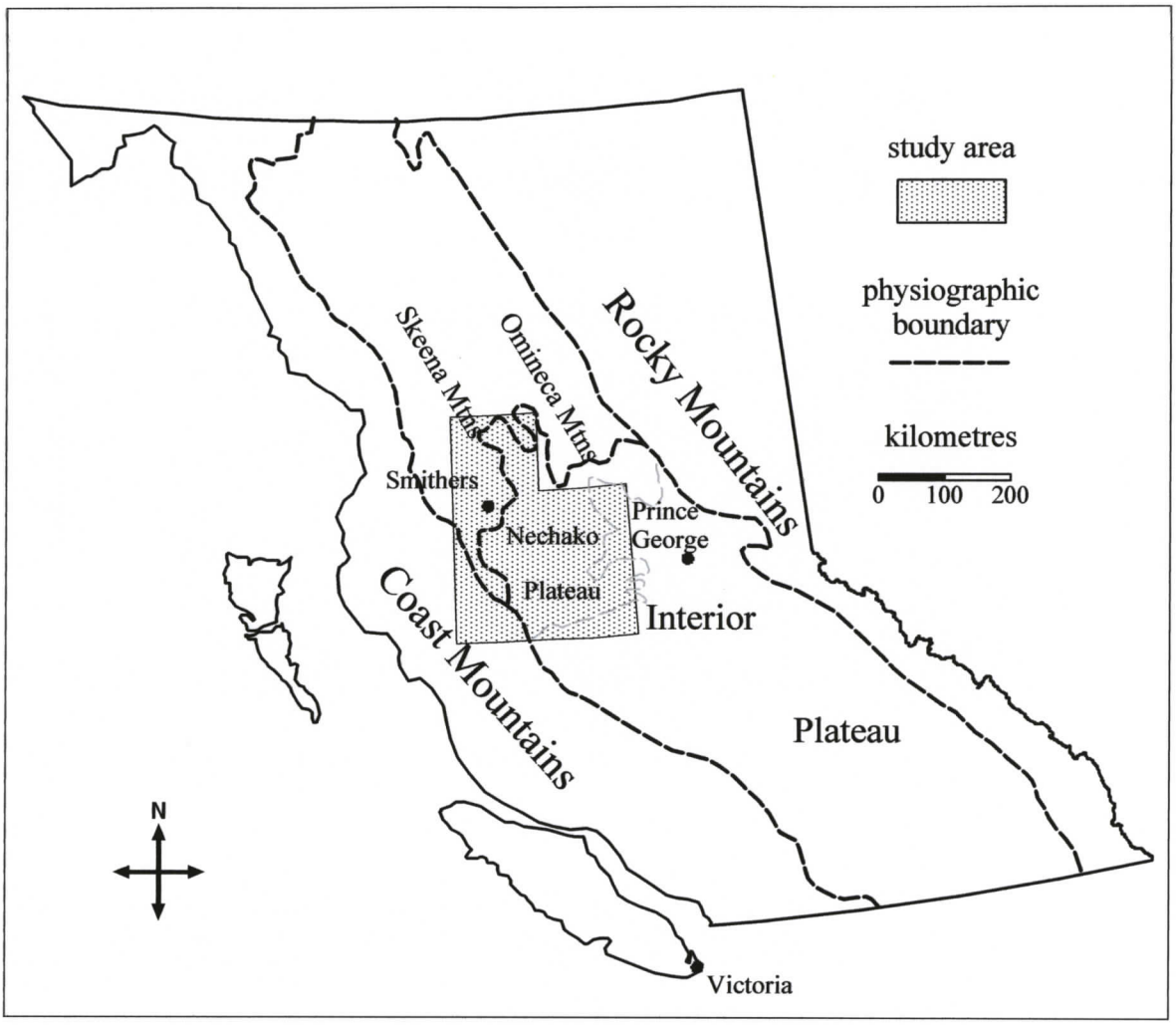

Figure 1. Study area location, major physiographic boundaries from Holland (1964). The lighter dashed line represents the boundary between the Nechako Plateau and the rest of the Interior Plateau.

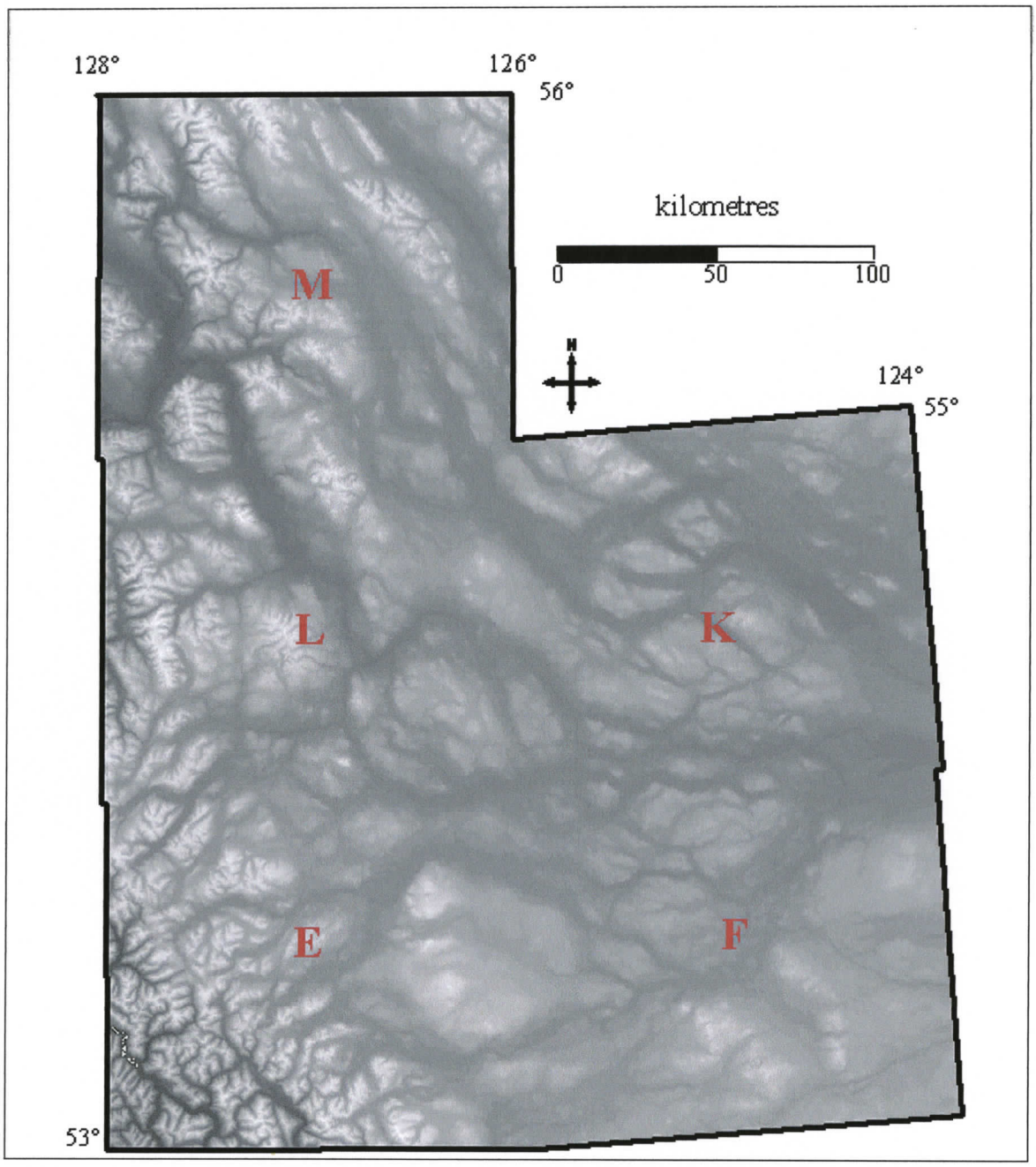

Figure 2. Topography of study area showing centers of NTS 93E, 93F, 93K, 93L, and 93M. Shaded elevation contours are from 0 m (dark grey) to 2600 m (white) above sea level.

Clague (1989) provided a description of the entire Cordilleran Ice Sheet, with growth history and flow directions. Ryder and Maynard (1991) focused on the Cordilleran ice sheet history and flow directions in northern British Columbia, north of and including the northern part of the study area. A north-south ice divide located in central British Columbia at the peak of the Wisconsinan glaciation was deduced by Levson *et al.*(1998) and Stumpf *et al.* (2000).

Clague (1984) described the Quaternary geology and geomorphology of the Bulkley and Skeena river valleys extending from Smithers to Prince Rupert. The Quaternary geology of northeast NTS 93L and southeast NTS 93M was discussed by Levson (2001, 2002). Quaternary geology and stratigraphy studies that included the northeastern parts of NTS 93E in the vicinity of Ootsa Lake are presented by Mate (2000) and Mate and Levson (2001). Ferbey (2004) conducted field research in NTS 93E in the Huckleberry Mine region, in the boundary area between the Coast Mountains and the Nechako Plateau.

A surficial geology map at 1:250 000 scale has been produced for all of NTS 93F (Plouffe *et al.*, 2004). Surficial geology of the Fawnie Creek (Levson and Giles, 1994), Tsacha Lake (Giles and Levson, 1995), Entiako Lake (Plouffe and Levson, 2004a), and Tatelkuz Lake (Plouffe and Levson, 2004b) areas in NTS 93F has been published. Plouffe (1998a, 1998b) prepared 1:100 000 scale surficial geology maps of the Tahultzu Lake and Binta Lake areas in NTS 93F. The Ootsa Lake and Cheslatta River and Lake areas in northeastern 93F were discussed by Mate (2000) and Mate and Levson (2001). Levson and Giles (1997) presented surficial geology studies in the context of till geochemistry for parts of the Nechako and Fraser plateaus. Both surficial

and bedrock geology of the Chedakuz Creek map area in the southwest corner of NTS 93F was discussed by Diakow *et al.* (1995). A 1:100 000 scale map showing bedrock and surficial geology of the south central part of 93F was produced by Diakow and Levson (1997). A digital elevation model of the Nechako River map area was produced by Lowe *et al.* (2001).

A surficial geology map at 1:250 000 scale has been produced for all of NTS 93K (Plouffe, 2000). Plouffe also prepared 1:100 000 scale surficial geology maps for the Tezzeron Lake (Plouffe, 1994), Burns Lake (Plouffe, 1996a), Cunningham Lake (Plouffe, 1996b), and Fraser Lake (Plouffe, 1996c) areas in 93K.

In addition to the studies listed above, terrain stability maps have been produced for large portions of the study area (Geological Survey Branch, 2003). This database was produced primarily as a result of the Forest Renewal BC government initiative. Terrain stability maps are maps of surficial material. Terminology and mapping objectives are somewhat different than those used in typical surficial geology studies.

A number of geologic maps and bedrock geology maps and studies have been completed for the study area. A geologic compilation map of the Skeena-Nass areas at a scale of 1:250 000 includes NTS 93E, 93L, and 93M (MacIntyre *et al.*, 1994a). Other studies in 93E have focused on Kemano-Tahtsa area (Stuart, 1960), Tahtsa Lake District (MacIntyre, 1985), and Nanika Lake map area (Diakow and Timmerman, 1990). The bedrock geology of the Tahtsa Ranges has also been investigated by Diakow and Koyanagi (1988) and Diakow *et al.* (1994).

Williams (1997) produced a 1:250 000 scale geologic compilation map for NTS 93F. Bedrock geology of the Fraser Lake and Nulki Hills areas in 93F has been mapped

at 1:100 000 scale (Struik, 1998a; Wetherup, 1998). Both bedrock and surficial geology in 93F are presented by Diakow *et al.* (1995) for the Chedakuz Creek map area and by Diakow and Levson (1997) for the southern Nechako Plateau.

Ash *et al.* (1993) studied the geology of the Stuart-Pinchi Lake area in NTS 93K. Struik *et al.* (2000) reported on bedrock geology in the Burns Lake map area in 93K. Bedrock geology maps at 1:100 000 scale have been published for the Endako (Struik and Whalen, 1998) and Tezzeron (Struik, 1998b) map areas in 93K. McIntyre and Schiazarra (1999) published the bedrock geology of Cunningham Lake.

MacIntyre (2001) produced a geological compilation map of the Babine Porphyry Copper District which lies in northern NTS 93L and in NTS 93M. Reports on bedrock geology in the Dome Mountain (MacIntyre *et al.*, 1987) and Fulton Lake (MacIntyre *et al.*, 1996) areas in the east half of 93L, and the Telkwa Valley (MacIntyre *et al.*, 1989) in the western part of 93L are also available.

Brown (1960) published a bulletin on the Rocher Deboule Range in southern NTS 93M. MacIntyre *et al.* (1998) present the bedrock geology of the Old Fort Mountain map in southeastern 93M. The geology of the Babine Mountain Recreation Area has also been published (Gaba, 1992).

1.1.4.2. Ice flow history

Ice flow history across the study area during the Fraser Glaciation has been described in several studies. Glacial flow indicators are interpreted in these studies as recording shifts in ice flow direction related to ice sheet growth and retreat. During ice advance, flow was generally out of cirques and down valleys (Plouffe, 2000; Levson,

2002; Plouffe *et al.*, 2004). Southeast, valley-parallel flow dominated the northern part of the study area and ENE flow emanated from the Coast Mountains (Plouffe, 2000; Stumpf *et al.*, 2000; Ferbey and Levson, 2001; Levson, 2002; Ferbey, 2004). Easterly flow in the northeast part of the study area is thought to have been deflected towards the north by flow from the Cariboo Mountains, located southeast of the study area (Plouffe, 2000).

As the ice sheet became thicker there was less influence of topography on ice flow direction. At glacial maximum, the ice divide located over the Coast Mountains migrated easterly over the Interior Plateau in a general region extending southward from east of the Babine Valley to east of the Quanchas Range (Stumpf *et al.*, 2000; Levson, 2002) (Figure 3). Uphill flow towards the west in the Babine Range, the Hazelton Mountains (Stumpf *et al.*, 2000; Levson, 2002) and in the Whitesail Range (Ferbey and Levson, 2001; Ferbey, 2004), and uphill flow towards the east in NTS 93K (Plouffe, 2000) are thought to have occurred during glacial maximum.

Ice retreat resulted in a return to valley directed flow. Southeast flow indicators that post-date westerly flow indicators are present in the Babine Valley (Stumpf *et al.*, 2000; Levson, 2002). East flow from the Coast Mountains during glacial retreat is proposed by Ferbey (2004).

1.1.4.3. Physiography

The study area lies entirely within the Canadian Cordillera and comprises parts of both mountain and plateau physiographic areas (Figure 1). Mountainous terrain dominates the north and west parts of the study area. The central and eastern sections of

the study area include the northwest extremities of the Interior Plateau. Relief in the study area ranges from sea level to 2700 m above sea level.

The western and northern sections of the study area include terrain of the Coast, Hazelton, and Skeena Mountains (Figure 3). The Skeena Mountains extend into the northern parts of the study area as generally southeast oriented ranges including the Hogem, Bait, and Babine Ranges. Matterhorns, north and east facing cirques, and serrated ridges characterize the upper peaks of the high mountains. Uplands below about 1830 m elevation are rounded. The ranges are separated by generally broad valleys.

The Hazelton Mountains extend into the west central part of the study area, and comprise the Nass, Kispiox, Bulkley, and Tahtsa Ranges (Figure 3). The Hazeltons lie between the Coast Mountains on the west and the Skeena Mountains and Nechako Plateau on the east. The upper peaks of the Hazeltons are serrate and demonstrate cirque erosional forms.

The Tahtsa Ranges are an en echelon series of smaller northeast oriented ranges including the Morice, Sibola, and Whitesail Ranges. The Tahtsa Ranges are separated by valleys occupied by lakes located between about 800 and 950 m elevation. The lakes drain eastward to the Fraser River.

The Nass Basin extends into the western part of the study area in NTS 93M (Figure 3). The basin is an area of low relief, generally lying below 750 m, drained by the Kispiox and Skeena Rivers.

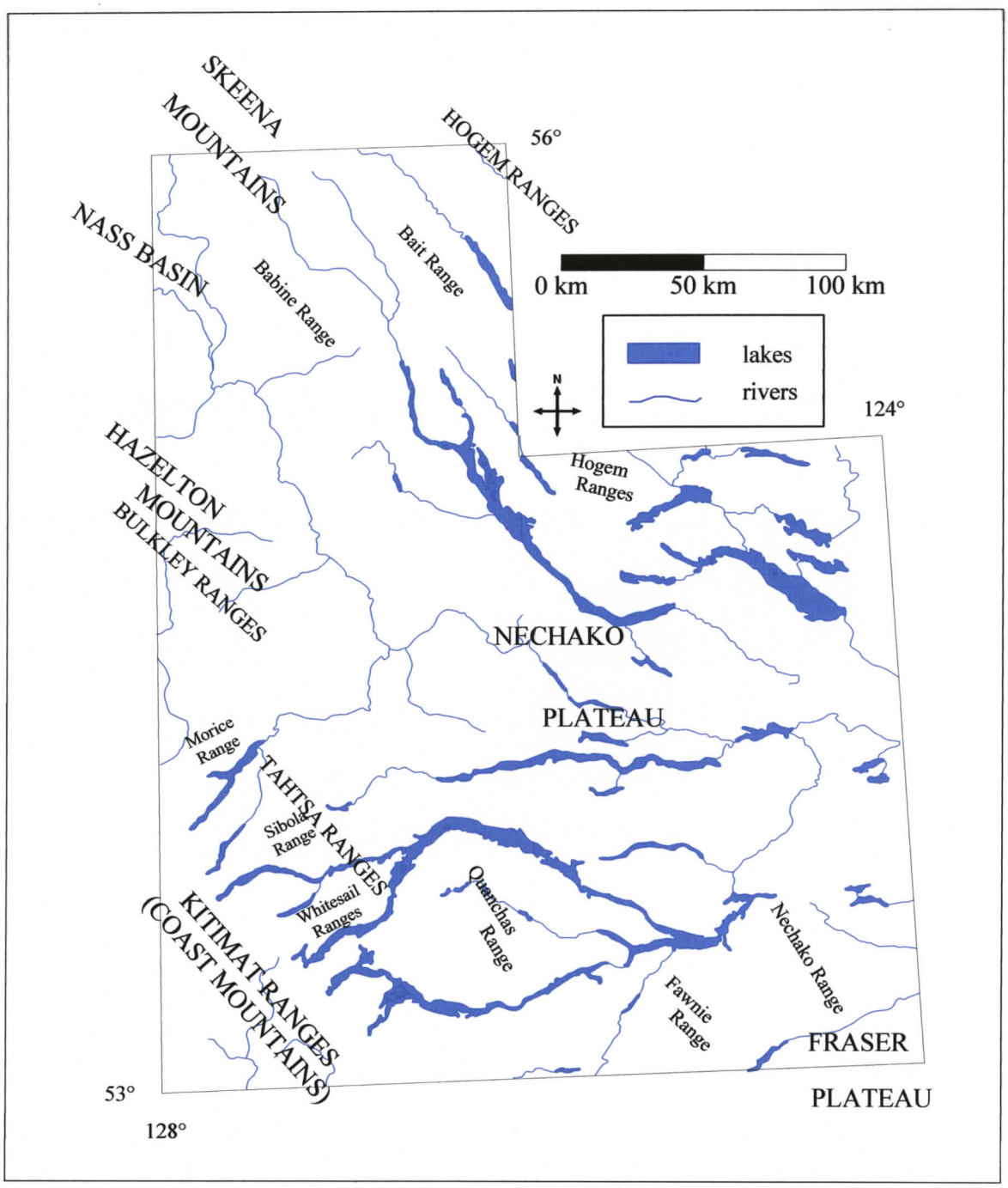

Figure 3. Mountain ranges, plateaus, and basins of the study area.

The central and eastern parts of the study area cover most of the Nechako Plateau, which is part of the Interior Plateau, an elongate basin in central British Columbia rimmed by mountains (Holland, 1964; Tipper, 1969). The boundary between the previously discussed mountain ranges and the adjacent plateau areas is generally drawn at about the 1500 m contour (Holland, 1976). The Nechako Plateau is less rugged than the western terrain, rarely exceeding 2000 m elevation (Tipper, 1969). Relief generally ranges between 450 m and 1500 m.

The plateau is characterized by rounded, and often elongated, uplands defined by a network of curvilinear or linear lowlands (Figure 2). The plateau surface generally lies between 1200 m and 1500 m elevation. Some parts of the lowlands are very long and broad and hold reservoirs, natural lakes, and rivers. Isolated, rugged monadnocks are found on the plateau, including Shass Mountain between Babine and Stuart Lakes, and including the principle peaks of the Quanchas, Nechako, and Fawnie Ranges in NTS 93F (Figure 3).

Drumlins, crag-and-tails, and flutings are found over almost the entire study area. They are most common on the plateau and in the lowland areas of the mountains, although they are also found on mountain ridges as high as 1900 m asl (Levson, 2002).

1.1.4.4. Surficial geology

Figure 4 is a generalized map (Fulton, 1995) used here to provide an overview of study area surficial geology. Greater surficial geology detail of various parts of the study area, including delineation of units not shown on Figure 4, is available in several publications (see Previous Work, this chapter).

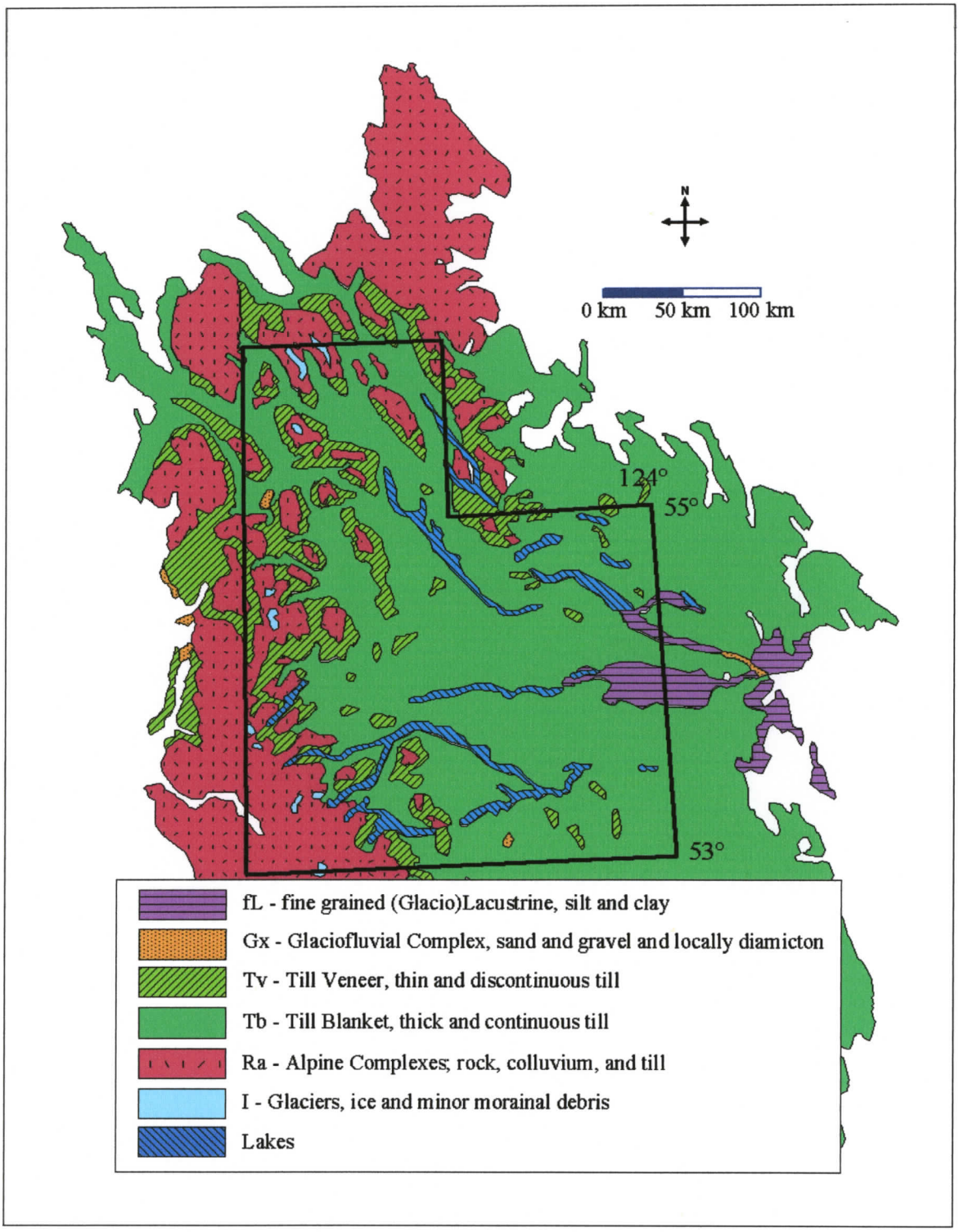

Figure 4. Generalized surficial geology of the study area. Produced from digital data, GSC Map 1880A, Fulton (1995).

Till accounts for approximately 70% of the surficial material in the study area (Figure 4). Most of the ground cover is interpreted as till blanket, indicating thicknesses greater than one metre. Till veneers, less than one metre thick, are discontinuous and may include extensive areas of rock outcrop. These units are generally associated with mountainous areas, and often separate Alpine Complex (Fulton, 1995) surficial materials from lower elevation till blankets. Most of the plateau area and mountain lowlands have till blanket cover.

Glaciofluvial Complex (Gx) sediments are interpreted as ice contact sediments with stratified drift and outwash (Fulton, 1995). The unit defined as fL on Figure 4 consists of glaciolacustrine deposits in the study area. These deposits often obscure older glacial landforms.

1.1.4.5. Bedrock geology

Due to widespread glacial sedimentation, bedrock exposures are limited in the study area. On the Nechako plateau and in major river valleys, only about 5 – 10 % of the bedrock is exposed. About 10 – 20 % of the bedrock is exposed over the entire study area.

The Canadian Cordillera is divided longitudinally into five morphogeological belts (Gabrielse *et al.*, 1991). The study area lies largely within the Intermontane Belt; although, the extreme southwestern corner of the study area is part of the Coast Belt. Both belts are interpreted as accreted superterranes (Gabrielse *et al.*, 1991). The Intermontane Belt is generally lower topographically than the Coast Belt to the west

and the Omineca Belt to the east, with the exception of the rugged, high relief Skeena Mountains.

About half of the bedrock that underlies the study area is of volcanic origin (Figure 5). The approximate relative percentages and bedrock types that underlie the study area are 49% volcanic, 33% sedimentary, 15% intrusive, 3% metamorphic, and <1% ultramafic.

The Skeena Mountains largely comprise folded sedimentary rocks. The Hazelton Mountains, including the Kispiox and Bulkley Ranges, are primarily Mesozoic sedimentary and volcanic rocks with some granitic intrusions that are mostly Cretaceous. Most sedimentary rocks in the study area belong to the Cache Creek, Skeena, Bowser Lake, Hazelton, and Takla Groups and dominantly comprise undivided, fine- and coarse-grained sediments (MacIntyre, 1994; Schiarizza *et al.*, 1994; Bellefontaine, 1995; Massey *et al.*, 2003a; Massey *et al.*, 2003b).

Volcanic rocks underlie much of the Nechako Plateau and account for almost half of upper bedrock units across the study area (Figure 5). Flat to gently dipping Tertiary volcanics cover rocks of the Takla and Hazelton Groups. Most of the volcanic rocks are members of the Hazelton, Nechako Plateau, Kasalka, Endako, and Ootsa Lake Groups. About half of the volcanics are of calc alkaline and andesitic composition. Rhyolite and felsic volcanic centres are also present, for example, near the Skeena Arch, an east-west tectonic feature in the northern part of the study area. Basalt flows also occur.

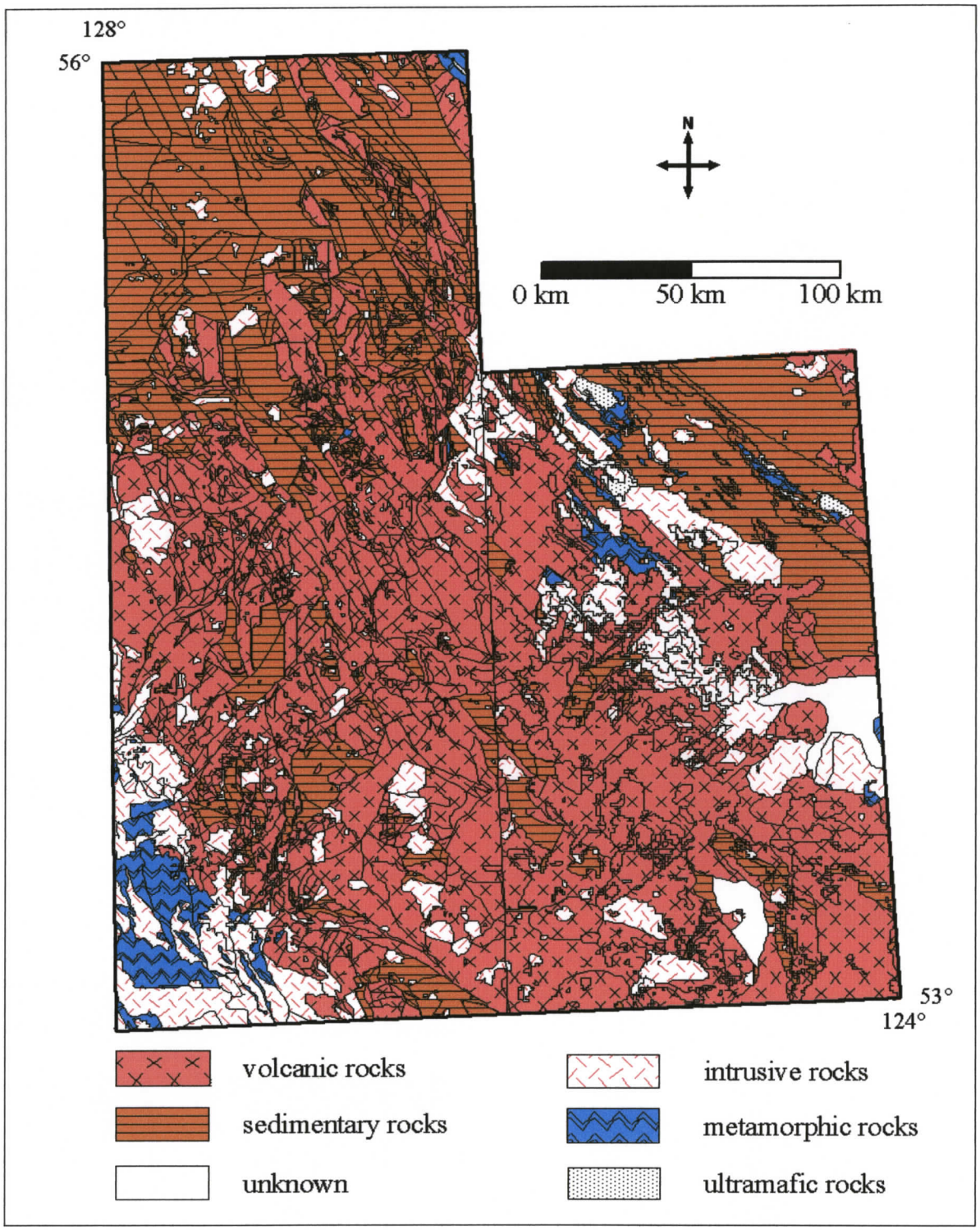

Figure 5. Bedrock geology of the study area. Most bedrock is covered by glacial sediments and outcrop limits are often inferred. Compiled from Massey *et al.* (2003a) and Massey *et al.* (2003b).

Granitic plutons intrude volcanic and sedimentary rocks. The Kitimat Ranges, of the Coast Belt, occupy the southwest corner of NTS 93E and are primarily granitic (Figure 5). Principle intrusives include quartz diorite, granodiorite, diorite and undivided granitic rocks. The main metamorphic rocks include orthogneiss, greenstone and greenschist facies rocks, and lower amphibolite/kyanite grade rocks. Ultramafic rocks are mainly members of the Cache Creek Group.

Fault patterns in the study area reflect the tectonic history of the Intermontane Belt. Long, northwest-trending faults generally parallel the contacts between adjacent belts, and are associated with accretionary tectonics. They include strike slip and thrust faults. Extensional tectonics resulted in the development of horst and graben structure defined by northwest-trending faults and generally shorter, northeast-trending faults (Figure 6) (MacIntryre, 1996).

1.2. STREAMLINED FORM DESCRIPTION AND CLASSIFICATION

1.2.1. Defining streamlined forms

Streamlined forms are sediment or bedrock forms shaped by and aligned parallel to flow. *Streamlined* is used to describe natural forms shaped like airfoils (Flint, 1957). Streamlined forms, in plan view, may look like the cross sections of two airfoils placed back to back. In side view, they may resemble a single airfoil cross section (Figure 7).

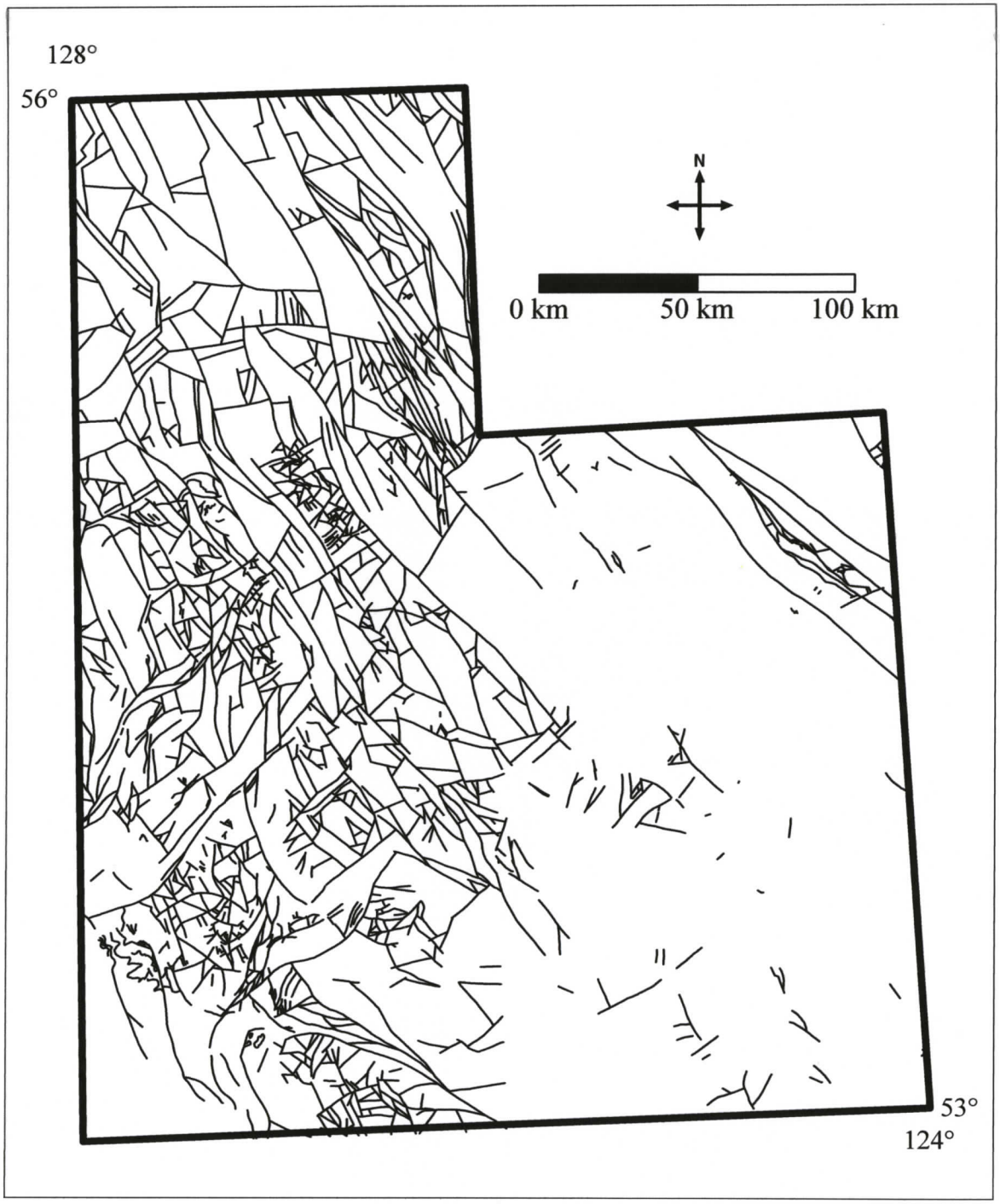

Figure 6. Study area faults, digital data from MacIntyre (1996). Note the lack of fault traces in the eastern part of the study area, due partially to the extensive Quaternary sediment cover.

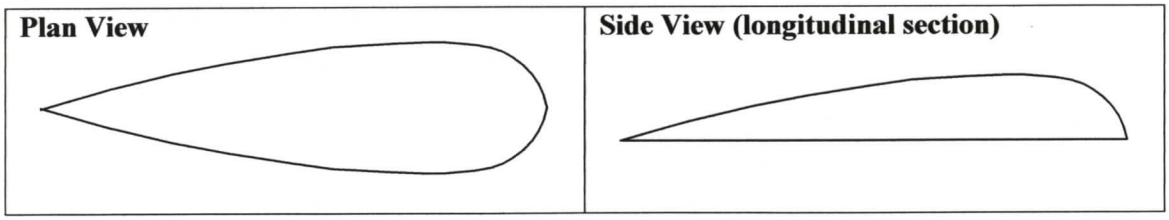

Figure 7. Streamlined shapes

Streamlined forms are a common feature in glaciated terrain; the most well known is the drumlin. Other common streamlined forms are flutes and rat-tails. Streamlined forms usually occur in groups, called fields or swarms. They are rarely found alone. Streamlined forms are composed of unlithified sediment, *in situ* bedrock, or both. Lengths may vary from centimetres to more than 70 km (Clark, 1993). The common characteristic of SF is a streamlined shape.

The term *streamlined*, as applied to landforms and bedrock forms in glaciated terrain, is based on the similarity of form between the glacial features and man-made and naturally occurring minimum-drag surfaces. Komar (1983) demonstrated that streamlined islands in flowing water represent minimum-drag shapes; their shape presents the least resistance to flow. Streamlined forms in glaciated terrain have been described as shapes that "offer the minimum of resistance to the flowing medium..." (Doornkampf and King, 1971). However, this statement is an assumption, since it has not been shown that these glacial terrain forms represent minimum-drag surfaces. Nonetheless, SF in glaciated terrain strongly resemble experimentally and observationally known minimum-drag shapes and, because of this resemblance, they are described as streamlined. In this dissertation, a streamlined form is defined as a

sediment or bedrock form that appears to have been rounded or smoothed by flow, and is elongated along the inferred flow axis (*e.g.*, Figure 8).

Streamlined forms have distinctive shapes. Viewed in longitudinal section, they are usually asymmetric, with a steeper rounded or rough end and another more gently sloping or tapered end. SF are more rarely symmetric in side view. Viewed perpendicular to the long axes (in cross section), SF commonly have convex tops, rounded and smoothed sides, and will sometimes have concave furrows on either side along the form base; they can be symmetric in cross section, or they can be asymmetric with the low areas along each side of the form at different elevations. In plan view, SF are frequently symmetrical across the long axis. They usually have a rounded, semi-circular or parabolic end that usually tapers but may widen towards the other end. Lateral furrows are sometimes observed along the sides of a tapered form; the furrows may widen as the tail tapers or they may narrow as the tail widens. The former is the more common case.

1.2.2. Streamlined forms classification

All groups of ridge and groove landforms in glaciated terrain are referred to as *streamlined moulded forms*, or *flutings* by Flint (1957). Rose (1987) uses the term *streamlined forms* for all streamlined forms (SF) found in terrain identified by other evidence, *e.g.* till occurrence, as being glacially modified. Drumlins, crag-and-tails, fluted surfaces, and streamlined erosional bedrock forms are all included in this broad class. The diagnostic feature of all forms is streamlined shape. Size and composition are

variable. Length categories used for study area SF are: very small (< 5 cm), small (5 cm – 1 m), medium (1 – 10 m), medium large (10-100 m), and large (> 100 m).

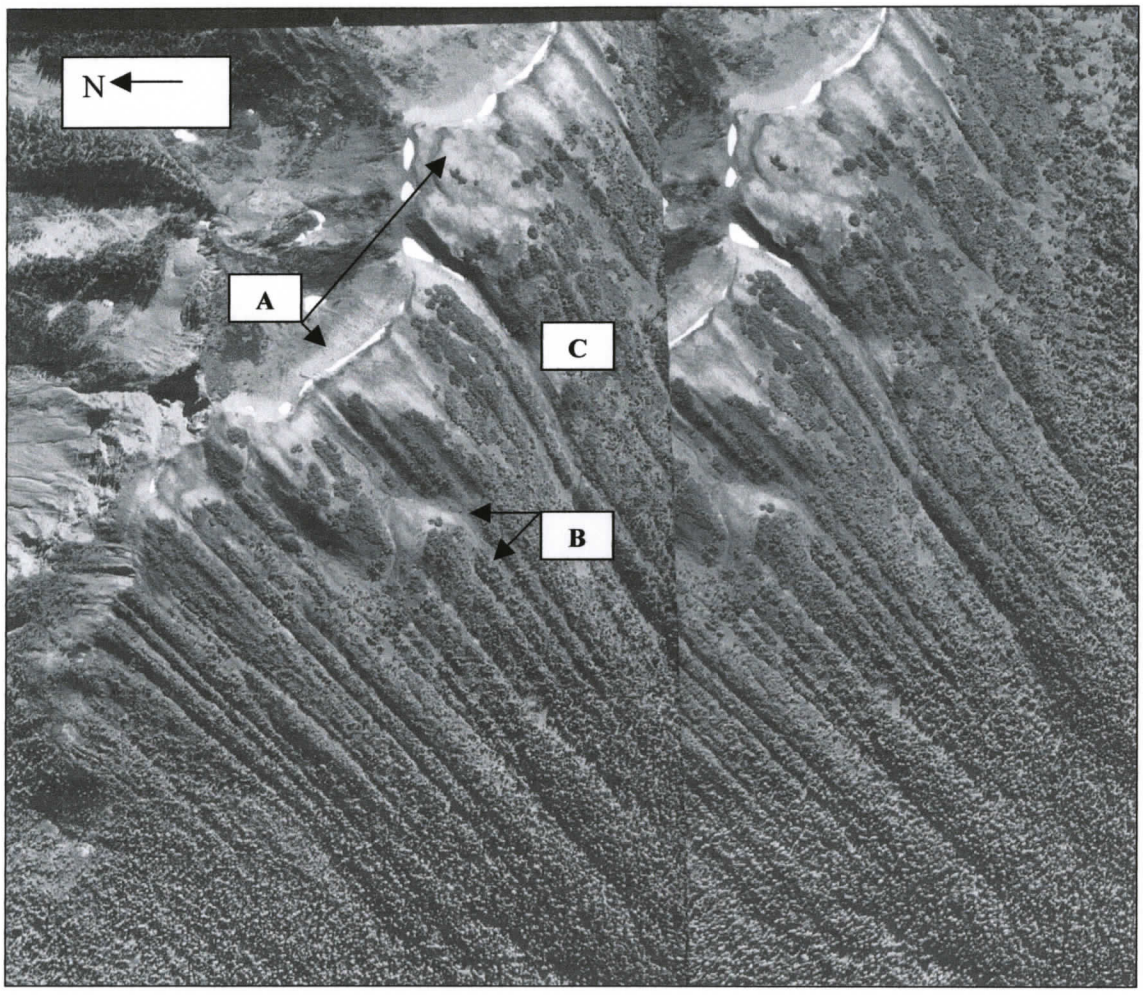

Figure 8. Stereo pair of drumlins (flutings) on Hazelton Mountain. Flow is downhill and towards the bottom right of the photos. Some of the stoss (up flow) ends of the drumlins are truncated by cliff faces (A). Stoss-end crescentic furrows are visible that merge with lateral furrows separating the drumlins, producing U-shaped furrows (B). Note the curvilinear drumlins and furrows towards the top of the photo (C). Province of British Columbia air photo 30BCC 94080 No. 55 and 56.

Streamlined forms often consist of sets of positive relief (ridge-type) and negative relief (groove-type) features. The ridges and grooves generally occur as alternating, interdependent forms, but either form can occur without the other. A U-shaped furrow within a flat till plain is a groove (negative relief) form occurring without an associated ridge form. A drumlin elevated above a flat till plain is a ridge (positive relief) form occurring without a groove form. Figure 9 shows schematic drawings of streamlined forms discussed in the following paragraphs. Of the forms shown in Figure 9, the following are observed during this study: typical drumlins, crag-and-tails, bedrock-cored drumlins, rock drumlins, flutings, drumlins with hairpin erosional marks, and rat-tails. Rat-tails are generally less than one metre in length and are, therefore, small- to very small-scale forms. Drumlins, flutings, and crag-and-tails in the study area range from medium large to large. Thus, streamlined forms discussed here range in length from centimetres to kilometres.

1.2.2.1. Drumlins

Drumlins are part of the group of ridge-type streamlined forms. Boulton (1996) defines them as large-scale drift lineations formed by erosion or deposition. The "typical" drumlin may have a steeper, higher, and broader stoss (proximal or up flow) end and a tapering lee (distal or down flow) tail (Figure 9) (Flint, 1957; Boulton and Hindmarsh, 1987; Shaw, 1996; Kor and Cowell, 1998; Knight, 2002; Jorgensen and Piotrowski, 2003; Rattas and Piotrowski, 2003), or it may have a more symmetric ovoid or less elongated egg shape (Armstrong and Tipper, 1948; Harry and Trenhailie, 1987; Boyce and Eyles, 1991).

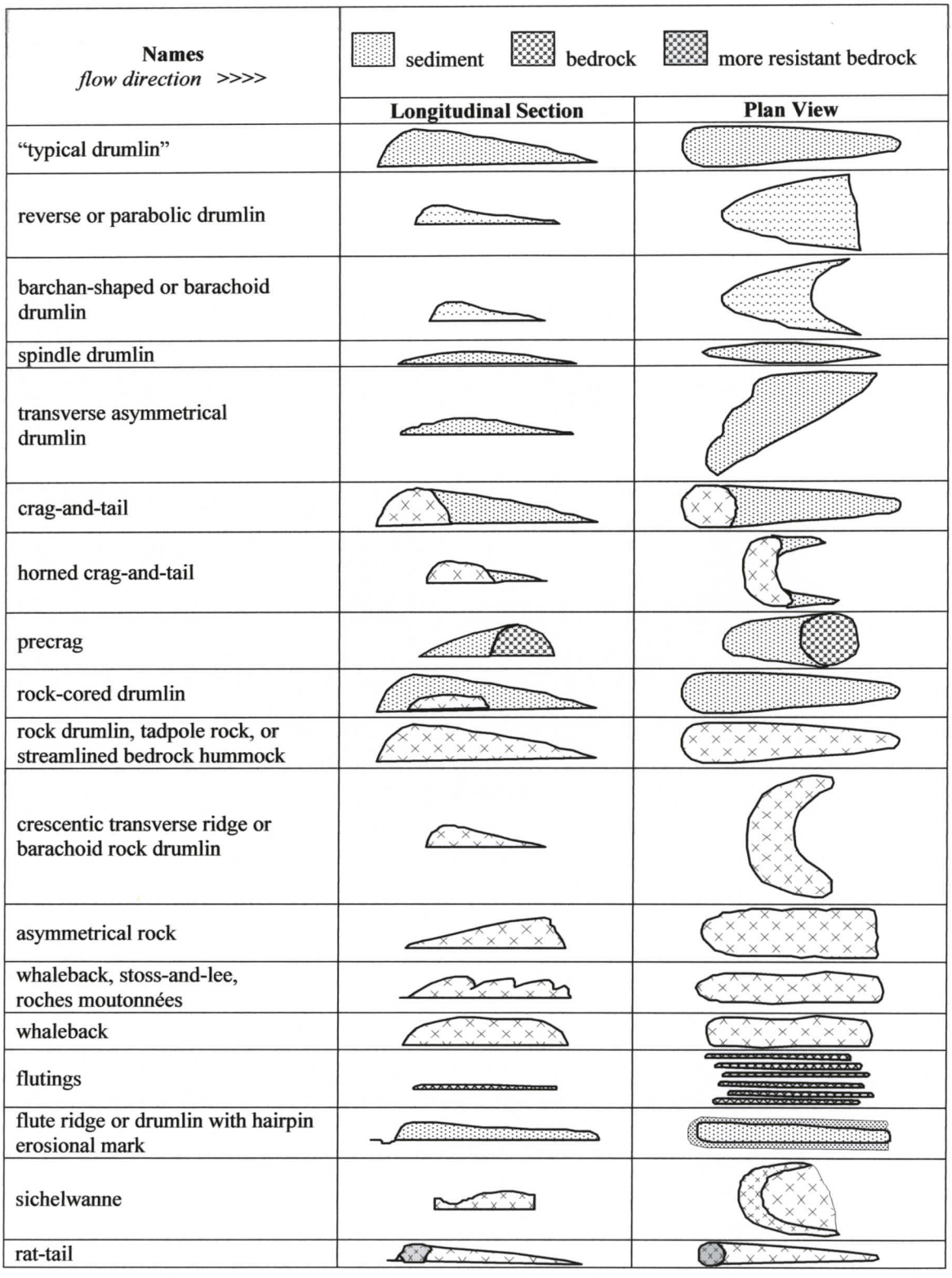

Figure 9. Long sections and plan views of streamlined landforms

Some workers have offered size and elongation ratio limits for defining streamlined ridges as drumlins. Rose (1987) uses size limits of 200 – 1000 m and an elongation ratio (length:width) less than four for defining drumlins. Forms with elongation ratios greater than four are classified as flutes. Clark (1993) states a drumlin is between 100-1000 m long. However, other researchers use drumlin for forms ranging up to and exceeding 6 km in length, and with elongation ratios of as much as 25:1 (Armstrong and Tipper, 1948; Doornkampf and King, 1971; Dionne, 1987; Harry and Trenhaile, 1987; Mills, 1987; Shaw and Sharpe, 1987; Boyce and Eyles, 1991; Clark, 1993; Kor and Cowell, 1998; Knight, 2002; Jorgensen and Piotrowski, 2003; Rattas and Piotrowski, 2003; Stalsberg *et al.*, 2003).

"Atypical" drumlins include *reverse* or *parabolic* drumlins (Figure 9), which, viewed from above, widen toward the lee end (Hanvey, 1987; Harry and Trenhaile, 1987; Sharpe, 1987; Boulton, 1996; Shaw *et al.*, 1996), and *barchan-shaped* or *barachoid* drumlins (Figure 9) which are comprised of crescentic ridges transverse to flow with the curved ends pointing down flow (Boulton and Hindmarsh, 1987; Hanvey, 1987). Although *spindle* can be used to describe a "typical" drumlin shape with a tail tapering down flow, spindle is also used to describe a drumlin with a sharp end pointing up flow or that is pointed on both ends (Shaw, 1996; Shaw *et al.*, 1996; Benn and Evans, 1998), or to describe long drumlins that are symmetric in plan view and longitudinal section (Harry and Trenhailie, 1987; Sharpe, 1987). *Transverse asymmetrical* drumlins (Figure 9) are low, spread out ridges sometimes overprinted by pointed spindle drumlins (Shaw and Kvill, 1984; Harry and Trenhailie, 1987; Shaw, 1996); the ridges are oriented oblique to the flow direction indicated by the spindle

drumlins. The long axes of transverse asymmetrical drumlins extend obliquely down flow either to the right or left of the flow direction (Shaw and Kvill, 1984; Shaw, 1996).

The term *megadrumlin* is used to describe extra large drumlins (Shaw and Kvill, 1984; Shaw, 1996); Rose (1987) assigns them a length range of 1-1.5 km. Small ridges of till in front of retreating glaciers were described as drumlins by Hart (1995) and Hart and Smith (1997). These forms are metres to tens of metres in length and smaller than most ancient drumlins.

Although drumlin may be used to refer to forms composed entirely or partly of bedrock (*in situ* rock), more exact terms are often used. C*rag-and-tail* (Figure 9) refers to a streamlined form with a bedrock stoss end and tapering tail composed of unlithified sediment (Dionne, 1987; Rose, 1987; Shaw and Sharpe, 1987; Hattestrand *et al.*, 1999; Knight, 2002). *Precrags* (Figure 9) are reverse crag-and-tails found in Finland, where streamlined drift ridges are developed on the proximal side of rock knobs (Menzies and Rose, 1987). *Horned crag-and-tails* (Figure 9) are bedrock flow obstructions that lack sediment tails immediately behind the centre of the ridge or peak. Instead, each form has two parallel sediment tails extending down flow of either side of the ridge or peak (Jansson *et al.*, 2003). *Rock-cored* drumlin (Figure 9) refers to a drumlin with a bedrock inner core covered with unlithified sediment (Dionne, 1987).

Bedrock forms that have been shaped by erosion into a typical drumlin shape are called *streamlined bedrock hummocks* (Boulton, 1974), *tadpole rocks* (Dionne, 1987; Sawagaki and Hirakawa, 1997), or *rock drumlins* (Kor *et al.*, 1991; Kor and Cowell, 1998) (Figure 9). Crescent-shaped bedrock forms are called *barachoid rock drumlins* (Knight, 2002) and *crescentic transverse ridges* (Sawagaki and Hirakawa,

1997) (Figure 9). *Roches moutonnées* (Dionne, 1987; Evans, 1996), *stoss-and-lee* (Flint, 1957), and *whaleback* (Dionne, 1987) are used to describe groups of bedrock bumps or hills with smooth inclined faces on the up flow side and rough, steeper, quarried down flow sides (Figure 9). Whaleback, however, is also used to describe symmetrical, in side profile view, rock drumlins (Evans, 1996; Knight, 2002). Bedrock eroded into a reverse drumlin shape is named an *asymmetric rock* (Dionne, 1987) (Figure 9) and is a larger more isolated form than similar roches moutonnées.

1.2.2.2. Flutings

Fields of alternating parallel groove and ridge patterns in bedrock and/or unlithified sediment are also common in glacial terrain (Figure 9). The positive- and negative-relief features together are called *flutings* (Flint, 1957; Shaw, 1996; Beaney and Shaw, 2000; Shaw *et al.*, 2000; Stalsberg *et al.*, 2003) or *fluted terrain* (Munro-Stasiuk and Shaw, 2002) (Figure 9). The parallel, erosional grooves (Dionne, 1987; Munro-Stasiuk and Shaw, 2002) and the ridges between the grooves (Rose, 1987; Smalley and Piotrowski, 1987; Boyce and Eyles, 1991; Clark, 1993; Clark, 1994; Knight, 2002; Stalsberg *et al.*, 2003) are also called flutings or *flutes*. So, different researchers use the same term to describe both positive- and negative-relief forms. The negative-relief troughs in fluted terrain are also called *groovings* (Armstrong and Tipper, 1948), *grooves* (Flint, 1957; Shaw, 1994), *furrows* (Kor *et al.*, 1991; Shaw, 1994), *giant flutes* (for grooves kilometres long) (Shaw *et al.*, 1996) and *grooved bedrock* (Jansson *et al.*, 2003). Shallow longitudinal scours in bedrock with pointed upstream ends and open or closed downstream ends are called *spindle flutes* (Kor *et al.*,

1991). The ridges between the grooves are called flutes (see above), drumlins (Armstrong and Tipper, 1948), "long narrow drumlins" (Munro-Stasiuk and Shaw, 2002), *elongate ridges* (Flint, 1957), *bedrock flutes* (for long, thin, low bedrock SF) (Knight, 2002), and *drumlinoids* (Dionne, 1987).

A fluting ridge is often distinguished from a drumlin as having greater elongation ratios and lower amplitudes than drumlins. Rose (1987) classified flutes as streamlined forms less than 100 m long and with length to width ratios exceeding four, and Clark (1993) concurred with a flute range from 10-100 m. However, other researchers use the term flute to refer to SF up to 15 km long (*e.g.*, Boyce and Eyles, 1991; Knight, 2002; Munro-Stasiuk and Shaw, 2002). *Megaflutes* are given a size range of 100-200 m and 100-1000 m by Rose (1987) and Clark (1993), respectively. Stalsberg *et al.* (2003) use megaflute to refer to forms up to 20 km long and about 7 m high. *Large-scale fluting* is used for erosional grooves and remnant ridges with ridge amplitudes and lengths measured in the tens of metres and kilometres, respectively, some exceeding 30 km (Shaw, 1996; Beaney and Shaw, 2000). Shaw (1996) distinguishes large-scale fluting from *small-scale fluting* found in the forefront of some modern glaciers. The modern fluted terrain in front of glaciers is similar in appearance to ancient fluted terrain. Some modern flutes appear to derive from a constructional process involving a clast with a ridge of smaller-grained material behind and sometimes in front of the clast (Hart, 1995; Shaw, 1996; Hart and Smith, 1997). Clark (1993, 1994) reports flute ridge-type linear features in Canada up to 70 km long that he names *mega-scale glacial lineations*.

1.2.2.3. Other streamlined forms and more general terms

Other terms are encountered in the literature for drumlin-like or fluting-like features. *Streamlined hill* is used by Rose (1987) for hills greater than 1.5 km in length and with length to width ratios less than four. Crescentic furrows that wrap around the stoss end of flute ridges, some drumlins, and some erosional bedrock forms and join seamlessly with drumlin lateral furrows or flute grooves are called *hairpin erosional marks* by Shaw (1994) (Figure 9). The morphology of these landforms is discussed in more detail later in this thesis.

More general terms are used by some researchers. Hattestrand *et al.* (1999) use *glacial lineations* for drumlins and flutes. They also suggest practical size categories based on length: small (500 m to 1.5 km), medium (1.5 to 8 km) and large (over 8 km). Fisher and Taylor (2002) use *lineaments* for aligned hummocks and streamlined forms not resembling classical drumlins. Stokes and Clark (2002) use lineaments and *attenuated bedforms* for linear landforms (that would probably be defined by others as drumlins or flute ridges) from 500 m to 14 km in length with length to width ratios up to 14. *Till lineation* is used by Jansson *et al.* (2003) for drumlins, flutes, crag-and-tails, and horned crag-and-tails.

1.2.2.4. Streamlined erosional marks in bedrock

Erosional marks in glaciated bedrock are called *p-forms* (**p**lastically eroded by ice) by some workers (Dahl, 1965; Boulton, 1974; Gray, 1982; Rea *et al.*, 2000; Evans, 2001), and *s-forms* (**s**culpted) by others (Kor *et al.*, 1991; Shaw, 1996; Pair, 1997; Sawagaki and Hirakawa, 1997). S-forms appears later in the literature than p-forms. It

is preferred by some because it does not assume a known genesis of features, the origin of which is in dispute. Other researchers use s-forms to refer to features known or inferred to have been eroded by water other than glacial meltwater, water sources including: tsunamis (Bryant and Young, 1997; Aalto *et al.*, 1999), surface flood waters flowing through caves (Springer and Wohl, 2002), and strong surface flows (Tinkler, 1993).

Rat-tails, *small-scale crag-and-tails*, and *micro-crag and tails* all refer to a streamlined form comprised of a resistant bedrock clast and a tapering tail of less-resistant bedrock (Figures 9 and 10) (Gray, 1982; Shaw, 1996; Sawagaki and Hirakawa, 1997; Glasser *et al.*, 1998; Stumpf *et al.*, 2000; Jansson *et al.*, 2002; Levson, 2002; Levson and Mate, 2002). These features are smaller than landscape-scale crag-and-tails and are composed entirely of bedrock. Lengths range from centimetres to metres. The tail is inferred to extend down flow of the clast (Gray, 1982; Shaw and Sharpe, 1987; Shaw, 1996; Sawagaki and Hirakawa, 1997; Jansson *et al.*, 2002), the result of a zone of non-erosion developed on the downstream side of the clast during flow. The resistant clast is sometimes lost to plucking or weathering after the rat tail has formed (Gray, 1982). A rat-tail is sometimes outlined by a crescentic scour that wraps around the stoss side of the clast and may extend in a straight groove down one or both sides of the tail (Shaw and Sharpe, 1987; Sawagaki and Hirakawa, 1997). The negative-relief grooves are part of the rat-tail form, and are called hairpin erosional marks by Shaw (1994).

Sichelwannen (singular *sichelwanne*) are sickle-shaped erosional scours in bedrock, with the horns of the sickle pointing downstream in glacial settings (Allen, 1982b; Gray, 1982; Kor *et al.*, 1991; Shaw, 1996; Sawagaki and Hirakawa, 1997).

Reverse orientations, horns pointing upstream, have been reported in tsunami-eroded bedrock (Bryant and Young, 1996). Sichelwannen can occur on level, sloping, near-vertical, or vertical rock faces (Allen, 1982b; Gray, 1982). The form includes both a negative-relief crescentic scour and can also include a positive-relief rock ridge. The rock ridge is often streamlined, having a broad, rounded upstream part and a tapering tail in plan and side view.

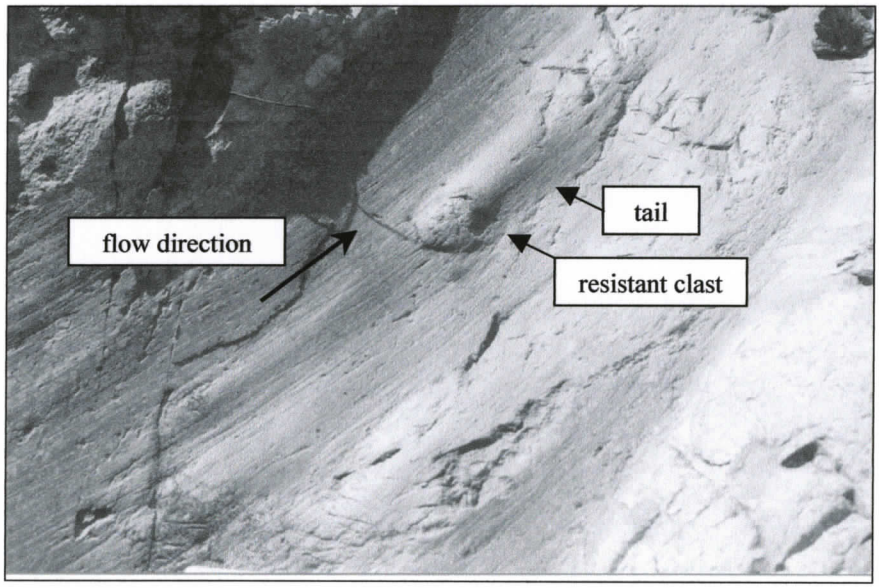

Figure 10. Rat-tail at Dome Mountain Mine, inferred flow direction indicated by arrow. Clast is about 3 cm across.

Comma forms resemble sichelwannen, except that only one arm of the crescentic ridge has developed (Kor *et al.*, 1991; Sawagaki and Hirakawa, 1997). According to Kor *et al.* (1991), *furrows* refer to linear troughs oriented along flow, much longer than wide, that are straight when viewed in their entirety but can be sinuous along their length; they carry other erosional marks and remnant ridges along their beds. *Cavettos* are curvilinear, undercut channels commonly carved into vertical or near-vertical rock surfaces. Sichelwannen, comma forms, cavettos, and furrows can range in length and width from centimetres to tens of metres (Smith, 1948).

Some bedrock erosional features are not streamlined, although they are associated with streamlined forms. *Striae* are scratches or grooves in bedrock generally considered to be eroded by debris trapped in the overriding glacial ice (Flint, 1957; Benn and Evans, 1998). Striae are usually straight, but may follow curved paths around an obstacle. They do not appear streamlined. In contrast, a hairpin erosional mark of the same dimensions as a striation is considered a streamlined feature because it includes a rounded crescentic furrow on the up flow side; its curvilinear shape, when viewed from above, implies streamlining. Muschelbrüche are transverse features shaped like mussel shells that occur with other s-forms (Kor *et al.*, 1991; Shaw, 1996; Benn and Evans, 1998). Transverse troughs, also found with s-form assemblages, are smoothed furrows aligned transverse to flow. Undulating surfaces are low-amplitude undulations, non-directional with respect to flow, that are found on the down flow side of bedrock humps, and potholes are near circular depressions a few centimetres to several metres deep (Benn and Evans, 1998).

1.2.3. Terms used in this dissertation

Since streamlined form classification and naming is not rigorous, it is necessary to state what terms for streamlined forms will be used in this dissertation. Drumlins, bedrock-cored drumlins, crag-and-tails, rock drumlins, flutings, streamlined hills, hairpin erosional marks with medial ridges, rat-tails, and roches moutonnées are referred to here as streamlined forms (SF).

Drumlin is used here to describe streamlined landforms similar in size and shape to typical drumlins; their lengths here are usually between 100 m and 1000 m. Their composition is primarily sediment. Fluting is used to describe a parallel assemblage of alternating streamlined ridges and grooves (Figure 9).

Streamlined bedrock forms (SBF) refer to SF composed of bedrock. SBF include rock drumlins, defined here as a bedrock form with "typical" drumlin shape; rat-tails; and roches moutonnées, used for bedrock bumps or hills with smooth sloping surfaces facing up flow and with rough, quarried lee sides (Figure 9).

Rock-cored drumlin and crag-and-tail are used as described above. Streamlined landforms greater than 2 km in length, with length to width ratios less than four, and with substantial bedrock composition are defined as streamlined hills.

1.3. ORIGIN OF DRUMLINS AND STREAMLINED BEDROCK FORMS

A number of explanations for drumlin origins have been proposed over the past century. Two previously suggested drumlin forming mechanisms are differential sediment dilatancy beneath high shear stress ice (Smalley, 1966; Smalley and Unwin, 1968) and kinematic deposition by helical flow cells in ice (Shaw and Freshauf, 1973).

Most current hypotheses invoke constructional and/or erosional drumlin formation by ice, subglacial meltwater, or combinations of both mediums.

1.3.1. Drumlins formed by glacial ice

One widely accepted drumlin origin theory proposes that drumlins are a consequence of preferential subglacial sediment deformation by ice (Boulton 1987, 1996). This theory requires a heterogeneous glacial substrate with adjacent stronger and weaker areas. The stronger sediments are coarser grained and more permeable than the weaker sediments. Examples of stronger sediments would be coarse-grained outwash or sandy till. As meltwater infiltrates the subsurface, zones of saturated finer-grained sediments become weaker than zones of well-drained coarser-grained sediments. As the mobile till layer and ice sheet move across this heterogeneous surface, the stronger zones become drumlin cores, and the weaker zones are eroded and/or remoulded around and behind the stronger cores to form streamlined landforms (Figure 11). In this model, both deposition and erosion contribute to drumlin formation. The model can also account for crag-and-tails and rock-cored drumlins, with bedrock serving as the drumlin core instead of strong till.

The preferential sediment deformation model is supported by a drumlin field study in Estonia (Rattas and Piotrowski, 2003). Differences in drumlin density, size, and attenuation were correlated with differences in permeability of both drumlin substrate and composition. A group of larger drumlins, mean aspect ratio of 3.0 and mean area of 5.65 km^2, was compared to a group of smaller drumlins, mean aspect ratio of 7.0 and mean area of 0.3 km^2. The larger drumlins are found where the bedrock

beneath the drumlins was more permeable. The smaller drumlins are found where the bedrock is more impermeable. All the drumlins are composed of diamicton, but finer-grained diamicton was found in the smaller drumlins.

The interpretations of drumlin distribution and composition in some drumlin fields do not entirely support the application of the sediment deformation model. Mills (1980, 1987) found little or no influence of bedrock lithology, till texture, drift thickness, regional slope, and relief on drumlin mean width, height, length, and aspect ratio (length to width ratio) among 1347 drumlins in 17 fields in the north-central and northeastern United States. The sediment deformation model described above postulates a correlation between sediment texture and drumlin location. It could be inferred that sediment texture would also influence drumlin shape. Little or no correlation between texture and drumlin shape, as reported by Mills (1980, 1987), does not conform well with the sediment deformation model.

Aario (1987) concluded that drumlin locations are primarily related to wave-like flow in glacial ice. Thus, drumlin location is not a function of differences in surficial material, but a function of ice sheet flow perturbations. This result is also contrary to the basic premise of the above-described sediment deformation model; that is, drumlin locations are related to variation within the forming mechanism, not to substrate differences.

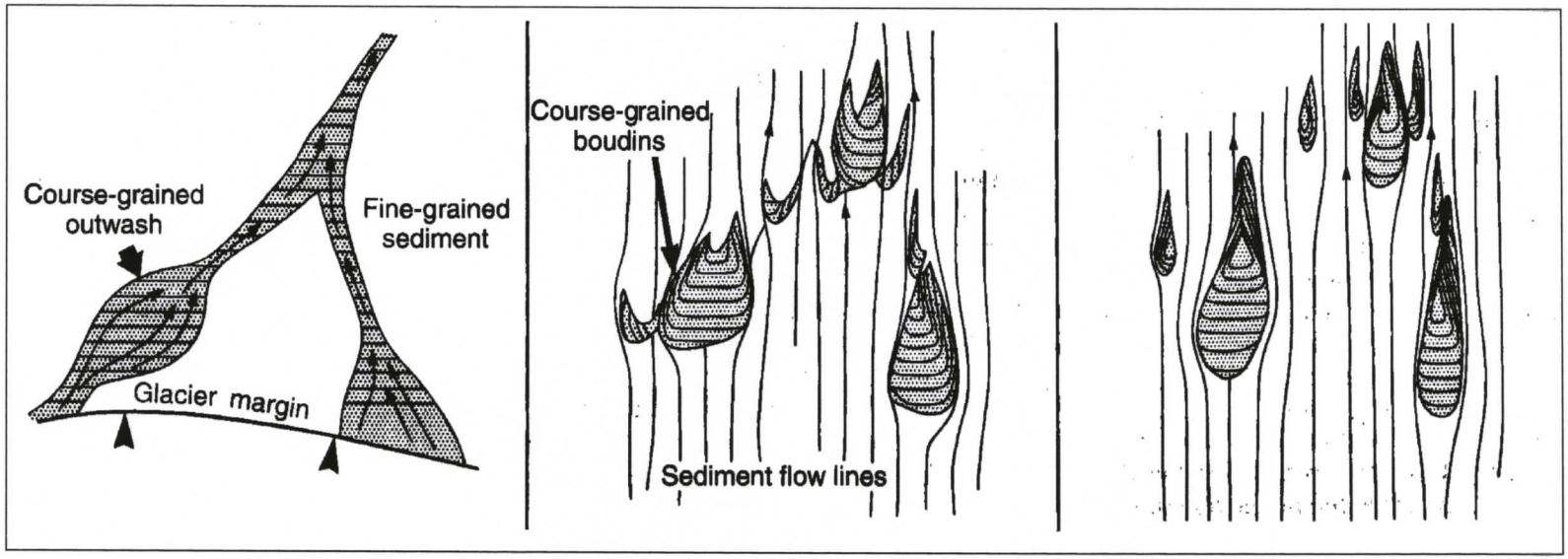

Figure 11. Drumlin formation by subglacial sediment deformation, from Boulton (1987). Reproduced from 'A theory of drumlin formation by subglacial sediment deformation by G.S. Boulton from Drumlin Symposium, eds. J. Menzies and J. Rose, www.tandf.no/boreas, 1987, pp. 25-80, by permission of Taylor & Francis AS.

Drumlin density in England and New York state was statistically analyzed by Doornkampf and King (1971). They used chi-square tests that compared local drumlin density to expected, average density for a given drumlin field. One drumlin field in England and an extensive drumlin field in central New York showed random drumlin distribution; there were no significant differences in expected drumlin density versus observed density. Drumlin distribution in the other drumlin field in England was not random. The two areas of random drumlin density were of subdued relief compared to the more rugged terrain showing non-random (clustered) drumlin density. The implication is that the relative roughness of the terrain determined whether the drumlins were distributed regularly or were clustered. More rugged relief resulted in clustered drumlins.

Francek (1991) interpreted the random distribution of New York drumlins as supporting the till deformation model. He assumed that coarse clasts and subglacial aquifers would be randomly distributed, would contribute to rapid drainage from the surface and subsequent sediment strengthening, and result in a random distribution of drumlins. Jauhiainen (1975) found clustered to random drumlin distribution in northern central Europe by nearest neighbour analysis, but did not suggest reasons for the distribution.

Other researchers propose drumlin formation by sediment deformation, but either specify that the distribution is unrelated to substrate lithology (Aario, 1987; Menzies, 1987; Rose, 1987; Smalley and Piotrowski, 1987; Boyce and Eyles, 1991) or make no substrate requirement. Differences in drumlin form at different locations in drumlin fields have been attributed to wave-like glacial flow (Aario, 1987), variable

thickness of ice (Rose, 1987), and variable ice velocity (Rose, 1987; Clark, 1993; Clark, 1994; Stokes and Clark, 2002; Rattas and Piotrowski, 2003). Menzies (1987) proposed that the influence of ice, substrate, and climatic factors combine and reach a triggering threshold where ice shear stress exceeds bed strength, at which point drumlins are initiated. Most of the sediment deformation models utilize constructional processes for drumlin formation.

Erosional formation by ice or streaming till is deduced for drumlins in the Peterborough, Ontario drumlin field (Boyce and Eyles, 1991) and for Boston Harbour drumlins (Newman and Mickelson, 1994); strata within drumlins are truncated at the drumlin surface. Hattestrand *et al.* (1999) found no signs of deformation of older drumlins or flutings in Sweden that were cross-cut at almost right angles by a later drumlin-forming event. They suggested that the later, cross-cutting event was "dominated by erosional processes rather than deformation or deposition..." (Hattestrand *et. al.*, 1999, p. 151).

An example of an unusual streamlined glacial form, the horned crag-and-tail, is found within the Ungava Bay landform swarm. Jansson and Kleman (1999) suggest that these landforms are best explained as resulting from bedrock crags that penetrate into the cold based layers of the ice sheet. Deposition does not take place behind the centre of the crag because of the cold based conditions effective at the upper elevations of the crag; whereas, sediment "horns", that extend down flow from each side of the crag, are deposited by lower elevation, warm based layers of the ice sheet.

1.3.2. Drumlins formed by moderate subglacial meltwater flows with or without the contribution of ice

Sequences of sorted sediments on the lee-side of some Irish drumlins were interpreted as evidence of meltwater deposition during drumlin formation, although ice deformation and erosion were thought to also contribute to the drumlin form (Dardis and McCabe, 1987; Hanvey, 1987). Knight (2002) suggested that horizontal strata found in drumlins were deposited and subsequently truncated by several meltwater flow events that emanated from glacial lakes. Mate (2000) suggests meltwater enhancement of ridges that were initially formed by glacier flow.

1.3.3. Drumlins formed by catastrophic subglacial meltwater floods

The subglacial meltwater flood theory makes provision for the formation of three types of drumlins (Shaw, 1996, 2002): drumlins formed by infilling of streamlined glacial cavities in the glacier sole; erosional drumlins left as remnant forms beneath streamlined cavities in the glacier sole; and erosional drumlins initiated as remnant ridges between hairpin furrows. This theory is applied to most, if not all, types of drumlins, transverse bedforms, and streamlined bedrock forms (see later in this chapter).

Cavity infill drumlins are proposed to have been formed by deposition of sorted sediments in inverted erosional marks in the glacier sole (Figure 12) (Shaw, 1983; Shaw and Kvill, 1984). The theory is supported by the stratigraphy and morphology of drumlins at Livingstone Lake in Saskatchewan: sorted sediments in the drumlins reflect water deposition, sediment strata conforms to the drumlin shape, and the drumlin shape

is streamlined. Irish drumlins with sorted, shape-conforming sedimentary sequences support the cavity infill model (Dardis, 1987; Dardis and McCabe, 1987; Hanvey, 1987). The shape of northern Saskatchewan drumlins is interpreted otherwise by Boulton (1987) as being fold traces caused by subglacial sediment deformation.

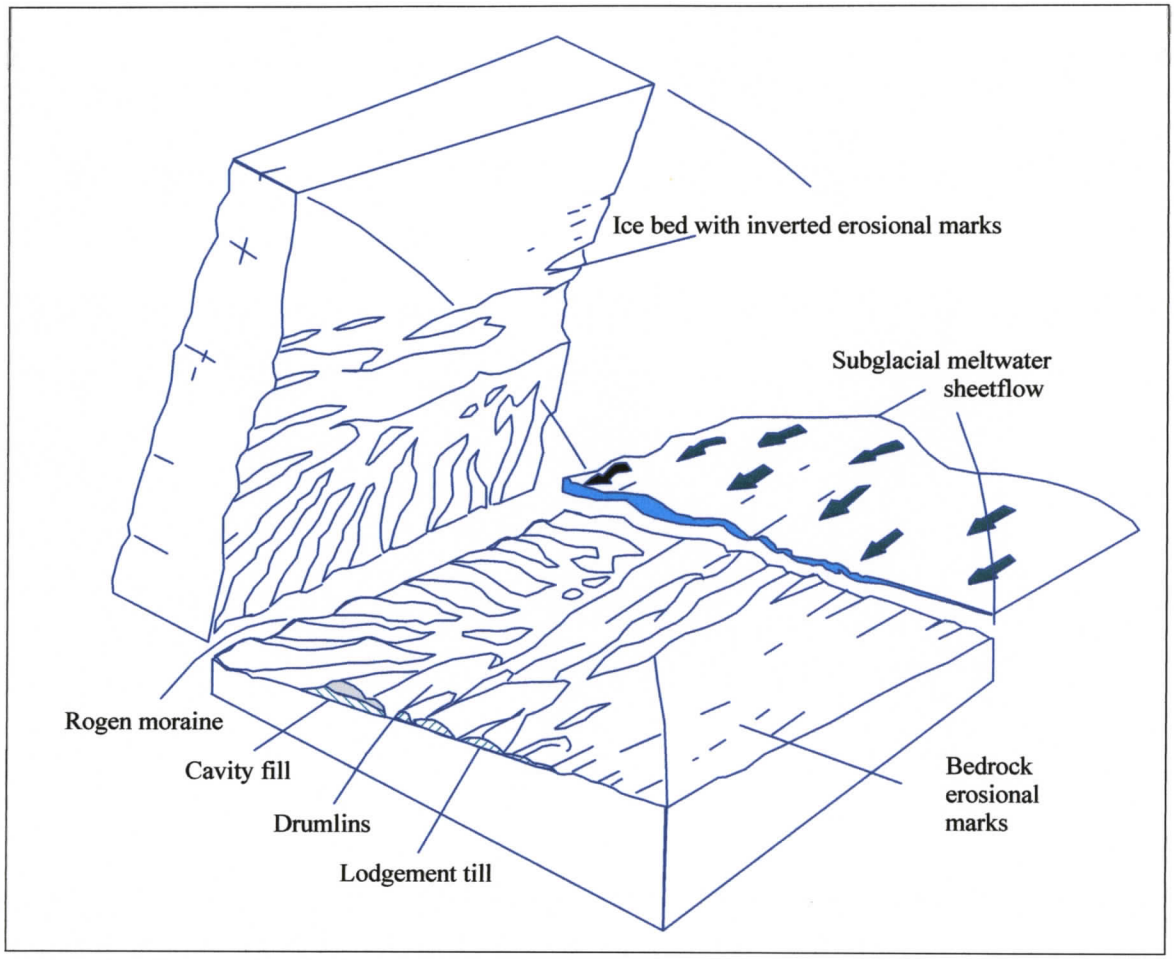

Figure 12. Drumlins formed by infilling of subglacial cavities, re-drawn after Fisher and Shaw (1992).

Some drumlins with the same shape as the Livingstone Lake drumlins have truncated bedding planes and are clearly erosional forms. In explanation of these forms,

Shaw (1996) proposed that streamlined inverted erosional marks, like those in which cavity infill drumlins form, cause lateral differences in erosional power during flooding. For example, less erosion would take place under an inverted flute mark than under an adjacent area where the ice sheet is closer to the substrate. The differences in erosional power would have resulted in an eroded landscape that would fit into the inverted, overhead erosional marks in the ice.

The third type of streamlined landform explained by the meltwater theory is another form of erosional drumlin (Shaw and Sharpe, 1987; Shaw, 1994; Shaw *et al.*, 2000; Munro-Stasiuk and Shaw, 2002). These drumlins are believed to be part of a continuum of streamlined forms ranging from rat-tails a few centimetres long to drumlins and flute ridges many kilometres long. The theory proposes that these forms began as hairpin furrows created by horseshoe vortices (Figure 13). Continued meltwater erosion further defined the remnant ridges. If the meltwater flood persisted long enough, it erased traces of the hairpin furrows and streamlined the remnant ridges.

Support for the meltwater flood theory is partly derived by similarity of glacial forms with those known to have been formed by water. Experimentally produced erosional marks resemble some inverted cavity infill drumlins (Allen, 1982), as do flutes at the base of turbidites, (Shaw, 2002) and other fluvial erosional marks (Allen, 1982; Richardson, 1968; Dreimanis, 1993; Tinkler, 1993). Some drumlins resemble streamlined islands in rivers and streamlined erosional hills in the Washington Scablands (Baker, 1973; Komar, 1983; Baker *et al.*, 1987); the streamlined islands and hills were both streamlined by water erosion.

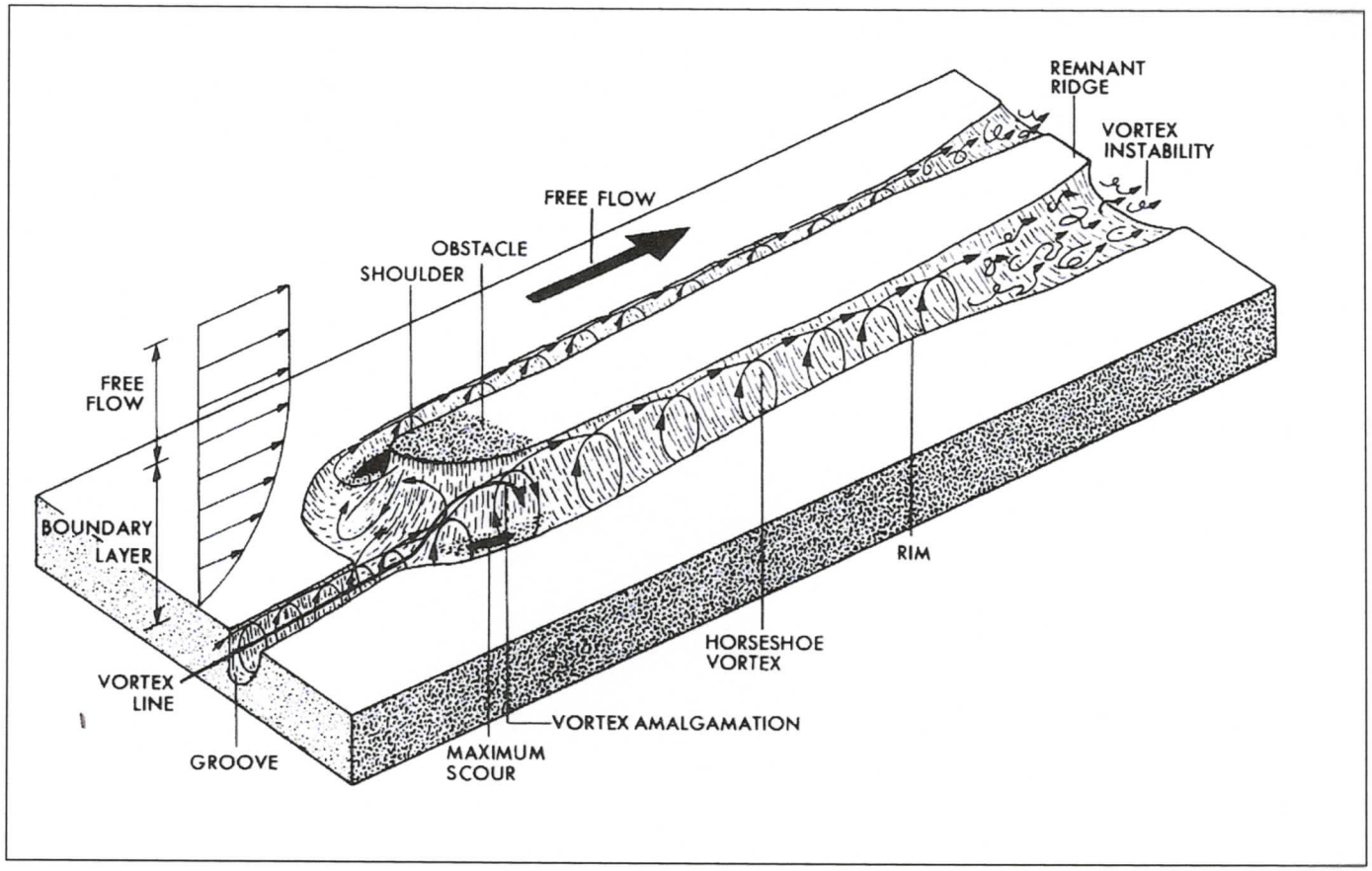

Figure 13. Erosion of hairpin scour by horseshoe vortex. Longitudinal vortex from an upstream hairpin furrow merges into the next horseshoe vortex such that hairpin scours do not cross-cut one another. Reprinted from Sedimentary Geology, v 91, J. Shaw, Hairpin erosional marks, horseshoe vortices and subglacial erosion, pp 269-283, 1994, with permission from Elsevier.

Drumlin shapes are also interpreted as evidence against the meltwater flood theory. Numerical analysis of drumlin dimensions by Komar (1984) indicated that only 34 of the 76 drumlins he investigated had streamlined shapes indicative of optimal streamlining, 34 had elliptical shapes, and 8 had reverse streamlined shapes. He concluded that the drumlins were not formed by water, but by ice. (Komar, 1984; Komar, personal communication).

Although many researchers have documented evidence of large floods in ancient glacial terrains (Baker, 1973; Baker *et al.*, 1987; Bryan *et al.*, 1987; Sugden *et al.*, 1991; Rains *et al.*, 1993; Kor and Cowell, 1998; Shaw *et al.*, 1999; Beaney and Shaw, 2000; Rampton, 2000; Shaw, 2001; Beaney, 2002; Fisher and Taylor, 2002; Munro-Stasiuk and Shaw, 2002; Lowe and Anderson, 2003), suggested sources for the flood(s) have not been proven. This remains a large problem for the meltwater flood origin theory. Some workers have proposed large subglacial lakes as water sources (Shoemaker, 1991, 1992, 1995; Munro-Stasiuk and Sjogren, 2002). Dowdeswell and Siegert (1999) estimated the total volume of about 70 Antarctica subglacial lakes to be between 4000 and 12,000 km^3. They stated: "Our estimates ... do not necessarily conflict with the possible significance of large meltwater floods during the deglaciation of former midlatitude ice sheets... (Dowdeswell and Siegert, 1999, page 254)." A second important problem of the meltwater model is the lack of sedimentary evidence for the debris that would result from the erosional event.

1.3.4. Streamlined bedrock form origins

Two different mechanisms are commonly proposed in the literature to explain the formation of streamlined bedrock forms (SBF): debris-rich glacial ice (Boulton, 1974) and subglacial meltwater (Kor *et al.*, 1991). Striae are considered in both the glacial abrasion and meltwater models to be formed by ice.

The glacial abrasion model explains formation of both SBF and striae. It is assumed in the glacial abrasion model that striae are a middle member between polished rock and giant glacial grooves (Smith, 1948; Flint, 1957); striae are interpreted as small grooves or scratches. Streamlined bedrock forms are sometimes overprinted by striae that are parallel, subparallel, or that cross-cut the SBF at high angles (Armstrong and Tipper, 1948; Smith, 1948). The meltwater model explains striated SBF as resulting from re-grounding of the ice sheet and minor glacial abrasion after meltwater erosion produced the SBF (Shaw, 1994).

In the glacial abrasion model, debris-laden ice at the glacier sole is diverted around bedrock obstacles (Boulton, 1974, 1979). The consequence of this diversion is concentration of debris along the sides of the obstacle, causing the erosion of a lateral furrow. The furrow deepens until bridging of the ice across the furrow removes pressure from the bed. The debris concentration of the ice over-riding the obstruction is less than that of the diverted ice. As the diverted ice proceeds past the obstacle, the ice bridges across the furrows, pressure causing abrasion lessens, and the furrow shallows, widens, and finally terminates.

The glacial abrasion theory is supported by observations beneath modern glaciers, observations of glaciated bedrock, and theoretical modeling. It has been

proven experimentally that modern glaciers produce striae (Boulton and Vivian, 1973). Boulton (1974) observed concentration of debris around bedrock obstacles within a modern glacier sole, and also observed subglacial sichelwannen and cavettos, which he attributed to formation by glacial abrasion. The glacial abrasion model requires that ice deform plastically, a property that has been observed (Boulton, 1979; Theakstone, 1979; Rea and Whalley, 1994; Rea *et al.*, 2000). In some cases, ice that simultaneously flowed more than one direction at different levels in the glacier was observed, an ice property inferred by Sharp *et al.* (1989) based on striae patterns in deglaciated terrain. Curving striae and structurally-controlled striae trending oblique to regional ice flow have also been observed in deglaciated terrains (Gray, 1982; Sharp *et al.*, 1989; Rea *et al.*, 2000).

Streamlined bedrock forms have been described that support the glacial abrasion model based on their association with striae. Rock drumlins in eastern Canada are covered with striae, chattermarks, grooves, and polished surfaces (Dionne, 1987). Glasser and Nicholson (1998) reported grooves, aligned with flow, that were eroded into heavily striated bedrock, the grooves also being striated. Both the grooves and the striae were inferred to be ice-formed features. Rea *et al.* (2000) concluded that fluted precipitate ("precipitate" presumably refers to mineral deposits from glacial meltwater) in the foreland of a receding glacier represented glacial abrasion, since the location of the fluting was not conducive to formation by meltwater. They also examined a large comma form on the flank of a rock drumlin. The comma form was striated to the same degree as the surrounding bedrock, the striae were slightly deflected by the form shape, and widened toward the lee end of the comma form. They concluded that the comma

form was eroded by glacial abrasion, its location initiated by a joint in the bedrock surface.

Boulton (1974, 1979) theoretically modeled bedrock erosion by glacial abrasion. He was able to numerically produce both stoss-and-lee (roches moutonnées) and typical rock drumlin asymmetry with his model by varying the amount of ice overburden pressure. Low pressure produced the stoss-and-lee form, and high pressure the rock drumlin. Evans (1996) also proposed a glacial abrasion model to account for patterns of whaleback (symmetric rock drumlin) and stoss-and-lee form occurrence in British Columbia. He suggested that whalebacks formed under high velocity, low viscosity ice streams, where bed separation on the lee of the forms was suppressed.

The most extreme meltwater model hypothesizes erosional formation of SBF by catastrophic outburst floods tens of metres deep and hundreds of kilometres wide (Kor *et al.*, 1991; Shaw, 1996). The same model is used to explain drumlin formation (see preceding section). In the model, SBF are formed subglacially over a period of days or weeks by high volume sheet floods beneath the ice (Shoemaker, 1991; Shoemaker, 1995; Rampton, 2000). The model requires that the ice sheet was lifted by the flow, and re-grounded as flow waned. Preservation of SBF after re-attachment implies that subsequent ice erosion was minimal. Spindle flutes, sichelwannen, comma forms, potholes, and rat-tails are interpreted as products of erosion by vortices in turbulent flow. Variations on the catastrophic model suggest more modest and/or localized meltwater flows, acting closely, in space or time, with abrading ice (Gray, 1982; Pair, 1997; Glasser and Nicholson, 1998). At the least, meltwater is considered by most researchers to have been responsible for subglacial pothole formation (Boulton, 1979).

The meltwater model is supported by form similarity of SBF with erosional marks clearly formed by water, interconnected SBF assemblages, co-occurrence of similarly shaped forms of widely different sizes, SBF morphology, and striae relationships. These are discussed below.

Crescentic scours around the proximal ends of rat-tails and rock drumlins are similar to forms produced experimentally by water flows or produced by water and wind in nature (Allen, 1970; Richardson, 1968; Karcz, 1981; Komar, 1983; Dargahi, 1990; Dreimanis, 1993; Tinkler, 1993; Shaw, 1994; Bryant and Young, 1996; Allen, 1982b; Herget, 2005). When water- or wind-produced crescentic scours extend around obstacles to flow, remnant ridges resemble some rock drumlins and rat tails (Figure 14). Bryant and Young (1996) also noted the resemblance of tsunami-formed flute ridges to rock drumlins and rat-tails.

Interconnecting erosional troughs are integral to some SBF assemblages. The lateral furrows of hairpin-shaped erosional marks merge into other hairpin furrows located down flow. Entire smaller sets of interconnected hairpin furrows can be located within a single larger trough, the larger trough itself being part of an interconnected series of larger hairpin furrows. These assemblages are known to extend across areas hundreds of metres to kilometres broad and are considered suggestive of contemporaneous formation by water erosion (Kor *et al.*, 1991; Shaw, 1994, 1996; Kor and Cowell, 1998). Sichelwannen or hairpin furrows of the same size in some SBF fields do not cross-cut; rather, the lateral furrows that define a rock drumlin merge down flow with the proximal, crescentic furrows that wrap around subsequent, down flow rock drumlins. Flow is also capable of eroding a wide size range of SBF, small

centimetre- or metre-scale forms nested within and upon forms one or more orders of magnitude larger, reflecting a flow process or processes that acted independent of scale.

Streamlined bedrock form morphology, particularly sharp edges of eroded scours, is considered to be indicative of water formation (Allen, 1982b; Kor *et al.*, 1991; Tinkler, 1993; Bryant and Young, 1996; Pair, 1997; Sawagaki and Hirakawa, 1997). Water is known to produce SBF-like forms, but it is not known if ice has the same capability. Furthermore, it is thought that ice is incapable of advancing over a rock lip without rounding or breaking the sharp edge characteristic of some SBF furrows.

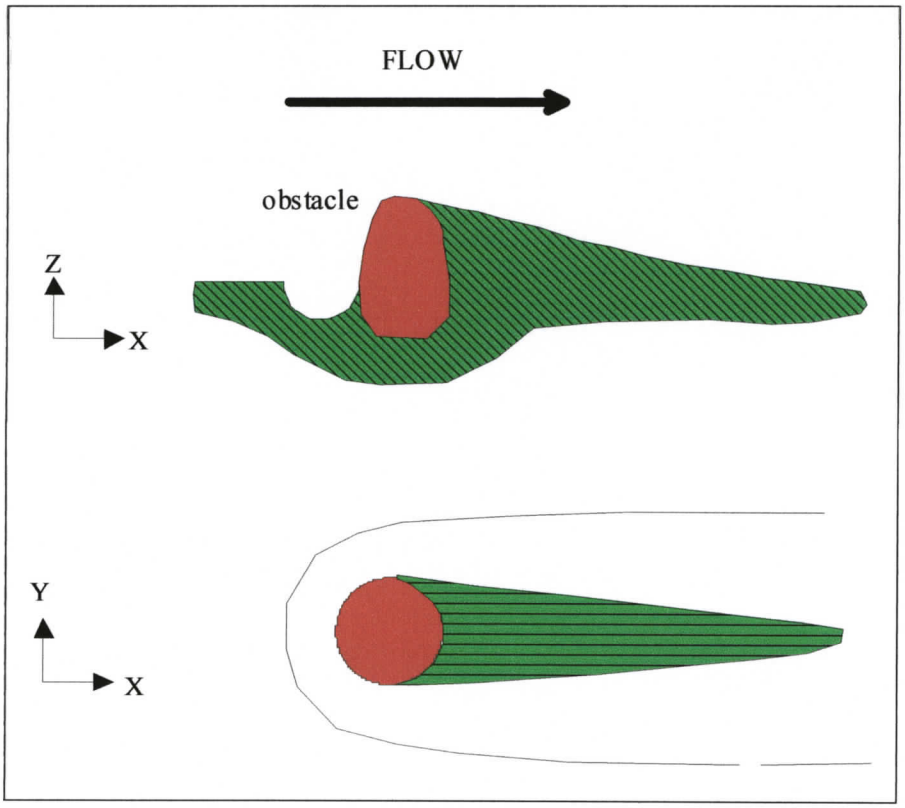

Figure 14. Remnant ridge left by water or wind flowing around an obstacle. Area immediately down flow of the obstacle is a zone of low shear stress (Allen, 1982).

Arguments for meltwater formation of SBF based on striae relationships present examples of negative-relief SBF (depressions) that are lightly striated or unstriated, but are eroded into or near expanses of heavily striated bedrock (Gray, 1982; Glasser and Nicholson, 1998; Kor *et al.* 1991, Shaw; 1994,). In these examples, meltwater erosion is thought to follow and erase signs of initial glacial abrasion, and in some cases to be followed by renewed, but minor, glacial abrasion. Pair (1997) interpreted rat-tails as initially shaped by water, but subsequently planed and striated by ice flowing parallel to the earlier water flow.

2. STREAMLINED FORMS MAPPING

2.1. INTRODUCTION

The principle objective of this chapter is to map streamlined forms (SF) in the study area. Following this introduction, there is a review of previous work relevant to this chapter, including SF and drumlin mapping in the study area and previous glacial flow studies relevant to the study area. Results of SF mapping are then presented. Patterns of SF occurrence are discussed.

After the literature review, methods used to produce the SF maps are detailed. The SF map is presented, and a subsection is devoted to comparison of this map with other study area SF maps. The latter sections of this chapter discuss patterns of SF occurrence observable from the SF map.

2.2. PREVIOUS WORK

Streamlined forms locations in parts of the study area have been mapped by several researchers. Clague (1984) mapped drumlins and crag-and-tails in the lowland valleys from Smithers to Prince Rupert, including parts of NTS 93L and NTS 93M. Tipper (1994) mapped streamlined forms in NTS 93L. Locations of several thousand drumlins, flutes, and crag-and-tails are shown on Quaternary geology maps of NTS 93F (Plouffe *et al.*, 2004) and NTS 93K (Plouffe, 2000). Streamlined landforms verified in the field are included on surficial geology and ice flow maps for parts of the Nechako plateau and in the Hazelton mountains (Stumpf *et al.*, 2000; Ferbey and Levson, 2001;

Levson, 2002; Levson and Mate, 2002). References to surficial geology, terrain, and bedrock geology maps are given in Chapter 1.

The Cordilleran Ice Sheet, at the last glacial maximum, is believed to have covered most of British Columbia (Clague, 1989); there are several explanations as to the configuration of this ice sheet at its maximum. Outward flow from a central dome located over the Interior Plateau is suggested by some (Kerr, 1934; Davis and Mathews, 1944; Fulton, 1991). Tipper (1971b) and Clague (1989) propose that glacial maximum in the Cordillera consisted of a series of separated smaller domes and ice caps. A shifting ice divide located in central British Columbia, with an axis oriented generally north-south, has been recently proposed (Stumpf *et al.*, 2000; Ferbey and Levson, 2001; Levson, 2002). General expected flow directions are: 1) valley controlled and downhill from the Coast Mountains and Skeena Mountains during advance, 2) radial outward flow from ice sheet highs during glacial maximum, and 3) return to topographically-controlled flow during retreat.

Regional ice flow studies that include parts of the study area indicate that the dominant observed flows converge towards the central part of the Nechako plateau (Tipper, 1971a, 1971b; Ryder and Maynard, 1991; Levson and Giles, 1997; Levson *et al.*, 1997; Plouffe, 2000; Stumpf *et al.*, 2000). Flow is thought to have been to the east from the Coast mountains out onto the Nechako plateau and to the southeast from the Skeena mountains down the Nass, Bulkley, Babine River, and Takla valleys Major exceptions to these flow directions are outlet westward-flows towards the Pacific Ocean (Clague, 1984; Ryder and Maynard, 1991), variable flow due to a second advance in the southeast part of 93F (Tipper, 1971b), and the development of a shifting ice divide

during glacial maximum driving east and west flow (Fulton, 1991; Levson *et al.*, 1997; Stumpf *et al.*, 2000; Ferbey and Levson, 2001; Levson and Mate, 2002). Local flow directions can deviate greatly from the general orientations stated above, and the sequence of flow events can change from one site to another (Stumpf *et al.*, 2000; Levson, 2002).

Flow from the Skeena Mountains during advance phase was topographically constrained by the sides of southeast trending valleys (Ryder and Maynard, 1991; Stumpf *et al.*, 2000). Advance phase eastward flow from the Coast Mountains was interpreted as being partially influenced by topography (Tipper, 1971b; Levson and Giles, 1997); uphill flow is common across the Nechako Plateau, but flow also follows valleys (Stumpf *et al.,* 2000). Flow that produced west-trending SF, interpreted as glacial maximum features, acted, for the most part, independently of topography. Lack of topographic control is deduced primarily by glacial flow direction indicators that point uphill and cross elevated ridges (Clague, 1984; Levson *et al.*, 1997; Stumpf *et al.*, 2000).

2.3. METHODS

Maps presented in this section were produced by digitizing streamlined form long axes on digital elevation model (DEM) shaded relief images, SPOT satellite images with 10 m resolution, and Landsat satellite images, with 15 m resolution. Each streamlined form is represented as a line segment consisting of two points.

Satellite images are georeferenced bitmap files comprised of many adjoining squares of identical size. The satellite image resolution refers to the length of each

square. For example, the squares that make up Landsat images used in this study are 15 m by 15 m. Each square can have only one colour or shade.

The DEM grid files, with 25 m horizontal spacing, are derived from the British Columbia TRIM I mapping project. All digitized features and maps in the dissertation use the Universal Transverse Mercator (UTM) projection with 1983 North American Datum (NAD 83).

Golden Software's Surfer version 7.04 is used for DEM grid operations and final map production, and Golden Software's Didger version 3.02 for projection conversion, calibration, and digitizing. Surfer allows the "sun" (illumination) position to be varied horizontally and vertically to create different shaded relief views of the same map area. Sun positions were varied in different parts of the study area to yield the clearest depiction of SF. In general, a low sun angle at about right angles to SF long axes is best for mapping SF. This configuration casts a "shadow" along SF ridges. Hairpin furrows, used for flow direction determination (discussed later in this chapter), are more easily observed by using a light source oriented parallel to flow. Surfer does not allow different "look directions", *i.e.* oblique views, for shaded relief images; all images are viewed from directly overhead.

The minimum, mappable SF length using these methods is about 100 m, though a few shorter forms are mapped. The average mapped SF length is 525 m. Streamlined forms that are not recognizable using these methods are not mapped, with two exceptions. First, SF near the top of Hazelton Peak are mapped using air photos combined with satellite imagery. These drumlins are included because they were observed in a field visit and appear to be related to the large drumlin swarm located

south of Hazelton Peak at lower elevations. Secondly, flutings in NTS 93L at some high elevation locations are mapped using high resolution orthophoto imagery in an attempt to define flow direction in those areas. Air photos were also used to confirm flow directions in some areas.

Landforms are mapped as streamlined forms if they have one or more of the following characteristics: elongated ridges with one rounded, semi-circular or parabolic end that tapers or maintains a constant width towards the opposite end; elongate ridges enclosed by hairpin furrows; and broad or protruding elevated areas with tapering tails. Streamlined forms are assumed to be straight, non-curving features relative to the horizontal plane, although some slightly curving forms are mapped if they are associated with other SF that are straight and of similar size.

It is assumed in this study that drumlins in the study area derive their shape and size characteristics primarily from the forming process(es). This assumption is based on the general similarity in size and shape of drumlins both within local swarms and across the entire study area. Bedrock ridges that have apparently been streamlined are also mapped, but are designated "low confidence" SF because some may be structurally controlled features. They are not included in numerical analyses of SF (Chapter 3). These type landforms are found primarily in NTS 93M, where dominant SF-producing flow was toward the southeast, parallel to dominant regional structural trends.

2.4. RESULTS

2.4.1. Streamlined forms map

More than 50,000 streamlined forms are mapped in the study area (Figure 15, in map pocket, and 20 maps in Appendix A). The lengths of the lines representing SF is drawn to scale.

2.4.1.1. Comparison of thesis map with other streamlined forms maps

The map of SF presented in this chapter (Figure 15) is compared to maps of parts of the study area prepared by other researchers. The purpose of this comparison is to compare results obtained using different methodologies and for quality control.

Streamlined forms locations are often included on surficial geology maps and on maps delineating glacial flow indicators. Study area maps that include streamlined forms often determine the location and orientation of streamlined forms using air photos. A drumlin, crag-and-tail, or fluting mark on these maps can be used to represent either a single streamlined form or a number of SF. The orientation of the SF symbol corresponds to the orientation of a single SF or the average orientation of more than one SF. The length of the map mark does not usually correspond to the length of SF. This approach is different than that used in this study. Each SF mark on Figure 15 represents the location, length, and orientation of a SF.

Other maps of the study area that include SF are used for quality control of Figure 15. Locations, orientations, and relative densities of SF are qualitatively compared. Figure 15 data are also compared to streamlined forms data from a digital surficial geology map of NTS 93K (Plouffe, 2000).

The most comprehensive maps of study area drumlin, crag-and-tail, and fluting occurrences compiled prior to the thesis map are surficial geology maps of NTS 93F (Plouffe *et al.*, 2004) and NTS 93K (Plouffe, 2000). The map of 93K is available in digital format. Streamlined forms occurrences in 93K are digitally available as points with azimuth attributes; SF lengths were not obtained. Plouffe's original maps of the area, produced using air photo interpretation, included most SF (Plouffe, 1994, 1996a, 1996b, 1996c); however, the density of the symbols was reduced for the 1:250 000 compilation. Thus, a single symbol was often used to represent more than one SF. All SF in the study area that are recognizable using satellite or DEM images are presented on Figure 15. As a result of this difference in mapping objectives, Figure 15 shows a great deal more SF than are included on Plouffe's map. Plouffe's (2000) map of 93K includes 2,363 SF. The thesis map includes more than 20,000 SF in 93K.

Another difference between Plouffe's map and Figure 15 is related to scale. Air photo interpretation allows the recognition of smaller and/or lower relief SF than are recognizable using the thesis methodology. Hence, Plouffe's map would be expected to include SF that are not included on Figure 15.

Distribution of SF on Figure 15 and on Plouffe's map are compared (Figure 16). Distribution is calculated as percent of total drumlins per 4 km^2 area. Since a single SF symbol is frequently used on Plouffe's map to represent more than one SF, then strict quantitative comparison of drumlin densities as indicated by the two different studies (Plouffe, 2000 and this study) is not meaningful. The data sets are known to be unequal. However, qualitative comparisons of SF locations and densities are possible.

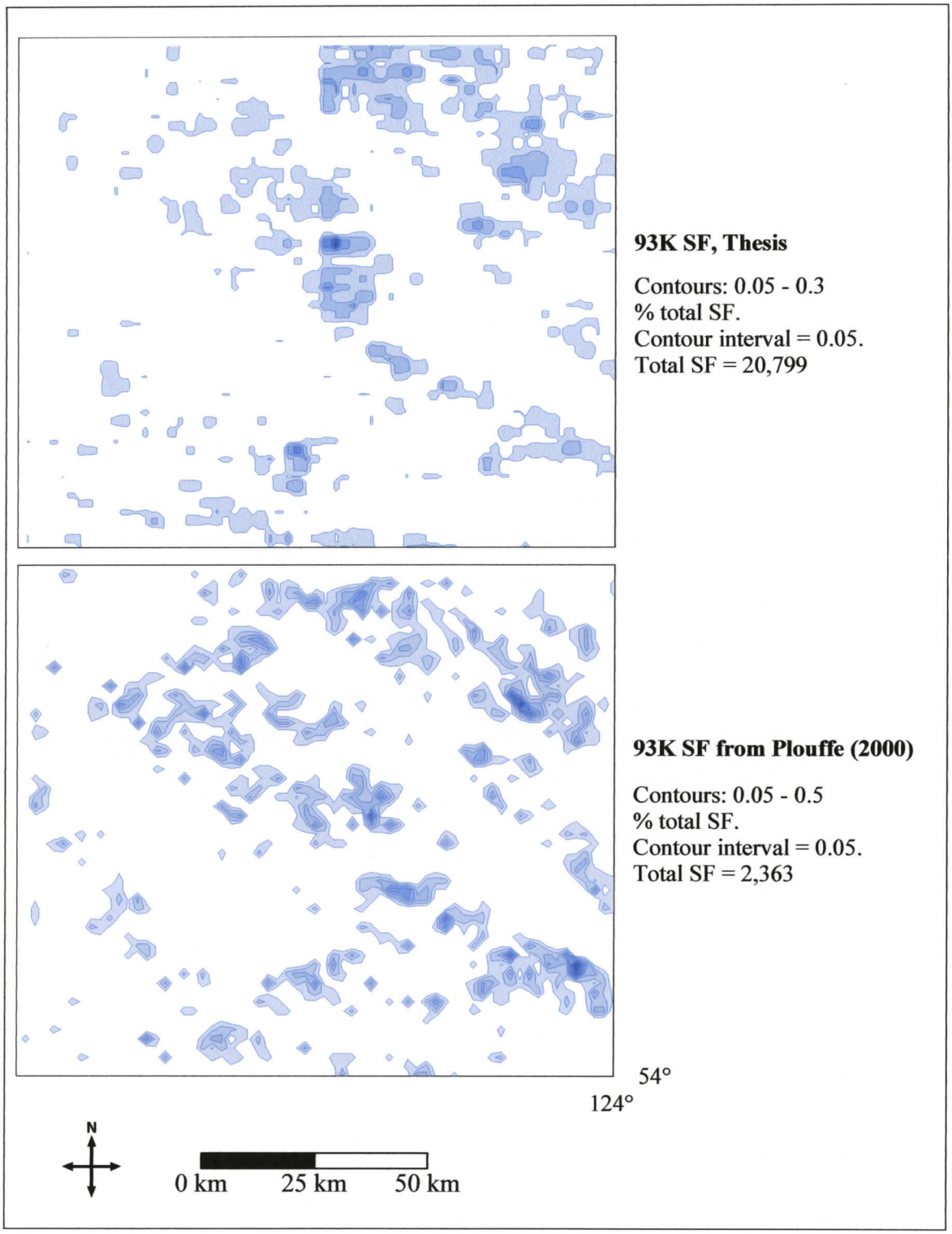

Figure 16. Comparison of streamlined forms distribution for NTS 93K. Contours represent percent total streamlined forms per four square kilometre area.

Some similarities of distribution are apparent. Low drumlin density can be correlated on both maps with two generally southeast-trending lowland areas, the northeasternmost containing Stuart Lake and Stuart River and southwestern lowland containing Babine Lake (Figures 15 and 16). Some areas of higher concentration coincide (*e.g.* northeast of Tembleur Lake and northeast of Tezzeron Lake; Figures 15 and 16).

Some differences in concentration are also apparent. Plouffe's map indicates more areas of high concentration than are evident from Figure 15. Higher SF concentrations on Plouffe's map than on Figure 15 are observed south of Stuart River, in lowlands between Fraser and Babine Lakes, and west of Stuart Lake (Figure 16). Air photos are higher resolution images than the satellite and DEM images used in this study. This difference in reported drumlin densities in these areas could be because thesis imagery does not detect SF that were observed by Plouffe using air photos.

Streamlined forms orientations reported by Plouffe (2000) and in this study are also compared. Since definite flow directions are not known for every mapped SF, the orientation of each SF is restricted to a value from 0 - 180° for the purpose of this comparison. This directionless SF property is called a strike in this study; however, in most cases these values probably represent the true bearing of the SF since almost no westerly flow is indicated in NTS 93K (Tipper, 1971a; Plouffe, 2000; Stumpf *et al.*, 2000; this study). Frequency plots of SF indicate similar distribution of 93K SF strikes reported by Plouffe (2000) and in this thesis (Figure 17). The thesis map, however, includes a somewhat greater percentage of SF mapped with strikes from 20° – 70° and

from 120° - 150°. Plouffe's map shows a greater percentage of SF with strikes from about 70° – 120°.

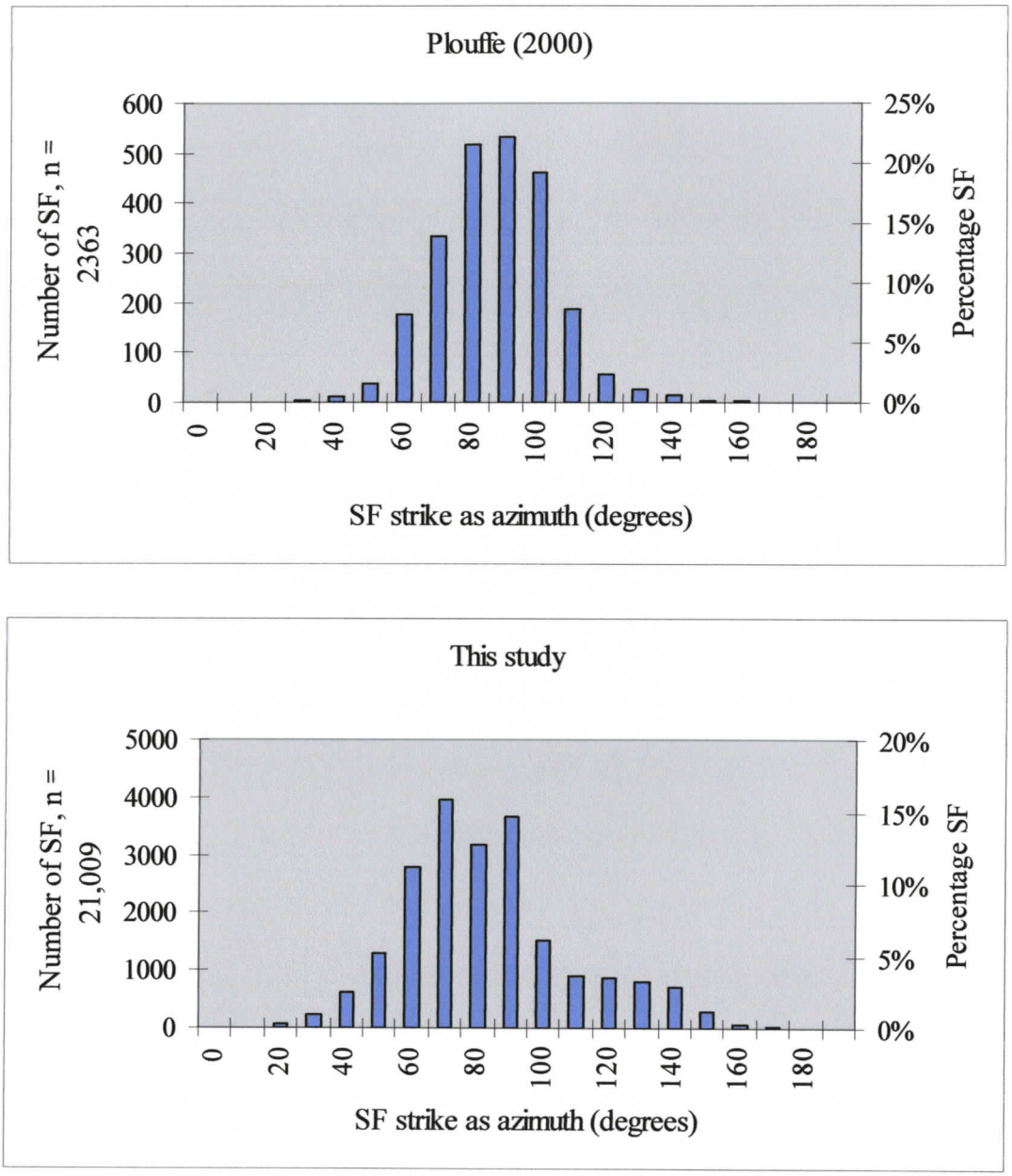

Figure 17. Distribution by strike of streamlined forms in NTS 93K. Strike is given as an azimuth. A somewhat higher percentage of SF bearing southeast and bearing between 60 - 70° are depicted on Figure 15 than are shown on Plouffe's map.

A possible explanation for the differences shown in Figure 17 are that Plouffe's map includes higher relative concentrations of SF northwest and northeast of Fraser Lake than are indicated by Figure 15 data (Figure 16). Plouffe's map shows mainly east-trending SF in these areas. This disparity results in a relatively greater percentage of 70° – 120° SF on Plouffe's map compared to Figure 15 SF bearings. This difference could be due to higher resolution air photo mapping used by Plouffe. The higher percentage of SF in the 120° - 150° range on Figure 15 than on Plouffe's map may reflect a tendency for the mapping methodology used here to identify SE-trending, structurally controlled forms.

Figure 15 also indicates a higher concentration of SF in the north and northeast parts of NTS 93K than is indicated on Plouffe's map (Figure 16). Streamlined forms in this area predominantly bear northeast, less than 80°, according to Figure 15. This results in a relatively higher percentage of SF bearings less than 80° for the thesis map compared to Plouffe's map. The difference here could be attributed to the different mapping methods. Since SF bearings are uniform in this area and densities are high, Plouffe may have often used a single symbol to represent a number of close-packed, parallel SF. Figure 16 represents every identified SF. The different methods would result in a greater relative density of SF in this area on Figure 15 than on Plouffe's map.

Clague (1984) prepared a surficial geology map that included the Bulkley Valley north from Smithers to Hazelton and southwest to Terrace. His map included parts of the Bulkley and Skeena valleys in the study area, spanning parts of both NTS 93L and NTS 93M. He mapped a few SF in the Bulkley Valley from Smithers north to Hazelton. He also shows west-trending SF where Trout Creek empties into the Bulkley

Valley and west-trending SF at the north end of the Bulkley valley. These results are comparable to Figure 15. He also mapped the remarkable field of SF in the Skeena River valley west and southwest of Hazelton; these forms are also on Figure 15.

Some minor differences between Clague (1984) and Figure 15 are noted. Figure 15 shows the SF field west of Hazelton extending to a greater elevation up the side of Hazelton Peak than was shown by Clague (1984). This is probably because Clague restricted his study to lower elevations with significant Quaternary deposits (Clague, 1984). Figure 15 also indicates SF trending E-W where the west flowing Suskwa River empties into the Bulkley River immediately prior to the Bulkley – Skeena confluence. These forms are not mapped by Clague. As is common on surficial geology maps, Clague (1984) does not indicate SF lengths.

Streamlined forms are included on a map of NTS 93L compiled from air photo study, field studies, and published information (Tipper, 1994). Tipper (1994) maps three types of SF that he calls glacial grooves or lineations, drumlins, and rock drumlins. Directions are sometimes indicated for drumlins and rock drumlins. Most of the SF on the map are described as glacial grooves or lineations with unknown direction. SF lengths are not indicated. The locations and strikes of SF on Figure 15 concur with Tipper's map of 93L with some exceptions. Examples of concurrence are converging SF fields north of Morice Lake and west of Hudson Bay Mountain in the western part of the study area, southeast flow up the Babine valley, and east-trending SF in the southern part of 93L.

Tipper (1994) shows generally more widespread and uniform occurrence of SF than the thesis map, including more occurrences at higher elevations. More SF are

shown by Tipper in the Bulkley Valley, particularly north of China Nose Mountain and west of Grouse Mountain. These differences are possibly due to the better resolution of air photos compared to satellite and DEM images; shorter and lower-relief features can be recognized using air photos than can be recognized using the satellite and DEM images used in this study. Figure 15 shows more SE – NW trending SF in the higher elevations of China Nose and Grouse mountains. It is possible that, in this case, the SF are more apparent on DEM shaded relief images than on air photos. It was noted during Figure 15 mapping that, in some cases, SF that are not initially found on satellite images are apparent on DEM shaded relief images. This is due to the "lack" of vegetation cover on a DEM image. When digital elevation models are made, the elevation of the ground surface is used, thereby effectively "removing" vegetation. Vegetation obscures landform shapes. In this sense, DEM images have better resolution than air photos.

Stumpf *et al.* (2000) reported on ice flow indicators in a study area comprising NTS 93L and NTS 93M, the north half of NTS 93E, and parts of the western margins of NTS 93F and NTS 93K. Most of the ice flow orientations depicted in their study correspond to the strikes of drumlin swarms on Figure 15. One exception is the northern part of Babine River in 93M, for which Stumpf *et al.* show a greater bearing variance than was detected using thesis methods. Many of the ice flow directions indicated by Stumpf *et al.* were obtained in the field. It is very likely that some ice flow indications found in field studies are not observable using remote imaging mapping. This would be especially applicable in the Babine River area where evidence of an earlier western flow has been largely erased by a southeast flow event (Stumpf *et al.*,

2000; this study). Isolated evidence of western flow is preserved in locations protected from southeast flow.

Streamlined forms in the north central and northeast portion of NTS 93E were mapped by Ferbey and Levson (2001) using air photo interpretation and extensive field observation. There is generally good agreement between the strikes of thesis SF and Ferbey and Levson's map. For example, both works show the curved path of SF varying in orientation from west to southwest up Nanika Lake and from northeast to east around the north bend of Ootsa Lake (Figure 15). However, some differences in the maps are apparent. Ferbey and Levson show a swarm of east-trending SF south of Nadina Lake, which is approximately 20 km north of Tahtsa Reach (Figure 15). This swarm is not shown on Figure 15. This SF swarm is recognizable using air photos, but is not found using satellite and DEM images used for Figure 15. Figure 15 shows some southeast-trending forms north of Tahtsa Lake that are not shown by Ferbey and Levson.

Crag-and-tails, drumlins, and flutings are included on a surficial geology map that includes the southeast part of NTS 93M and northeast part of NTS 93L (Levson, 2002). The general trend of SF on that map and the thesis map is toward the southeast. Both maps record a change in SF orientation to a more easterly trend in the vicinity of Fulton Lake (Figure 15). Figure 15 includes more SF than are included on Levson's map, an expected disparity due to different mapping objectives. Levson (2002) was interested in SF occurrence relative to till dispersal; whereas, it is the intent here to map all recognizable SF in the study area.

Levson and Mate (2002) mapped SF locations in NTS 93F/5 and NTS 93F/12 . The swarm of east-northeast bearing SF on their map (Figure 18) corresponds to the thesis map. Also, the lack of SF in the valley connecting Ootsa Lake and Cheslatta Lake is apparent on both maps (Figures 15 and 18).

Differences between Figure 15 and SF mapped by others suggest relative advantages and disadvantage of mapping approaches. The approach used in this thesis results in a data set that includes most SF in the study area that are recognizable using the Landsat, SPOT, and DEM TRIM I imagery. The data set includes locations, orientations, and lengths of all mapped SF. The data set does not, however, represent all SF in the study area. There are many SF that are of too little relief or too small to be detected by thesis methods. One of the greatest advantages to the thesis mapping methodology is the ability to create an extensive detailed SF map of a large area relatively quickly.

Other studies that produced maps of the study area made extensive use of air photos for SF recognition and mapping. The higher resolution of air photos permits the detection of SF that are not detectable using thesis methods. Some of the studies also included extensive field verification of significant portions of the map. This adds quality control to the map and allows the collection of relevant data that is not obtainable remotely.

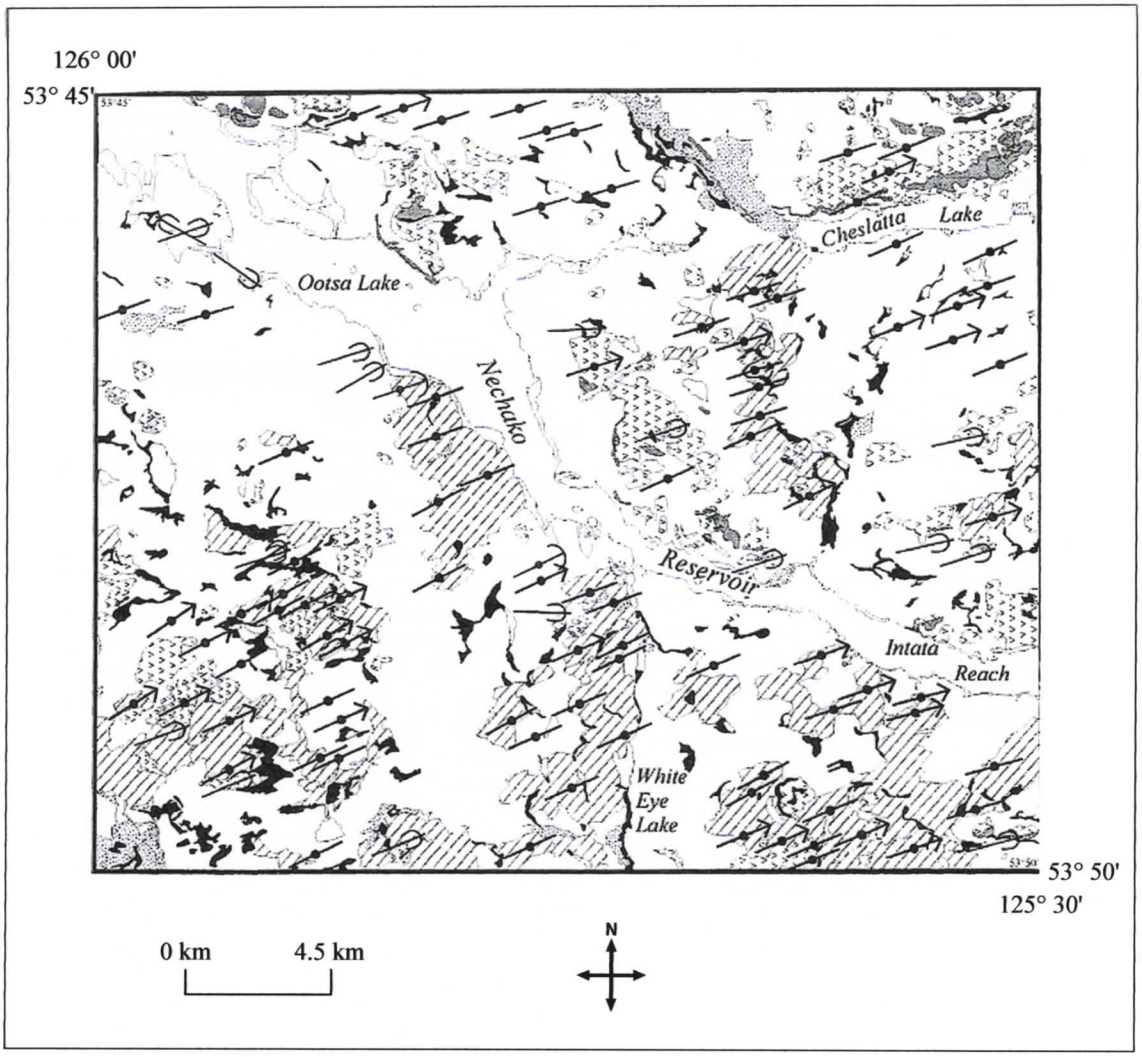

Figure 18. Drumlins, flutings, and crag-and-tails near the east reach of Ootsa Lake, modified from Levson and Mate (2002). The lack of SF in the lowland area from Ootsa Lake to Cheslatta Lake is noted both here and on Figure 15.

2.4.2. Flow directions

Flow directions are interpreted from satellite and DEM images based primarily on hairpin furrows and on tapering, in the horizontal plane, of SF. The justification for using hairpin furrows is discussed below. Tapering tails are common on drumlin and crag-and-tail SF (see Chapter 1). If a group of SF show a consistent flow direction based on one or both of these criteria, then that flow direction is assigned to that location. Most flow directions reported here are based on remote evaluation. Reports by other workers of flow directions indicated by field studies in some parts of the study area (see above) are also considered in the evaluation of flow directions. A field study conducted as part of this thesis (Chapter 5) also resulted in determination of flow directions in some parts of the study area. Air photos were used to confirm flow directions in some areas.

Hairpin furrows are considered reliable indicators of flow direction. The rounded crescentic scour occurs on the upstream part of the hairpin, and the lateral furrows extend down flow. This unidirectional property has been demonstrated experimentally with water as the eroding mechanism (Allen, 1982b; Komar, 1983), and is observed in natural settings where erosion was by both water and wind (Allen, 1982b; Komar, 1983; Dreimanis; 1993; Bryant and Young, 1996). Bryant and Young (1996) compared scours around erosional flutes on tsunami-swept headlands with glacial hairpin furrows. In ancient glacial terrains, the lateral furrows of the hairpins consistently point downstream relative to inferred flow directions (Armstrong and Tipper, 1948, 1971a; Aario, 1987; Boulton, 1987; Shaw and Sharpe, 1987; Clark, 1993;

Shaw, 1994, 1996; Munro and Shaw, 1997; Pair, 1997; Sawagaki and Hirakawa, 1997; Benn and Evans, 1998; Mate, 2000; Plouffe, 2000; Stumpf *et al.*, 2000).

Hairpin furrows have distinctive shape characteristics. In its simplest form, a hairpin furrow consists of two parallel furrows connected by a crescentic furrow (Figure 19). The erosion of the furrows leaves a remnant ridge between the eroded troughs (Figure 14). The lateral furrows generally broaden and become shallower away from the crescentic furrow. This lateral widening corresponds to tapering, in the horizontal plane, of the remnant ridge. One of the two lateral furrows emanating from the crescentic furrow may be less developed than the other furrow, or missing entirely. Hairpins are eroded into both bedrock and unlithified sediments.

Hairpin furrows occur at different size scales, and frequently are interconnected: the lateral furrows of one hairpin will often terminate at a down flow crescentic scour of another hairpin, but will not cross-cut the next furrow in the group. The interconnectedness of a group of furrows can result in en echelon arrangements (Kor *et al.*, 1991; Shaw, 1994, 2002; Mate, 2000) (Figures 20, 21, and 22). Sets of smaller hairpin furrows sometimes occur within larger hairpin furrows or crescentic scours (Kor and Cowell, 1998; Mate, 2000).

Some examples of flow direction determination are presented below. Figures 21 and 22 show a satellite image of the western part of NTS 93M. Flow direction at this site is inferred to be towards the southeast based on hairpin furrow arrangements. The lateral furrows point down flow. The ridges between the lateral furrows are mapped as SF on Figure 15. Ryder and Maynard (1991) indicate that southerly ice flow occurred in the Nass Basin. The Nass Basin extends into the western part of 93M (Figure 3).

Figure 23 shows a DEM image of the Hazelton drumlin field, located near the confluence of the Skeena and Bulkley Rivers, west of the village of Hazelton. Figure 24 is the same image with traced hairpin furrows. Flow direction is indicated by both tapering SF and by hairpin furrows. Figure 8 is an air photo stereo pair of drumlins located on Hazelton Peak north of the main Hazelton drumlin field (Figure 23). The drumlins in Figure 8 are not detectable using DEM imagery. Southwest flow direction in this area agrees with Clague's (1984) findings and is confirmed by field study (Chapter 5).

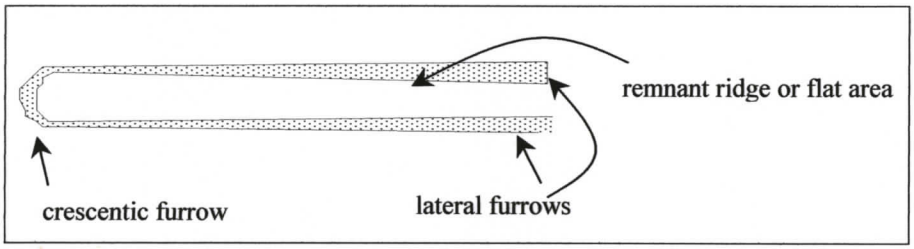

Figure 19. View from above of simple hairpin furrow. Flow is to the right. Shaded area represents negative relief troughs.

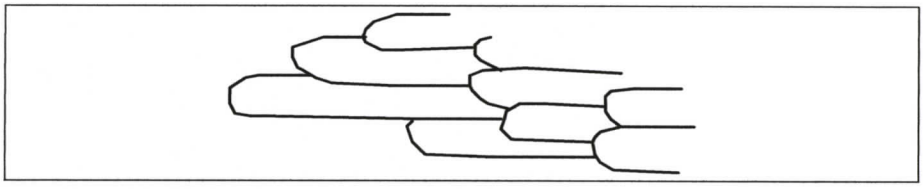

Figure 20. Stylized interconnected hairpin furrows. Flow is to the right.

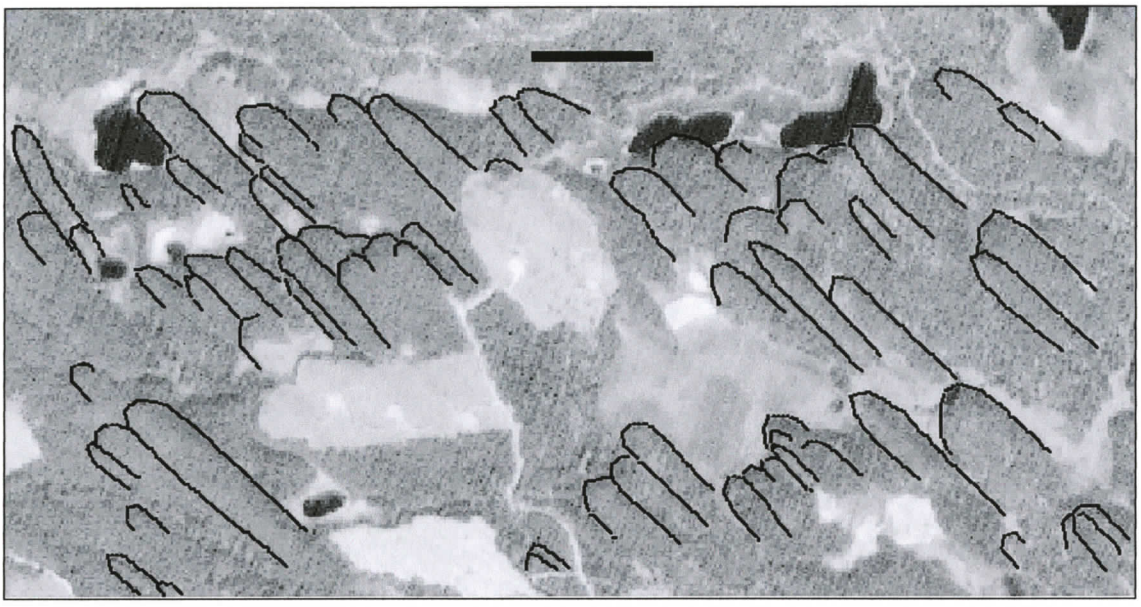

Figure 21. SPOT satellite image of traced hairpin furrows around drumlins in NTS 93M 051. Figure 22 is the same view without tracings. Flow was to the southeast. Scale bar = 500 m. North is at the top of the figure.

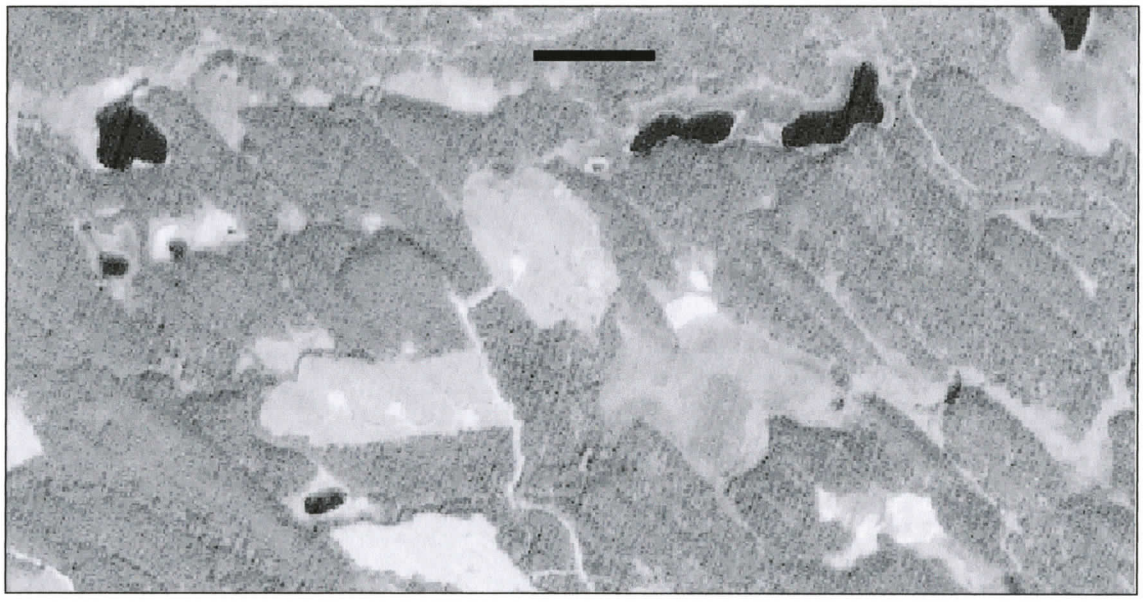

Figure 22. SPOT satellite image of part of NTS 93M 051. Hairpin furrows are shown traced in Figure 21. Scale bar = 500 m. North is at the top of the figure.

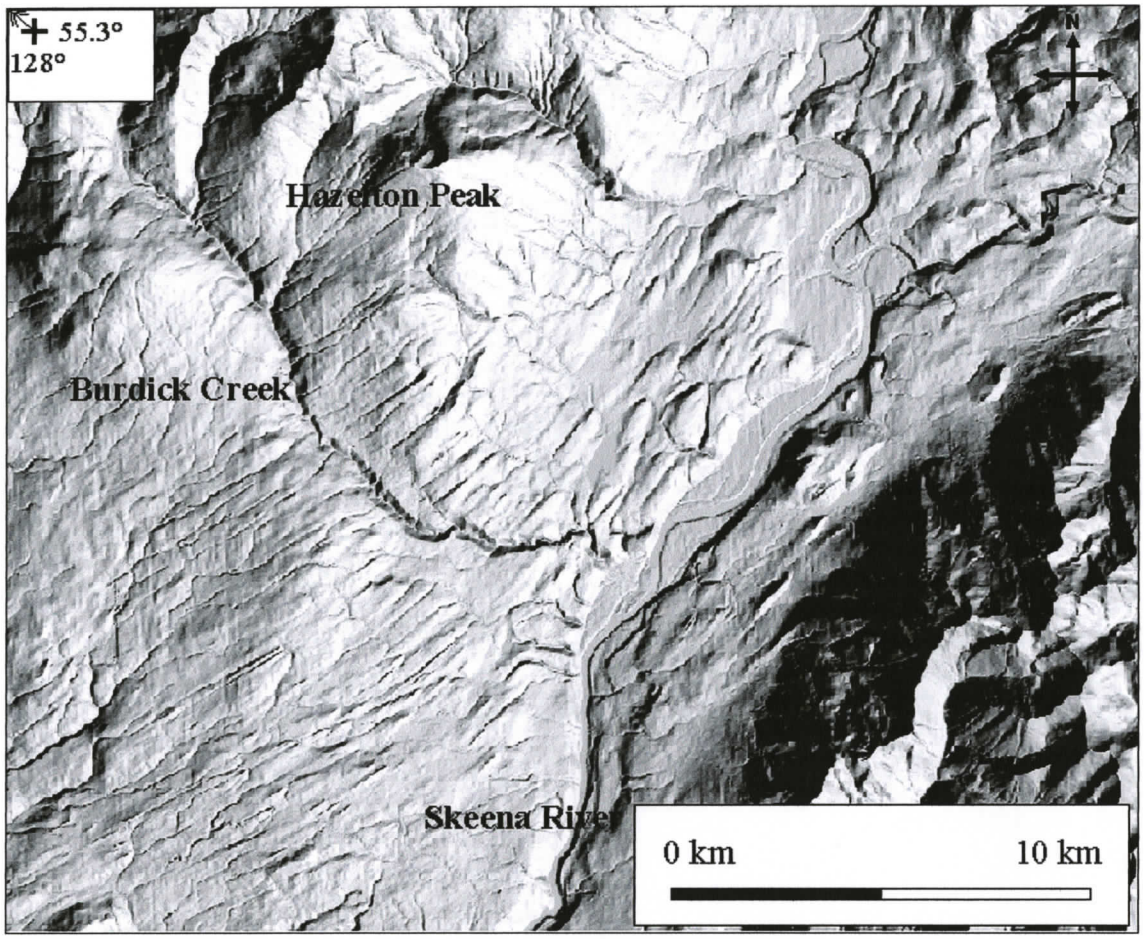

Figure 23. DEM image of the Hazelton drumlin field. Tapered SF and hairpin furrows are visible. Flow was towards the southwest. Figure 24 shows the same image with hairpin furrows traced.

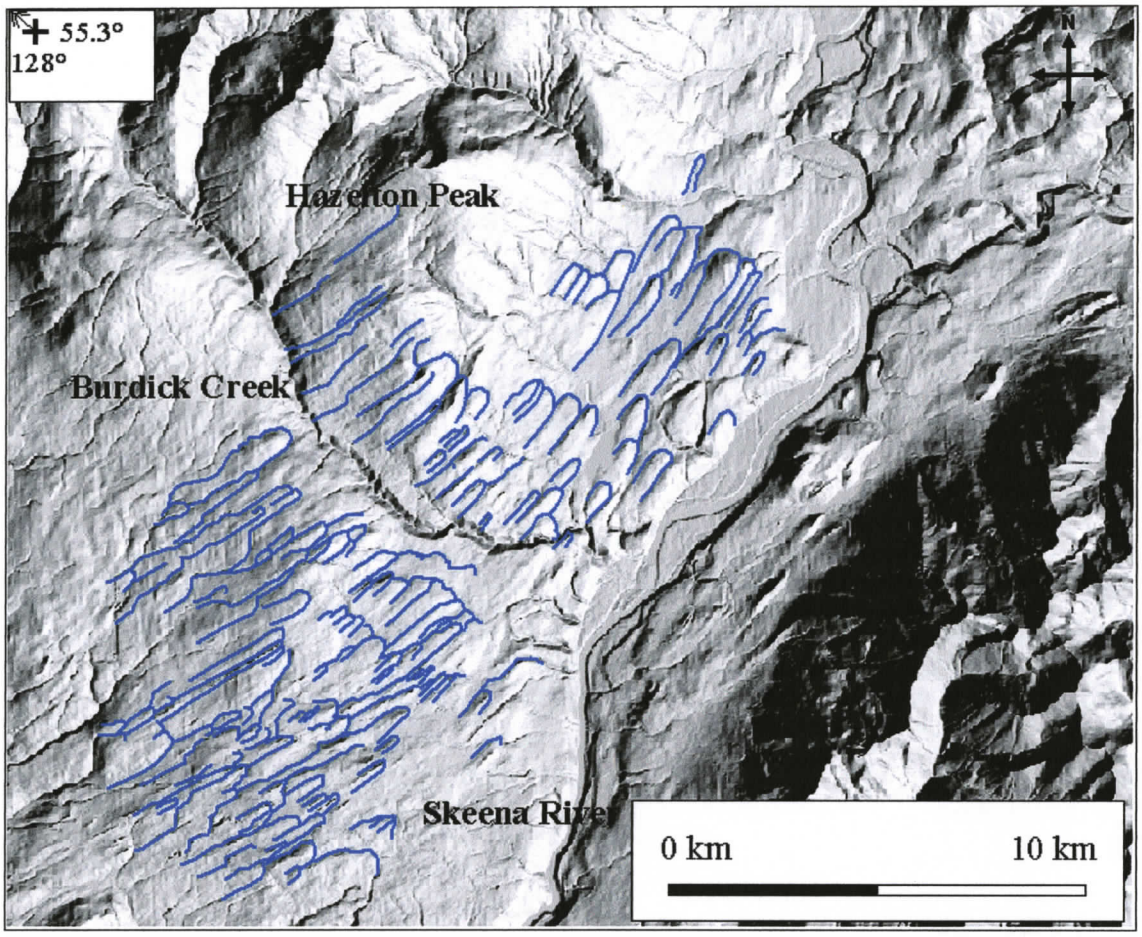

Figure 24. Furrows traced on a DEM image of the Hazelton drumlin field. Figure 23 is the same DEM image without traced furrows. Flow was to the southwest.

Figure 25 shows a DEM image from the southeast part of NTS 93M. Flow is interpreted as being towards the south-southeast in this area. This result is in agreement with other studies (Ryder and Maynard, 1991; Stumpf *et al.*, 2000; Levson, 2002). Figure 26 shows two satellite images of NTS 93F and NTS 93K. Flow direction is inferred to be towards the northeast based on tapering SF and hairpin furrows.

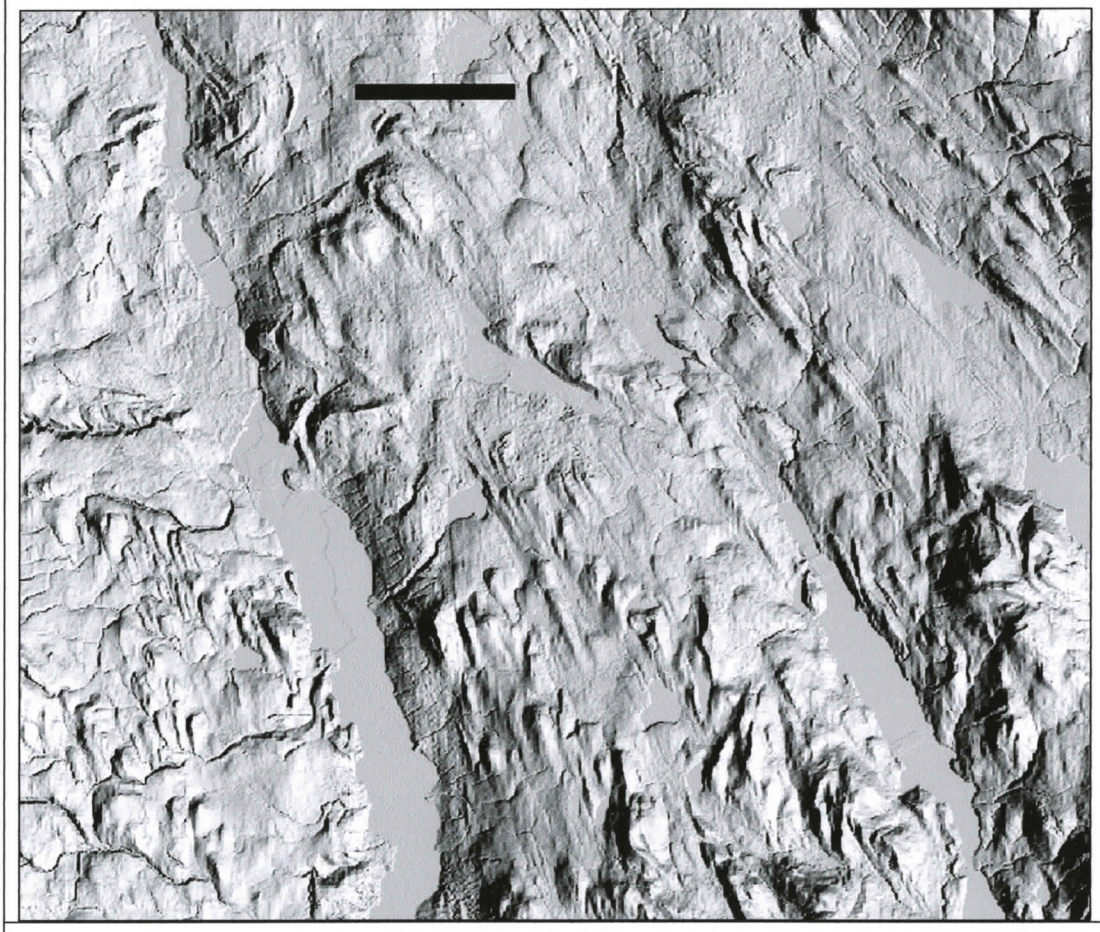

Figure 25. DEM image of southeast part of NTS 93M, the Babine River valley. Flow is interpreted as being towards the south-southeast based on tapering forms and hairpin furrows. Scale bar is approximately 4 km long and north is towards the top of the photo.

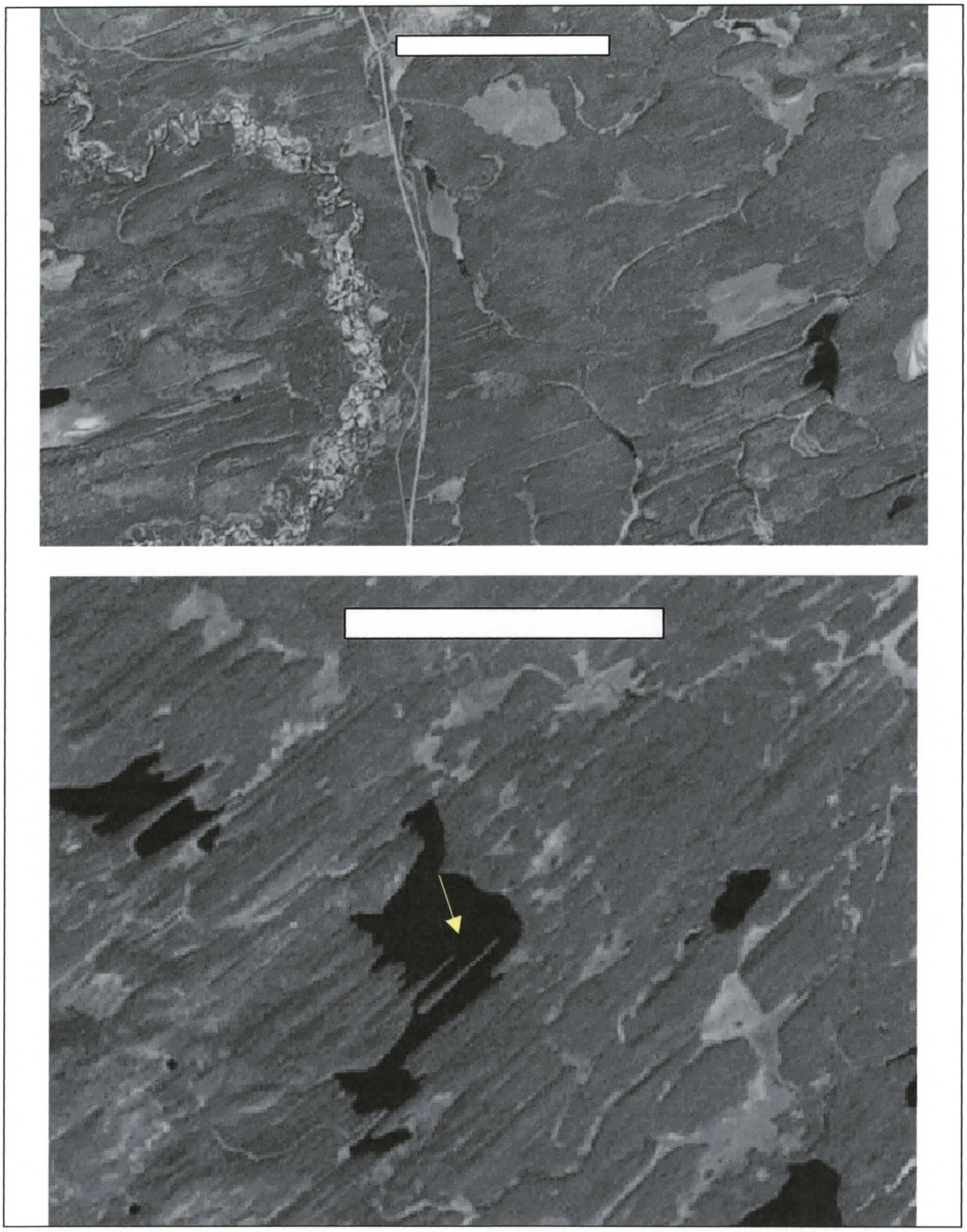

Figure 26. Landsat satellite images of SF in the SE part of NTS 93F (bottom) and NE corner of 93K (top). Flow is interpreted as being towards the NE and ENE, respectively. The white scale bar is approximately 2 km long. Note the tapered SF shown in the lake (arrow). North is toward the top of the figure.

A flow direction map is compiled based on observations including those presented as examples above. The flow direction map indicates four main flow directions across the study area: southeast, west, east-northeast, and in the western part of NTS 93M, south and southwest outlet flow towards the coast (Figure 27). The outlet flow towards the coast is possibly connected with the SE flow down the Babine and other SE-oriented valleys in the eastern part of NTS 93M. Southeast flow indicators are dominant in the north, and rare in the south. Flow parallels Babine Lake, the Bulkley Valley, and other valleys and lakes in the northern sections.

Indications of west and west-southwest flow are most common in the western third of the study area. West or WSW flow in the southwest is most common along the east side of the Coast Mountains, where those mountains diagonally cross the southwest corner of the study area (Figures 3 and 27). West-southwest flow indications are found on alpine ridges on either side of the Bulkley Valley (see Chapter 5).

The most dominant flow in the southeast, including all of NTS 93F and the east half of NTS 93E, is towards the ENE. Some SE flow indications are mapped within the area of dominant ENE flow (Figure 27). Only limited evidence is found using the thesis methods of ENE and WSW flows occurring together; however, other workers have reported the adjacent occurrence of east and west ice flow indicators (Stumpf *et al.*, 2000; Ferbey and Levson, 2001; Ferbey, 2004).

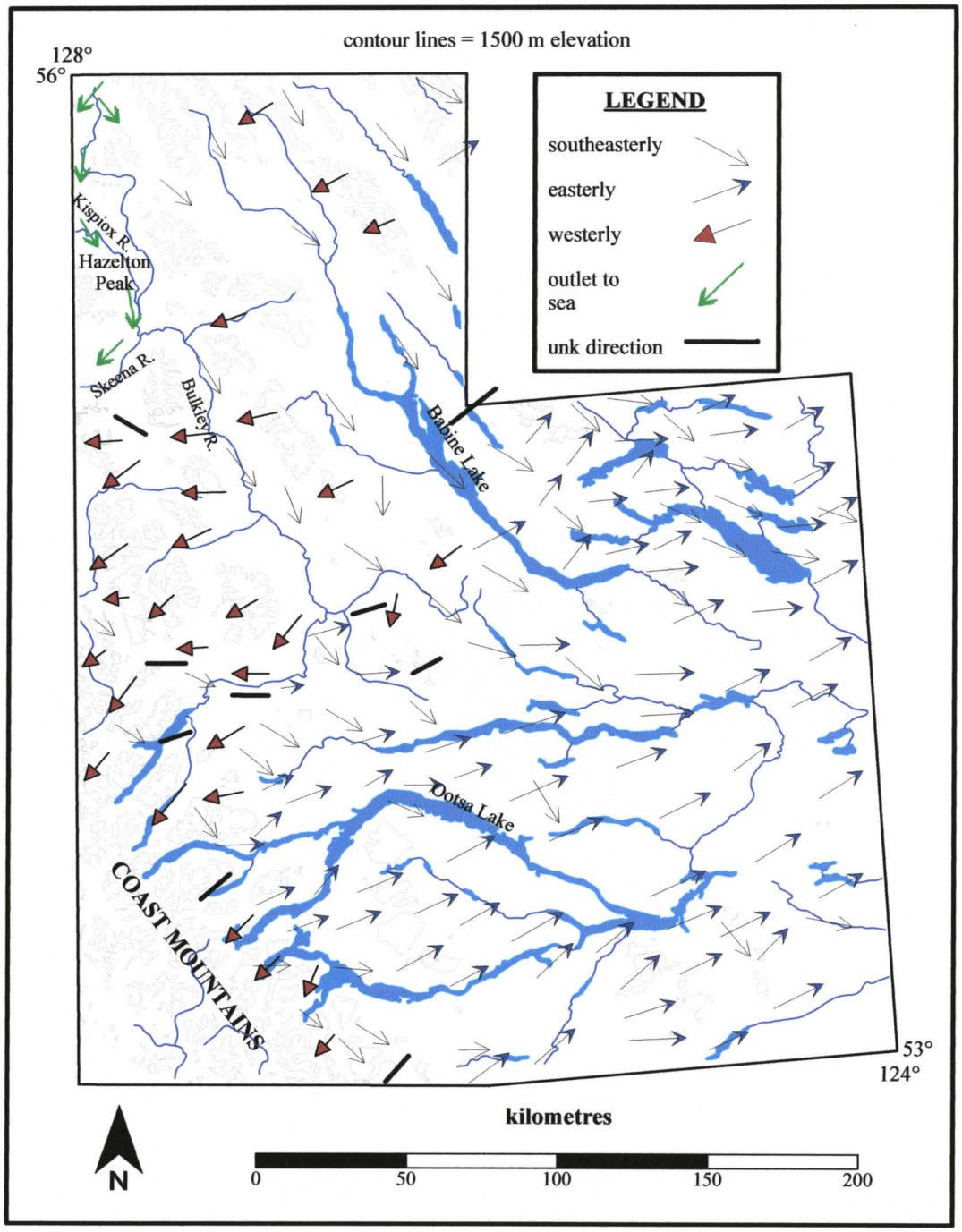

Figure 27. Flow directions from streamlined forms mapping.

Outlet flow to the Pacific Ocean (Clague, 1984; Ryder and Maynard, 1991) is apparent in the northwest. Southward flow followed the Kispiox Valley, then curved to the southwest at the junction with the Skeena and Bulkley Rivers, and flowed out of the study area down the Skeena Valley towards the coast (Figure 27, green arrows). Drumlins on top of Hazelton Peak (Figure 27), about 1525 m a.s.l. (see Chapter 5), parallel the valley flow. This outlet flow, indicated by the green, double-headed arrows on Figure 27, branches at the northwestern corner of the study area and is possibly contiguous there with the southeastern flow (indicated by single-headed black arrows). That is, flow down the Kispiox and Skeena Valleys may be a branch of the flow that dominated the eastern half of NTS 93M.

2.4.3. Streamlined forms occurrence and flow patterns

The streamlined forms map (Figure 15) is a record of SF location, orientation, and length relative to study area topography. Some characteristics of flow that created SF can be inferred from observations of the relationships between SF and topography. Observed flow patterns include SF that parallel valleys and SF that cross valleys. Low SF densities are found in many study area valleys. Low densities could be a result of later deposition or erosion. Both possibilities are discussed later in this chapter.

2.4.3.1. Relationship of valleys to paths of streamlined forms

Many SF swarms follow paths that parallel valleys. Many of these valleys are curved. Some major examples are the SF fields along the Kispiox and Skeena Rivers in NTS 93M, the SF path along the west side of Whitesail Reach and continuing around

the north side of Ootsa Lake, and the slightly curving SF swarms on either side of the Nechako River in NTS 93F (Figure 15). Other sites where SF follow curving valleys include: streamlined forms trending up valley, towards the west and southwest along the Morice River, Telkwa River, Tahtsa Reach, Whitesail Lake, and in valleys north and west of Hudson Bay Mountain; southeast-bearing SF along the Driftwood River and Takla Lake in 93M; and ENE-trending SF along Tsacha Lake in southern 93F (Figure 15).

On the other hand, some SF flow paths cross valleys or are cut by those valleys. This flow characteristic shows clearly in the west part of NTS 93F (Figure 28). Cheslaslie Arm, Euchu Reach, Natalkuz Lake, Intata Reach, and the east end of Ootsa Lake run contrary to a wide spread field of ENE-trending SF in this area. East-northeast flow also continues on both sides of ESE-trending Inzana Lake in the northeast corner of NTS 93K (Figure 15). Streamlined forms west and north of Ootsa Lake follow a curving path around the north side of the lake along its western reach, but most SF are oblique to the lake in the area along its eastern reach (Figure 29).

2.4.3.2. Valleys and gaps in streamlined forms occurrence

Valleys in the study area are often sites at which only a few or no SF are mapped. These valleys constitute gaps in SF occurrence. Both valleys that are parallel or subparallel to flow and valleys that are oblique to flow ("cross valleys" in this thesis) show SF gaps. Gaps in the major valleys and lowlands in the eastern part of the study area can be attributed to glaciolacustrine (LG), glaciofluvial (FG) and alluvial deposits

that partially or completely obscure or mask earlier features (Plouffe, 2000; Levson, 2002) (Figure 30). Some SF are still visible through a veneer of glacial lake sediments.

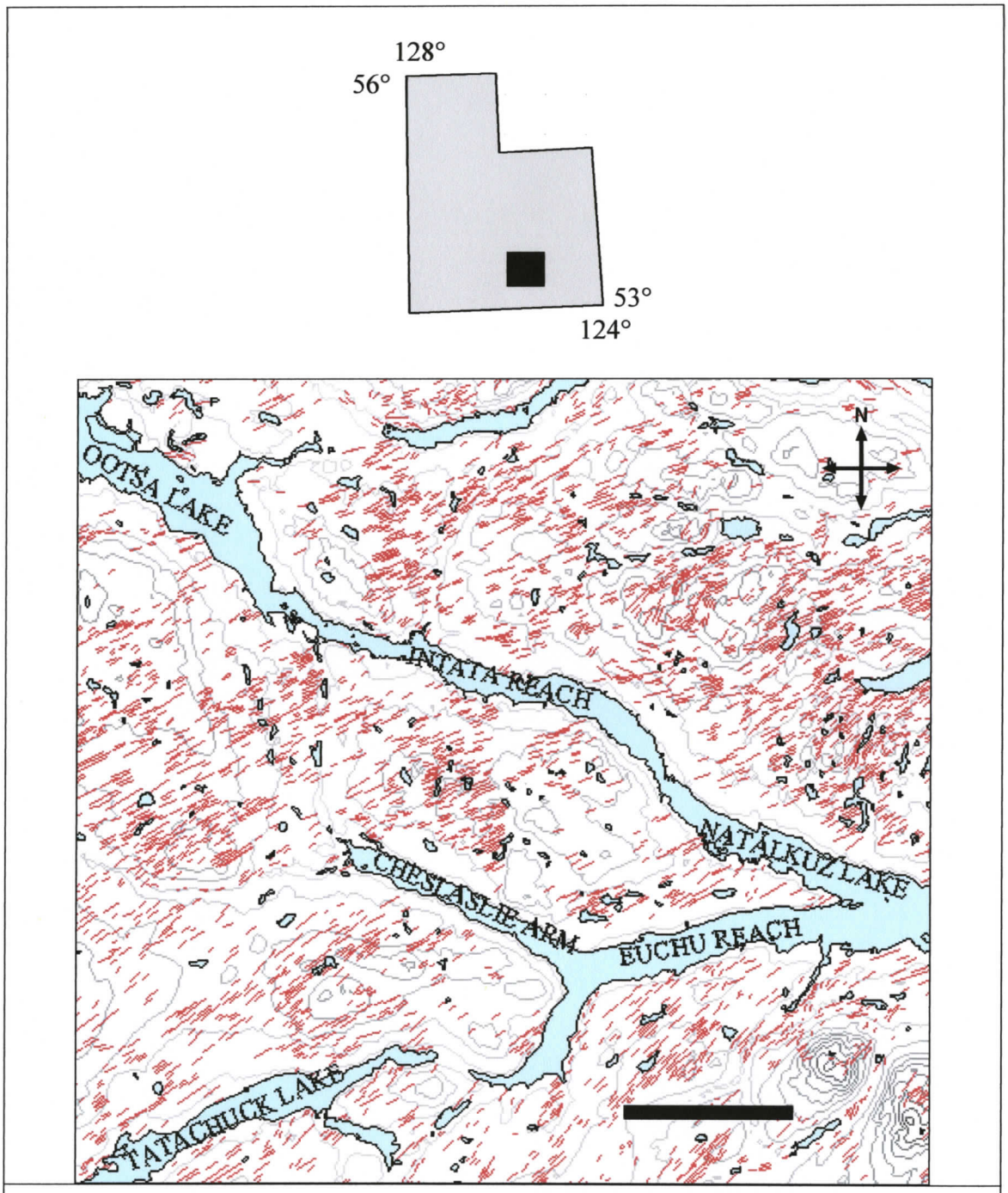

Figure 28. East-northeast trending SF crossing valleys oblique to flow in east Ootsa. Scale bar = 10 km.

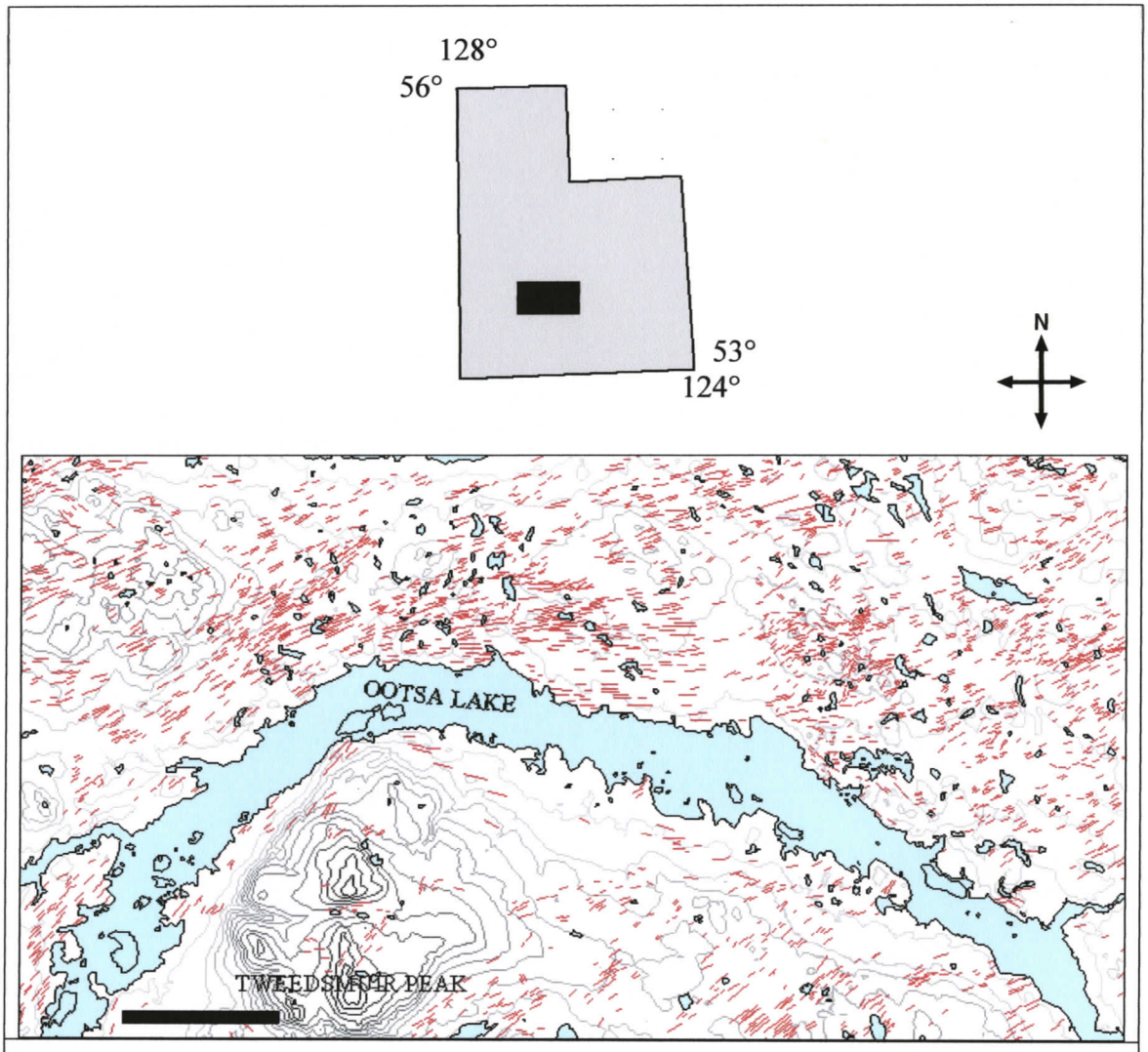

Figure 29. Northeast-trending SF parallel the bend around the western reach of Ootsa Lake, and then continue obliquely to the eastern reach of Ootsa. A few SF run southeast and parallel the eastern reach of Ootsa. Streamlined forms to the south of Ootsa's eastern reach bear ENE, oblique to Ootsa Lake in this location (see also Figure 28). Scale bar = 10 km.

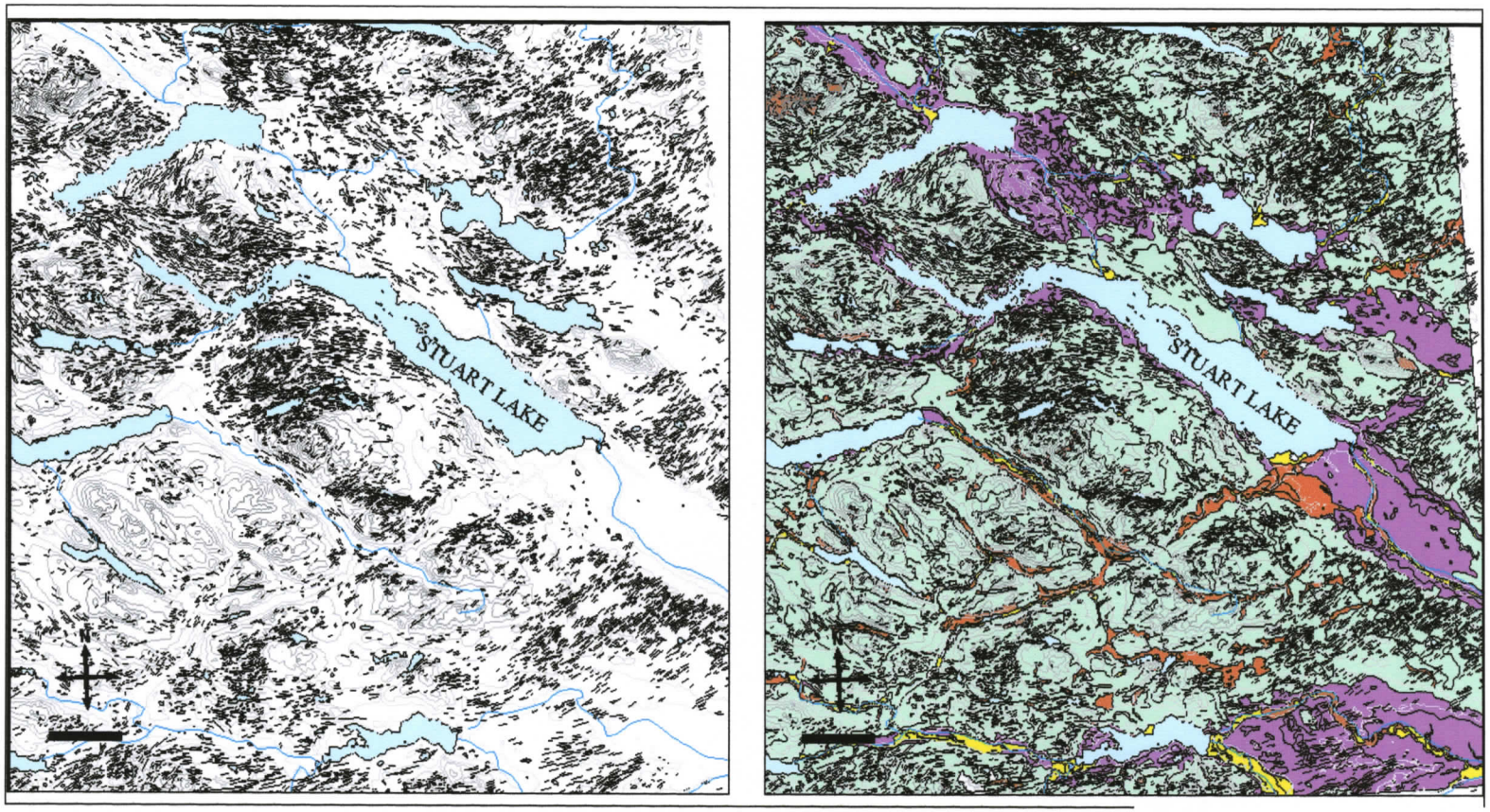

Figure 30. Two maps showing the relationship between glaciolacustrine (purple), glaciofluvial (orange), alluvial (yellow), and bedrock\colluvium (brown) deposits and SF occurrence in NTS 93K. Some areas of low SF density (left map) coincide with glaciolacustrine, glaciofluvial, and alluvial sediments (right map). Surficial geology units from Plouffe (2000). Scale bar = 10 km.

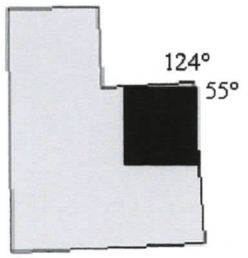

However, other valleys with low SF densities are not associated with later LG deposition. Clague (1984) mapped the Bulkley Valley primarily as moraine, drift, organic, and alluvial deposits from Smithers northward; Levson (2002) compiled mapping in part of the Bulkley Valley northwest of Decker Lake, and showed no LG sediments in the vicinity of that valley. Nonetheless, very few SF are apparent along almost the entire length of the Bulkley Valley from Decker Lake northward (Figure 15). Some valleys in the Skeena and Babine watersheds also demonstrate SF gaps (Figure 31), as do valleys in the vicinity of Francois Lake (Figure 32).

The Telkwa and Morice river valleys are sites of generally WSW flow. Although SF are conspicuous to the north and south of the Morice River, the Morice valley bottom shows only minor SF occurrences. Similarly, few SF are noted along the Telkwa River.

2.4.3.3. Streamlined forms density

Review of the SF map (Figure 15) allows some general observations about SF densities in the study area. A more quantitative discussion of SF distribution is included in Chapter 3. High SF concentrations are apparent at several locations: northwest of Morice River, north of Natalkuz Lake, northwest and southeast of the Nechako River, southwest of Stuart River, west of Inzana Lake, and northwest of the Skeena River (Figure 15). Low concentrations are found in many valleys and troughs and where glaciolacustrine, glaciofluvial, and/or alluvial deposits are pervasive. Also, few SF are mapped on the upper peaks and ridges of high mountains.

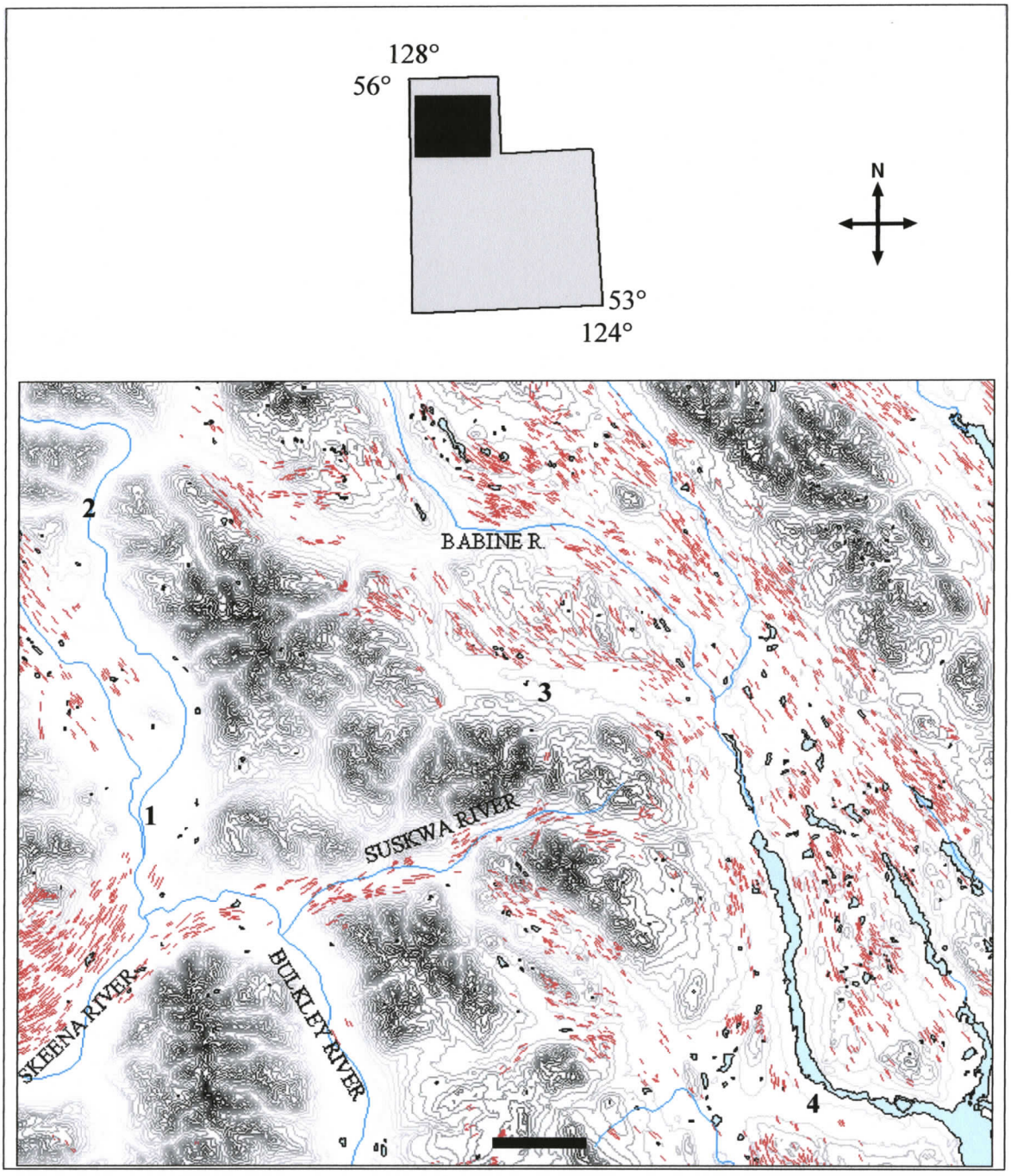

Figure 31. Valleys with low SF densities in NTS 93M. Valleys 1 and 2 are parallel to southeast flow. Location 3 is subparallel and location 4 is a cross valley. Note the westward oriented SF path along the Suskwa River that crosses the north end of the Bulkley Valley and leads into the Skeena River valley. Scale bar = 10 km.

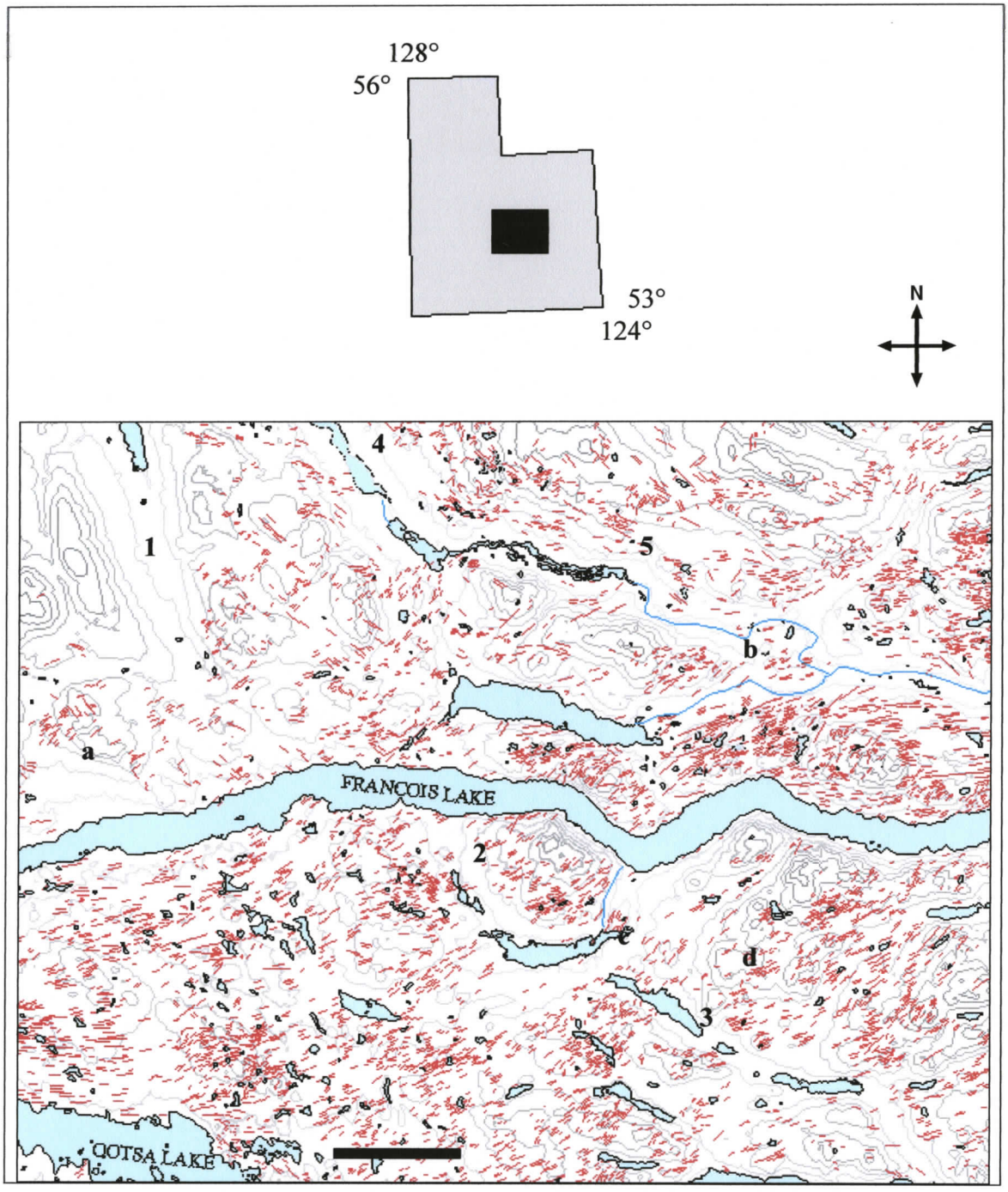

Figure 32. Valleys / lowlands with low SF densities near Francois Lake. Five lowland areas (labelled 1-5) trend approximately SE and are cross valleys to ENE flow. Relatively few ENE SF occur in the valleys. Four NE- or ENE-trending lowlands with low SF density are labelled a-d. Scale bar = 10 km.

Field evidence (Chapter 5) indicates the occurrence of SF at elevations as great as 1800 m; however, these alpine SF were rarely detectable using thesis mapping methods. The alpine SF have lower relief and are smaller than many lowland SF. Subsequently, they are not detectable using the satellite and DEM images used here.

2.4.3.4. Flow out of cirques

Streamlined forms emanate from cirques at some locations, for example, northwest of Trembleur Lake in the Hogem Ranges, in the Telkwa Range (Figure 33), and possibly at Tweedsmuir Peak (Figure 15). The cirques open towards the northeast.

2.5. DISCUSSION

2.5.1. Principle flow directions

Streamlined forms are records of uni-directional movement. Based on SF orientations, three principle flow directions are evident in the study area: south-southeast to southeast, northeast to east-northeast, and west-southwest to west (Figure 27). In addition, a SF swarm with a south-southwest to southwest orientation is evident in the southwest part of NTS 93M along the Skeena River (Figures 15 and 27). The flow that formed this field of drumlins can be traced northward up the Kispiox River to the northwest corner of NTS 93M (Figure 15). Based on SF mapping in this corner of 93M (Figure 15), it appears that ice or water from somewhere north of the study area split and flowed south down the Kispiox River and also flowed southeast into and along the Babine River valley. The southwest-oriented SF along the Skeena River are interpreted here as being formed by flow related to the dominant southeast flow found

in the eastern half of 93M, *i.e.* the generally south-trending SF in both the eastern and western parts of 93M are spatially connected.

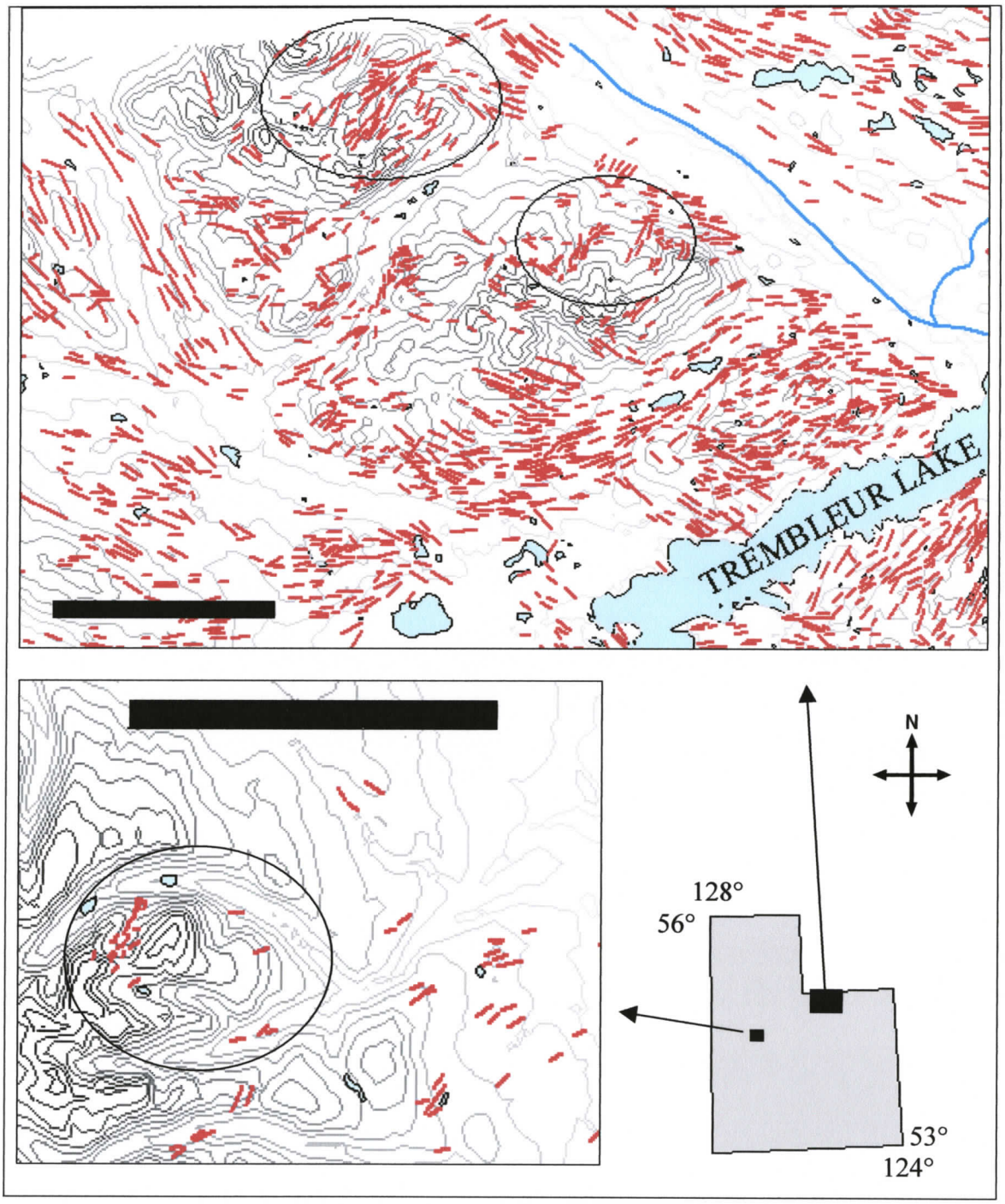

Figure 33. Northeast trending SF emanating from cirques (circled). Top map shows SF in the Hogem Ranges. Left bottom map shows SF in the Telkwa Range. Scale bars = 10 km.

It is not clear whether all south-trending SF in NTS 93M formed during the same ice advance and/or meltwater flood. However, it is possible that these generally south-trending SF were formed at about the same time.

However, ice flow indication data in the eastern parts of NTS 93M and NTS 93L are interpreted by Stumpf *et al.* (2000) as indicating two southeast ice flow events, one during advance and one during retreat, separated in time by ice divide-driven flow towards the west. Thus, it is possible that the SF in the Kispiox and Skeena river valleys were not formed by the same event(s) that created the southeast-trending forms in the east part of NTS 93M. Some field studies indicate more complex flow history in the study area than is observed in this remote imaging study (Stumpf *et al.*, 2000; Ferbey and Levson, 2001; Ferbey, 2004). Remote imaging is clearly limited at discerning relationships between site-scale glacial features that allow deduction of complex flow orders. Remote imaging cannot replace field investigations. Nonetheless, remote imaging allows the analysis of large areas relatively quickly and provides a "large view" of glacial flow. An efficient method for studying glacial flow would be to use DEM and satellite imaging combined with air photo interpretation and field investigation.

2.5.2. Source areas based on principle flow directions

Streamlined forms were probably formed by glacial ice, meltwater floods, or a combination of the two processes. The three principle flow directions of study area SF suggest locations for a driving water or ice surface. The source of ice or water that

formed the southeast-trending forms was located north of the study area. The Skeena Mountains are a probable location for that source (Ryder and Maynard, 1991; Stumpf *et al.*, 2000; this study). Most southeast flow indications on Figure 15 occur in lowlands or valleys. Some exceptions are noted, for example, in the Hogem Ranges in northwest NTS 93K (Figures 3 and 15).

The southeast part of the study area is dominated by east-northeast flow. The Coast Mountains are one possible source for this flow (Figures 3, 15, and 27) (Stumpf *et al.*, 2000, Ferbey and Levson, 2001; Ferbey, 2004; this study). Another possible source is an ice divide located in the east part of NTS 93E, running north-south approximately along the Quanchas Range (Stumpf *et al.,* 2000) (Figure 3).

Uphill west flow indications are found in this study on peaks on either side of the Bulkley River valley (Chapter 5). This field evidence supports the interpretation of SF mapped in the Telkwa River and Morice River valleys as west-trending SF. These SF indicate west flow up valleys located west of the Bulkley River, a finding also reported by Clague (1984) and Stumpf *et al.* (2000).

A source for this westward flow is not apparent from Figure 15. Field evidence presented in Chapter 5 shows that a driving head for streamlining flow must have existed at an elevation exceeding 1680 m somewhere east of Dome Mountain, a peak located just east of the Bulkley Valley (Chapter 5). These field data are discussed in more detail later. Stumpf *et al.* (2000) postulate a generally north-south ice divide crossed the study area at the last glacial maximum resulting in west flow towards the Coast Mountains and Hazelton Mountains. If ice is the forming mechanism for SF, then this study supports the idea of such an ice divide in principle. However, the location of

the ice divide as presented by Stumpf *et al.* (2000) is not entirely supported by SF paths shown on Figure 15. Stumpf *et al.*(2000) suggest an ice divide that runs approximately north-south along the ridge of the Quanchas Range (Figure 3). Figure 15 indicates SF flow paths that appear to be continuous across the Quanchas Range ridge; that is, there is no apparent division of east and west flows along the ridge based on remote imaging.

2.5.3. Causes of low streamlined forms densities in valleys and lowlands

Low densities of SF are often associated with lowlands and valleys in the study area. Lakes fill many of these lowlands and whether SF occur on the lake bottoms is unknown. However, in several locations SF fields occur up to lake margins, for example, along the south shores of Intata Reach, Cheslaslie Arm, and Euchu Reach in NTS 93F (Figure 15). It is likely that fields of streamlined forms extend across at least part of the lake bottoms in these areas.

A difference in SF density in NTS 93F is apparent by observation of Figure 15. If 93F is divided by a line drawn from the southwest to northeast corner, the southeast half has fewer SF than the northwest half. The lower density could be associated with different glacial environments in the two diagonal halves. The different environments are indicated by a greater occurrence of glaciofluvial, ice contact sediments in the southeast part of 93F (Plouffe *et al.*, 2004).

Low SF densities in NTS 93K are similarly associated with lowlands containing glaciofluvial deposits (Figure 30). Low SF densities in 93K are also related to lowlands containing glaciolacustrine and fluvial deposits (Figure 30). Low densities in areas of glaciolacustrine deposition are inferred here to be a result of masking of SF by glacial

lake deposition that occurred after SF formation. Low densities in areas dominated by fluvial sediments are possibly due to the removal of SF by high-energy meltwater flows.

Some areas of low SF density in NTS 93K are located where thick till, till blankets, and/or till veneers are the dominant surficial deposit. Although these upland areas are covered by till (Plouffe, 2000), significant glaciofluvial deposits are located in adjacent lowlands (Figure 34). This spatial association is similar to that discussed above for NTS 93F. It is suggested here that low SF densities in some parts of 93F and 93K are due to the association of the low density areas with relatively higher-energy fluvial or glaciofluvial settings.

If SF are the product of glacial meltwater floods, then low densities of SF could be related to the higher energy parts of meltwater flows. Higher SF densities would be found in lower energy flood areas. The idea here is that if meltwater flow velocities are too high and/or the flow is overly turbulent, then possibly drumlins will not form. It is reasonable to suppose that there would exist both an upper and lower limit on flow velocity favouring the formation of drumlins. There is some support for this supposition based on studies of subaerial glacial spillway channels in the northern Great Plains (Kehew and Lord, 1986). Longitudinal grooves are found along some of the outer zones of these glacial spillways, but not in the deeper inner channels. Given sufficient duration of flow, groups of parallel longitudinal grooves could develop into fluting assemblages and/or drumlin fields.

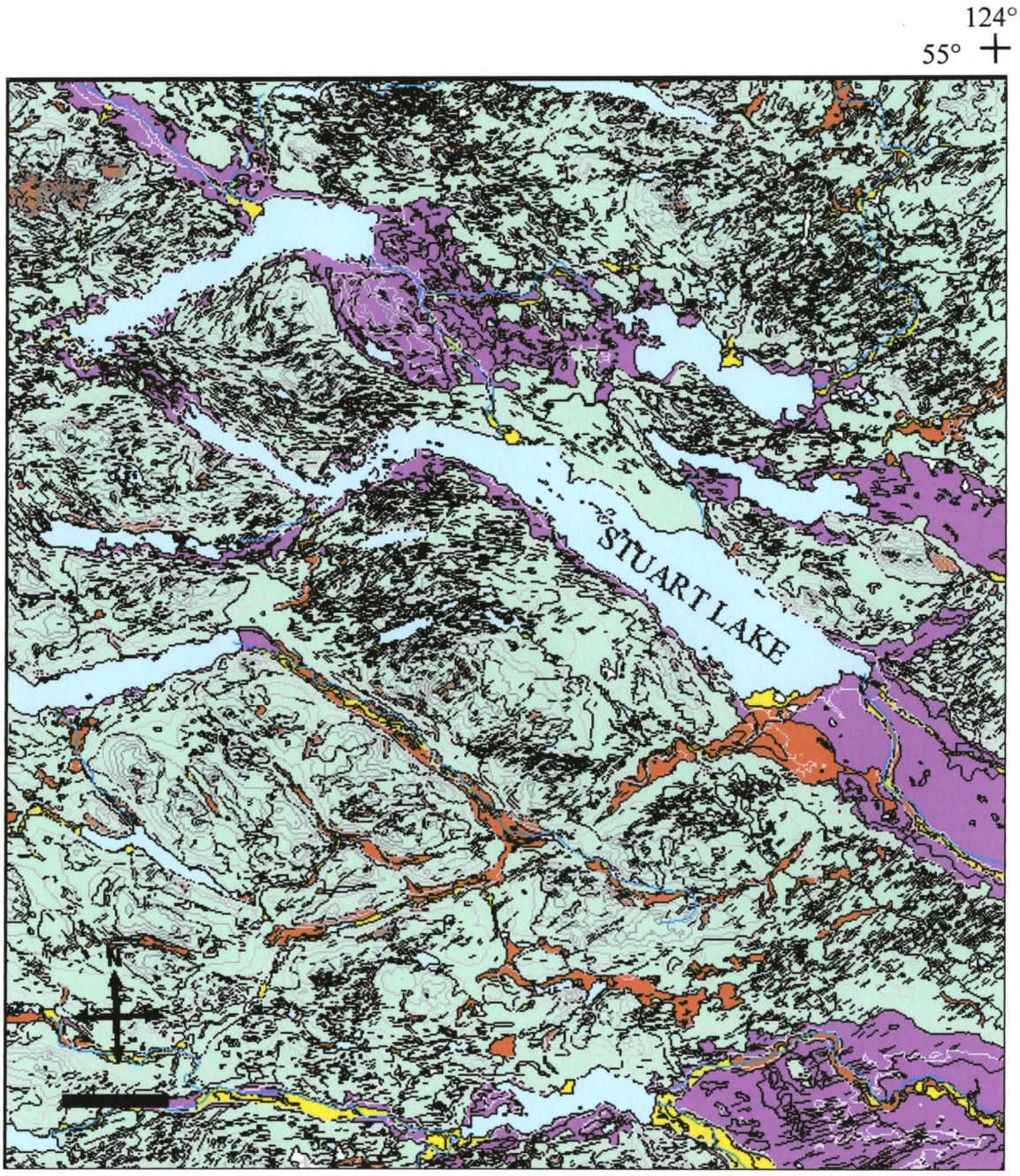

Figure 34. Streamlined forms (black lines) and surficial geology in NTS 93K. Streamlined forms density is less in the southern half of the map. Glaciofluvial (orange) and fluvial (yellow) deposits are greater in the southern half of the map. Till is pale green and glaciolacustrine sediments are purple. Surficial geology from Plouffe (2000). Scale bar is 10 km long.

Areas of low SF densities in NTS 93L and NTS 93M are presented above. Areas of interest are the broad lowlands, particularly the Bulkley, upper Skeena, and Telkwa River valleys. Pervasive glaciolacustrine (LG) deposition, like that found in eastern NTS 93K, is not present in these areas, although LG sediments are found in the Bulkley Valley (Clague, 1984). Glaciolacustrine sediments were observed during this study about 10 km up the Morice River valley from the Bulkley River and about 1 km north of the confluence of the Telkwa and Bulkley Rivers. In both cases, the LG strata are exposed by road cuts and are overlain by diamicton.

Several explanations for the lack of SF in these valleys are possible. Streamlined forms may have been removed by high energy meltwater flows; glacial lakes may have been in place in these valleys during streamlining events; the valleys may have been ice-filled during formation of SF; subsequent till deposition by stagnating ice may have covered existing SF; streamlining flow down or up these valleys may have been blocked; and/or flowing ice may have planed down most pre-existing SF. Conditions either were not favourable for producing SF during glaciation and/or existing SF were removed or covered.

2.5.4. Orientations of valleys and streamlined forms

Streamlined forms follow curving paths parallel to and along some study area valleys and lowlands. Streamlined forms also cross some valleys. Areas where large fields of SF run oblique to significant valleys or lowlands are described above. In most of these cases, the SF are bearing east or northeast and cross southeast-trending valleys (Figure 15). In a few cases, southeast-trending SF run up to east-trending valleys.

Streamlined forms follow the curve of Ootsa Lake around the north side of the Quanchas Range (Figures 3 and 15). Orientations change from NE to E. East of the Quanchas Range, the SF north of Ootsa Lake no longer follow Ootsa Lake, which is oriented southeast at this point, and the SF bear ENE. The flow path merges with the ENE flow path that emanates from the east and southeast sides of the Quanchas Range, the same SF flow path that obliquely crosses the east end of Ootsa Lake and Intata Reach.

This relationship implies that the valley holding Ootsa Lake was formed prior to the event that formed the ENE-trending SF in NTS 93E and NTS 93L. If the Ootsa Lake valley was a consequence of the same flow that formed the SF, then it would be expected that the SF would follow the Ootsa Lake valley along its entire length. This is not the case, and SF parallel the west end of Ootsa Lake and cross the east end of Ootsa Lake. Ootsa Lake is interpreted here as a pre-existing lowland that acted as a conduit for SF-producing flow. The driving force behind the SF flow was primarily directed towards the ENE. Deviations from that course are due to deflection around topographic highs.

An alternative explanation to that given above is that the SF that follow Ootsa Lake and those that cross the eastern part of Ootsa Lake were formed at two different times. Valley-parallel SF and the Ootsa Lake lowland could have formed during topographically controlled flow. Subsequently, SF that cross Ootsa Lake could have formed during a larger scale ice or meltwater flow that acted independently of topography.

Similar topographic deflection is observed in curving flow paths that trend up valley in the Coast Mountains and Hazelton Ranges (Figures 3 and 15). Main valleys where this occurs are the Morice River valley, northeast-draining valleys located about 30 km north of Morice Lake, the Telkwa River valley, and the valleys located due west of Hudson Bay Mountain (Figure 15). Field evidence presented in Chapter 5 confirms uphill flow at elevations exceeding 1600 m in the Hazelton and Babine Ranges on both sides of the Bulkley River valley. Other work has documented uphill flow indicators in the Tahtsa Reach and Tahtsa Lake areas of NTS 93E, which are also in the Coast Mountains (Ferbey and Levson, 2001; Ferbey, 2004). The SF located in these valleys indicate uphill, west flow. The SF follow curving paths up the valleys.

Streamlined forms in NTS 93K are more variable in flow direction than the other parts of the study area (Figures 15 and 27). Valley orientations are also variable. Southeast-northwest and ENE-WSW valleys predominate (Figure 35). Streamlined forms both parallel valleys and run obliquely up to valleys. For example, SF follow a curving path from ENE to ESE around the north end of Stuart Lake, whereas ENE-trending SF are observed on both sides of the SE-flowing Stuart River (Figure 15).

Swarms of SF that are oriented oblique to adjacent SF swarms are apparent in several locations in NTS 93K (Figure 36). Both NE and SE flows are well represented in the northern two-thirds of 93K. This area is interpreted as being the location of merging SE and ENE flow from the Skeena Mountains and Coast Mountains, respectively. The flows may have been contemporaneous during some period of SF formation.

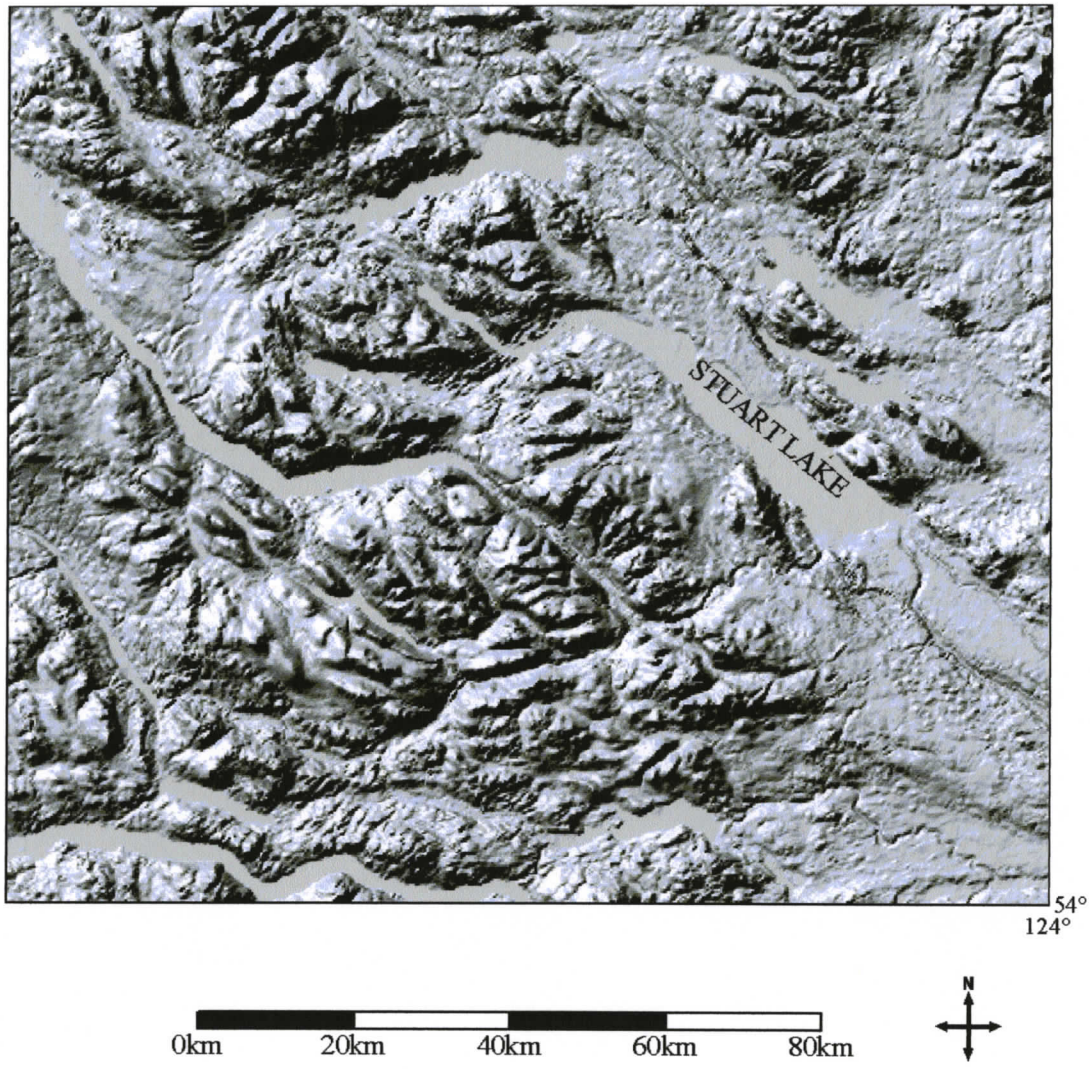

Figure 35. Shaded relief image of NTS 93K. Note prevalent northeast and southeast trending valleys and lakes in northern two-thirds of the map sheet, corresponding to two of the dominant flow directions in study area. Contour intervals = 50 m.

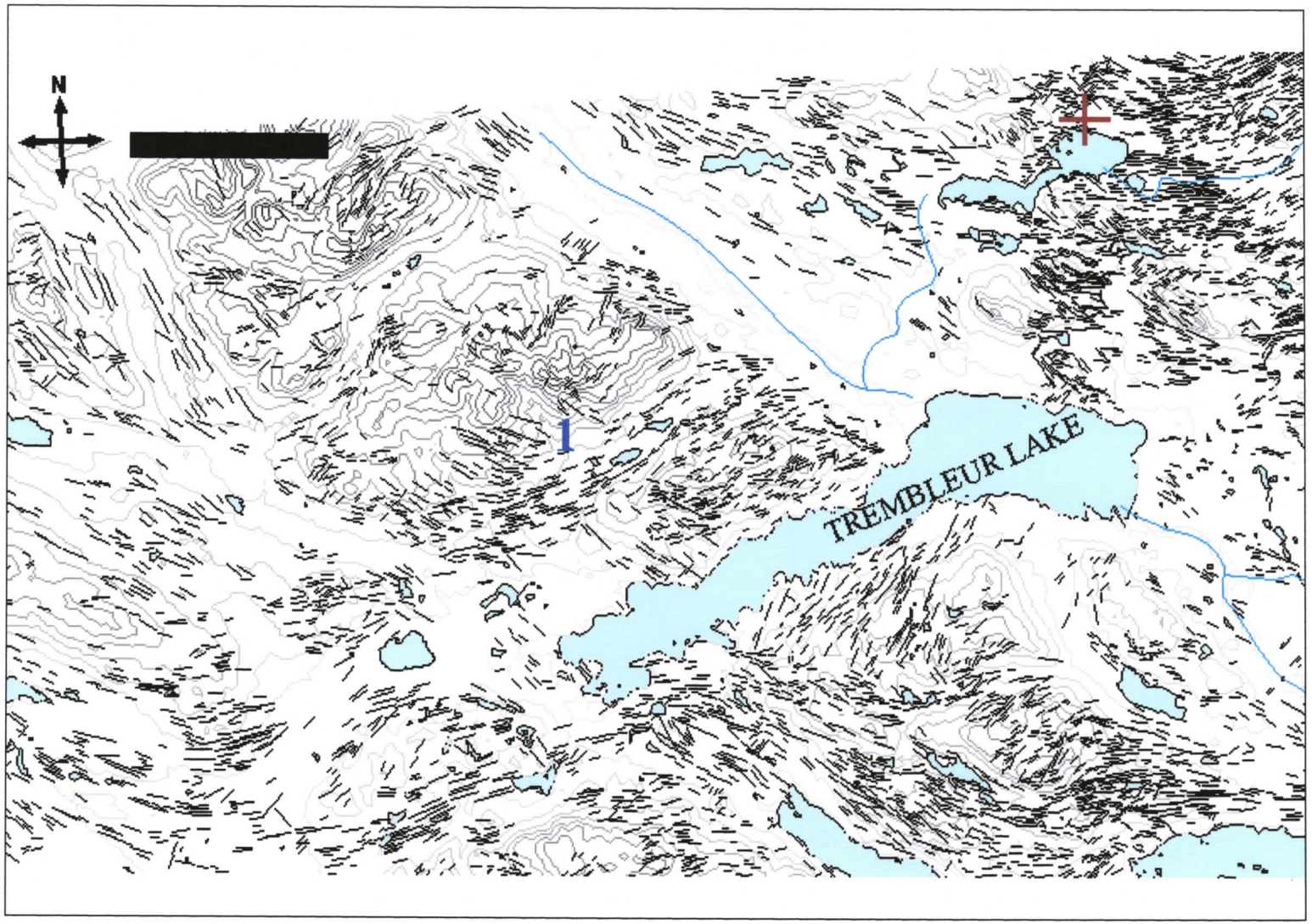

Figure 36. Streamlined forms in northern part of NTS 93K. ENE-trending forms cross-cut SE-trending SF at loction 1. Scale bar = 10 km. Red cross is located at about 125°W and 55°N.

Neither flow is dominant in the central part of NTS 93K; however, east-northeast flow dominates the southern and northeastern parts of 93K. Streamlined forms cross-cut SE-trending valleys in the southern and northeastern parts of 93K; therefore, streamlined forms-producing flow is interpreted as occurring after the formation of the southeast-trending valleys in these areas.

Plouffe (2000) proposed that east flow across the north part of NTS 93K was deflected to the north by flow from the Cariboo Mountains, southeast of the study area. In the western part of 93K, it can be seen that southeast and east flows are deflected towards the east and northeast, respectively (Figures 15, 36). It is possible that this deflection is due to convergence with the ENE flow that comes from the Coast Mountains. Thus, flows from both the Coast and Cariboo mountains may have deflected southeast and east-trending flows in 93K. This would suggest the possibility that southeast flow from the Stikine Mountains, ENE flow from the Coast Mountains, and northward flow from the Cariboo Mountains may have at some time been simultaneous.

Upland southeast-directed SF are apparently cross-cut in some locations in 93K by SF swarms trending east or east-northeast along lowlands (Figures 15, 36). This cross-cutting relationship is not apparent on surficial geology mapping in the region (*e.g.* Plouffe, 2000). A possible explanation for this, as previously mentioned, is that SE-trending forms shown on Figures 15 and 36 are often structurally controlled. Flow deflection of such forms would perhaps not be apparent. Another possibility is that east-northeast flow may have persisted, at least in some locations, after southeast flow

ended. In either case, deflection of southeast and east flows by simultaneous northeasterly flows is still possible.

2.5.5. Streamlined forms and cirques

Streamlined forms that emanate from cirques are observed in NTS 93K in the Hogem Ranges and NTS 93L in the Telkwa Ranges (Figures 3, 33, and 37). The cirques open towards the northeast. The simplest explanation for these forms is that they were produced by alpine glaciers located in the cirque valleys. This interpretation favours an ice origin for these SF. Cirque flow would have occurred during glacial advance and possibly during retreat.

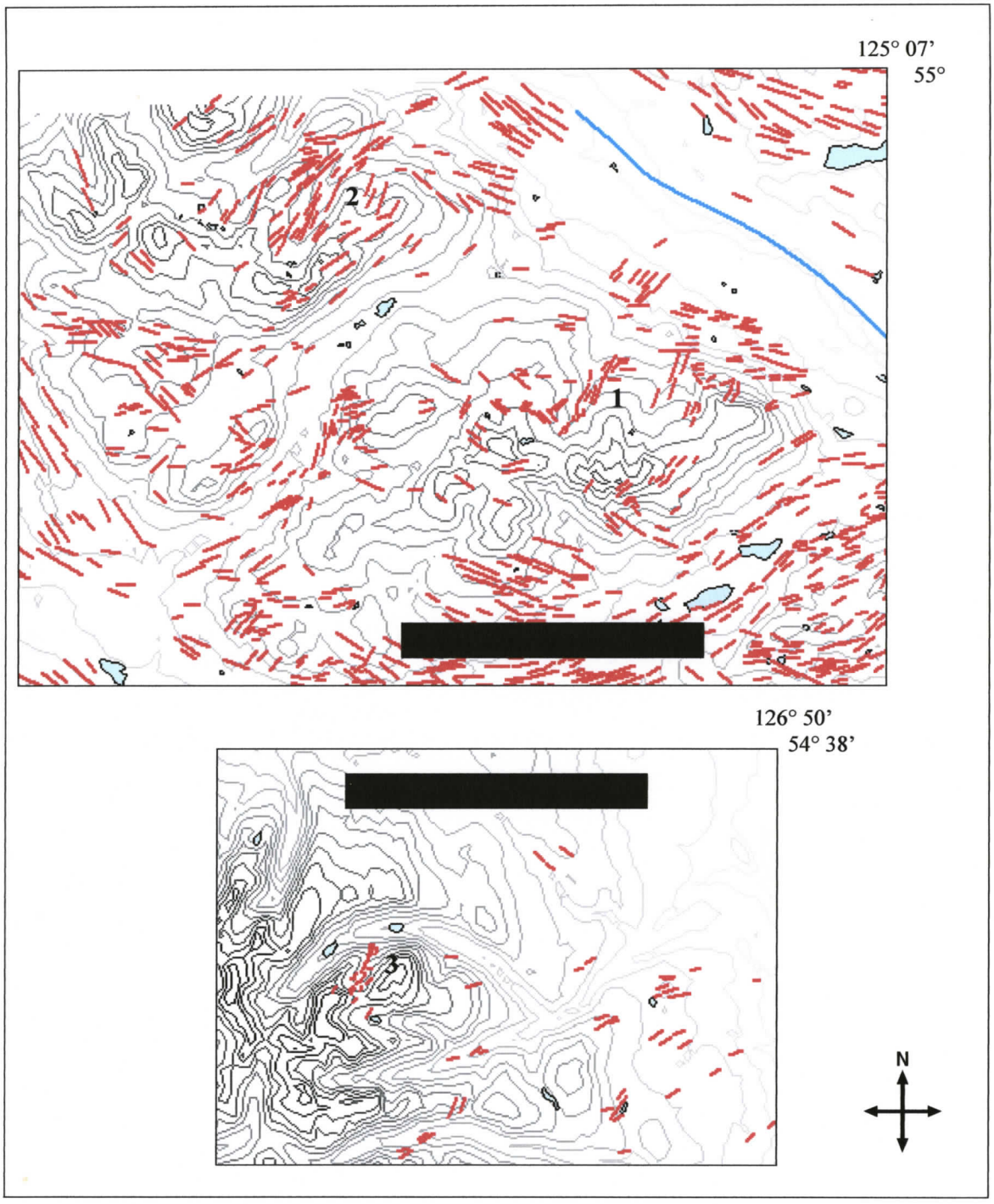

Figure 37. Streamlined forms emanating from cirque valleys in NTS 93K (top) and NTS 93L (bottom). Locations of SF paths emanating from cirques are indicated by numbers 1-3. Scale bar = 10 km.

3. STATISTICAL ANALYSES

3.1. INTRODUCTION

Data from streamlined forms mapping are used in this chapter to analyze the statistical relationship between various terrain attributes and streamlined forms (SF) properties. The terrain attributes included in the analyses are geographic location, elevation, and slope; the SF properties that are tested are density of occurrence, length, and bearing deviation.

The purpose of the statistical tests is to determine if terrain attributes can be statistically related to SF properties and to make inferences about the SF-forming mechanism based on the test results. If terrain attributes have no or little correlation with SF properties, then SF properties are more likely related to regional-scale flow processes than to local terrain effects. If terrain attributes have pervasive, measurable relationships with SF properties, then these relationships can be compared to effects that would be predicted due to either ice or water as a formative mechanism.

Several hypotheses are formulated here to define the nature of the mechanism that created study area SF; the main objective of these tests is to differentiate between characteristics that could be attributable to water versus those attributable to ice. Some observations are made that are not directly relevant to the main question of SF origins attempted by this thesis; however, information about the nature of the SF-producing flow is still gained. Hypotheses are testable using the statistical data analyses methods developed in this study and the SF data set presented in Chapter 2.

A main objective of this aspect of the study is to develop computer-driven methodologies for automating complex analyses of large databases. Computer processing is necessary due to the large SF database size produced and investigated in this study.

The previous chapter discusses areas of low SF density that are observed on Figure 15. Density statistics are used in this chapter to quantitatively confirm these visually observed low density areas. Some areas of low density are associated with lowlands and valleys. The timing of valley / channel formation versus SF formation is addressed by the hypothesis: major valleys were formed prior to the formation of major fields of streamlined forms. This hypothesis is tested using density statistics and analysis of the effects of elevation and slope on SF bearing deviation.

Water and ice would be expected to behave differently on downhill slopes in some situations. Ice would tend to accelerate on downhill slopes. Downhill unconfined water flow could also accelerate; however, subglacial water velocity would vary depending on the distance between the ice roof and the ground surface. This velocity variation is discussed later. The following hypothesis is tested by statistically analyzing the effect of terrain slope, relative to flow direction, on SF length: If streamlined forms were formed by ice or unconfined water flows, then SF on moderate down slopes will be longer than SF on more horizontal surfaces.

Visual examination of Figure 15 indicates regional-scale SF flow paths that are tens of kilometres wide. This observation is quantitatively tested by the hypothesis: Flows that formed most mapped SF were thick/deep and of regional scale; streamlined forms were not formed by a number of small scale local events. This hypothesis is

indirectly relevant to the question of SF origins. The meltwater hypothesis addressed here for SF origins specifies large, regional-scale flow(s). An ice mechanism for streamlined form creation does not necessarily require regional-scale flow; that is, ice lobes could have been active at different times in different local areas. It is possible that SF were formed by a number of local events that occurred at different locations at different times If numerical analyses falsify the hypothesis, then an ice origin for SF is supported. The hypothesis is tested by analyzing variation in SF size across the study area and across elevation. The relevance of these SF characteristics to scale of flow is discussed.

3.2. PREVIOUS STREAMLINED FORMS NUMERICAL ANALYSES

Previous studies of streamlined form morphometry generally include a compilation of SF locations, dimensions, and/or orientations and visual or numerical analyses of these variables (Doornkampf and King, 1971; Jauhiainen , 1975; Mills, 1980; Evans, 1987; Mills, 1987; Boyce and Eyles, 1991; Francek, 1991; Clark and Wilson, 1994; Hattestrand *et al.,* 1999; Stokes and Clark, 2002; Rattas and Piotrowski, 2003). Dimensions evaluated include SF length, width, height, the distance of the SF apex from one of the ends, and/or the distance between the widest part of the SF and one of the ends. Various ratios of measured dimensions may be employed in the analysis, the most common being length-to-width which characterizes SF elongation. Streamlined forms lengths are the only dimension included in some morphometry studies (Clark and Wilson, 1994; Hattestrand *et al.*, 1999). This simplifies data collection and facilitates analysis of large groups of lineaments. On the other hand,

Evans (1987) introduced analysis of a high level of morphometric complexity using terrain attributes (altitude, gradient, aspect, vertical curvature, contour curvature) for points spaced 50 m apart on just seven SF.

Streamlined form morphometric studies have been used by several authors to classify and compare SF shapes and spatial arrangements in order to make inferences about SF origins and flow behaviour (*e.g.*, Harry and Trenhaile, 1987; Mills, 1987; Stokes and Clark, 2002). Comparisons of SF shapes and sizes may be compared within a single SF field, or across two or more SF fields. Statistical differences in dimensions among SF can be detected using the Student's t-test (Doornkampf and King, 1971; Francek, 1991) or analysis of variance (ANOVA) (Doornkampf and King, 1971; Jauhiainen, 1975). Nearest neighbour analysis is used to indicate distribution patterns (Jauhiainen, 1975; Harry and Trenhaile, 1987; Francek, 1991; Clark and Wilson, 1994). Other statistical tests including correlation are also employed (Mills, 1980; Evans, 1987; Mills, 1987).

3.3. METHODS

Streamlined forms properties are from the database produced during the SF mapping (Chapter 2). A Universal Transverse Mercator (UTM) projection is used for mapping. Streamlined form coordinates are expressed in metres. Data sets containing the SF coordinates are contained in text files exported from Didger, the software used for digitizing (Chapter 2, Methods). An Excel Visual Basic for Applications (VBA) program (all VBA programs mentioned in this dissertation were written by the author) imports the SF data into an Excel spreadsheet, and computes SF lengths, strikes, and,

where flow directions are known, bearings. Streamlined forms are mapped (Chapter 2) as single lines instead of as shapes or intersecting axes to allow collection of more data and study of a larger area. Large-scale data collection facilitates the analysis of large-scale variations and region-wide spatial arrangement.

Streamlined forms density is determined using a VBA program that divides the study area into 2-km squares, locates SF whose midpoints are within each square, and calculates a density value for each square. A grid is generated from this data using Surfer software, allowing the density data to be depicted as a contour map.

Elevation is determined for each SF using a VBA program that accesses Surfer software's grid operation methods. The Surfer GridSlice function outputs elevations for all grid intersection points for a given SF line. Each SF elevation is calculated as an average of all output elevations for that SF.

DEM grids for each NTS map sheet contain approximately 25 million nodes. In order to calculate average study area elevation, DEM grids are "recalculated" using Surfer to 1% of the original size. As explained by Surfer documentation (Golden Software, Inc., 1999):

> "When the grid is recalculated, all the grid nodes in the smoothed grid are completely recalculated. This option can either increase or decrease the number of rows and columns in the smoothed grid relative to the original grid. The original grid values are lost unless their locations correspond exactly with the grid nodes in the output grid. The smoothed grid file will still be an accurate representation of the original data." (Surfer help topic: Gridding | Smoothing Grids | Recalculating a Grid)

Surfer recalculation is utilized as a tool to perform initial averaging of the grid file and to reduce the exported grid data to a manageable file size. After recalculation, the resulting grid files are exported into text files consisting of latitude and longitude UTM

coordinates and elevation. The text files are imported into Excel, and average elevations are obtained.

Slope is determined using VBA access of a Surfer GridCalculus method. The amount of slope in the direction of flow is determined for an extracted DEM grid slightly larger than and completely surrounding each SF. This "area of influence" is defined as a rectangle that exceeds the minimum and maximum x and y values of the SF by a buffer value, the buffer being equal to 1/10 of the SF length (Figure 38). The buffer size is intentionally small in order to measure the slope of the local area immediately surrounding the SF; the intent is to test the local effect of slope on each SF. The slope is returned as rise over run, negative values indicating downhill flow.

"Uphill" or "downhill" slope is relative to the direction of movement. In order to use an automated procedure effective over a wide area, it is necessary that the flow direction be known over the entire area to which the procedure is applied. For this reason, the programmatic slope determination methods developed here are restricted to regional-scale areas with known flow directions across the region. This restriction is discussed more in the relevant subsection of this chapter.

A "moving squares" VBA program was written to allow the testing of smaller area squares across the larger study area. The program builds a set of defining coordinates for a series of squares of specified size. It finds the midpoints of SF which fit within each square and performs mathematical operations on the SF data of that square. ANOVA is run on each square's data and/or on a data set compiled from all the squares. In the first case, data are compiled and analyzed square-by-square. In the second case, the squares serve as bins from which data are collected for a single

statistical analysis. ANOVA, frequency histograms, and descriptive statistics are obtained using Excel data analysis tools.

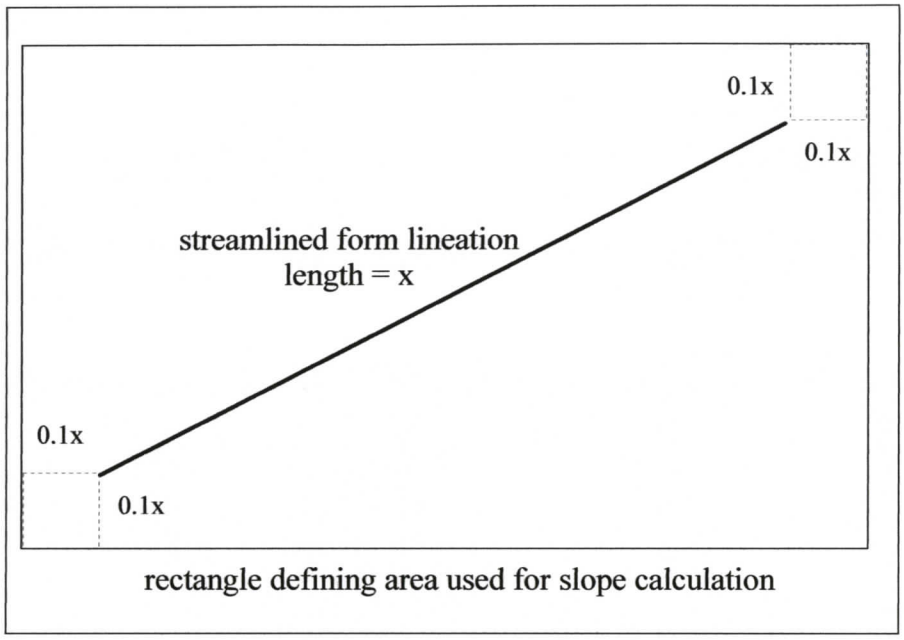

Figure 38. Derivation of rectangle used for computing local terrain slope for a SF.

In statistical terms, ANOVA allows the comparison of variance between samples, due to treatment, and variance within samples, due to inherent variation (experimental error) (Neville and Kennedy, 1968). An example of "treatment", in the context of the methods developed here, is the effect of landscape attributes, *e.g.* elevation, on SF characteristics, *e.g.* length. The variances are compared using the 'F test'. The calculated F-value is the sample variance (mean square treatment) divided by

the inherent variance (mean square error). An F-critical value is known for the given ANOVA probability level, the P-value. $P < 0.05$ is used in this thesis, meaning that if F-calculated exceeds F-critical, there is less than 5% probability that the null hypothesis is true. The null hypothesis is that there is no effect due to treatment. If the calculated F exceeds the critical F for the given probability, then the alternative hypothesis is accepted, that is, there is an effect due to the treatment.

In non-statistical terms relevant to this study, ANOVA allows a statement to be made as to whether a given landscape attribute (*e.g.*, slope, elevation) affected a SF characteristic (*e.g.*, length, orientation). ANOVA essentially measures differences in the SF characteristics relative to the landscape attributes. If the F-calculated value exceeds the F-critical value, then there is a 95% probability (with a P-value < 0.05) that the given SF characteristic is related to the landscape attribute being tested. There is an "effect" due to the landscape attribute.

3.3.1. Geographic areas for different analyses

The statistical analyses presented here require data sets that can be analyzed using automated computer methods. The geographic areas used for the statistical analyses vary depending on the type of analysis. Analyses that require known flow directions are restricted to those areas from which flow directions can be obtained automatically using the computer methods developed here.

NTS map areas 93F and 93K comprise most of the plateau portion of the study area (Figure 2 and Figure 3). NTS map areas 93E, 93L, and 93M include extensive mountainous areas. In the study area, dominant flow directions on the plateau are

almost all towards the southeast, east or northeast (Plouffe, 2000; Stumpf *et al.*, 2000; Levson, 2002; Plouffe *et al.*, 2004; this study). This characteristic allows directionless SF strikes, derived from the database, to be programmatically converted to directional bearings. For example, the database may record a SF strike of 45°. In an area with less well known flow directions, that strike could be interpreted as a bearing of 45° or 225°. Since orientations in the eastern half of the study area are all generally towards the northeast, east, or southeast, then all strikes can be assumed to represent bearings between 0-180°. The plateau region, represented by eastern map areas NTS 93F and NTS 93K, is thus suited to analyses that require known flow direction.

On the other hand, streamlined forms created by both westward and eastward flows are common in the mountainous western half of the study area (Levson *et al.*, 1998; Mate, 2000; Stumpf *et al.*, 2000; Ferbey and Levson, 2001; Levson and Mate, 2002; this study) Automated, programmatic conversion of SF strikes to bearings is not possible in this area using thesis methodologies. Consequently, analyses requiring known flow directions are restricted to the eastern half of the study area.

Analyses that are not directionally dependent are applied to the entire study area. These analyses include descriptive statistics on SF density, elevation, and length. Streamlined form frequency relative to elevation is graphically compared to study area elevation. The effect of elevation on SF length is tested.

Slope mode, uphill or downhill, is a terrain attribute that is directionally dependent. The same section of ground can be defined as uphill, downhill, or level depending on the direction of movement across the ground. Since slope determination depends on known flow direction, then only SF in the eastern half of the study area are

tested using slope statistics. The statistical effects of slope on SF frequency and on SF length are tested.

The detection of differences in bearing deviation caused by local terrain effects requires testing of local variation within a larger region with minimal bearing deviation; otherwise, local terrain effects are likely to be masked by regional effects. Computation of bearing statistics also requires known flow directions. The southeast portion of the study area shows little regional-scale bearing deviation and flow directions are known. Almost all SF are in northeast-trending flow paths. The southeast part of the study area is conveniently represented by the NTS 93F map area; hence, SF in 93F are tested for the effects of elevation and slope on bearing deviation.

Differences in SF lengths due to elevation are analyzed at the local scale. This is accomplished by dividing the target area into smaller squares. The square size is varied for specific runs. Streamlined forms in each smaller square are tested for the effect of elevation on length.

Differences in SF lengths due to slope are also analyzed at the local scale using the same method. The target area is divided into smaller squares of specified size. Slope measurements require known flow directions; hence, the target area is the eastern half of the study area. The effect of slope on SF length is also tested at a regional scale using the SF data for the eastern half of the study area.

3.3.2. Quality control of database and analyses

Elevation, length, strike, and slope values of SF are calculated within the analyses programs. In order to check these calculations, five to twenty SF were randomly

selected from the database for each type of automated calculation. Each selected SF was located on a digital version of Figure 15, the SF map. The elevation, length, strike, and slope of the located SF were measured by observation and "manual" calculations. The strike of a given SF was measured with a protractor, its elevation was measured using topographic contours, slope was calculated from the topographic contours, and length was measured using GIS software. These "check" values verify the accuracy of the program calculations. All manually checked values corresponded to computer-derived values.

Descriptive statistics were cross-checked by importing SF data into an Excel worksheet. Streamlined forms means and counts were determined using both the Analysis Toolpack (an Excel addin providing numerical analysis functions) and using manual Excel formulas and functions. Streamlined forms density contours were compared visually to SF concentrations observable on the main SF map (Figure 15).

ANOVA results were spot checked by calculating treatment effects by two different methods. Excel provides ANOVA functionality using the Analysis Toolpack which comes packaged with Excel 2000. ANOVA is also possible using spreadsheet formulas. All ANOVA used in the research methodologies uses the Analysis Toolpack; however, to cross check the results of the Toolpack, spreadsheet ANOVA solutions were constructed. Random ANOVA calculations were performed using both methods in order to verify the Toolpack results.

Random sample squares were spot checked to see if the SF being assigned to that square by the moving square program were indeed within the square. The properties of the SF in the checked squares were also verified.

3.4. RESULTS AND DISCUSSION

The following subsections present results of the statistical analyses. Some discussion of the results are presented within each subsection. The final section of this chapter is a summary of these discussions relative to the hypotheses set forward in the chapter introduction.

3.4.1. Average topographic elevation by map sheet

Average elevation is determined using elevation data from recalculated DEM grids as explained in the Methods section. The lowest average elevation is in the northeast corner of the study area (Table 1 and Figure 39). About 75% of topographic elevation values, calculated from DEM files, are between 700 and 1200 m (Figure 40).

The northeast corner is also characterized by adjacent, non-parallel groups of SF (Figures 15 and 36). This juxtaposition of northeast- and southeast-oriented swarms of SF indicates that flow paths from the southeast and northeast merged in this area, though NE and SE flows were not necessarily contemperaneous. Northeast flow paths that apparently crossed the Stuart River can be traced up flow to the south-central part of the study area. Some northeast flows in the northern half of NTS 93K may be unrelated to NE flow paths originating further south, and may record change of direction of southeast flow originating from the Skeena Mountains to the north.

Table 1. Streamlined forms counts, lengths, and elevations by NTS sheet						
	93E	**93F**	**93K**	**93L**	**93M**	**All**
Number SF	4383	16686	21008	7024	4344	53445
Average SF elevation (m)	1101	1049	953	1061	870	1003
Average topographic elevation (m)	1124	1038	921	1057	1038	1036
Maximum elevation of 99% of mapped SF (m)	1640	1564	1466	1724	1450	1724
Maximum elevation of mapped SF (m)	2040	1882	1865	1966	1743	2040
Maximum topographic elevation (m)	2757	1932	2007	2758	2582	2758
Average SF length (m)	537	495	488	430	666	501
Minimum SF length (m)	74	83	62	28	89	28
Maximum SF length (m)	3074	3343	6710	2141	4388	6710
Standard deviation of SF length	291	271	288	247	401	294

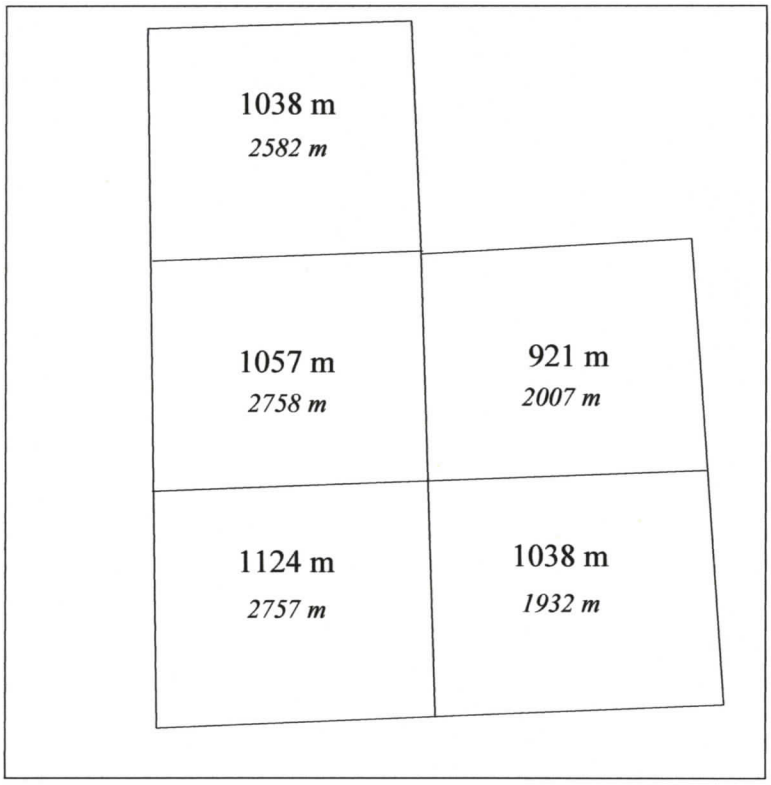

Figure 39. Average and maximum elevations by NTS sheet from DEM grid files. Average values are in normal, larger font; maximum values are in italics.

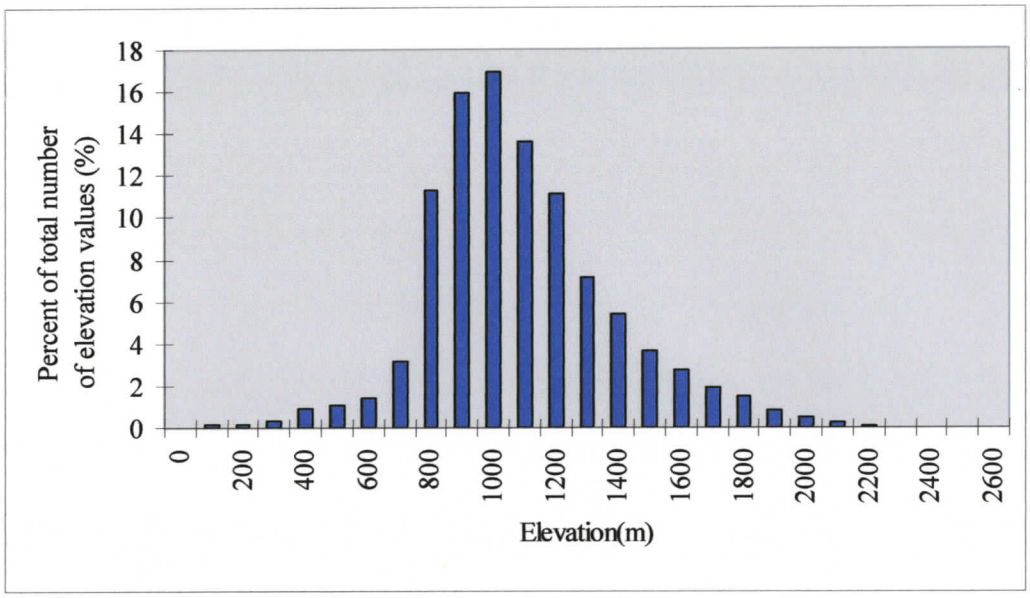

Figure 40. Distribution of point values for recalculated DEM grids for NTS map areas 93E, F, K, L, and M. DEM grids were recalculated using a Surfer grid function to reduce grid sizes to one percent of initial size.

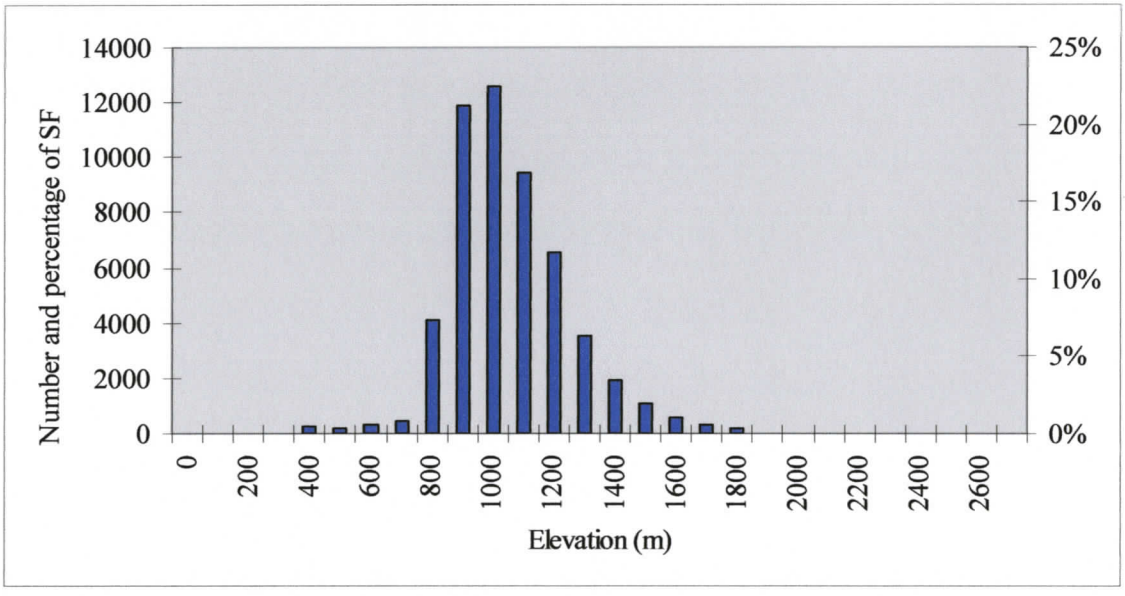

Figure 41. Number of SF within elevation intervals in the study area. Each bar represents the number of SF found between the next lower elevation and the bar's elevation.

The northeast corner of the study area could represent a sink towards which ice or water from the northwest and southwest flowed. If the northeast corner acted as an area of convergence, then the juxtaposition of northeast and southeast forms is explained by this convergence. Alternatively, the relatively lower elevation of the northeast corner of the study area could be a result of possibly more intensive erosion created by contrary flows as compared to erosion resulting from more unidirectional flow. Other factors unrelated to ice or water flow could also account for this relatively lower terrain, for example, the area could represent a downthrown fault block. Existing faults may be covered here by Quaternary sediments (Figures 4 and 6). It is speculated here that the relatively lower elevation is possibly due to a downthrown fault block, and that flow from the west and from the northwest was flowing downhill towards this low area. Horst and graben structures are known to exist in the study area and the northwest corner of the area is partially bounded by major faults (Figure 6). It is reasonable to suppose that flow from the mountains to the west and northwest would flow in a downhill direction.

3.4.2. Streamlined forms distribution by elevation

The average elevation of SF occurrence by NTS map sheet corresponds to the average topographic elevation in all NTS sheets except for 93M (Table 1). However, this correlation does not hold when SF distribution is considered by incremental elevation "bins" (Figure 41). About 75% of mapped SF in the study area occur at elevations between 800 and 1200 m a.s.l. (Figure 41). About 75% of elevation points are found between 700 and 1200 m (Figure 40). However, SF frequency exceeds

elevation frequency between about 850 m and 1250 m elevation and SF frequency is exceeded by elevation frequency in most other elevation bins (Figure 42); *i.e.*, higher percentages of SF are found at intermediate elevations than are found at lower or upper elevations. This relationship suggests some degree of non-random distribution across elevations.

On the other hand, the discrepancies between SF and elevation frequencies may be explained by causes not related to vertical limits of streamlining flow. It can be seen on Figure 42 that SF frequency is exceeded by elevation frequency in the 300 – 800 m elevation range. In the study area, this range corresponds generally to longitudinal lowlands and valleys. The relationship between lowlands and low SF density is noted in the preceding chapter and also discussed later in this chapter in the context of SF density analyses. It is probable that flow that acted at 800 m elevation also affected lower elevations. Lower SF frequencies at these elevations must be related to some factor or factors other than the existence of flow.

Low SF frequencies at higher elevations may be related to lack of diamicton at these elevations. As discussed previously and as observed in field studies during this research (Chapter 5), most SF in the study area are comprised of diamicton. Another possible reason for low densities at higher elevations is size related. Bedrock drumlins and flutings observed at higher elevations (this study) are generally smaller than lowland SF. The remote mapping methods used to collect SF data are not able to detect many of these smaller high altitude SF. Although low till availability and/or non-recognition of small SF may account for lower SF density at higher elevations, there

still appears to be a vertical limit to major SF-producing flow. Ninety-nine percent of mapped SF occur below 1724 m elevation (Table 1).

It is suggested here that the discrepancy between SF and elevation frequency below about 1700 m is probably not due to flow thickness or depth limitations. Streamlined forms were probably formed at all elevations below about 1700 m. The maximum elevation in NTS 93F exceeds the maximum mapped SF elevation by only 50 m (Table 1). Since minimum elevations in 93F are about 600 m, then east-northeast flow in 93F produced SF over almost one kilometre of vertical extent.

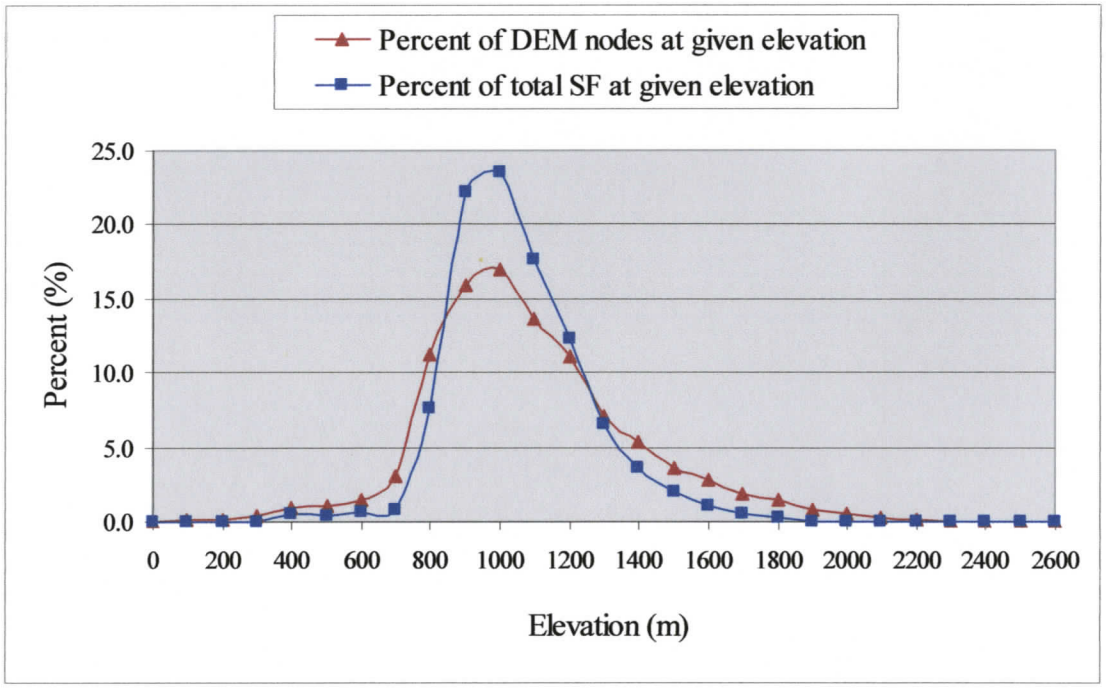

Figure 42. Comparison of SF frequency by elevation and topographic elevation frequency. SF frequency follows same general trend as topographic elevation frequency, but shows a greater percentage of SF between about 850 m and 1250 m elevation than would be expected if SF were randomly distributed across elevation.

3.4.3. Streamlined forms density

Streamlined forms density is defined here as number of SF per square kilometre (SF/km^2) . The area of greatest SF density is the Nechako plateau (Figure 43, Table 1, Figure 3). Comparison of elevation contours with SF density (Figure 43) suggests two patterns of SF occurrence, one for mountainous and one for plateau areas. In the mountainous regions along the western and northern margins of the study area, lowest SF concentrations are associated with upper elevations. Areas of high concentration are found in a number of the principle valleys and on the mid-elevation uplands along these valleys. The main areas of concentration are to the north of Morice Lake in NTS 93E, north and west of Hudson Bay Mountain in NTS 93L, and along the Skeena, Kispiox, and northern Babine valleys in NTS 93M (Figure 15 and Figure 43).

In the plateau region, the lowest concentrations are generally in valleys and the highest concentrations are at mid-elevations. An example of the juxtaposition of high density and low density areas is in the northeast half of NTS 93K (Figure 43). The high concentration of SF in this corner of the study area is disrupted by a broad NW-SE trending lowland that includes the Stuart River and Stuart Lake (Figure 15), and by other NE-SW and NW-SE valleys. The low densities in the northern half of 93K can to some degree be attributed to lakes that may cover SF.

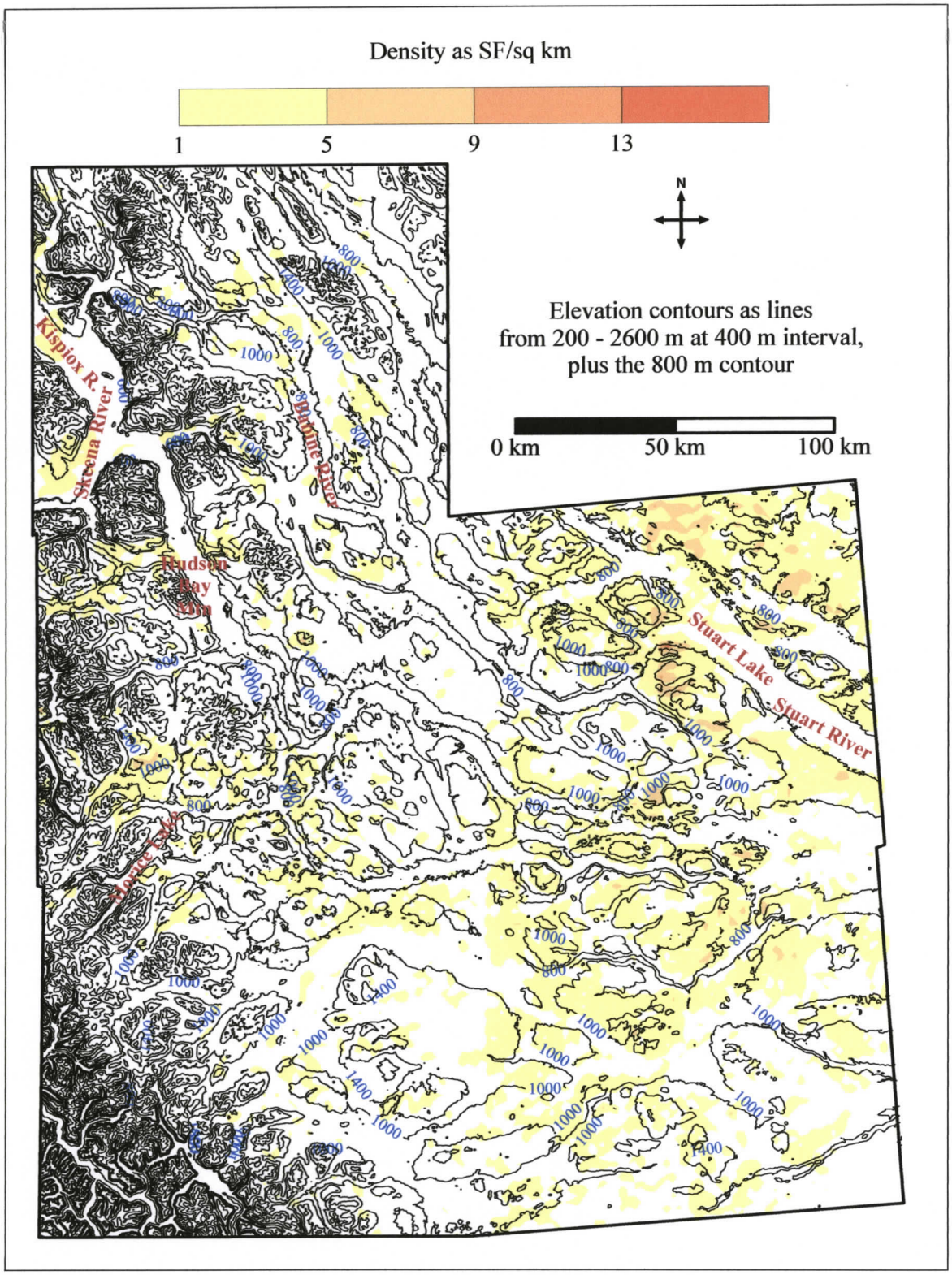

Figure 43. Study area SF density as number of SF per square kilometre. Shaded areas represent SF density values and lines represent elevation contours (see legend).

A reason other than cover by lakes or lake sediments must be used to explain two other broad areas of low density in the plateau region. The NE half of NTS 93K and the NW half of NTS 93F have higher SF concentrations than the SW half of 93K and the SE half of 93F, respectively. This observation is also made in Chapter 2 and is verified here by numerical analysis. The areas of low concentration in both these map sheets are not associated with extensive lakes and lowlands. On the contrary, the areas of lower SF concentration, in both cases, correspond, in a regional sense, to areas with generally greater elevation. This can be seen by comparing the low density areas in 93F and 93K to the elevation contours (Figure 43). The southeast half of 93F has greater elevation than the northwest half of 93F; similarly, the southwest half of 93K has greater elevation than the northeast half of that NTS map area.

3.4.4. Elevation effects

3.4.4.1. Elevation and streamlined form length

The effect of elevation on length is statistically tested over local areas using a moving sample square. The reason for this approach is to isolate local terrain effects on SF length. Streamlined form size variation can be due to a number of factors including variability in sediment thickness across a SF field or relative location within a larger SF field. Boyce and Eyles (1991) noted that larger drumlins are associated with thicker till in the Petersborough drumlin field in central Canada. Stokes and Clark (2002) demonstrated that SF lengths vary depending on location in a large (~500 km by 50 km) SF field northwest of Hudson Bay. The SF flow path includes an area of flow constriction in which SF lengths are greater than in unconstricted parts of the SF field.

Using smaller sample squares within a larger area allows larger-scale effects on SF length to be filtered out. For example, lengths of SF may vary over many tens of kilometres due to convergence and divergence of flow. At a local scale, on the order of kilometres, those regional-scale differences are not perceptible. The use of smaller sample sizes permits the detection of possible local elevation effects on lengths.

The moving square program testing local elevation effect on all SF lengths is run using sample squares that are 2, 5, 10, 20, 30, 40, 50, and 60 km on a side. Following is an example of the general processing during a moving square "run" using a 5 km square size in UTM zone 10:

1. NTS 93F and NTS 93K grids are divided into equal, adjacent squares, each 5 km on a side.
2. For each square:
    a. Lengths and elevations of all SF having midpoints within the squares limits are found.
    b. Streamlined forms are divided into two equal groups based on elevation.
    c. ANOVA is run on the two groups.
3. Results are compiled noting whether a significant difference is found between SF lengths at lower elevation and SF lengths at higher elevations.

Outputs of this analyses include elevation effects on SF length, percentage of significant squares, and SF population in squares (Table 2). The 2 km square size

results in the lowest percentage of populated squares, 50% (Table 2). This lower value is the truest representation of SF distribution since larger square sizes can include large areas in which no SF are mapped. A testable square is one that contains sufficient SF to perform ANOVA; in this particular analysis, at least four SF are required. The percentage of significant squares is calculated with respect to the number of testable squares. Percentages of populated, testable, and significant squares increase with an increase in square size, for example, from just 7% significant 2 km squares to 60% significant 50 km squares (Table 2).

The number of significant squares with longer high or longer low elevation SF is almost evenly divided at square sizes up to 10 km. Larger square sizes show a trend towards more significant squares with longer low elevation SF (Table 2).

Table 2. Effect of elevation on SF length; moving square sampling and ANOVA, $P < 0.05$

Square side length (km)	Percentage of squares with >1 SF	Percentage of testable squares (>3 SF)	Squares with significant results / testable squares	Number squares with longer high elevation SF	Number squares with longer low elevation SF	Percentage squares with longer high elevation SF	Percentage squares with longer low elevation SF
2	50%	26%	7%	188	168	53%	47%
5	74%	62%	14%	147	130	53%	47%
10	85%	81%	22%	63	86	42%	58%
20	88%	88%	40%	27	51	35%	65%
30	97%	96%	50%	15	33	31%	69%
40	98%	98%	51%	5	25	17%	83%
50	97%	97%	60%	5	16	24%	76%
60	100%	100%	60%	4	14	22%	78%

Another moving square program captures local elevation effects by testing only those SF located in the lower elevations of each local square. The purpose of this test is to isolate small relief differences at lower elevations. Square sizes of 5, 10, 20, 30, 40, 50, and 60 km are used. Zones 9 and 10 are processed separately, and the results compiled. An example of the processing on UTM zone 9 for the 40 km square size is as follows:

1. NTS 93E, 93L, and 93M grids (zone 9 grids) are divided into equal, adjacent squares, each 40 km on a side.
2. For each square:
    a. Lengths and elevations of all SF having midpoints within the squares limits are found.
    b. Streamlined forms are divided into eight fractions based on relative elevation.
    c. ANOVA is run on the lowest two fractions, that is, those SF in the lowest elevation interval are compared to those in the next-to-lowest elevation interval.
3. Results are compiled noting whether a significant difference is found in the average lengths of the lower two SF fractions.

Results of this analysis (Table 3) are somewhat different than the analysis of all SF in each square (Table 2). Sixteen SF, instead of four, are needed to comprise a testable square, resulting in somewhat lower numbers of testable squares for the 5 km

and 10 km sample sizes. The percentages of significant squares range from 6% (5 km square) to 33% (60 km square). This reduced significance is also reflected by the results of the ANOVA testing. Although the 10 km square size shows more squares with longer high elevation SF, the 60 km square size has longer low elevation SF. The rest of the square sizes indicate an approximately even split between longer low and high SF.

Table 3. Effect of elevation on SF length; moving square, lower 2/8 fraction sampling, and ANOVA, P < 0.05

Square side length (km)	Percentage of squares with >1 SF	Percentage of testable squares (>15 SF)	Squares with significant results / testable squares	Number squares with longer high elevation SF	Number squares with longer low elevation SF	Percentage squares with longer high elevation SF	Percentage squares with longer low elevation SF
5	74%	36%	6%	30	35	46%	54%
10	85%	68%	9%	34	18	65%	35%
20	88%	85%	19%	20	16	56%	44%
30	97%	95%	18%	10	7	59%	41%
40	98%	97%	22%	7	6	54%	46%
50	97%	97%	29%	6	4	60%	40%
60	100%	100%	33%	3	7	30%	70%

3.4.4.2. Discussion of elevation and streamlined form length

Based on moving squares analysis, elevation does not have an effect on SF length at a local level. A local level is considered here to be represented by 2 – 10 km square sizes in which all SF are tested. Only 7 – 22% of testable squares at this size range are significant, and squares with significant results are split, approximately evenly, between longer SF in upper elevations and longer SF in low areas (Table 2).

The maximum number of significant squares is 33% of testable squares (Table 3). Therefore, no statistical local elevation effect on SF lengths is detected.

A possible significant relationship is found at a sub-regional scale, not at a local scale. Larger square sizes, from 20 – 60 km, in moving square analysis show from 40 – 60 % significant squares (Table 2). About three-quarters of those significant squares (about 3/8 of testable squares) indicate longer low elevation SF. A possible reason for this difference is thicker till at lower elevations.

3.4.4.3. Elevation and bearing deviation

The statistical effect of elevation on bearing deviation is tested using moving sample squares as bins for holding bearing deviation values. For reasons given above, this analysis is restricted to 93F. The test is run using sample square sizes of 5, 10, 15, 20, 25, 30, 35 and 40 km. An example of the processing is as follows:

1. NTS 93F is divided into equal, adjacent squares, each 20 km on a side.
2. For each square:
    a. Bearings and elevations of all SF having midpoints within the squares limits are found.
    b. Streamlined forms are divided into lower, middle, and upper elevation groups.
    c. The standard deviation of the bearing for each elevation group within each sample square is determined.

3. After collection of standard deviation values from all squares, ANOVA is run to determine if there is an effect of elevation on bearing standard deviation.

Significant results are found using 15-30 km square sizes (Table 4). Streamlined forms at lower elevations have greater bearing deviation than those at medium and upper elevations for each significant sample square. Streamlined forms at mid-elevations have less bearing deviation than either upper or lower elevation SF.

Table 4. Elevation effect on bearing deviation, NTS 93F. Bold values are significant results at P < 0.05.

Square size (km)	Standard Deviation			F calculated	F critical
	Low Elevation	Medium Elevation	High Elevation		
5	8.1	7.4	7.7	1.9	3.0
10	10.7	9.3	9.6	3.0	3.0
15	**12.1**	**9.4**	**10.3**	6.3	3.0
20	**12.3**	**10.0**	**10.9**	3.3	3.1
25	**12.6**	**9.9**	**11.4**	3.8	3.1
30	**13.4**	**10.5**	**11.6**	3.4	3.2
35	13.1	11.5	11.9	1.1	3.2
40	13.4	11.3	11.4	1.9	3.3

3.4.4.4. Discussion of elevation and bearing deviation

Significant results for 15-30 km square sizes indicate greater bearing deviation at lower elevations. Although results are not statistically significant, the same trend is noted in other square sizes, that is, lower elevations have greater bearing deviation. One possible explanation for this difference is that more large channels and valleys are

located at lower elevations than at higher elevations. Streamlined forms-producing flow would possibly have been influenced by these large valleys. Flow obliquely crossing a valley would be diverted to orientations more parallel to the valley. Curving SF flow paths along valleys described in Chapter 2 (*e.g.*, Figure 29 and flow paths in the Coast and Hazelton Mountains, Figure 15) support this interpretation.

Cross-cutting valley / SF relationships are observed on Figure 15 and discussed in Chapter 2. Streamlined form / valley relationships are interpreted as indicating the pre-existence of the valleys relative to the development of SF fields. The relationship between bearing deviation and elevation can be interpreted as supporting the inference that many of the major lowlands and valleys were formed prior to SF-producing flow. Another possibility is that low elevation SF formed at a different time than higher elevation SF; the earlier flow event may have been more controlled by topography. This explanation fits with a model of SF formed at different times during the growth of an ice sheet.

3.4.5. Slope effects

3.4.5.1. Slope and streamlined form frequency

The effect of slope on SF frequency is determined using four slope bins. Streamlined forms are divided into four categories: those on moderate and gentle uphill slopes, and those on gentle and moderate downhill slopes. The slope cut-off value used to divide moderate slopes from gentle slopes is the standard deviation, 0.08, of slope values for all SF in NTS 93F and NTS 93K. This value is equal to a 4.6° dipping surface. The maximum dips of uphill and downhill surfaces around mapped SF are

about 33° and 34°, respectively. Fifty-six percent of mapped SF occur where SF-forming flow was downhill, and 41% of total SF occur on gentle downhill slopes (Figure 44). Seventy-five percent occur on slopes < 4.6°.

3.4.5.2. Slope and streamlined form length

The same four slope bins as used in the preceding analyses are also used to investigate the regional effect of slope on SF length. Streamlined forms located on gentle downhill slopes in NTS 93F and NTS 93K average longer than SF found on other slopes (Figure 45).

Analyses of local slope effect generates similar results to the regional effect reported above. ANOVA of combined values from sample squares is used to test whether differences in SF lengths attributed to slope were significant. The analysis and processing are similar to that used to test the effect of elevation on bearing deviation. Sample square sizes are 10, 20, and 40 km. Streamlined forms are divided into bins with increments of three degrees dip, from 0° to 12° and greater than 12° (Table 5).

Significant results are found for all square sizes (Table 5). At all square sizes, average SF lengths are longest on the most level slopes. Note that there is a steady decrease in average SF length as slope increases, in both downhill and uphill directions (Table 5). Calculated F values greatly exceeded critical F values; hence, there is a significant effect on SF length due to slope.

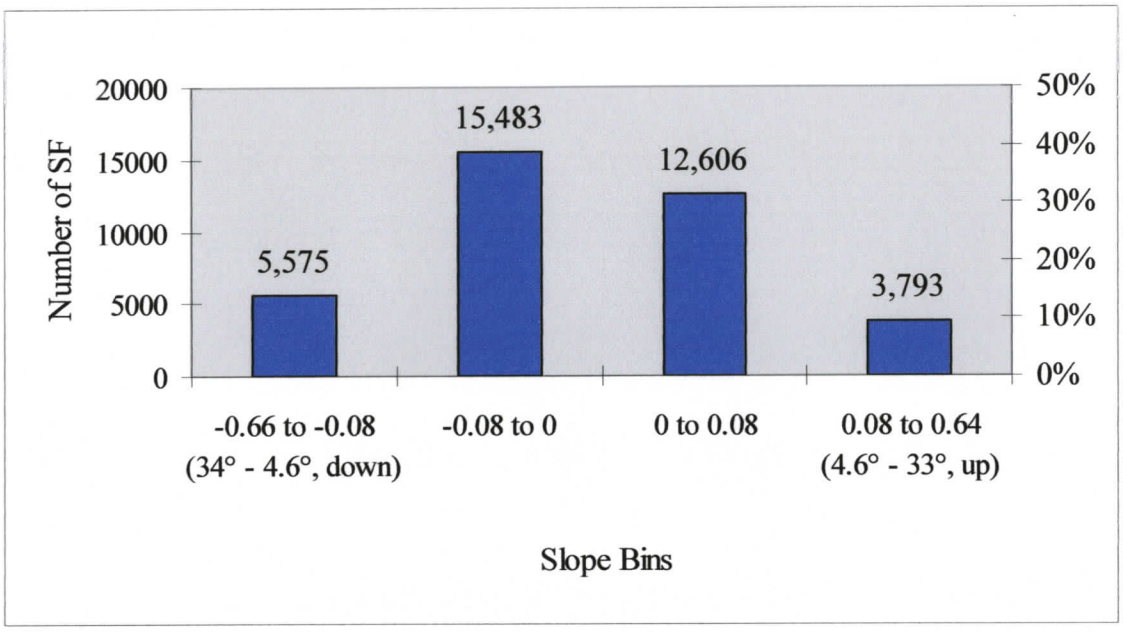

Figure 44. Streamlined form frequency by slope, NTS 93F and NTS 93K.

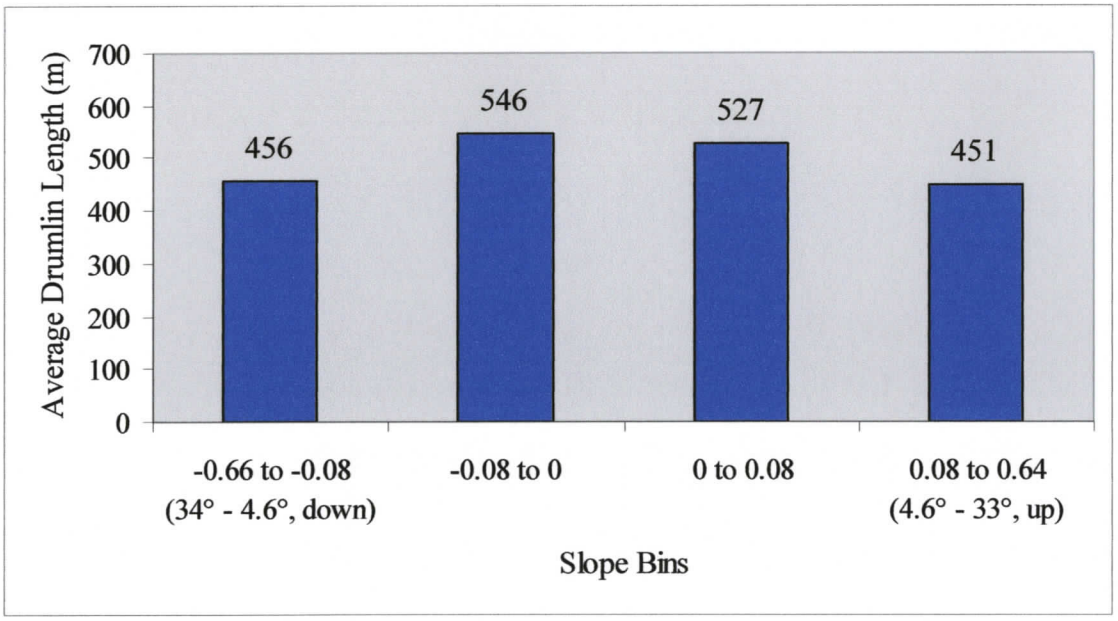

Figure 45. Average lengths of SF by slope intervals, NTS 93F and NTS 93K.

Table 5. Slope effect on SF length, NTS 93F and NTS 93K, P < 0.05; top two average lengths per square size are in bold.			
	Average SF length (m)		
dip (degrees), downhill flow	10 km square	20 km square	40 km square
>12°	419	398	396
9° – 12°	426	434	436
6° – 12°	465	470	466
3° – 6°	506	504	504
0° – 3°	**543**	**548**	**551**
dip (degrees), uphill flow			
0° – 3°	**522**	**534**	**533**
3° – 6°	469	489	480
6° – 12°	447	454	441
9° – 12°	439	442	420
>12°	392	376	378
calculated F	14.2	20.1	18.5
critical F	1.9	1.9	1.9

3.4.5.3. Discussion of slope and streamlined form length and frequency

The relationship between slope and SF length is relevant to the question of an ice versus a water origin for SF. Downhill flowing ice could be expected to accelerate due to gravity, so ice on downhill slopes would have greater velocity than ice on level slopes. There would be cases where it probably would not accelerate, for example, where the flow path leads downhill into a low area without an outlet, i.e., a "box canyon" type of configuration. However, at the scale of drumlins in the study area, there are possibly a number of areas where downhill flow could be supposed to accelerate. Some examples of areas where this slope-velocity relationship would appear to be applicable are flow down the east side of the Quanchas Range, flow up the Babine

Valley towards the southeast (the downhill gradient of the Babine Valley is towards the north), and flow down the numerous upland areas on the Nechako plateau. Stokes and Clark (2002) demonstrated that the length of SF in a constricted part of a SF flow path had greater lengths than SF in unconstricted parts of the same flow path. They inferred that an increase in ice velocity occurred where flow converged into the constriction, and that the increased velocity produced relatively longer SF. Assuming an ice origin for SF and accepting the inference that greater ice velocities yield longer SF, then longer SF should occur on steeper downhill slopes.

Moving square analyses of the effect of slope on SF length show that SF on more level slopes are longer than SF on both downhill and uphill steeper slopes. There is also a pattern of longer SF on downhill slopes that on uphill slopes. However, the amount of slope appears more important than the direction of slope. This conclusion is drawn by the observation that SF on uphill slopes between 0°-3° are longer than SF on downhill slopes between 3°-6°. The same relationship is observed for all slope bins (Table 5). The data indicate that the more level the slope, the greater the SF length; that is, as uphill or downhill surface inclination increases, shorter SF are formed. Based on a secondary tendency for longer SF on downhill slopes, these data are interpreted as somewhat supportive of an ice origin for SF.

The length of SF also may be related to factors such as sediment availability rather than just the flow mechanism itself. For example, the finding that longer SF occur on more level slopes suggests the possibility that SF length is related to the availability of sediment. In many cases, more level areas reflect sites of greater sediment accumulation, partly because sedimentary deposits tend to accumulate in lows

and thus level out the topography. The interpretation that the thickness of sediment may be a major control on SF length is also suggested by the finding that, at sub-regional scales, longer SF are associated with lower elevations. Lower elevations typically have thicker sediment sequences than upland areas as they act as depositional sinks.

Higher frequency of streamlined forms on downhill slopes (Figure 44) may be a function of the regional topographic trend. NTS 93K has the lowest elevation of the study area map sheets (Figure 39). Two of the three principle flow directions are southeast from north of the study area and east-northeast from the southwest. Based on these flow directions and observation of Figure 15, it can be seen that most SF flow was towards NTS 93K, the lowest part of the study area. Hence, greater frequency of SF on downhill slopes could be because there are relatively more downhill than uphill surfaces in the principle flow paths.

3.4.5.4. Slope and bearing deviation

The effect of slope on bearing deviation is tested using the same methodology and processing as that used for testing the effect of slope on length. Two slope bin configurations are used in the bearing deviation analysis: analysis with just two slope bins (downhill and uphill) and analysis with four slope bins (steep downhill, gentle downhill, gentle uphill, and steep uphill). Square sizes are 5, 10, 20, and 40 km.

Significant results are found for all square sizes by ANOVA using two slope bins (Table 6). Streamlined forms pointed downhill have less bearing deviation than those pointed uphill for each significant sample square. Bearing deviation increases as

the square size increases. Significant results are not found for ANOVA using four slope bins (Table 7).

The reason for the lack of significant findings using four slope bins could be due to the non-linear variation of bearing deviation by slope (Figure 46). Most of the variation among the four slope bins is in the steep uphill bin. Variation in the other three slope bins is too small to be significant at the probability level employed in the analyses. Nonetheless, the data show that bearing deviation is greatest on steep upslopes. This would seem an obvious result; flow that encounters a bluff obstacle would tend to divert. One possible location of steep upslopes could occur where oblique flow crosses a lowland channel or valley and encounters the far valley wall. Bearing deviation would be expected. Such a situation is suggested earlier in this chapter as a possible reason for greater bearing deviation at lower elevations.

Table 6. Slope effect on bearing deviation, 93F, two slope bins, $P < 0.05$. Greatest deviation in bold.

Square size (km)	Bearing deviation		F calculated	F critical
	Downhill	Uphill		
5	7.9	**8.9**	7.4	3.9
10	10.1	**11.3**	4.1	3.9
20	10.7	**12.9**	7.4	4.0
40	11.7	**14.4**	7.7	4.3

Table 7. Slope effect on bearing deviation, 93F, four slope bins, P < 0.05. No significant effect.

Square size (km)	Bearing Deviation				F calculated	F critical
	Steep downhill (>2.3°)	Downhill (0 to 2.3°)	Uphill (0 to 2.3°)	Steep Uphill (>2.3°)		
5	12.0	12.2	12.3	13.2	1.6	2.6
10	14.7	14.7	15.2	16.1	1.4	2.6
20	16.8	16.6	18.1	19.5	1.9	2.6
40	18.1	17.4	18.6	20.8	0.8	2.7

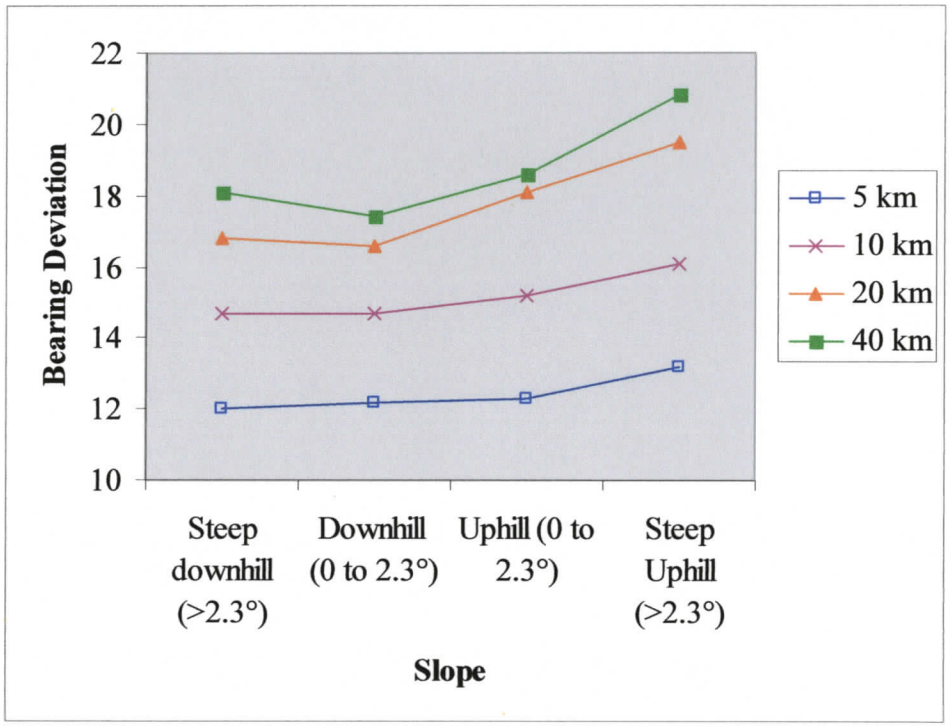

Figure 46. Graph of bearing deviation for four slope bins, data from Table 7. Square sizes are indicated in legend.

3.5. SUMMARY

3.5.1. Timing of valley and streamlined forms formation

Streamlined form densities (Figures 15 and 43) indicate greater, more evenly distributed concentration patterns on the plateau than in the mountain regions. This is probably largely due to a greater abundance of till in the plateau area. Some broad valleys and lowlands in the study area with low or no concentrations of SF are discussed in Chapter 2. The SF density map presented in this chapter (Figure 43) verifies these low density areas. It is suggested in Chapter 2 that the system of lowlands that include Ootsa Lake was developed prior to major fields of SF in that area. Several possibilities for low SF concentrations in the lowland valleys are suggested here: streamlined forms are not observed in the channels because the channels were filled by stagnant ice or lakes during SF-producing flow, post-SF ice or water flow utilized existing channels and eroded existing SF; or SF are covered by lakes or by post-SF deposits.

Two statistical tests completed here are used to test the hypothesis that major valleys / channels formed prior to SF. A statistical effect of elevation on bearing deviation is noted in this chapter. Lower elevations tend to have greater bearing deviation over local-size sample squares in NTS 93F. This map sheet is also the site of some major valleys oriented oblique to the dominant east-northeast SF-producing flow. It is possible that greater bearing deviation at lower elevations is related to these cross valleys. Water, and possibly ice, flowing across valleys at oblique angles would tend to

be diverted along valley axes, thus resulting in greater bearing deviation. A statistical effect of slope on bearing deviation is also observed; bearing deviation is greater on uphill slopes.

3.5.2. Level slopes and streamlined form length

As discussed previously, Stokes and Clark (2002) reported that an increase in SF length is observed at a constricted area in a large SF flow path. They associated the increased SF length to increased ice flow velocity. Their interpretation, that higher velocity ice formed longer SF, is accepted here for the purpose of testing the relationship between SF length and slope.

Ice flowing downhill would have a greater velocity than the same ice flowing uphill or on a level surface. Hence, if longer SF are formed by faster ice, then longer SF should be apparent on downhill slopes. A statistical effect of slope on SF length is observed in this study. The primary relationship appears to be that the more level the slope, the greater the SF length. A secondary relationship was also observed, that is, SF lengths are longer on downhill slopes than uphill slopes for a given slope range. For example, SF on downhill slopes in the 0°-3° bin are longer than those on uphill slopes in the 0°-3° bin (Table 5). Given the assumption that faster flowing ice creates longer SF, this result is supportive of an ice origin for SF. Nonetheless, this trend is secondary to the primary trend indicated by Table 5, that is, that more level slopes result in greater SF lengths. Based on this primary trend, it is suggested here that one of the main controls on SF length is sediment availability and thickness. It is quite possible that more sediment would have been available on more level surfaces. This interpretation is

supported by the statistical relationship found here between SF length and elevation at a sub-regional scale, that is, longer SF occur at lower elevations. It would be reasonable to suppose that lower elevation sites would have been covered by thicker sediment sequences.

3.5.3. Scale of SF forming flow

Streamlined forms are consistently sized across the study area. The average lengths of SF for the five NTS sheets are all similar (around 450 – 550 m), with the 666 m average length of 93M SF being noticeably longer than the other sheet averages (Table 3). The 93M SF are probably longer due the dominance of SE flow in 93M, paralleling structural and tectonic trends.

East-northeast flow produced SF over a vertical range of more than 1000 m. The vertical extent of ENE flow may be a minimum value since the maximum elevations in 93F and 93K only slightly exceed the maximum elevation of mapped SF. It is possible that ENE flow overtopped all elevations in the plateau area. West SF-producing flow extended up to at least 2000 m elevation (Table 1 and Chapter 5). Southeast flows probably had less vertical extents.

Although SF are located across a large vertical extent, more than a kilometre in many locations, the timing of flows that produced the vertically separated SF is not clear in many areas. In the mountainous western part of the study area, southeast and west flows appear to have occurred at different times. However, in the plateau region and especially in 93F, the vertical range of SF distribution and consistent SF size supports the hypothesis that these SF were formed by regionally extensive flows. This

conclusion is supported by large groups of similarly sized, parallel and subparallel SF that are tens of kilometres wide. However, the occurrence of some SF oriented oblique to the main trends are suggestive of formation at different times, for example, flow out of cirques (Chapter 2).

4. INCREMENTAL GLACIAL EROSION ANALYSIS

4.1. INTRODUCTION

This chapter presents a two-dimensional computer analysis simulating the incremental erosion of a rock surface by a thick ice sheet. The tool used to conduct this analysis is an Excel 2000 workbook named: **igem.xls** (Incremental Glacial Erosion Model).The computer analysis tool is included on the CD in the back disk pocket of the thesis. A description of how to use the tool is detailed in the Methods section of this chapter. The computer analysis is referred to at times in this chapter as a "model", but it is important to note that the analysis is not a dynamic model based on complex ice physics. Rather, the analysis is a simple computer model that tests the effects of varying a selection of parameters that control rock erosion by glaciers.

The purpose of this analysis is to show site-scale distribution and time-wise variation of shear stresses at the base of an ice sheet, and to predict erosion patterns based on that changing stress distribution. Shear stresses have magnitude and direction, and will vary along the ice / rock interface as the orientation of the rock surface varies. In the analysis, the amount of erosion along the rock surface is assumed to be solely dependent on the shear stress acting along the surface at any given point and on the relative hardness of the surface at a given point. Given these assumptions, the rock surface is differentially "eroded", along its length, based on length-wise shear stress variations. This differential erosion then results in a new surface with, possibly, different orientations and a different stress distribution. The whole process is repeated, and the surface is programmatically eroded.

The results of this simulated erosion are applied to the problem of origins of streamlined forms. Two types of surfaces are eroded using the model: the long section of a typical rock drumlin, and a flat surface with a central core of more resistant rock. In the first case, the intent is to simulate what changes, if any, occur to a drumlin shape subjected to distributed glacial stresses. The hypothesis that a bedrock surface with a streamlined "drumlin" shape maintains its shape at a given location when subjected to distributed stresses at the base of an ice sheet is tested.

This hypothesis is used here as it provides insight into the stability of streamlined shapes at the base of an ice sheet. There are a number of examples of streamlined shapes that are stable fluvial end forms, for example, streamlined islands and erosional residuals (Baker, 1979; Komar, 1984; Kehew and Lord, 1986), streamlined flutes formed by tsunamis (Bryant and Young, 1996), and experimentally produced erosional marks and residuals (Allen, 1981; Komar, 1983). If the erosion analysis indicates streamlined forms are not stable shapes in an ice sheet, then the argument of an ice origin for streamlined forms is weakened since some streamlined forms are known to be stable in water flows.

The second type of surface, flat with a resistant core, imitates the preliminary surface from which a rat-tail is formed. The hypothesis is: When a surface with a resistant core is eroded by distributed shear stresses at the base of an ice sheet, a streamlined form will result. Streamlining will be evident by the projection of the resistant core up into the ice sheet, and a tapering tail extending down-ice of the core.

The next section of this chapter reviews two previous glacial erosion models with some similarities to and differences from the model presented here. Following

that, a methods section details formula derivation, design, operation, and assumptions of the analysis. Results and discussion follow. A working version of the analysis tool is included as an Excel file on the CD located in the back disk pocket.

4.2. PREVIOUS WORK

Harbor (1988) numerically simulated valley glacier erosion by linking an ice flow and landscape erosion model. The resulting three-dimensional model predicted the transformation of a V-shaped valley into a U-shaped valley. This model is similar to the analysis presented here in that it numerically simulates glacial erosion. However, Harbor's model is landscape scale and three-dimensional; whereas, the following simulation is site scale and two-dimensional.

Boulton (1974, 1979) theoretically modeled glacial erosion and deposition along a two-dimensional surface. He used an abrasion theory in conjunction with a sliding theory that predicted the pressure distribution over a low ridge transverse to ice flow. Differential erosion and deposition were determined by differences in normal pressure. Boulton stated that his theory simulated roches moutonnées, steps with depressions in their lee, and drumlin-like forms. His model is similar to the simulation presented here in that it simulated erosion of a two-dimensional surface beneath a glacier. However, Boulton's model related erosion to normal stresses and did not resolve the normal stresses into shear stress components, as is done here. Boulton's model also included areas of erosion and deposition, whereas the following simulation is entirely erosional.

4.3. METHODS

4.3.1. Shear stress derivation

Stress at the base of a sloping ice sheet due to the weight of the ice can be resolved into a normal and a shear component (Paterson, 1994). The normal stress is a function of the ice overburden. The shear stress is a function of the normal stress and the slope of the ice sheet.

Figure 47 diagrams the derivation of the stress formulae used in the analysis. On a level surface at the base of a level ice sheet, no shear stresses are active (Case 1, Figure 47). Case 2 is a level ice sheet over a sloping ground surface (Figure 47). The ice exerts a downward stress, which is broken into a normal and shear component at the ground surface. If the ice surface is sloping, then the stress from the ice sheet has a normal and shear component (Case 3, Figure 47). In such a case and if the ground surface is level, shear stress can be described by a single component (Case 3, Figure 47). If neither the land surface nor ice surface is horizontal, then shear stresses from the weight of the ice are described by two shear components (Case 4, Figure 47). The sum of the two components is the total shear along the surface at a given angle with the horizontal.

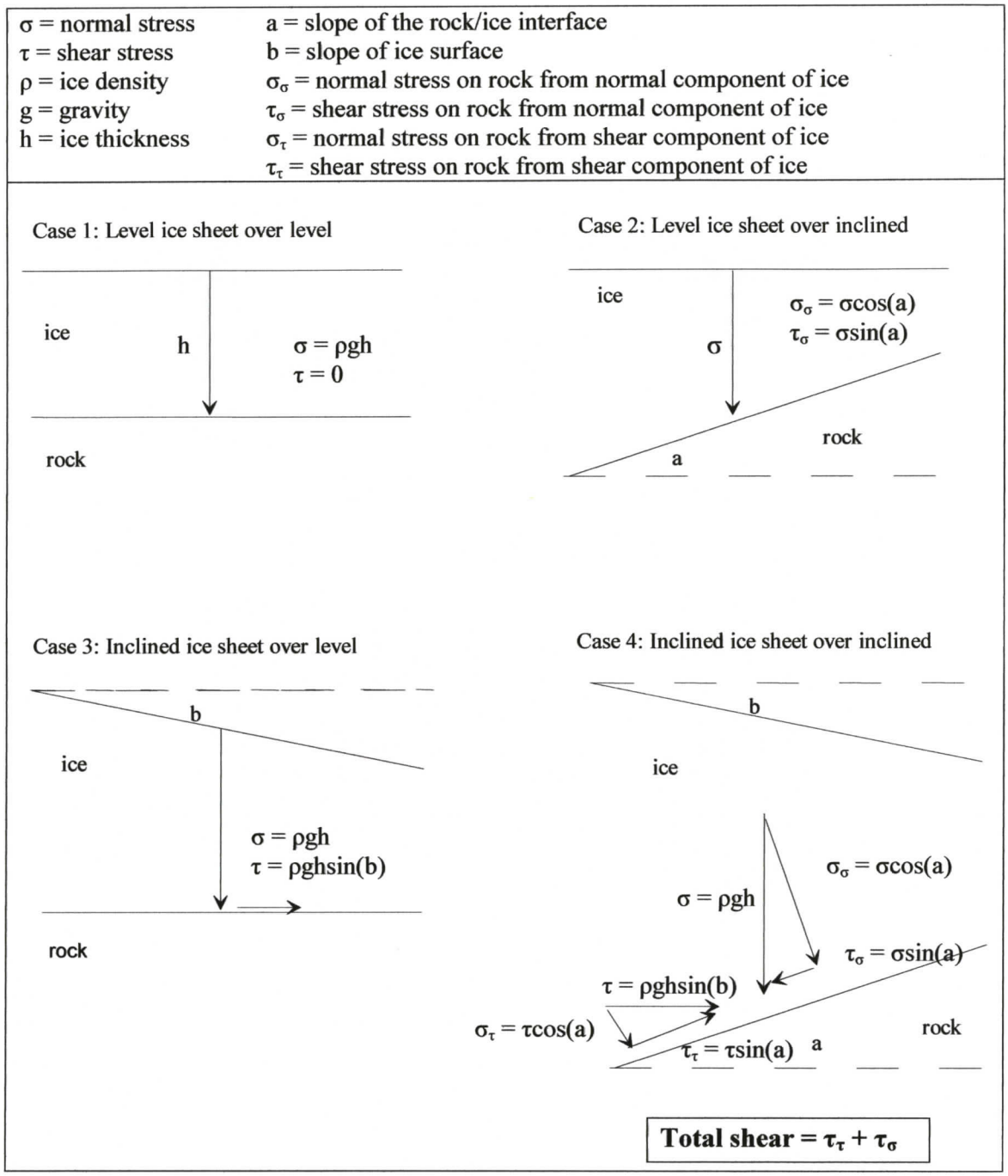

Figure 47. Derivation of total shear stress acting along a land surface due to the weight of an ice sheet.

4.3.2. Reverse shear and longitudinal shear stresses

The resolution of shear stresses from the ice weight sometimes results in the development of a total planar shear stress pointed opposite to the direction of ice flow (Case 4, Figure 47). This situation results where ice flows uphill, driven by an ice gradient originating up-ice. It is assumed in this analysis that the ice flows only in the direction indicated by the ice gradient, that is, reverse ice movement is not allowed. Since reverse movement is not allowed, then cases of reverse shear, acting in an up-ice direction, must be offset by force acting in the opposite, down-ice direction.

The "pushing or pulling effect" within an ice sheet is known as the longitudinal stress (Nye, 1969; Paterson, 1994; Benn and Evans, 1998). The longitudinal stress acts approximately parallel to the direction of flow and makes uphill flow possible. A calculated longitudinal stress component is not included in the analysis, but an estimate of this value is assumed in order to compensate for reverse basal shear stress. Longitudinal stress varies within an ice sheet. Analysis has shown that longitudinal stresses can be about the same order of magnitude as planar shear stresses (Hindmarsh, 2004); although, longitudinal stresses can greatly exceed planar shear stresses in some cases (for example, Wilchinsky and Chugunov, 2000).

Three methods for offsetting possible reverse shear stress in the analysis using an assumed longitudinal stress component are considered:

Method 1. A variable longitudinal stress value is calculated at each iteration as being equal to the absolute value of the minimum total shear stress

for that iteration. This constant is added to all shear stresses for that iteration. Only positive and zero value shear stresses result.

Method 2. A constant longitudinal stress value is assumed that is equal to the absolute value of the maximum possible reverse shear for a given set of analysis parameters, *i.e.* for an up-ice facing surface approaching the vertical. This constant is added to all shear stress values at each iteration of the model, thereby forcing positive shear stress values.

Method 3. If the total shear stress at a point is negative, the total shear stress at that point is set to zero.

Test runs were conducted to assess the three methods. The intention is to disallow negative total shear stress and to expose erosion patterns due to planar stress distributions, which are in turn derived from the weight of the ice sheet. On runs with Method 3, where the erosional surface dips steeply up-ice, all shear stresses on the erosional surface are negative; hence, no erosion takes place. Field examples where this is not the case are abundant; for example, the stoss sides of roche moutonnées are often extensively striated. With Method 2, the longitudinal stress is generally much greater than the planar stress and obscures erosion patterns due to planar stress distribution. Neither of these methods is compatible with the objectives of the analysis. Method 1 disallows negative stresses, but allows recognition of differences in planar stress distribution over time; therefore, Method 1 is used in the erosion analysis for reverse

stress compensation. It is suggested here that Method 1 more closely approximates reality than either Method 2 or Method 3 in many cases.

4.3.3. Analysis tool design and use

The analysis tool simulates the erosion, in longitudinal section (section along flow), of a rock surface. The length of the rock surface used in the analysis is 6.3 m; its height varies as simulated erosion takes place. This length was chosen as it is similar to the length of many rock drumlins observed during the field study (Chapter 5). The total length of the surface is divided into 1 cm increments along the x-axis; hence, the surface consists of 630 small, adjacent surfaces, called "slices" here. The two-dimensional shape of the surface, then, is described by 630 xy coordinate pairs. The x values are constant, but the y values decrease as the surface is eroded.

4.3.3.1. Platform and output

The platform for the analysis is an Excel spreadsheet and iterative runs are driven by a Visual Basic for Applications (VBA) program. Calculations are done using spreadsheet functions and formulas and VBA code. The surface is visually depicted as an Excel chart using xy coordinates of the erosion profile. Erosion is programmatically simulated by subtraction of model-determined increments from the y values; hence, the erosion and subsequent changes in the surface shape can be observed on the Excel chart as the model runs. This feature allows visualization of changes in stress distribution over time. The coordinates of the eroded surface can be saved after an erosion run. Excel was chosen as the analysis platform because it is readily available, commonly used, and allows a user interface for modifying analysis parameters.

4.3.3.2. Parameters

The parameters used in the analysis are acceleration due to gravity, the physical characteristics of the ice and rock surface, and specifications pertaining to erosional behaviour (Table 8). All the parameters can be varied by the user for a given run.

A typical drumlin shape is digitized using Didger, and the coordinates are imported into Excel and used as the beginning surface for rock drumlin erosion (Figure 48, top). The flat surface is represented by a line where y = 5 (Figure 48, bottom).

The number of iterations is the number of times erosion is simulated on the surface for a given run. It is a measure of the relative time over which erosion occurs.

The rock surface dip parameter accommodates uphill, level, and downhill flow. Although it is possible to use extreme slope angles in the analysis, the maximum dips selected for analyses are based on field observations and drumlin mapping. Although rock drumlins and rat-tails occur on an approximately 27° slope at the Dome Mountain Mine site (Chapter 5), more than 99% of the SF mapped in NTS 93F and NTS 93K occur on slopes less than 20° (this study).

The hardness ratio parameter is used for erosion of a flat surface with a resistant core (Figure 48, bottom). The hardness of the resistant core is defined as being two or four times the hardness of the rest of the rock surface (Table 8). The minimum X and maximum X values of the resistant core refer to the location along flow (along the x-axis) of the resistant core (Figure 48, bottom).

The erosion maximum (or, erosion "bit") is the maximum amount of erosion that occurs for an iteration. Each slice receives some percentage of this erosion depending on the basal shear calculations. The slice with the greatest basal shear for the

iteration receives the full erosion bit. Slices with less shear than the maximum receive a corresponding percentage of the erosion bit.

The break height is incorporated into the analysis in order to prohibit the development of high, thin slivers of rock beneath an ice sheet. If a slice in the analysis exceeds the break height, it is "broken" (see following section).

Neither the ice thickness nor the ice slope are varied. One reason for this is that modification of the ice thickness essentially has no effect. This is because at any point on the surface and for a given iteration, model erosion is a function of the percentage of the maximum shear stress (see discussion in following section).

Table 8. Parameters used for incremental glacial erosion analysis

Parameter	Value	Use*	Remarks	Range
acceleration due to gravity	9.81 m/s^2	C		Not Variable
ice density	900 kg/m^3	C	Paterson (1994), Benn and Evans (1998)	> 0
ice thickness	500 m	C		> 0
ice surface slope	5°	C	slope is always down in the down-ice direction	0 to 90
rock surface dip	-20°, 0°, 20°	V	dip of rock surface; negative numbers indicate dip in up-ice direction	-90 to 90
number of iterations	variable	V	number of erosion iterations for a particular run	Integer > 0
surface shape	two types, see remarks	V	typical drumlin and flat surface with resistant core	
erosion maximum	0.001, 0.01, 0.02 m	V	maximum amount of erosion per iteration	> 0
break height	0.01 m	C	height of a slice before it is 'broken' even with its neighbours	> 0
hardness ratio	2, 4	V	ratio of hardness of resistant core to hardness of surrounding rock	> 1
minimum X, core	4.5 m	C	specifies location of resistant core	0.8 to max X
maximum X, core	5 m	C	specifies location of resistant core	min X to 7.1

* V = varied for different runs; C = held constant but can be varied using model

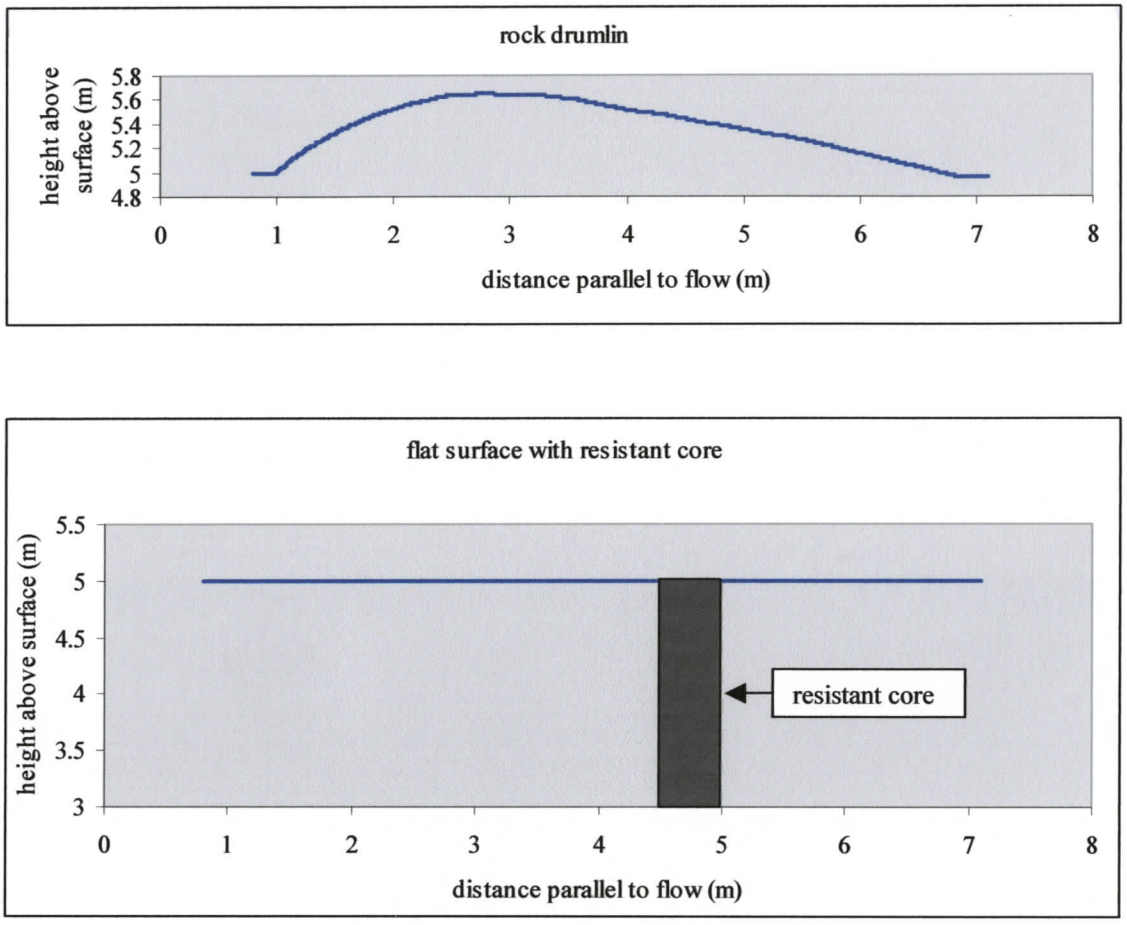

Figure 48. Starting surfaces for simulated erosion, rock drumlin (top) and flat surface with resistant core (bottom).

4.3.3.3. Erosional processing

After parameters are specified, the erosion process begins. Following is a summary of the processing of a typical run:

1. Y coordinates of the selected shape are loaded to a spreadsheet.

2. Surface inclinations of each slice, relative to the horizontal, are calculated using the difference in y values between that slice and the adjacent, down-ice slice.
3. Total shear stress from the weight of the ice acting on a slice is derived.
4. The minimum shear stress for all points along the surface is determined, and its absolute value is added to the shear stress values for each of the slices.
5. The maximum shear stress for all points along the surface at the current iteration is determined, and its value is used to calculate an erosion amount for each slice using the following formula:

$$\mathbf{e = (s / s_m)\ b_e}$$

e = erosion amount in metres
s = total shear stress at point
s_m = maximum shear stress for iteration
b_e = erosion maximum in metres (Table 8)

If the slice is part of the resistant core, then the following modification of the formula results:

$$\mathbf{e = (s / s_m)\ (b_e / hf)}$$

hf = hardness factor

6. The erosion amount for each slice is subtracted from the y value for that slice.
7. The height of each slice is compared to the height of its neighbouring slices. If it exceeds the height of either neighbour by the break height value (Table 8), then its height is made equal to the average height of its neighbours.

At this point, an erosional iteration is complete, resulting in a new erosional surface. Processing is continued for the specified number of iterations.

4.3.3.4. Analysis tool use

The analysis tool features are accessible from the "Main" worksheet of the **igem.xls** workbook included on the CD in the disk sleeve at the back of the thesis. Formulas used in the analysis can be found on the "Names" and "Erosion" worksheets, and in the code accessed through the Visual Basic Editor (Alt + F11). Although all worksheets and the VBA code are accessible, it is recommended that the analysis tool be used via the controls on the "Main" worksheet. Following are steps that can be applied for a test run of the erosion analysis tool:

1. Open Excel. Perform menu command: Tools | Macro | Security, and set security level to Medium.
2. Open the Excel workbook, **igem.xls**. It is located in the CD pocket at the back of the thesis. When prompted, choose Enable Macros.
3. If it is not selected, select the Main worksheet.
4. Select "flat surface with resistant core" and choose Method 1.
5. Set the erosion parameters as follows: rock surface dip = 0, number of erosion iterations = 100, erosion bit = 0.01, hardness factor = 2, and slope of ice surface = 5.

6. Click the button labelled ERODE SPECIFIED SURFACE. This starts the program and a flat surface with a resistant core is eroded.

4.3.4. Assumptions

Assumptions specific to a given analysis run are specified by the parameter settings. The analysis is also based on the following assumptions:

- The analysis is purely erosional and does not take into account deposition.
- The analysis is two-dimensional; the x-axis is defined as being oriented along flow, and parallel to the plane of the rock surface being eroded. In the case of the rock drumlin, the x-axis is parallel to the flat sections up-ice and down-ice of the rock drumlin shape (Figure 48, top). The beginning dip of the eroded surface is not evident from the chart orientation, but is incorporated into the calculation of shear stresses. The y-axis is defined as being perpendicular to the main plane of the rock surface.
- All erosion is assumed to be caused by shear stress parallel to the rock surface at the base of the ice sheet.
- Longitudinal stress is defined as acting parallel to the entire surface. Method 1 (section 4.3.2) is used for longitudinal stress calculation, as follows: If one or more slices are acted on by a negative total shear stress, the longitudinal stress is set to be equal to the absolute value of the minimum shear stress for that iteration. If no slices have a negative total shear stress, then the longitudinal stress is zero. The longitudinal stress value is calculated for each erosion iteration, and that value is added to the shear stress values acting on each slice.

- The erosional surface is assumed to be of homogeneous composition, with the exception of the embedded resistant core in the case of the initially flat erosional surface. The resistant core is also homogeneous and extends to an infinite depth.
- The portion of the ice sheet in contact with the rock surface is assumed to be homogeneous, with evenly distributed, similarly sized, fine-grained sediment. The rest of the ice sheet is also presumed to be of homogeneous density.
- The ice is assumed to maintain its original height above the surface as the surface is eroded; that is, the ice surface does not lower as the surface lowers.
- All movement of the ice is confined within the plane of the analysis.
- The abrasive ice sole is assumed to remain in constant contact with the rock surface. No separation of ice from the surface is permitted, for example, as sometimes occurs in the lee of obstructions to flow. No water film is permitted between the ice and rock surfaces. A water film would disrupt the analysis in two ways. It would separate the abrading ice sole from the rock surface, and it would disperse the stresses at any given point; pressure on the water would result in hydrostatic pressure acting in all directions through the water "body".
- No erosion takes place beneath overhangs or on undercut surfaces. This assumption essentially prohibits the development of such surfaces. In the two-dimensional flow analysis used here, erosive shear stress is unidirectional, that is, all erosive movement is down-ice. To allow erosion on undercut surfaces in a two-dimensional analysis requires permitting up-ice flow; that is, ice must flow in an up-ice direction to either enter or exit an undercut area. Up-ice flow is not permitted in the analysis.
- Plucking or quarrying of material is not included in the analysis.

4.4. RESULTS AND DISCUSSION

Results reported here are based primarily on 315 analysis runs, 105 of which are on a rock drumlin shape and 210 on a flat surface. The flat surface has one extra parameter, hardness ratio, that is varied and that is not applied to the rock drumlin erosions. Parameters that are varied for the different runs include surface type, hardness ratio (only applicable to flat rock erosion), erosion bit (ebit on figures), surface dip, and the number of iterations (Table 9). Iterations are systematically increased in order to produce a record of erosion patterns over time. Some runs require extended iterations to allow full development and recognition of erosional patterns.

4.4.1. Flat rock with resistant core erosion

Apart from the number of iterations, 30 combinations of hardness factor, erosion bit, and surface dip parameters are investigated for the erosion of a flat rock surface with a resistant core. The resistant core is located between 4.5 m and 5 m on the x-axis. Two supplementary runs are used to investigate longer term erosion with the smallest erosion bit and erosion using an alternate method of reverse shear compensation.

Table 9. Parameter values for simulated erosion

Surface type	Hardness ratio of resistant core	Erosion bit	Surface dip	Number iterations
typical rock drumlin	2	0.001 m	-20°	100
flat rock, resistant core	4	0.01 m	-5°	200
		0.02 m	0°	400
			5°	600
			20°	800
				1000
				1200

Consistent patterns show during the initial parts of the flat rock runs. First, a roche moutonnée shape is produced, then the shape changes into two slope-parallel surfaces separated by an inclined plane. The steep down-ice face of the roche moutonnée form corresponds to the resistant core location. The more gently sloping roche moutonnée surface extends up-ice from the resistant core. The rock ledge or step of the final stage of the form is located where the resistant core is located.

The roche moutonnée form is common to glaciated terrain. Although it forms readily in the analysis, it does not persist and is replaced by a rock ledge or step. Boulton (1974, 1979) produced roche moutonnée forms and steps with depressions in their lee in a theoretical model of glacial erosion. His model and the one presented here are compared later in this chapter.

The hardness ratio, or hardness factor (hf), for flat rock runs is set at 2 and 4. Runs with hf equal to 4 show more exaggerated differences in elevation between the resistant core and the main rock body; hence, form development due to the resistant core is more pronounced (Figure 49, top). Less erosion depth for a given number of iterations occurs with the higher hardness factor (compare y-axis values at top and bottom of Figure 49). However, when hf is equal to 4 and the maximum erosion bit (0.02) is used, "run-away" erosion on the down-ice side of the resistant core occurs at all surface dips (Figure 50). This run-away effect becomes more pronounced as the surface dip value increases from –20° to 20°. Run-away erosion also occurs with the higher hf value in combination with the 0.01 erosion bit value when surface dips are down-ice (5° and 20°). Run-away erosion is not consistent with observed glacial landforms.

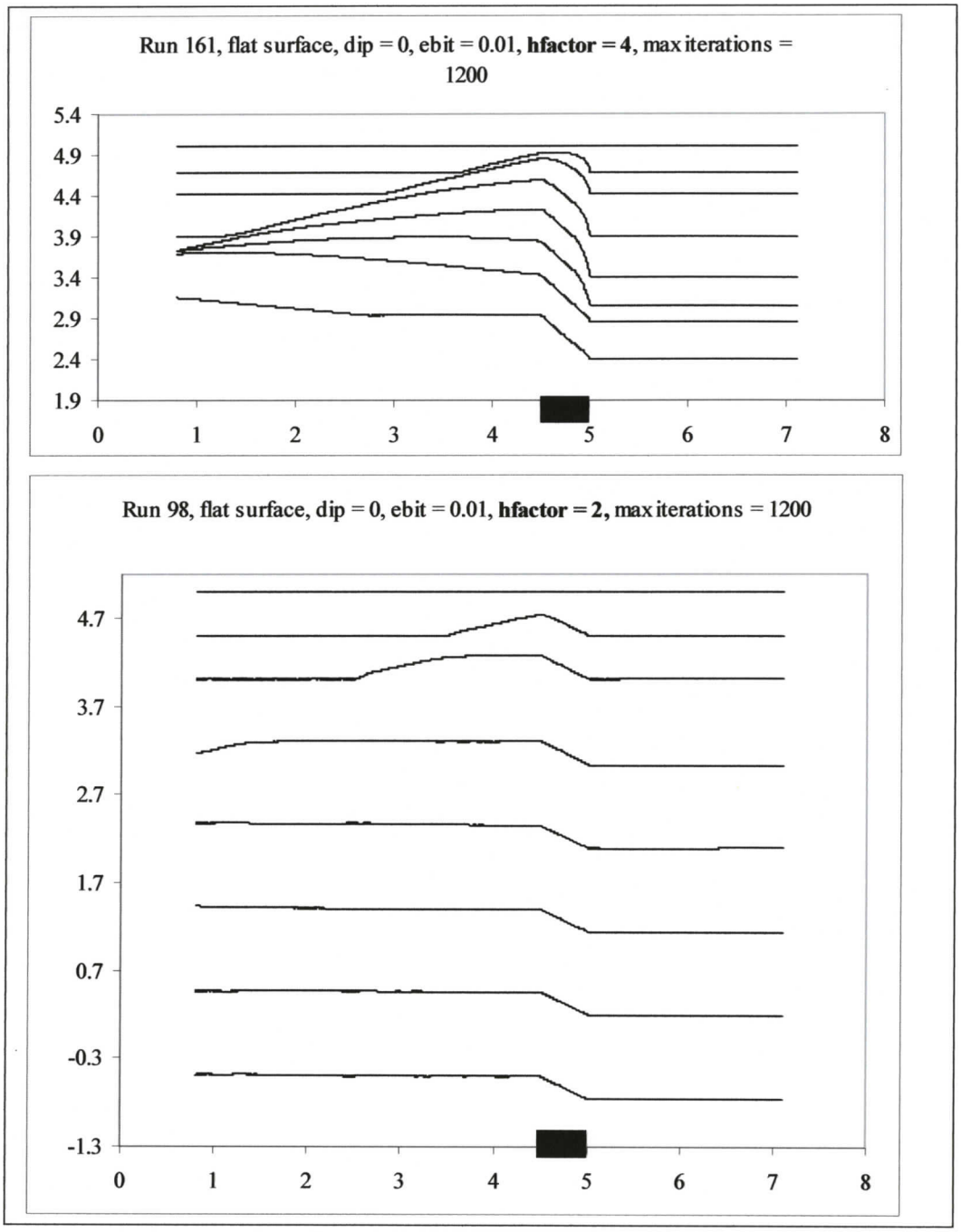

Figure 49. Flat erosion, difference in erosion patterns due to hardness factor variation. Iterations range from 0 to 1200 (see Table 9). All axes values in this and subsequent figures are in metres. Dark rectangle on x-axis represent location of resistant core. Flow direction is left to right.

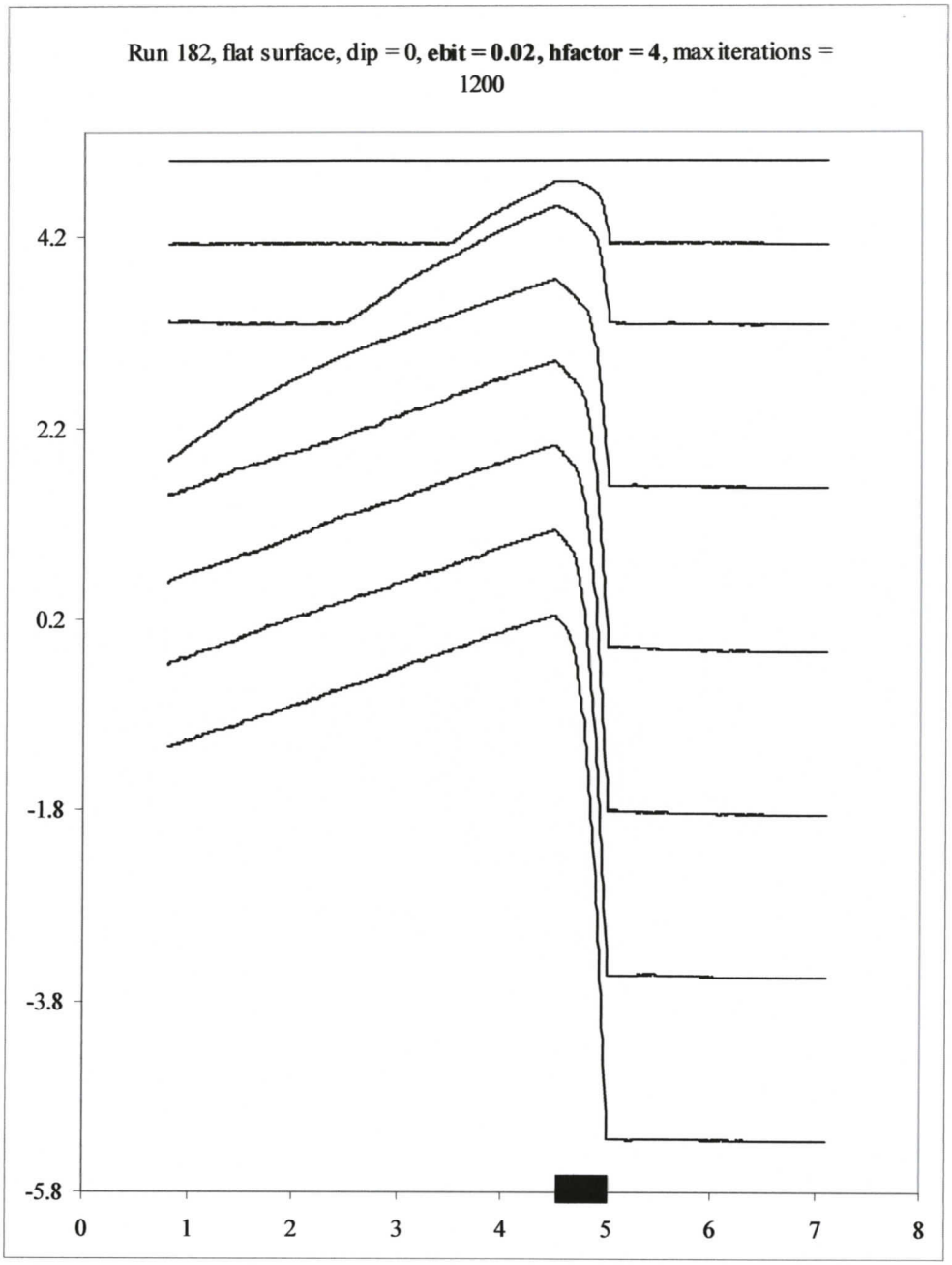

Figure 50. "Run-away" erosion on down-ice side of resistant core. Hardness factor = 4. Dark rectangle on x-axis represents approximate location of resistant core. Flow direction is left to right.

A possible reason for the model run-away erosion could be that "ice bridging" is not included in the analysis. It is known that ice flowing over a steep cliff will, at least in some cases, drop at a lesser angle than the cliff face (Boulton and Vivian, 1973; Boulton, 1974; Theakstone, 1979; Rea and Whalley, 1994; Rea *et al.*, 2000). This results in a void along and near the base of the cliff; the cliff face and part of the more horizontal rock surface near the cliff are ice free. No glacial erosion takes place on the ice-free areas.

In the analysis, ice flows down near-vertical and vertical surfaces and erosion takes place on those surfaces. Model erosion on steep surfaces is relatively greater than that on more horizontal surfaces because ice sheet weight is resolved primarily into an erosive shear component acting down the face. This results in run-away erosion. On a more horizontal surface, erosive shear stress due to ice sheet weight is relatively small compared to normal stress.

The erosion maximum, or bit, is given three values. The lowest value, 0.001 m, results in only minor lowering of the surface, and negligible form development (Figure 51). In order to further test erosion using this lowest value, a supplementary test is run using 10,000 iterations in 1,000 iteration increments. The results are similar; little erosional form development occurs (Figure 52). The quickest erosion occurs with the largest erosion bit, 0.02. The surface tends to be rougher and does not develop planar surfaces as readily as are formed using the 0.01 erosion bit (compare Figure 49 bottom and Figure 53). However, run-away erosion develops with the 0.02 erosion bit on 20° down-ice dips, even though the lower hardness factor is used. Possible reasons for run-away erosion are discussed above.

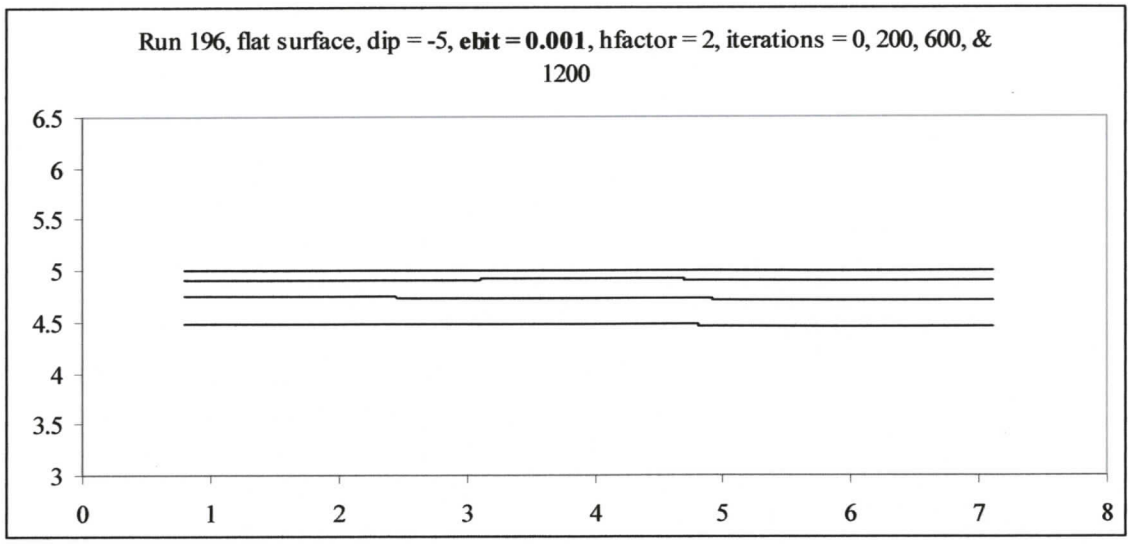

Figure 51. Flat surface erosion with erosion bit = 0.001. Only the beginning surface and iterations 200, 600, and 1200 are shown.

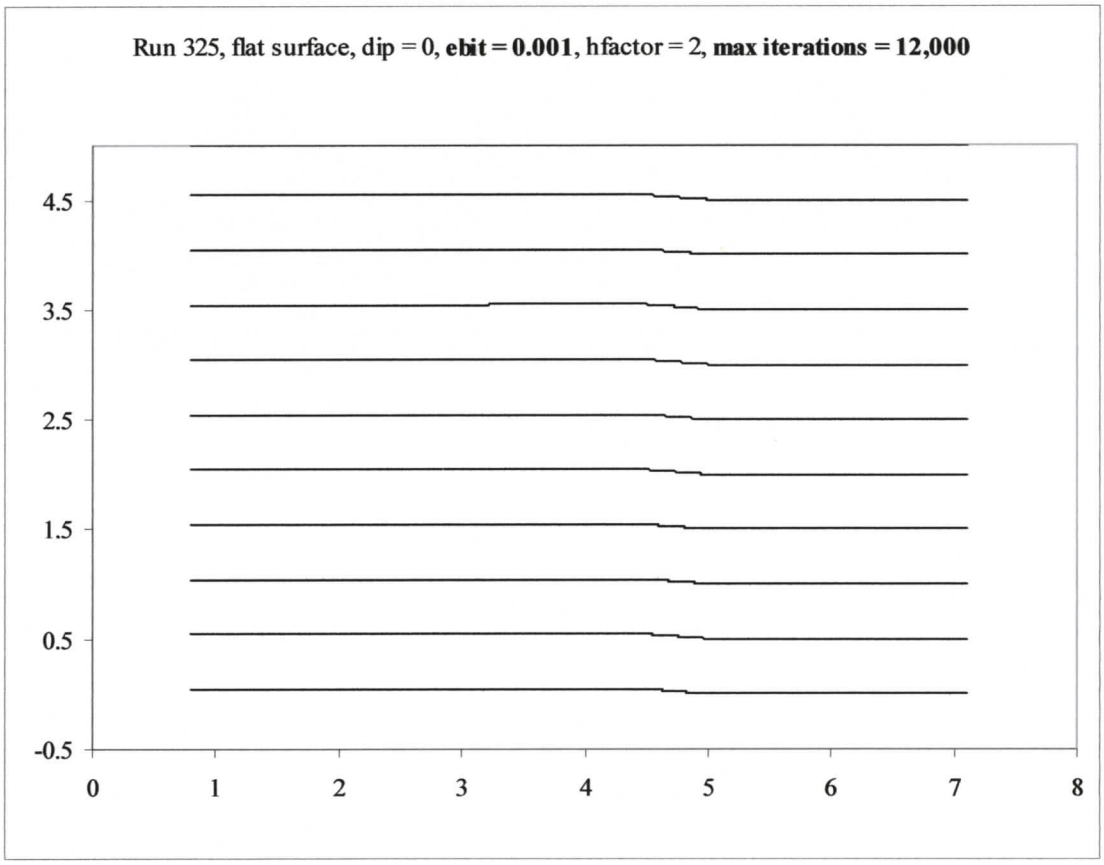

Figure 52. Extended flat surface erosion with erosion bit = 0.001. Iterations from 3,000 to 12,000, in increments of 1,000, are shown.

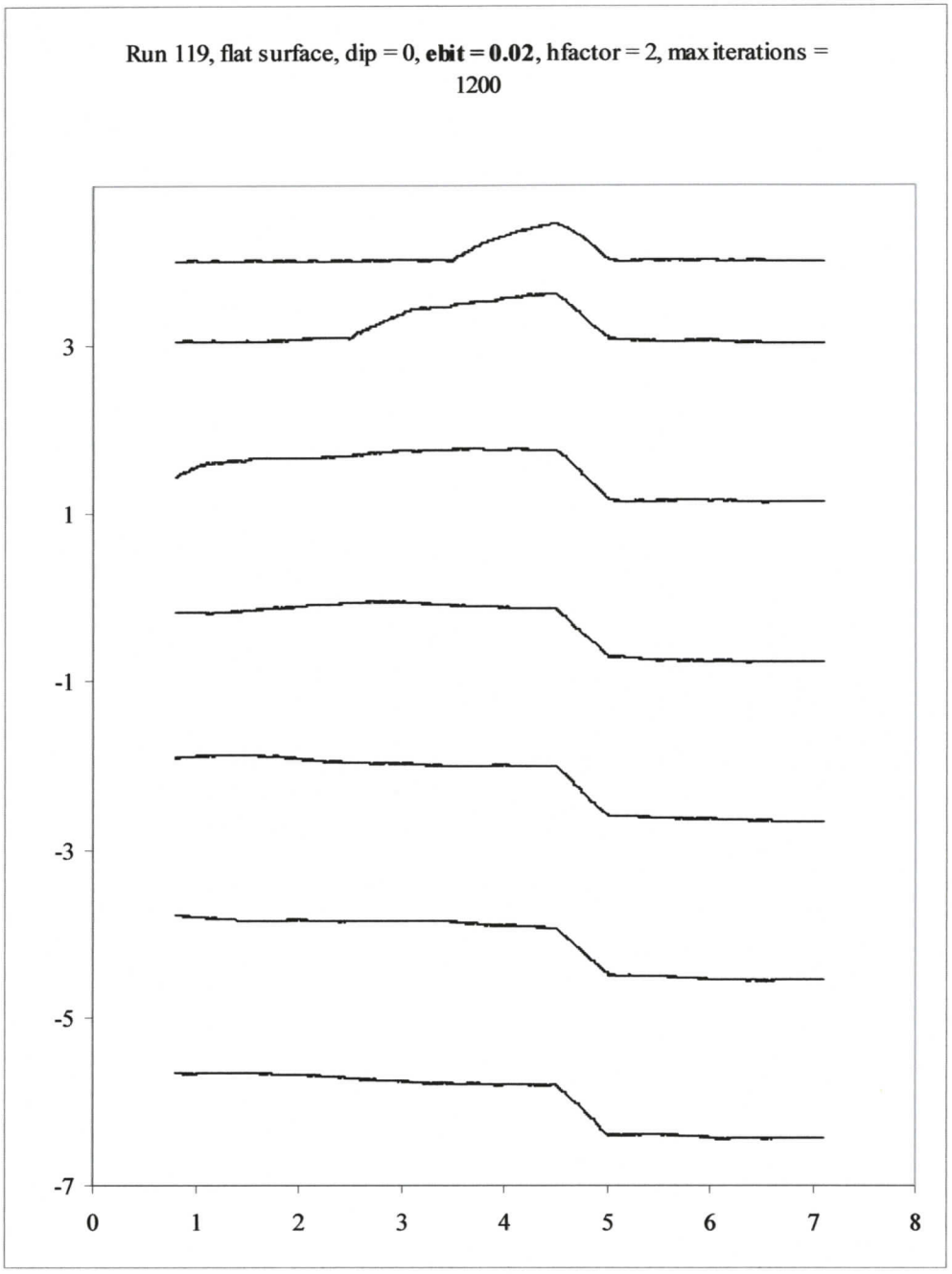

Figure 53. Flat surface erosion patterns with 0.02 erosion bit at 0° dip. Compare with Figure 49 bottom, in which parameters are the same as here except for the erosion bit. Iterations shown: 100, 200, 400, 600, 800, 1000, and 1200.

The reason for the low amount of form development with 0.001 erosion maximum is probably due to the lack of steep rock surfaces being eroded. The analysis tool calculates the slope between adjacent slices. When a greater erosion maximum of 0.01 is used, then adjacent slices are more likely to have greater elevation differences than when a 0.001 ebit is used. Differences in erosion amount per iteration are thus magnified by up to a factor of ten. Greater shear stress occurs on steeper surfaces because most of the stress of an ice sheet is directed down. With the smaller erosion maximum, erosion differences between adjacent slices are less, less elevation differences between adjacent slices are developed, and less erosion occurs on the more horizontal slopes between adjacent slices.

The rougher surfaces developed using the 0.02 erosion maximum are probably also due to this model characteristic. Greater differences in erosion can occur between adjacent slices due to the higher erosion maximum that is used. This has two effects: higher slope angles for each slice and greater differences in slope angles for adjacent slices. Both effects in turn cause even greater differences in erosion between slices. A rough erosion surface develops. The break height parameter limits the degree to which the surface roughness is propagated by "breaking" off slices. The break height limits height differences between slices.

The effect of surface dips on flat surface erosion are examined using a hardness factor of 2 and an erosion bit of 0.01. Surface slope is varied from –20° to 20° (Table 9), and produces approximately similar forms (Figures 54 and 55). However, some differences are noted.

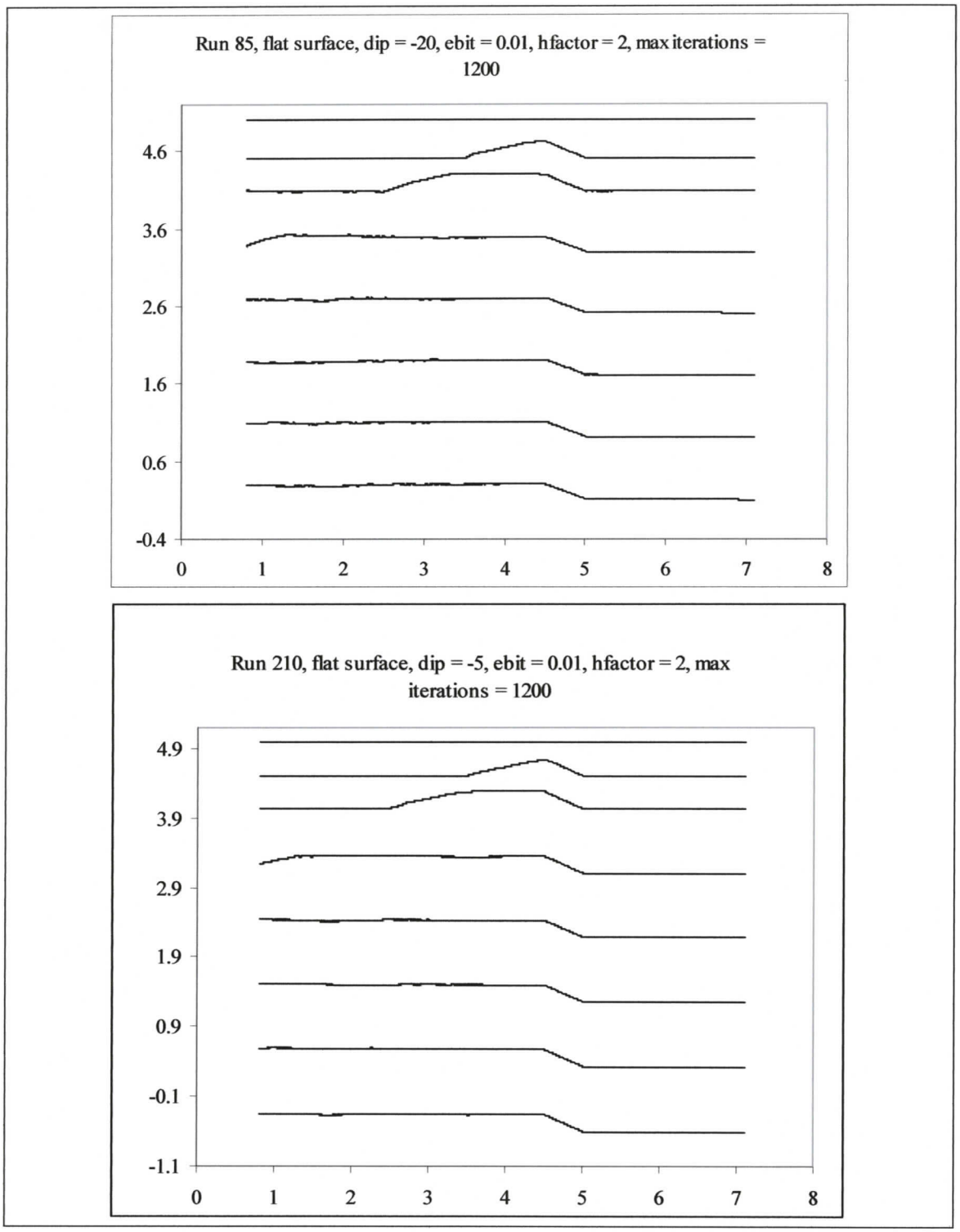

Figure 54. Flat surface erosion on uphill slopes. Dips = -20° (top) and –5° (bottom). Flow is to the right. Resistant core located between 4.5 and 5 on the x-axis. Iterations shown: 0, 100, 200, 400, 600, 800, 1000, and 1200.

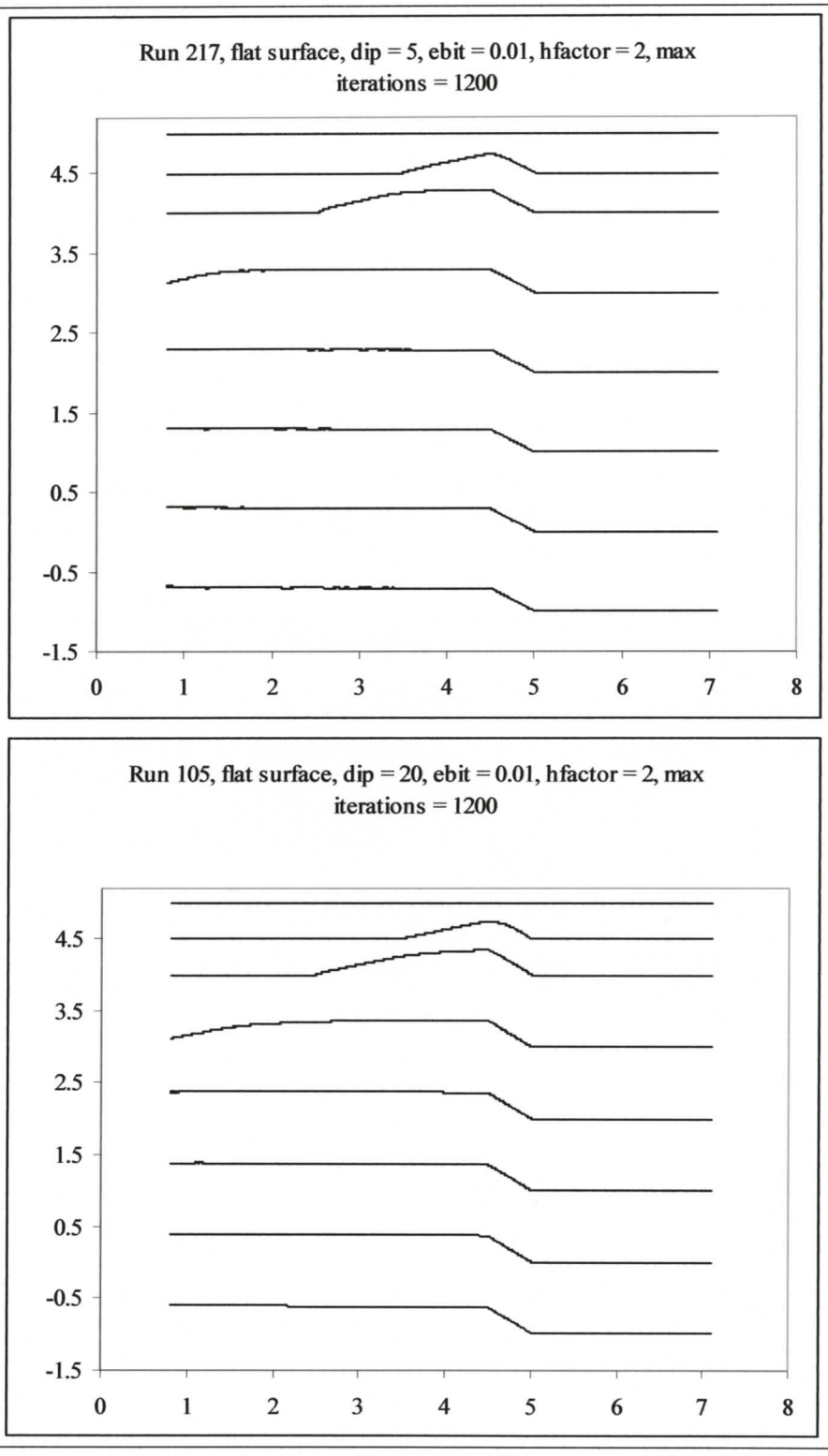

Figure 55. Flat surface erosion on downhill slopes. Dips = 5° (top) and 20° (bottom). Flow is to the right. Resistant core located between 4.5 and 5 on the x-axis. Iterations shown: 0, 100, 200, 400, 600, 800, 1000, and 1200.

Relative erosion depth increases as rock surface dip increases from –20° to 5°. Erosion depth is given by the y-axis. Erosion depth at 1200 iterations is shown on Figure 54 (top) as y = 0 for the surface dipping –20°. The 5° down-ice dipping surface is eroded to approximately y = –1 by iteration 1200 (Figure 55, top). Greater erosion occurs on the surfaces that dip down-ice than on the surfaces that dip up-ice. This is because more basal shear develops when the ice is flowing downhill. When the ice is flowing uphill, basal shear in the flow direction is dampened by basal shear acting in the opposite direction. The opposite shear is caused by a downhill pull on the ice sheet in the up-ice direction.

Smoother surfaces develop on down-ice dipping slopes than on up-ice dipping slopes (compare Figure 54 top to Figure 55 bottom). This effect is also related to the difference between uphill and downhill flow. Resultant shear stresses on up-ice surfaces are less than on down-ice faces since the downhill pull due to gravity on an up-ice face opposes the pull due to cohesiveness of the moving ice sheet. Lower shear stresses have the effect of increasing the percentage difference in shear stress values between adjacent slices. For example, two adjacent slices on a down-ice slope might have shear stresses of 2000 and 2100 kPa, respectively. Two adjacent slices on an up-ice face might have shear stresses of 200 and 300 kPa. The difference between the values is equivalent. However, the amount of erosion is calculated using a percentage of the maximum shear stress for a given iteration. The percentage difference in erosion between the adjacent slices would be greater on the up-ice face than on the down-ice face, resulting in a rougher surface.

Flat rock erosion form development occurs in two stages. Asymmetric hills, with steeper slopes on their down-ice sides, form in the first 200 to 400 iterations. By about 600 iterations, the surface shape reaches an equilibrium form which it maintains for all subsequent iterations. The equilibrium form is an inclined plane at the location of the resistant core; the inclined plane separates two surfaces that parallel the original flat surface. The angle between the steeper, resistant core surface and the rest of the surface increases from 20.8° for the –20° slope to 35° for the 20° slope. The variation is regular and can be expressed by a linear relationship with an R^2 value of 0.996 (Figure 56).

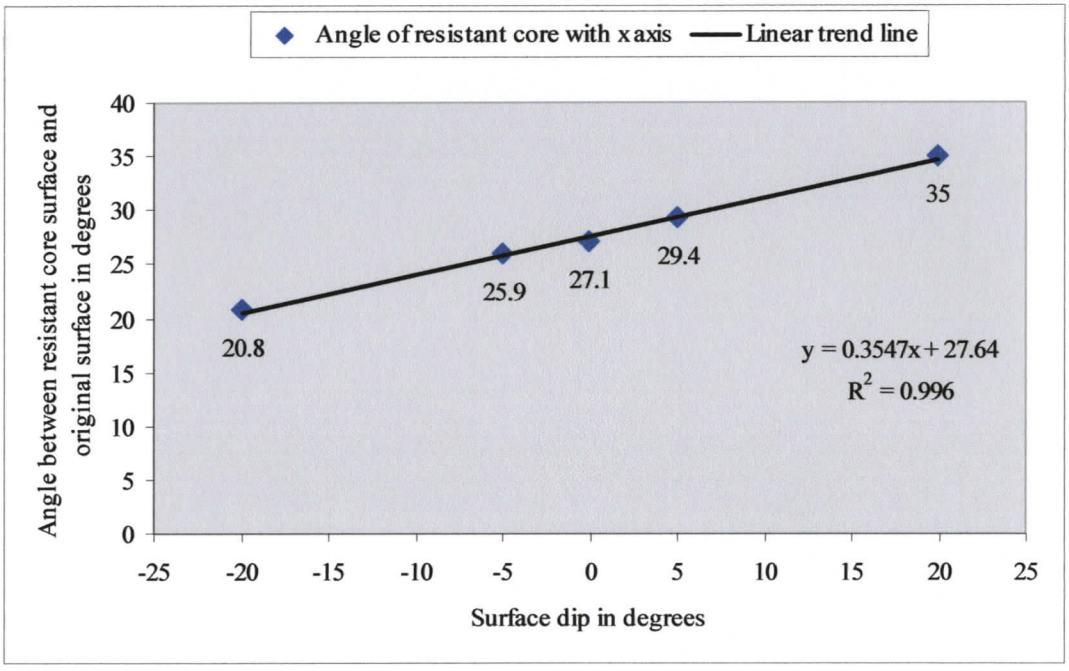

Figure 56. Inclination differences between erosion surfaces of resistant core and adjacent rock.

4.4.2. Rock drumlin erosion

Erosion bit and surface dip are varied for simulated erosion of a rock surface with a typical drumlin profile using the same values as simulated flat surface erosion (Table 9). The number of iterations is extended on 5° and 20° slopes with 0.02 erosion bit and on a 0° slope with 0.001 erosion bit in order to observe the point of form equilibrium. Form equilibrium refers to the point in the analysis run where further change to the shape of the surface does not occur; the only change to the surface is a progressive lowering. Another supplementary run is conducted to ascertain whether an "edge effect" is present with rock drumlin analysis runs. This is accomplished using a drumlin shape approximately one-half the size of the shape used in the other analyses. Flat surfaces extend in front of and behind the drumlin shape.

Almost no difference in erosion pattern is attributable to dip slope variation when an erosion bit of 0.001 is used. The analysis incrementally flattens the drumlin. A flat surface represents the stable surface configuration and is obtained before increment 3000 on 0° dip slope (Figure 57).

Erosion of the half-size drumlin demonstrates an edge effect (Figure 58). The drumlin shape does not persist in its original location, but is planed down. However, a modified drumlin shape is propagated up-ice. The modified shape has an up-ice facing surface similar to that of a roche moutonnée. The up-ice face changes from convex to concave. The down-ice facing surface of the propagating form has the same approximate slope as the original drumlin tail.

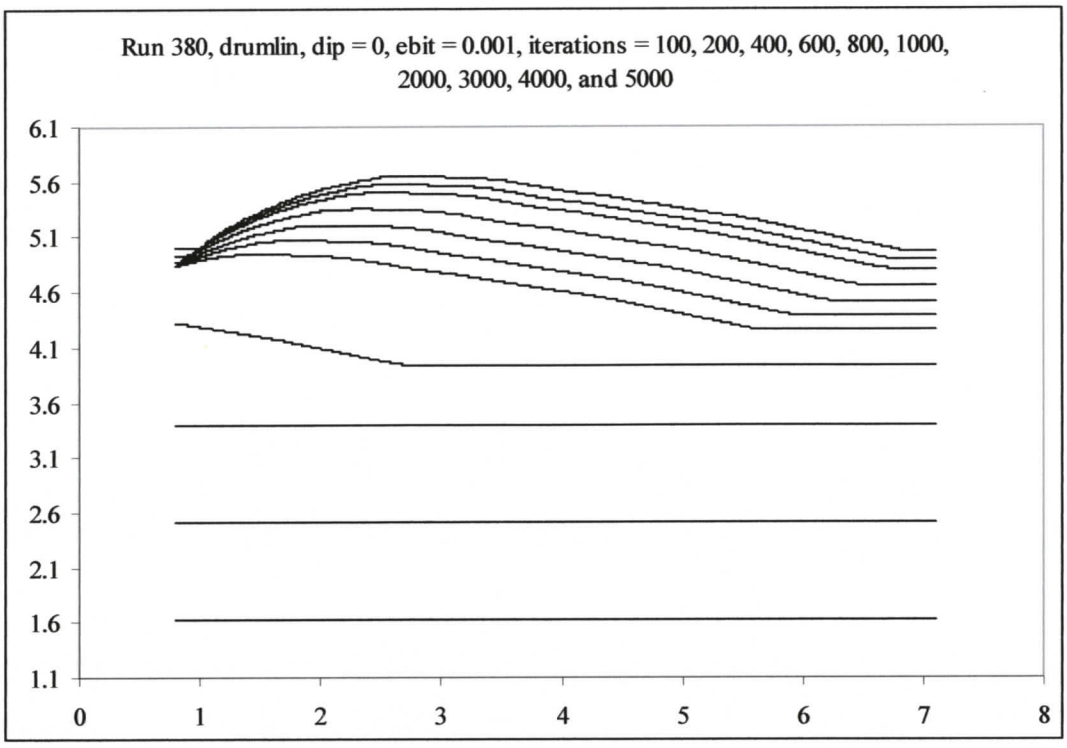

Figure 57. Rock drumlin erosion using ebit = 0.001.

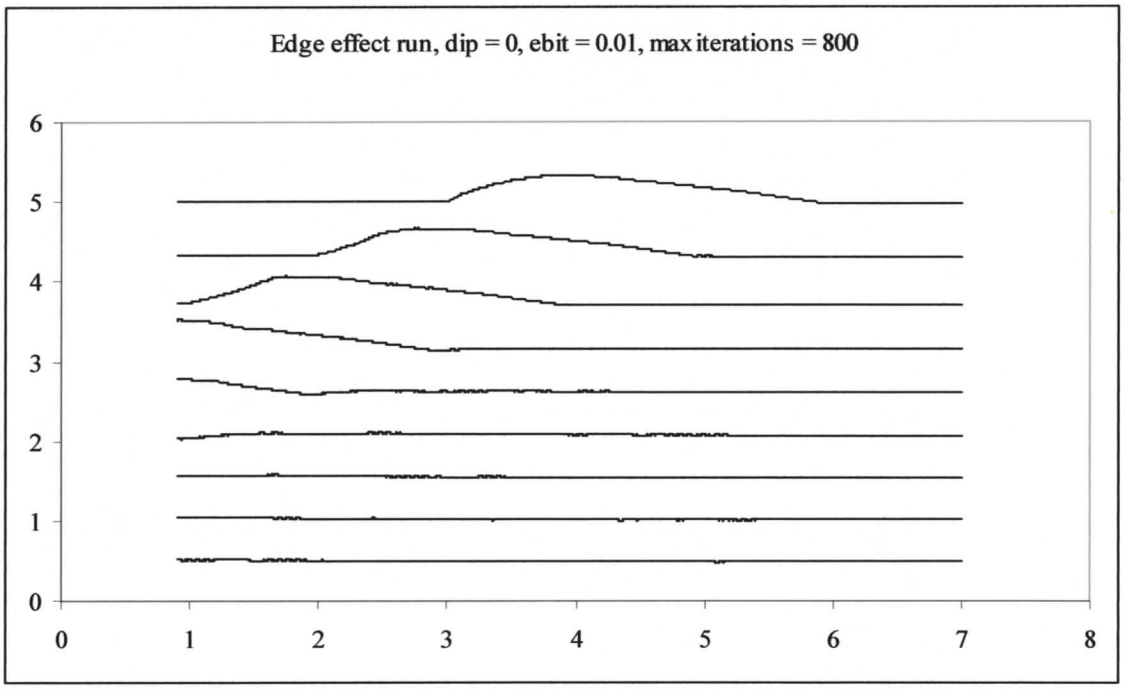

Figure 58. Edge effect of rock drumlin erosion. Drumlin shape is planed down in its original location, but modified shape is propagated up-ice. Flow is left to right. Iterations shown in the bottom figure are from 0 to 800 in increments of 100 iterations.

Three interpretations are made about the edge-effect run. First, the ice analysis tends to develop a roche moutonnée up-ice surface. Second, a rock drumlin shape does not persist in a single location, but is replaced by a slope-parallel plane. Third, an initial drumlin shape results in the propagation of a positionally unstable ridge in the up-ice direction. In terms of reality, this final result suggests that stress conditions beneath an ice sheet can favour the temporary existence of positive relief ridges.

Erosion of rock drumlins on all dip slopes using an erosion bit of 0.01 produces a planar surface by 600 - 1000 iterations. The planar surface is within 1° of the dip slope inclination. Depth of erosion increases as the dip value increases; that is, runs using –5° dip show greater erosion after 1200 iterations than runs using –20° dips. Maximum erosion depth occurs with the runs using a 20° dip slope. Erosion using the steeper dip slopes, -20° and 20°, produce the "roughest" erosion; the "smoothest" erosion occurs on the 5° dip slope, parallel to the ice surface (compare Figures 59 and 60).

The roughest erosion surfaces occur when the erosion bit is 0.02. Of these, the roughest surfaces occur on –20° and 20° dip slopes. The 0.02 erosion bit also results in greater erosion depth than occurs with the 0.01 erosion bit; erosion depth increases as the dip increases from –20° to 20°. Approximately stable surfaces with low relief occur by 1200 iterations for –20°, –5°, and 0° slopes (Figure 61). The 5° slope, parallel to the ice surface, does not reach a planar surface before the completion of 2400 iterations. The approximately planar surfaces at the end of the runs deviate as much as 6.2° from the original surface dips on the –20° and 20° dip slopes (Figure 62).

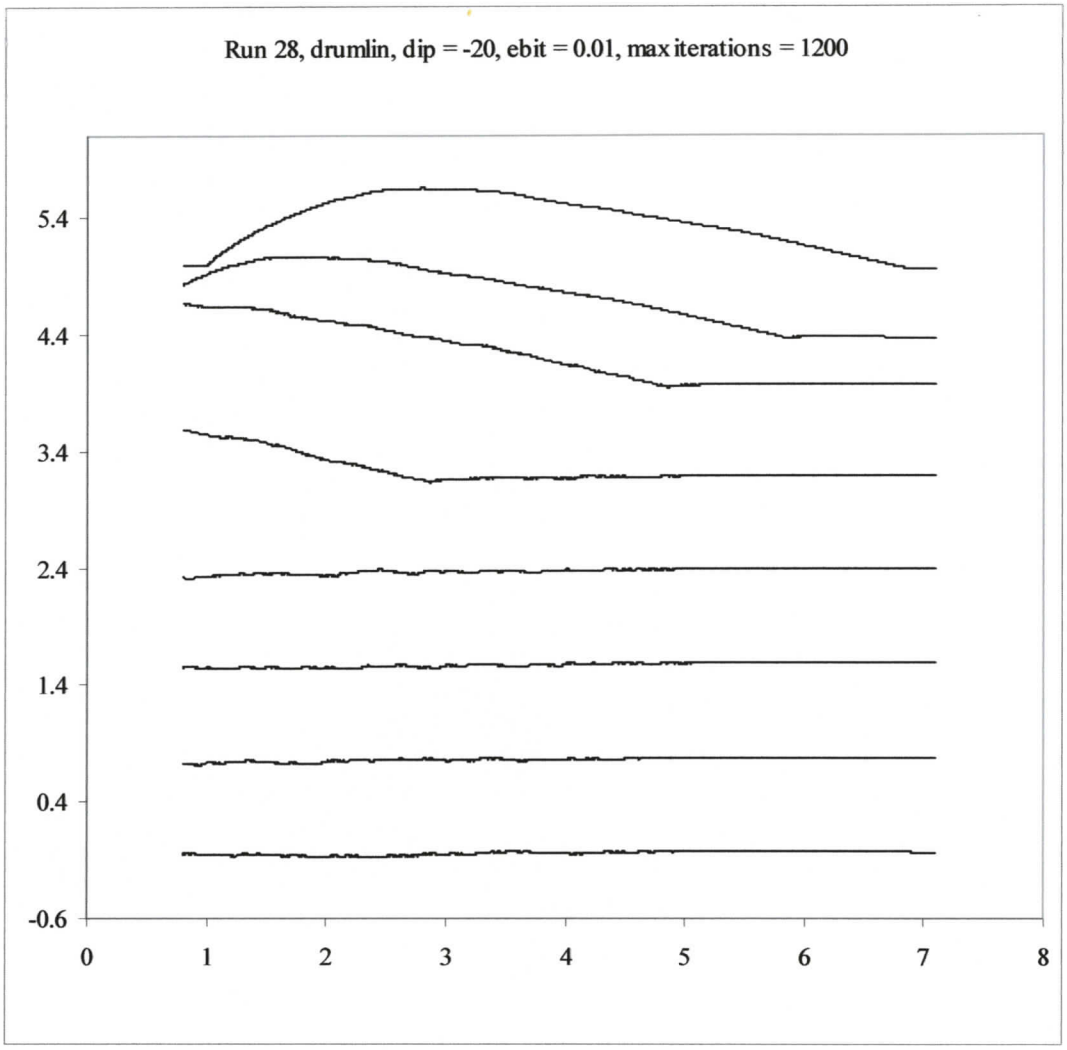

Figure 59. Rock drumlin erosion using ebit = 0.01 on uphill slope, dip = -20°. Iterations shown: 0, 100, 200, 400, 600, 800, 1000, 1200.

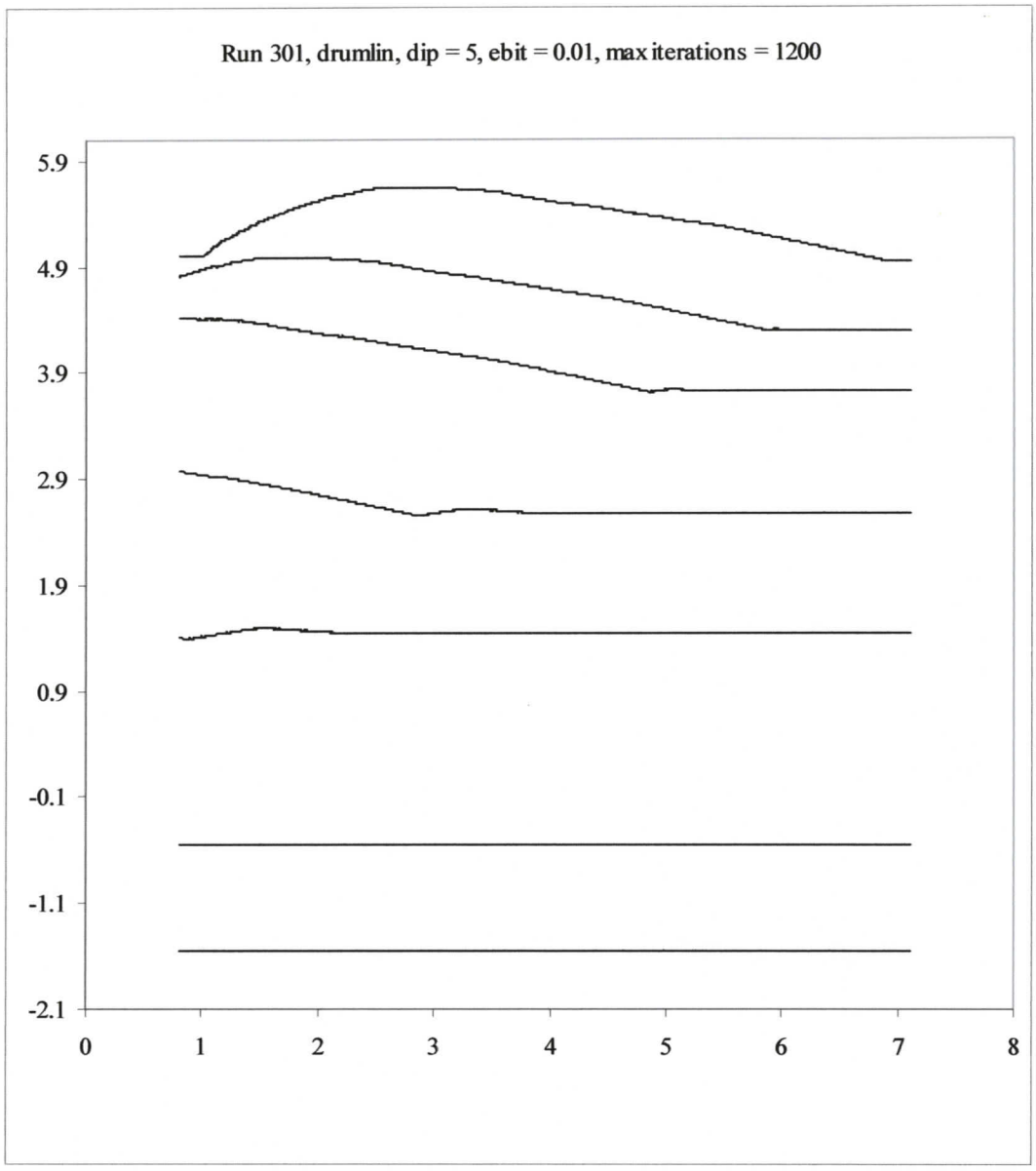

Figure 60. Rock drumlin erosion using ebit = 0.01 on downhill slope, dip = 5°. Iterations shown: 0, 100, 200, 400, 600, 800, 1000, 1200.

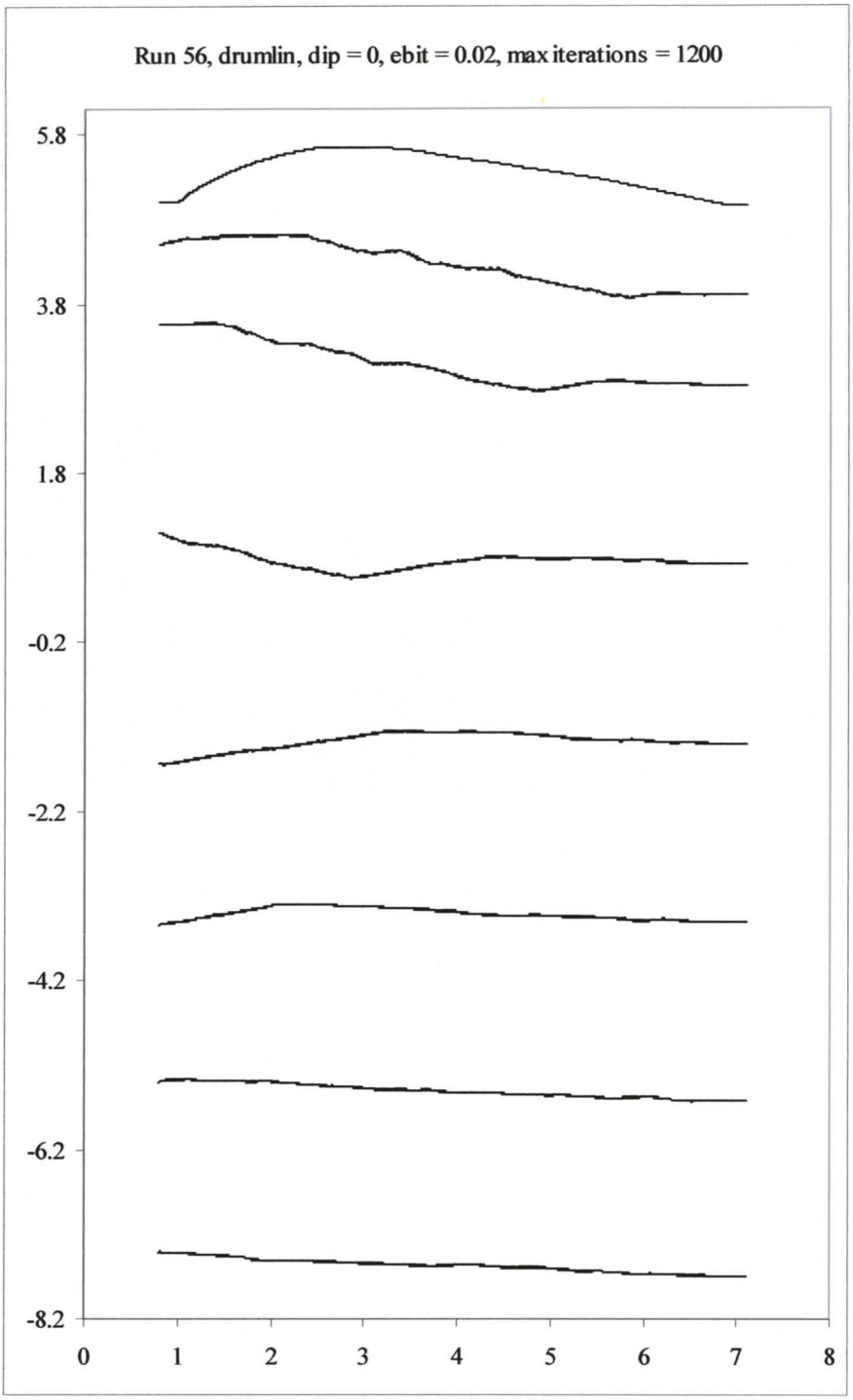

Figure 61. Rock drumlin erosion using ebit = 0.02 on level slope. Iterations shown: 0, 100, 200, 400, 600, 800, 1000, 1200.

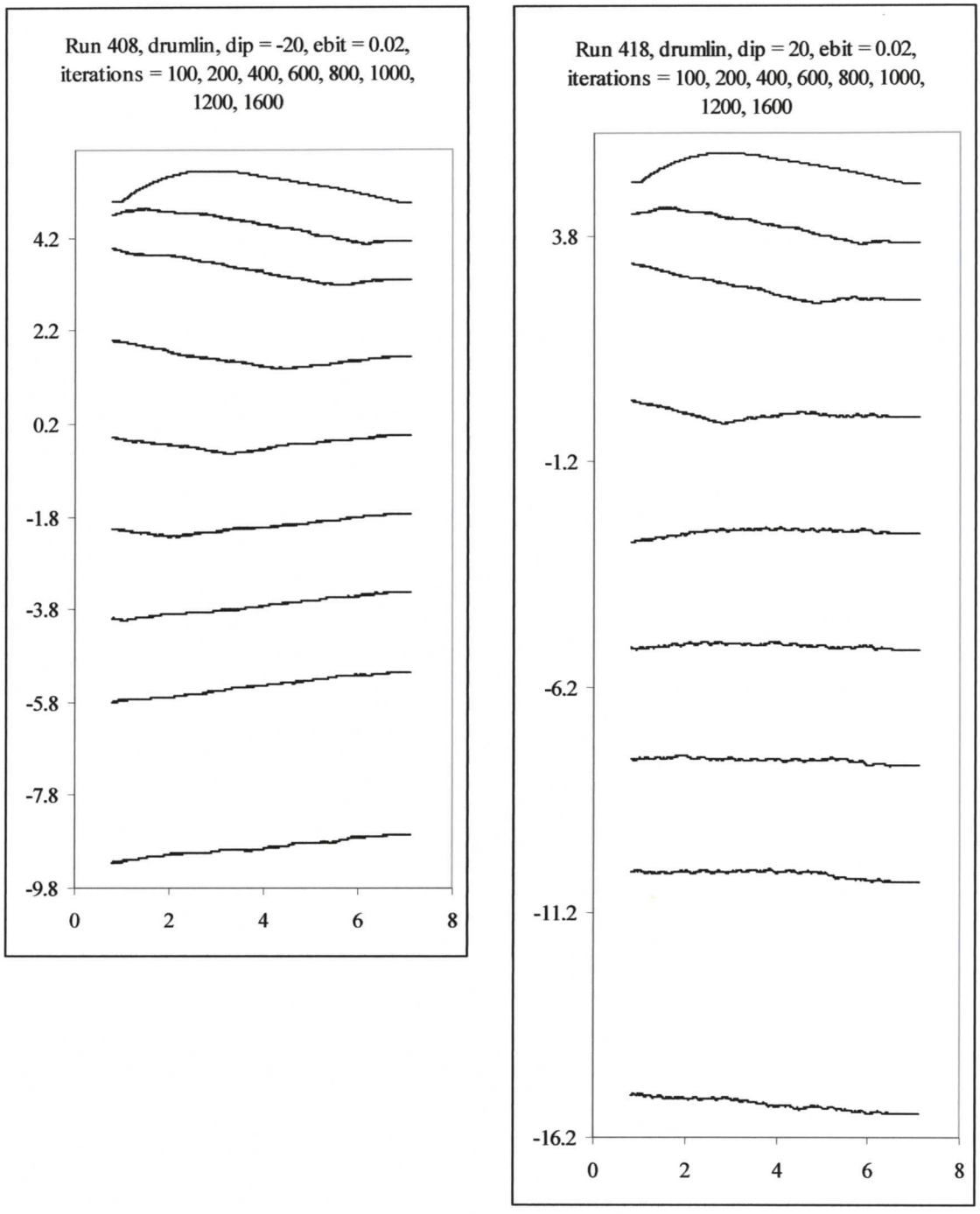

Figure 62. Rock drumlin erosion, -20° (left) and 20° (right) dips, ebit = 0.02.

4.5. SUMMARY AND DISCUSSION

The incremental glacial erosion analysis presented in this chapter allows for simulation and visualization of shear stress distribution over time at an ice sheet / rock surface interface. A shear stress distribution is used to differentially "erode" the rock surface, thereby producing a new rock surface that triggers a new stress distribution. The analysis is restricted to the set of assumptions presented earlier, and to specific parameter settings for a given run.

4.5.1. Discussion of analysis assumptions

One of the more important assumptions is the restriction of the analysis to two dimensions. The analysis is defined by a vertical axis and single horizontal axis. The second horizontal axis, which is perpendicular to the modeled axes, is not considered in the analysis. In some real-world cases, two-dimensional flow is more applicable than in other cases. For example, an assemblage of sedimentary rocks with near vertical dip might strike perpendicular to ice flow. In this case, rock properties along the strike of the beds are relatively consistent; whereas, inhomogeneous rock properties would be encountered along flow. If one layer in the assemblage is harder than overlying and underlying strata, then a situation exists in which the flat rock, two-dimensional analysis closely approximates actual conditions.

The analysis approximates conditions where little change in rock composition or morphology occurs perpendicular to the dimensions represented by the analysis. The non-modeled dimension of a streamlined rock drumlin is not constant perpendicular to modeled dimensions; that is, the drumlin shape changes in the directions perpendicular

to model dimensions at any given point along flow. However, it is assumed here that the two-dimensional model can still be validly applied to a drumlin shape due to the main directions of force at the ice sheet base. Most force is directed down and in the flow direction. Although forces may locally act in directions outside the plane represented by the model, these forces would probably be of less magnitude than the forces acting within the model plane.

The non-modeled dimension of flat rock erosion is more likely to be constant in the direction perpendicular to modeled dimensions. In this sense, the flat rock surface is more suited to two-dimensional erosion modeling than the rock drumlin surface.

It is assumed in the analysis that all erosion is caused by shear stress parallel to the rock surface, and that erosion is accomplished by abrasion. The abrasion source is visualized as similarly sized, fine-grained sediment evenly distributed within the ice sole. Although this assumption for the abrasion source is probably often not true, it is possible in areas where ice flow is over bedrock. In addition, inhomogeneities in the abrasive source would presumably even out across any one area over time, in many cases. Another major ice erosion process not included in the analysis is quarrying or plucking, a process in which fragments larger than about one centimetre across are fractured from the bed (Sugden and John, 1976). Freeze-thaw processes and inhomogeneous distribution of rock particles in the ice are also not included in the analysis. Nonetheless, abrasion is considered a major source of ice erosion (*e.g.*, Flint, 1957; Sugden and John, 1976), and it is likely that real locations and ice conditions existed where the erosion mechanism assumed here is a valid approximation of reality.

A discussion of longitudinal stress is included earlier in this chapter. No direct calculation of longitudinal stress is attempted in this analysis. It is suggested here that the method selected for simulating longitudinal stress approximates reality in at least some cases.

The homogeneity of the rock drumlin surface is assumed, and the inhomogeneity of the flat rock surface is rigidly defined in the analysis. This assumption would be valid for some real situations.

It is assumed in the analysis that the ice surface remains in constant contact with the rock surface. As mentioned earlier, this assumption of the analysis is a departure from known glacier behaviour at steep cliff faces, and possibly results in the "run-away erosion" effect described earlier. However, the assumption is valid for near-horizontal surfaces. It is suggested here that this assumption renders the analysis more applicable to near-horizontal slopes than to steeper slopes.

4.5.2. Asymmetric forms and inclined planes

Simulated erosion of a flat surface with an inner core of more resistant material is intended to provide insight pertaining to rat-tail bedrock forms. A streamlined form comprising a resistant core on its up-ice end and a tapering tail down-ice of the core is not obtained using the analysis. The analysis indicates a failure of ice to produce the forms. Given the restrictions on the analysis, no firm conclusions are possible, but the analysis results themselves are not supportive of an ice origin for rat-tails.

However, roche moutonnée forms, or "reverse drumlin" shapes, are consistently produced by the analysis. A partial roche moutonnée form is also produced during the

"edge effect" rock drumlin erosion run. These results suggest that the roche moutonnée form could be consistent with stress distribution patterns beneath some parts of an ice sheet. The roche moutonnée form does not persist indefinitely in analysis runs. It is replaced by two parallel planes separated by a steeper inclined plane where the resistant core is located.

The validity of the analysis results could be tested by a field study of roche moutonnée forms. Relative hardness of portions of the forms could be measured along flow. If greater hardness values are found on down-ice surfaces of roche moutonnée forms than on up-ice surfaces, then the analysis would be validated and ice as the forming mechanism of roche moutonnée would be supported by the analysis.

4.5.3. Simulated rock peneplains and propagating ridges

Given the assumptions of the analysis and in cases of homogeneous rock hardness, a drumlin shape is not positionally stable beneath an ice sheet and is rapidly planed down. The basal shear stresses tend towards a level surface at a given location. However, the "edge effect" analysis run indicates that a positive-relief ridge similar to a drumlin shape is propagated up-ice when erosion is applied to an existing drumlin surface.

4.5.4. Hypotheses

The first hypothesis is: A bedrock surface with a streamlined "drumlin" shape maintains this shape at a given location when subjected to basal ice sheet stresses. In model erosion, the stress field at the base of an ice sheet planes down a drumlin shape. Hence, the first hypothesis is rejected because the rock surface where the drumlin is

located at the beginning of the test is planed down. However, a modified drumlin shape is propagated up-ice. This up-ice surface of this modified shape has a gentler slope than the drumlin shape. This suggests that a ridge form can exist at a given time beneath an ice sheet. However, the ridge does not persist at a single location.

The second hypothesis predicts that a streamlined form results when a surface with a resistant core is subjected to shear stresses at the base of an ice sheet. The core will act as the up-ice end of the form, and a tail will extend down-ice from the resistant core. Such forms are not produced by the analysis and, strictly interpreted, analysis results do not support the second hypothesis. However, roche moutonnée forms are consistently produced, but not maintained, by the model. These forms have reverse asymmetry to rat-tails and crag-and-tails, but are nonetheless defined as streamlined bedrock forms in this thesis (Chapter 1).

4.5.5. Application to reality

The implications of these results are that at least two glacial terrain bedrock landforms are obtainable by ice sheet erosion as modeled: the roche moutonnée and the flat plane. Their formation by ice sheets is supported by the analysis results. Analysis results also suggest that, given an initial drumlin shape, bedrock ridges can persist temporarily at a given location beneath the ice.

Analysis results do not support formation of rat-tails at the base of the modeled ice sheet. Streamlined forms do not develop in the lee of resistant bedrock cores. At a given location, drumlin shapes are reduced to planar surfaces.

The analysis tool, as built, is probably not applicable to steep slopes that face down-ice since the analysis assumes constant rock-ice contact and does not incorporate ice bridging. The assumption of homogeneous ice and rock composition is valid in some cases over local scales. However, the larger the scale of application, the more likely that this assumption is not valid. The up-ice propagation of the ridge during the edge effect test is possibly due to the assumption of homogeneity. Up-ice inhomogeneity would possibly disrupt this propagation effect.

The analysis is best applied to locations and ice conditions where analysis assumptions most closely approximate reality. Optimum "reality" is obtained where the ground surface approaches horizontal, the ice sheet is homogeneously permeated with fine-grained sediments, and the ground surface composition varies minimally in the dimension not represented by the analysis. An example of a "analysis-friendly" environment is a uniformly "dirty" ice sheet advancing across a fairly level surface of inclined sedimentary beds. The strike of the beds is perpendicular to flow, and resistance to erosion of each bed is consistent within that bed.

4.5.6. Comparison to a similar analysis

The only analysis found in the literature review comparable to the analysis presented here was developed by Boulton (1974, 1979). Boulton (1974, 1979) uses an abrasion theory, in conjunction with a sliding theory, to theoretically model glacial erosion and deposition along a two-dimensional surface. Pressure distribution over a low, sinusoidal ridge oriented transverse to ice flow is determined according to Nye's (1970) glacial sliding theory. Differential erosion and deposition are determined by

Boulton's abrasion theory that establishes areas of relative erosion and deposition based on differences in normal pressure. Boulton applies a time transgressive analysis in which he calculates a new surface based on areas of erosion and deposition, re-synthesizes the model, and repeats the calculations. The analysis is run using two different values of ice overburden pressure, 7 bars and 24 bars (Boulton, 1974).

Boulton's model relates erosion to normal pressure, includes an ice velocity component that is part of Nye's glacial sliding theory, and does not consider down-ice directed pressure due to a sloping ice surface. The analysis presented here resolves the pressure due to the overburden and due to the slope of the ice sheet into shear stress components; erosion is related to shear stress instead of normal stress. The thesis analysis does not include an ice velocity component. Boulton's analysis starts with a hummock of sinusoidal profile. The thesis analysis erodes a rock drumlin shape, which is roughly similar to the sinusoidal hummock, and also erodes a flat surface with a resistant core. Both Boulton's analysis and this analysis are applied iteratively; Boulton presents up to five stages of form evolution representing five iterations of the analysis. The analysis presented above is usually run up to 1200 iterations for a given set of parameters. Boulton's analysis includes both erosion and deposition. The analysis presented here only includes erosion.

When run using a normal pressure of 7 bars, Boulton's theory produces a profile where the lee face is steeper than the up-ice face. This profile is compared to roches moutonnées forms. This form propagates in a down-ice direction. Boulton's run using 24 bars pressure results in a profile where the up-ice surface is steeper than the down-

ice surface. This form propagates in an up-ice direction. This profile is compared to a drumlin.

The analysis presented in this chapter has some similarities to Boulton's analysis. Both models produce roche moutonnée – like forms. The propagation of a form along the horizontal axis occurs with both models.

4.5.7. Field observations related to analysis results

Streamlined forms on Microwave Ridge in the Hazelton Range are discussed in Chapter 5. The ridge is comprised of generally north-south striking beds (Figure 63). The beds dip steeply towards the west. The topography of the ridge includes alternating north-south trending high areas separated by north-south trending low areas. The high areas are presumably composed of more resistant material than the low areas. Generally west-trending rock drumlins, rat-tails, and striae are present on many of the outcrops (Chapter 5).

The step-like topography is probably the result of differential erosion caused by the same flow that formed SBF and/or striae at the site. The analysis results suggest that this topography could have resulted from west-trending ice flow across the ridge. Abundant west-trending rat-tails occurring with east-west striae on outcrops indicate west-flowing ice.

Step topography and roche moutonnée forms occur in glaciated terrains. Results from the model research presented here support the interpretation that these glacial terrain features are produced by ice. A possible test of the applicability of the analysis

could be conducted on roche moutonnée forms. The analysis predicts that the lee end of these bedrock forms would be harder than the stoss ends.

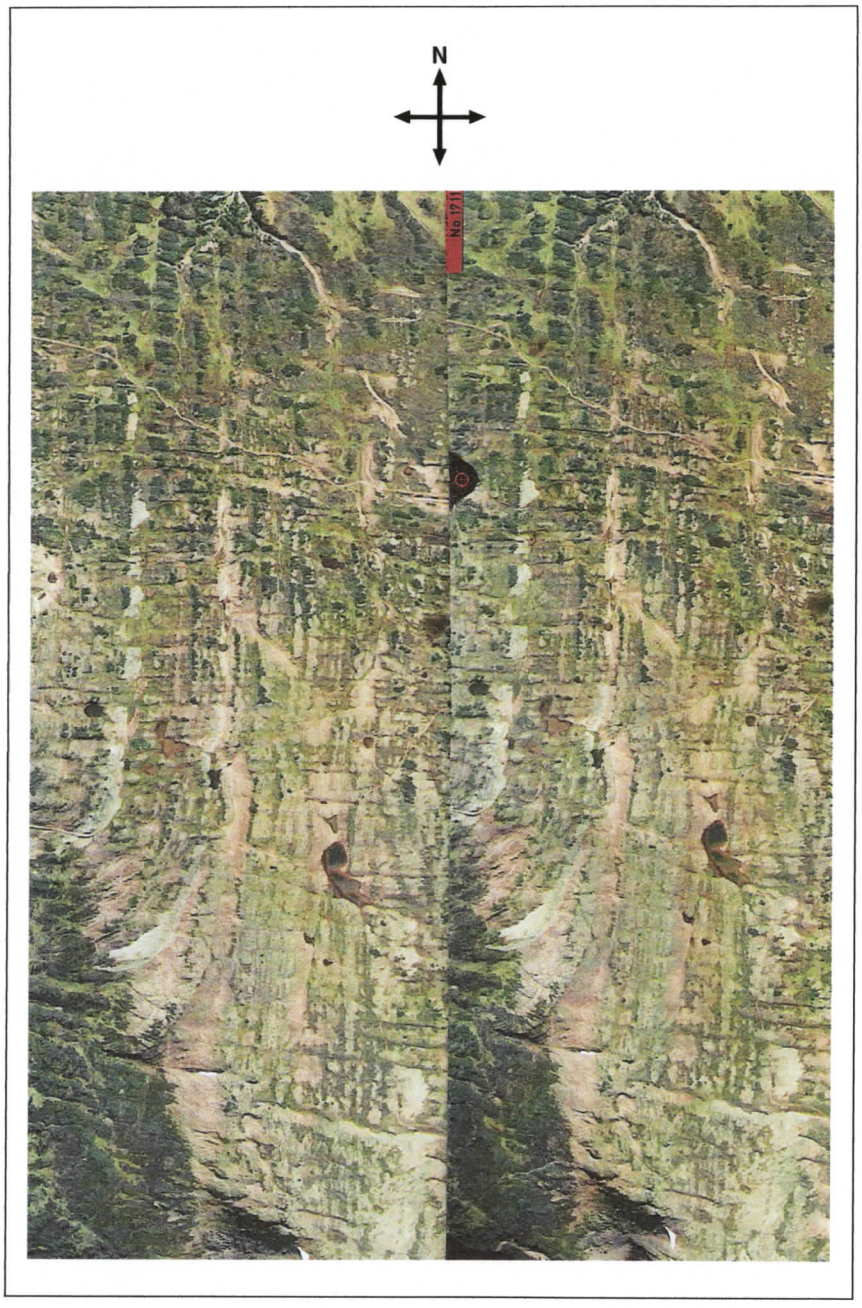

Figure 63. Air photo pair of Microwave Ridge. Streamlined forms at the site were produced by flow towards the west. Bedding planes on the ridge strike generally north-south and dip to the west. British Columbia Government air photos, SAS30C996133 – 459 and 460.

5. FIELD STUDIES

5.1. INTRODUCTION

One thesis research objective is to observe and describe streamlined forms (SF) in the field and relate those observations to SF origins. This chapter presents the results of field investigations of SF sections at several locations within the study area and detailed descriptions of several streamlined bedrock form (SBF) sites. There were several reasons for this part of the study. First, it was necessary to observe sediment streamlined forms in the field in order to better understand remote imaging data. Secondly, the study of drumlin sections is relevant to the question of SF origins. For example, sorted sediments could indicate fluvial action; deformed sediments could indicate glacial deformation; and, drumlin morphology and composition could help to determine if the forms are erosional or depositional features. These elements of the field analysis are discussed later in this chapter. Finally, the study of rat-tails allowed for determination of flow directions and rat-tail and striae occurrence patterns were needed to make inferences pertaining to SF origins and to evaluate theoretical results of the computer analysis.

Previous work pertaining to SF composition and bedrock erosional marks found in the field study is introduced below. In the methods section, study site locations and a summary of collected data types are provided. Field study observations are presented in the results section. Inferences and conclusions derived from the observations are then applied to the problem of the occurrence and origin of SF in the study area.

5.2. PREVIOUS WORK

5.2.1. Previous work pertaining to streamlined forms composition

Most drumlins are composed primarily of diamicton (Flint, 1957; Aario, 1987; Dardis and McCabe, 1987; Karczewski, 1987; Rose, 1987; Forbes and Syvitski, 1994; Newman and Mickelson, 1994; Knight, 2002); although, there are many examples of SF composed entirely or partially of well sorted sediments, ranging from clays and silts, implying low energy deposition, to sands, gravels, and boulders, indicative of high energy deposition. Most diamictons in drumlins are interpreted as tills, but some are considered to be debris flow deposits (Dardis, 1987; Dardis and McCabe, 1987; Shaw *et al.*, 2000). Submarine tills contain shell fragments (Stalsberg *et al.*, 2003).

Sediments comprising drumlins are found to both conform to the drumlin shape (Aario, 1987; Hanvey, 1987; Sharpe, 1987; Newman and Mickelson, 1994; Shaw, 1996) and to be truncated by a streamlined surface (Boyce and Eyles, 1991; Newman and Mickelson, 1994; Shaw, 1996; Knight, 2002). Reasonable evidence and convincing arguments are presented in the literature supporting drumlin formation by both erosional and depositional processes.

Drumlin stratigraphy can be complex (*e.g.*, Shaw *et al.*, 2000), with SF often containing more than one identifiable unit. Researchers report drumlins composed of dual diamicton layers (Aario, 1987; Newman and Mickelson, 1994; Knight, 2002), diamicton mantles draped over sorted sediments (Hanvey, 1987; Harry and Trenhailie, 1987; Sharpe, 1987; Boyce and Eyles, 1991; Newman and Mickelson, 1994; Stalsberg *et al.* 2003,), and diamicton interbedded and conformable with sorted sediments

(Dardis, 1987; Dardis and McCabe, 1987; Sharpe, 1987; Shaw *et al.*, 2000). Mate (2000) described SF in the central part of the thesis study area. Many SF in that area are crag-and-tails with bedrock stoss ends and diamicton tails.

5.2.2. Previous work pertaining to streamlined bedrock forms

Erosional marks cut into bedrock are characteristic of glaciated terrain. These marks include striae, rat-tails, furrows, troughs, rock drumlins, sichelwannen, muschelbrüche, comma forms, undulating surfaces, and potholes (Benn and Evans, 1996). Forms that demonstrate streamlining, as defined in Chapter 1, and that were observed during the field study are considered in this dissertation, including rat-tails, rock drumlins, roche moutonnées, and furrows. These are referred to here as streamlined bedrock forms (SBF). Observations of cavettos are presented as they relate to the question of SF origins. Hairpin furrows are discussed because where they occur in the study area they usually outline positive relief SF such as drumlins, crag-and-tails, rock drumlins and rat-tails. Sichelwannen are included because of their similarity of form to hairpin furrows (Kor *et al.*, 1991). Muschelbrüche, comma forms, undulating surfaces, transverse troughs, and potholes are not discussed here. General observations pertaining to striae are also discussed in this thesis. Rat-tails, rock drumlins, and roche moutonnées in the study area have been reported and used as flow indicators by several researchers (Stumpf *et al.*, 2000; Ferbey and Levson, 2001; Levson, 2002; Levson and Mate, 2002). They are also commonly used by researchers in other areas.

Assemblages of hairpin erosional furrows or sichelwannen commonly display interconnected arrangements (Kor *et al.*, 1991; Shaw, 1994), that is, hairpin furrows or

sichelwannen troughs do not typically cross-cut (see also Chapter 2, Figures 20, 21, and 24). The lateral furrows, if present, of interconnected hairpin furrows in some bedrock features lead into the proximal furrows of subsequent, down flow forms. This characteristic is also noted for the proximal and lateral furrows around some sediment SF (see Chapter 2). Kor *et al.* (1991) concluded that this spatial arrangement indicates contemporaneous formation of the interconnected forms.

Another characteristic of SBF assemblages is the occurrence of larger forms overprinted by groups of much smaller forms that generally parallel the flow direction indicated by the larger form (Kor *et al.*, 1991; Shaw, 1994; Pair, 1997; Sawagaki and Hirakawa, 1997; Kor and Cowell, 1998). The smaller forms occur within or upon the larger forms.

5.3. METHODS

Streamlined forms are examined in both lowland and alpine locations at 12 different sites in the study area (Figure 64). The internal composition and structure of lowland SF are examined using road cuts. Collected observations include composition, maximum clast size, percent clasts, clast angularity, matrix texture, and structures, if present. Streamlined form morphology is best observed in alpine areas due to the lack of vegetation. Coordinates of study site locations were marked using a Garmin 12 GPS set to a UTM projection and NAD 83 datum. UTM coordinates of SF sites where SF are composed of unconsolidated sediments, primarily diamicton, are given in Appendix B. Streamlined forms in bedrock, primarily in alpine areas, are included in Appendix C.

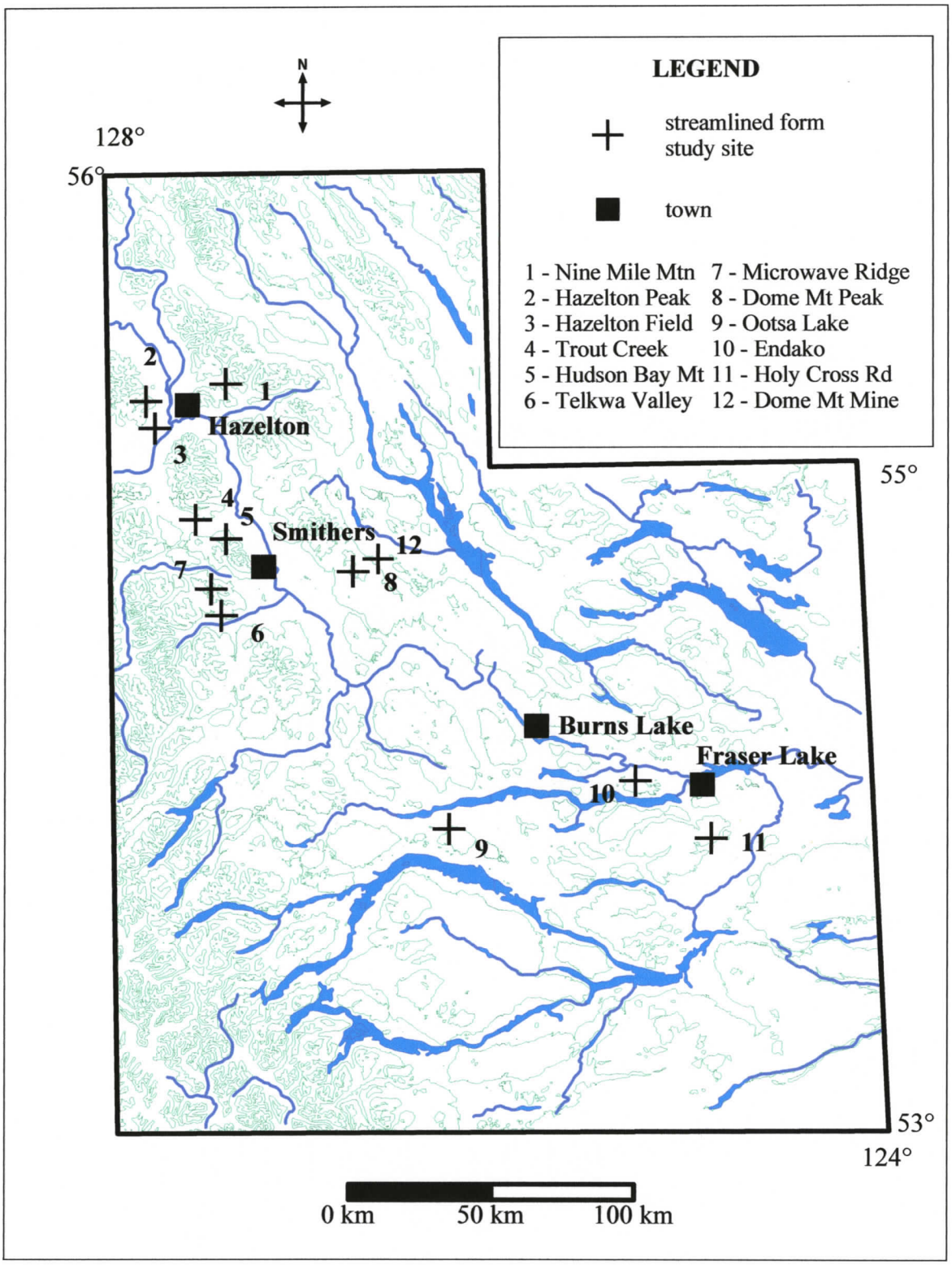

Figure 64. Streamlined forms field study sites. Contours are from 1000 m to 2500 m in 500 m intervals.

Streamlined bedrock form exposures are limited in lowland areas due, at least in part, to weathering, thick drift, and soil and vegetation cover; hence, most of the SBF study sites are in alpine areas where soil and vegetation cover is minimal and bedrock outcrops plentiful. Collected data include SBF orientation, slope mode (whether the form points uphill or downhill), elevation, and UTM eastings and northings (Appendix C). At each site, it is noted whether striae parallel rat-tail orientations, and if cross-cutting SBF or striae are evident.

5.4. RESULTS

5.4.1. Lowland streamlined forms

Almost all SF in lowland areas are composed of massive diamicton (Table 10). Based on air photo data, many are crag-and-tails. Even within a single area, there is wide variability of diamicton matrix texture, percent clasts in the matrix, rounding range, and maximum clast size. Of 78 matrix descriptions, the dominant texture of the matrix is clay in 17 samples, silt in 46 samples, and sand in 15 samples; 81% of the diamicton samples had silt or clay matrix textures. About 20% of the investigated SF had visible bedrock cores. However, the road cuts through the SF often did not extend down to the SF base, and if bedrock cores were present, they may not be exposed. It is likely that a higher percentage of SF have bedrock cores than is indicated, particularly in areas where most SF are defined by hairpin furrows which may be initiated by obstructions to flow (Karcz, 1981; Allen, 1982; Shaw, 1994).

Some SF were examined using road cuts to determine if there are lateral variations along flow or vertical variations in matrix texture, percent clasts, or clast size

(Tables 11 and 12). Percent clasts and maximum clast sizes are visual field estimates. Samples for vertical comparison are separated by one to two metres; top samples are one metre below the SF crest and bottom samples are 2-3 m below the SF crest. Lateral samples are spaced 5-50 m apart. All SF listed in the Table 11 and Table 12 are located in the Hazelton SF field (Figure 64).

Lateral variation of matrix texture, percent clasts, and maximum clast size within individual SF is present, but slight. Textural variation comprises minor fining or coarsening; for example, the diamicton matrix of SF 72 changes from silty to clayey silt in the down flow direction along one SF flank (Table 11). Differences in percent clasts and maximum clast sizes within individual SF are variable. No patterns of variation related to flow direction are recognized.

Table 10. Composition of lowland streamlined forms

	Number of SF examined					*Diamicton descriptions*			
Region	**Total**	**With bedrock cores**	**Percent bedrock cores**	**With sorted sed.**	**With diamicton +/– bedrock**	**Matrix texture range**	**Percent clasts range**	**Clast rounding range**	**Max clast size range (cm)**
Hazelton field	34	8	24%	0	34	clay to sand	5 - 65%	A to R	15-90
Trout Creek	9	2	22%	1	8	clay to silty sand		A to SR	30-40
Telkwa Valley	8	0	0	0	8	clay to silt	20%	SA to R	15
Ootsa Lake	5	2	40%	0	5				
Endako	3	1	33%	0	3	clay to silt	40%	A to SR	25
Holy Cross Road	13	1	8%	1	12	clay to sand	5 - 60%	A to R	10-70
All (sum)	72	14		2	70				
All (avg.)			21%				33%		37
All (range)						clay to sand		A to R	

Table 11. Lateral variation in streamlined form composition, Hazelton streamlined forms field

ID	Distance between samples (m)	Distance below SF crest (m)	Properties	Up-flow to down-flow locations, from left to right.				
70	10	2	texture*	cz	sz			
			% clasts	45%	40%			
			max. clast size (cm)	60	60			
72	5	1	texture	z	z	cz	cz	cz
			% clasts	5%	25%	45%	45%	45%
			max. clast size (cm)	90	90	90	90	90
73	20	1	texture	cz	cz	zc	zc	zc
			% clasts	20%	20%	15%	20%	5%
			max. clast size (cm)	20	20	40	60	25
82	15	1.5	texture	cz	cz	z	z	
			% clasts	40%		25%	15%	
			max. clast size (cm)	45	55	35	15	
83	50	3-10	texture	z	s	z	z	
			% clasts	40%	45%	35%	40%	
			max. clast size (cm)	50	60	75	50	

* c = clay, z = silt, s = sand

Last descriptor has highest relative percentage, *e.g.* cz is primarily silt.

Table 12. Vertical variations in streamlined form composition, Hazelton drumlin field. Top sample is 1 m below SF crest; bottom sample is 2-3 m below SF crest.

ID	Properties	Top	Bottom
50	texture	zc	z
	% clasts	10%	10%
	max. clast size (cm)	n.d.	n.d.
51	texture	sz	zs
	% clasts	15%	15%
	max. clast size (cm)	75	75
52	texture	zc	zc
	% clasts	10%	10%
	max. clast size (cm)	60	60
53	texture	c	zc
	% clasts	10%	10%
	max. clast size (cm)	35	35
54	texture	z	z
	% clasts	n.d.	n.d.
	max. clast size (cm)	60	60
56	texture	s	s
	% clasts	15%	15%
	max. clast size (cm)	30	30
69	texture	c	c
	% clasts	40%	40%
	max. clast size (cm)	40	40

* c = clay, z = silt, s = sand
Last descriptor has highest relative percentage, *e.g.* cz is primarily silt.
n.d. = no data

Vertical composition variations within individual SF are less than lateral variations, probably due to the closer sample spacing. Although minor textural differences are noted (*e.g.*, streamlined forms 51 and 53 show a slight coarsening downwards of the matrix texture), no consistent variation pattern is indicated.

No major lateral or vertical variations in SF composition are recognized. Although the number of sites observed are not sufficient to make confident conclusions, it appears that the minor composition variations observed do not follow any pattern related to flow or relative vertical location.

5.4.2. Alpine streamlined forms

Observations pertaining to SF morphology, spatial relationships, location relative to slope and flow direction, and composition were made at five upland areas (Figure 64). The SF discussed in this section range between 10 m and 100 m in length, *e.g.*, are classified as medium large SF in this thesis. Air photo and orthophoto examination show that Dome Mountain, Hudson Bay Range, and Microwave Ridge are covered by hundreds of SF, primarily composed of bedrock. Nine Mile Mountain and Hazelton Peak also show extensive fluting across their alpine areas. Streamlined forms at all the alpine areas are located above 1500 m elevation, and have orientations between 210-270° (Table 13). Some SF are pointed upslope. Implications of this uphill flow are discussed later.

Streamlined forms on Hazelton Peak (Figures 65, 66, and 8) and Nine Mile Mountain (Figure 67) consist of a significant amount of sediment. Although bedrock cores may be present beneath the surfaces of Hazelton Peak SF, only diamicton is

observed; bedrock cores are visible at the stoss ends and at isolated locations along the flanks of streamlined forms on Nine Mile Mountain indicating that diamicton cover is thin. Streamlined forms in both areas have typical streamlined shapes; the apices of the SF are closer to the stoss than lee end, and the stoss ends are broader and steeper than the tapered lee "tails". Interconnected furrows between SF ridges are evident on air photos of Hazelton Peak (Figure 8) and on photographs taken at the site (Figure 66).

Streamlined forms on Dome Mountain, Hudson Bay Mountain, and Microwave Ridge are primarily bedrock. Evelyn Mountain (part of Hudson Bay Range) SF were observed from the north side of Hudson Bay Mountain. Air photos show stoss end and lateral furrows (Figure 68). Concave lateral furrows occur along some rock SF flanks on north Hudson Bay Mountain (Figure 69).

Table 13. Streamlined forms in alpine areas

Field area	Approx. elevation (m)	Approx. Orientation	Surface slope in flow direction	Number of SF investigated	UTM easting, zone 9	UTM northing, zone 9
Dome Mountain	1680	255°	uphill	5 - 10	651117	6068858
Hazelton Peak	1525	210°	downhill	5	573991	6125452
Hudson Bay Mountain	1550	270°	uphill	5	610383	6071818
Microwave ridge*	1660	270°	uphill	5 - 10	600161	6062129
Nine Mile Mountain	1550	210°-240°	uphill, level, downhill	5 - 10	593815	6132441

* local name

Figure 65. Stoss ends of streamlined forms on Hazelton Peak. Flow was from right to left and downhill.

Figure 66. Lateral furrow between two streamlined forms on Hazelton Peak. Furrow bifurcates at stoss end of another SF. Flow was away from the viewer.

Figure 67. Composite photograph of SF on Nine Mile Mountain. View is to the east. Flow was from left to right and uphill.

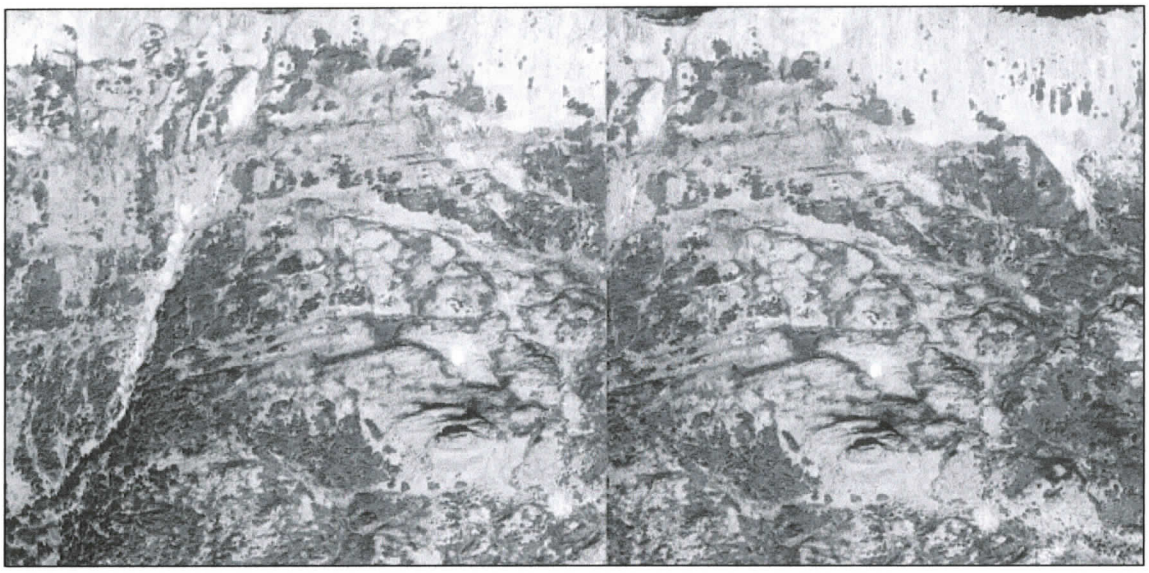

Figure 68. Stereo pair of streamlined forms on Evelyn mountain north of Hudson Bay Mountain. Composition is interpreted as primarily bedrock. North is at the top of the photo, and flow was to the west. British Columbia Government air photos, SAS30C996133 – 84 and 85. North-south lineations at top of photos mark steep, unvegetated scarp extending down from a sharp ridge

Figure 69. Lateral furrow along streamlined form flank on north side of Hudson Bay Mountain. Flow was towards the viewer.

Bedrock outcrops comprise roughly a third of Microwave ridge; alpine vegetation and small ponds make up the rest. Extensive flutings cover the ridge (Figure 70). The flow directions at the studied sites on the ridge are to the west (across the ridge) and commonly uphill. Measured dips of the uphill slope are as great as 24° towards the east.

Flutings on Dome Mountain are extremely weathered, and occur where flow was uphill (Figure 71). Flow direction was determined based on orientations of rat-tails located on larger streamlined forms and on nearby bedrock surfaces.

Alpine SF presented above range from 10 to 100 m in length. Heights of bedrock SF are usually less than 10 m. Hairpin furrows outline many bedrock SF and the diamicton SF on Hazelton Peak (Figures 8, 66, 68, and 69). Furrows are developed on both sides of the Hazelton Peak SF, but asymmetric furrow development is also observed. Broader and higher stoss (up flow) ends are common.

5.4.3. Rat-tails

Streamlined forms covered in this section are primarily rat-tails located at Dome Mountain Mine, Dome Mountain Peak, Microwave Ridge, and Hudson Bay Mountain field study sites (Figure 64). The study sites are streamlined bedrock outcrops located above timberline except for the Dome Mountain Mine site, which is located in a forested area at about 1370 m elevation. Bedrock erosional marks at the Dome Mountain Mine site were exposed when bedrock in the vicinity of a mine adit was mechanically cleared of overburden.

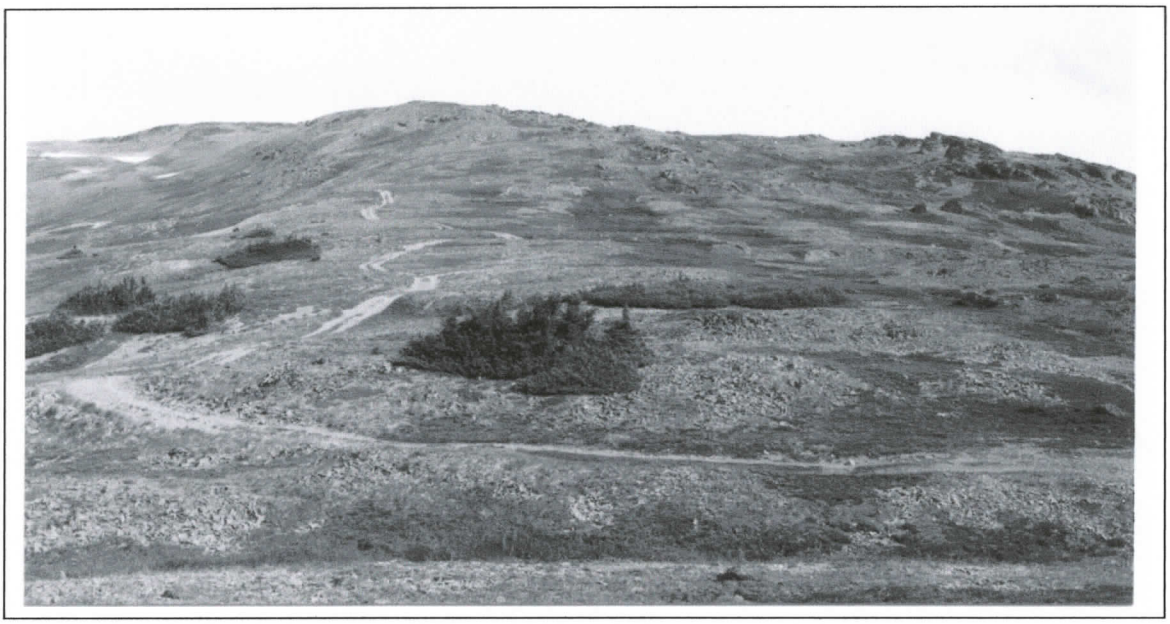

Figure 70. Streamlined forms on Microwave ridge; flow is from right to left.

Figure 71. Typical weathered bedrock SF on Dome Mountain. Flow was away from the viewer. The exposed bedrock ridge is about 12 m long and 2 m wide.

5.4.3.1. Spatial and size relationships

Rat-tails occur in swarms of parallel, similarly-sized forms (Figures 72 and 73), and commonly occur on larger rock SF, parallel to the streamlines that define the larger SF shape. Cross-cutting rat-tails were not observed, but one possible case of rat-tail swarm truncation by another rat-tail swarm (site 152o) is discussed later in this chapter.

In the field study areas, rat-tails were not found that were eroded onto other rat-tails of similar size; however, smaller rat-tails were found on larger SF. The orientation of the smaller rat-tails varies depending on their location on the larger form. Smaller rat-tails on the upper near-horizontal surface of a larger form or along its flanks or tail are oriented parallel to the larger form (Figures 74 and 75); whereas, smaller rat-tails on a larger form's more vertical stoss end are oriented oblique to the large form's bearing (Figure 76). The smaller forms in all cases appear to parallel the presumed flow-streamlines around the larger form.

Miniature rat-tails at field study sites demonstrate the persistence of erosional and flow processes at very small scales (Figure 74). All miniature rat-tails found in the field study are located on larger SF (for example, Figure 77). Some miniature rat-tails are outlined by fine hairpin furrows (Figure 78), as small or smaller than similar marks pointed out by Shaw (1996, 2002).

5.4.3.2. Flow response to surface irregularity

Characteristics of the erosive flow that formed rat-tails and rock SF can be inferred from the response of flow to surface irregularities. That response is deduced primarily from rat-tail trails and occurrence patterns. Some striae and grooves are

always observed in association with, and that follow the same paths as, rat-tails. The largest scale flow response observed at the study sites is uphill flow that occurred as a response to the "flow obstruction" of an uphill slope. Many SF and rat-tails were formed by uphill flow (for example, Figure 79).

Figure 72. Rat-tail swarm at site 112. Pen is 15 cm long and points downstream (uphill). Each rat-tail appears to be initiated by a clast in the bedrock.

Figure 73. Small rat-tail (circled) in rat-tail swarm at site 115. Note how even smaller streamlined features are located on the sides of the larger rat-tail. Flow was to the upper right.

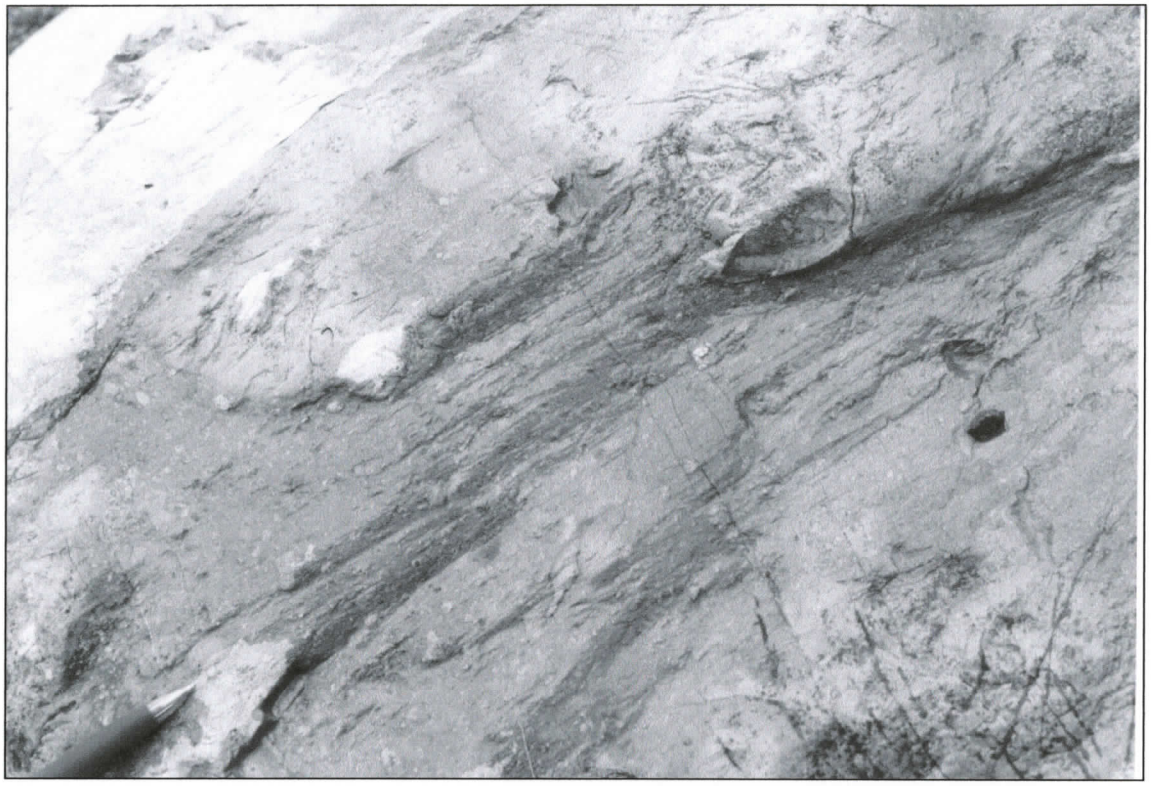

Figure 74. Very small- and small-scale rat-tails at site 152f. The clear part of the pen head (lower left) is about 1 cm long and points to a small rat-tail upon the tail of which are a number of parallel, very small rat-tails. Fine grains in the bedrock initiated the very small rat-tails. Flow was to the upper right.

Figure 75. Large, 50-cm long rat-tail with superimposed smaller rat-tail that formed along its side (see arrow), site 152j. The pen at the top of the photo is about 15 cm long.

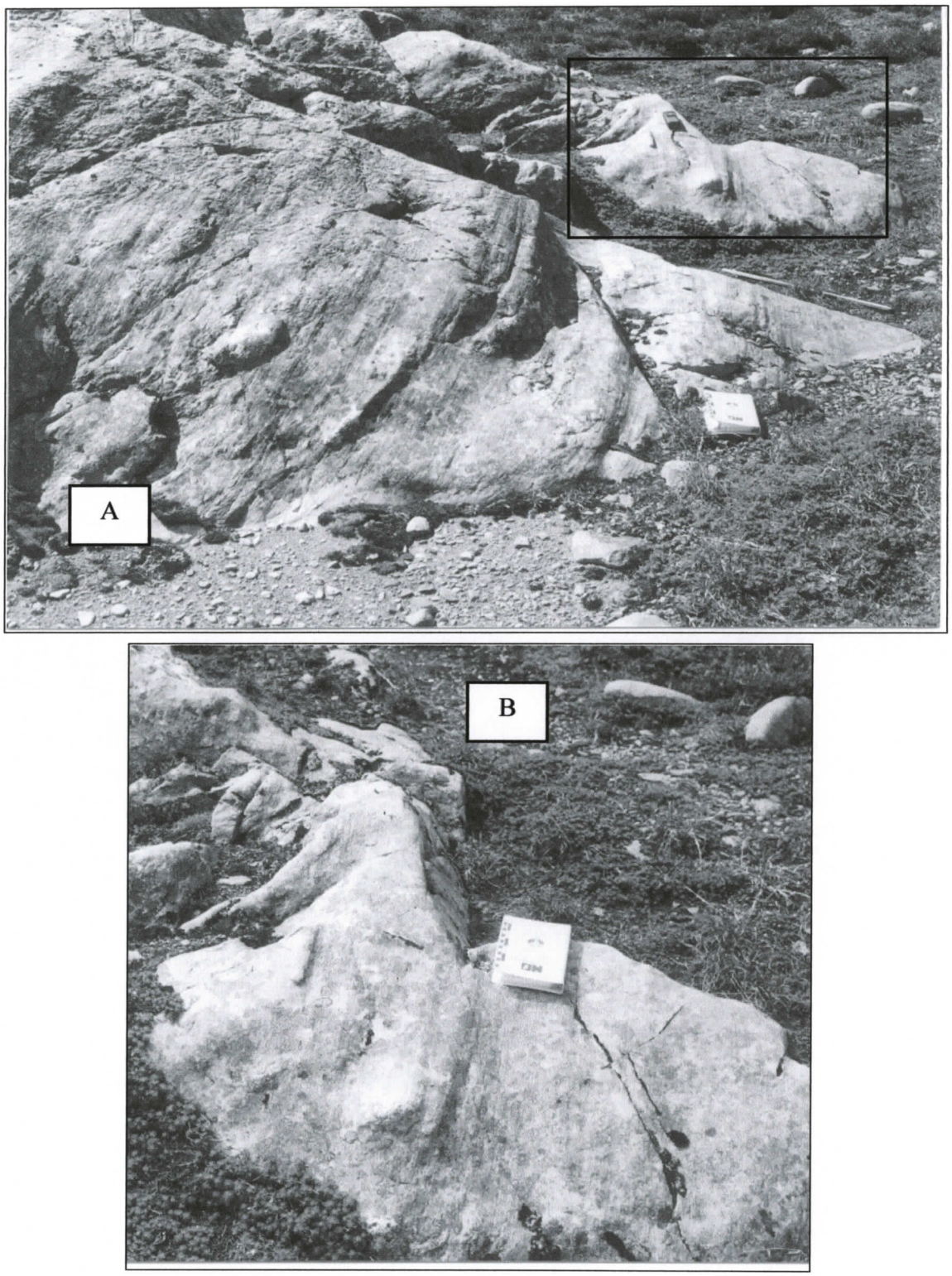

Figure 76. A) Small rat-tails on the right side (looking down flow) of a medium SBF at site 125. The smaller rat-tails follow the streamlines around and over the SBF. Flow was away from the viewer. B) Photo of approximate area enclosed by rectangle on photo A.

Figure 77. Swarm of very small rat-tails on stoss end of small SBF at site 128. Clear head of pen is about 1 cm long. Flow was toward the top right. The estimated dip of the rat-tail-covered surface is ~40° NE. Dominant flow at the site is to the west.

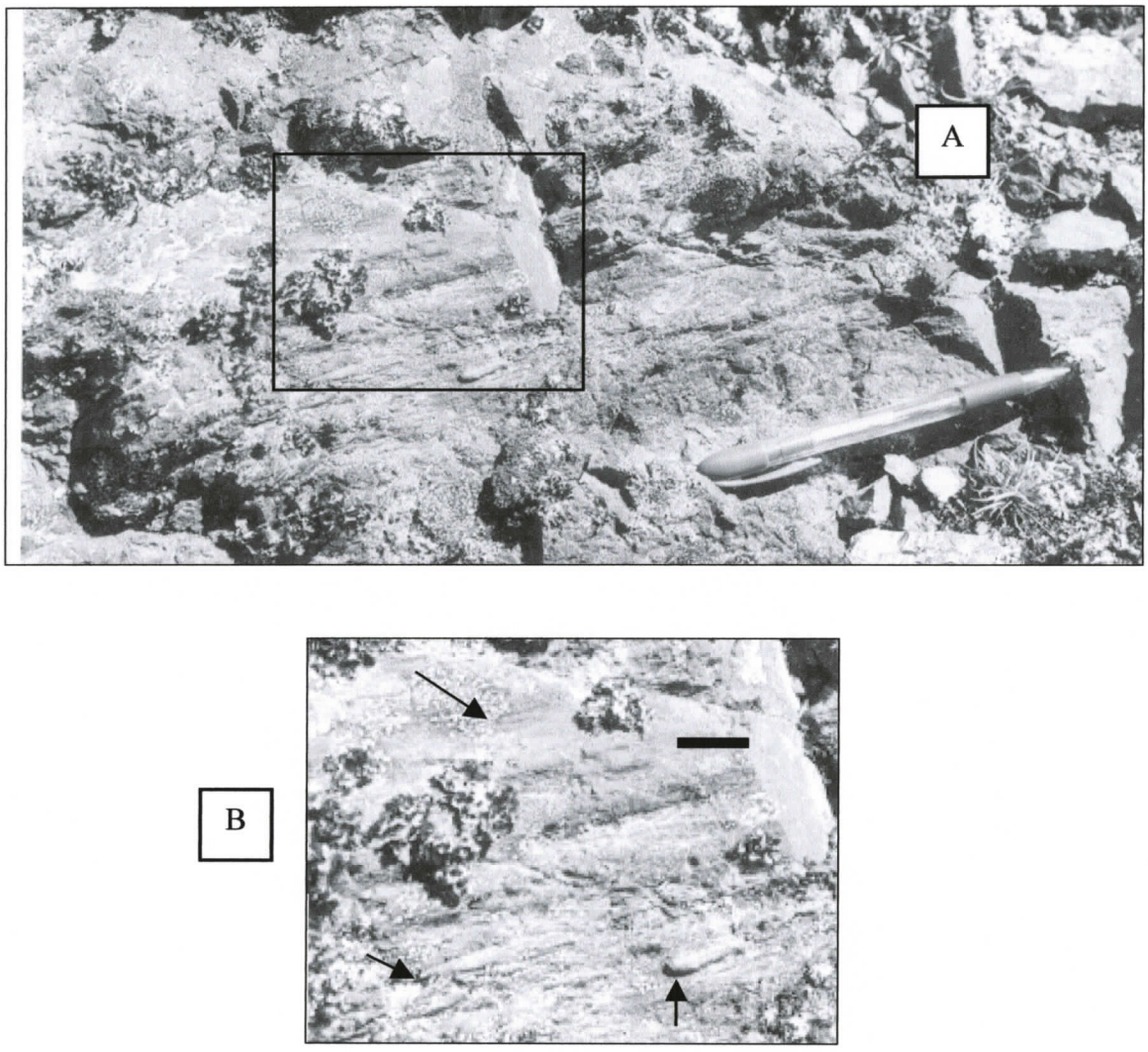

Figure 78. A) Very small rat-tails at site 162. Flow was to the right. The black rectangle indicates the area represented by photo B. B) Magnification of miniature rat-tails showing proximal hairpin scours, indicated by arrows. Scale bar equals approximately 2 cm.

Figure 79. Dome Mountain Mine site. Flow was to the right and uphill. The orientations of rat-tails at this site are generally parallel to the flow axes of the medium-scale SBF shown in the photograph.

One example of downward flow into a cavity was observed (Figure 80). Sub-parallel rat-tails, grooves, and striae indicate rat-tail forming flow descended into an angular joint cavity located on a larger bedrock SF (Figure 71). The rat-tail orientations are oblique to the axis of the larger SF. The angle between the larger SF axis and the orientation of the rat-tails, grooves, and striae systematically increases in the down flow direction of the larger form. No other similar exposures were found.

Rat-tail trails may form curved paths around larger SF. Figure 76 shows rat-tails near the base of the stoss end of a medium-scale SF that are oriented oblique to the main flow direction. Rat-tails on the more horizontal top surface of the larger SF and on its flank parallel the main flow direction. A curved rat-tail trail around the flank of a medium rock SF at site 152o may be truncated by and/or merges with a rat-tail swarm that parallels the main flow direction (Figure 81). Vertically curving flow paths were also observed (Figure 82).

Another type of flow obstruction is vertical or near-vertical bedrock faces that strike oblique or perpendicular to the main flow direction. Figure 83 shows this configuration. Rat-tails and other erosional marks run subparallel to the strike of the near-vertical face. At the intersection of this near-vertical face with the more horizontal upper bedrock surface, the erosional marks wrap up onto the more horizontal surface and return to the main flow bearing (Figure 83). The top edge of flow-obstructing, near-vertical faces are always rounded at field study sites. If the strike of a near-vertical bedrock face is near normal to flow, only minor rat-tail formation is present along the face. Instead, rat-tails are initiated just below the upper lip of the bedrock face (Figure

84). When the strike of vertical faces are subparallel or oblique to the flow direction, rat-tails may be found on the vertical face (Figures 85 and 86).

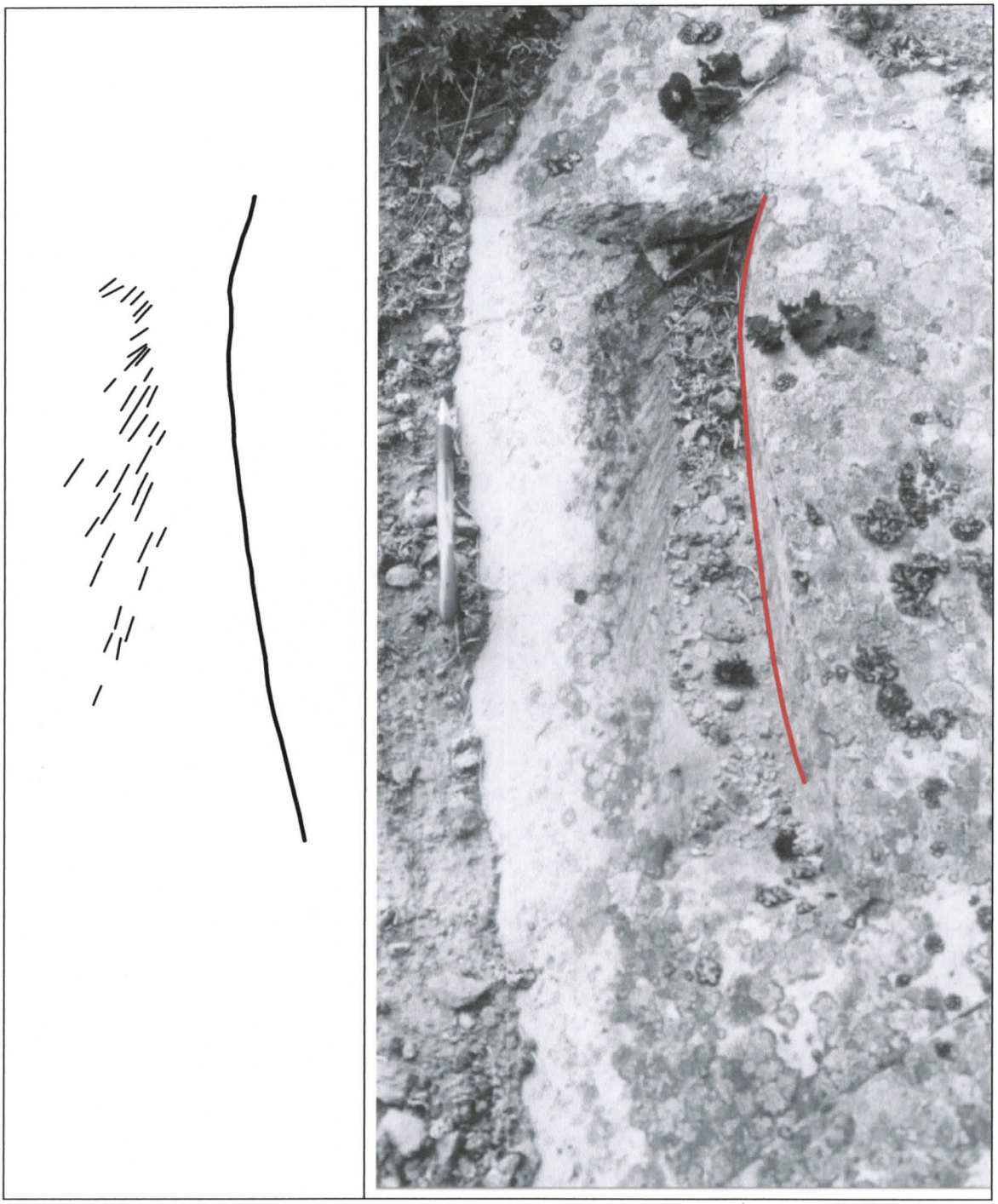

Figure 80. Looking down at rat-tails and striae descending into angular joint cavity at site 131. The cavity is on the tail of the medium-scale SF shown in Figure 71. Pen is 15 cm long and points down flow. Traces on left depict rat-tail and striae orientations relative to the cavity wall.

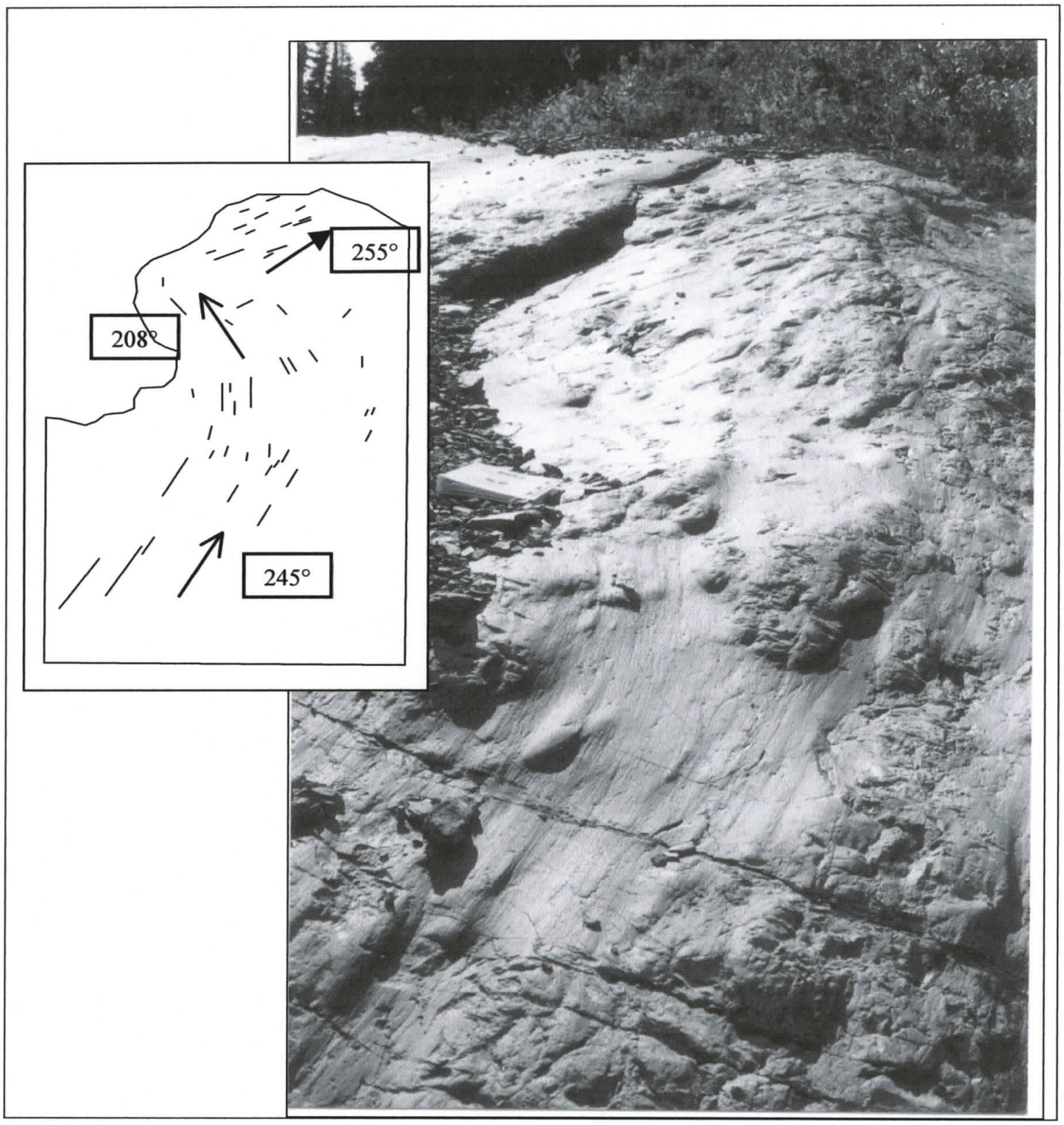

Figure 81. Curving rat-tail trail at site 152o. The line diagram on the left shows representative rat-tail traces. The curving path (open-head arrows) is following a furrow around a rock SF located to the left of the photo area. Flow that is oblique to and appears to converge with the curving path (closed-head arrow) is parallel to the main flow direction at the site. Representative rat-tail orientations are given on the line drawing.

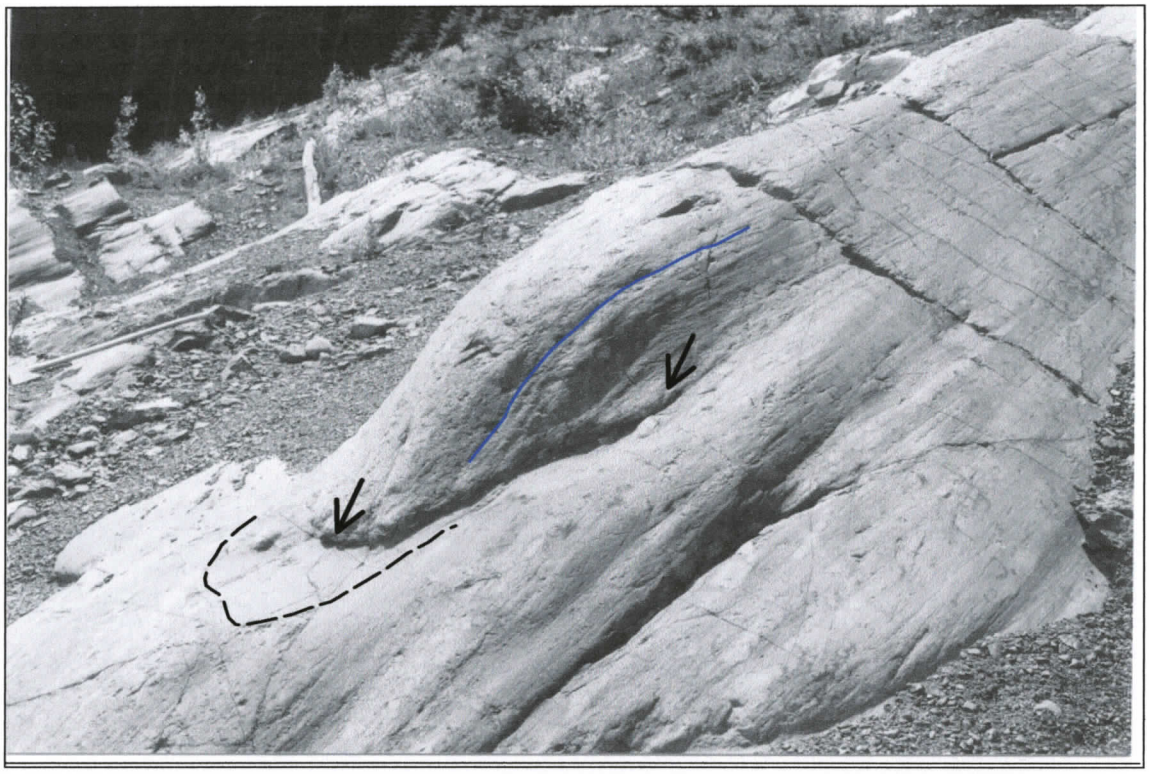

Figure 82. Medium-small-scale SF at site 152k. Solid line indicates curved path of small SF along the larger SF flank. Dashed line outlines proximal scour of larger SF. Arrows define ends of undercut SF base.

Figure 83. Streamlined rock face that modified flow direction at site 118. There is a continuum of orientation change of small rat-tails from bearings that are subparallel to the strike of the face, to the main flow direction on the upper surface of the outcrop. Flow was toward the top of the photo. The same changes in flow direction are noted in striae / grooves.

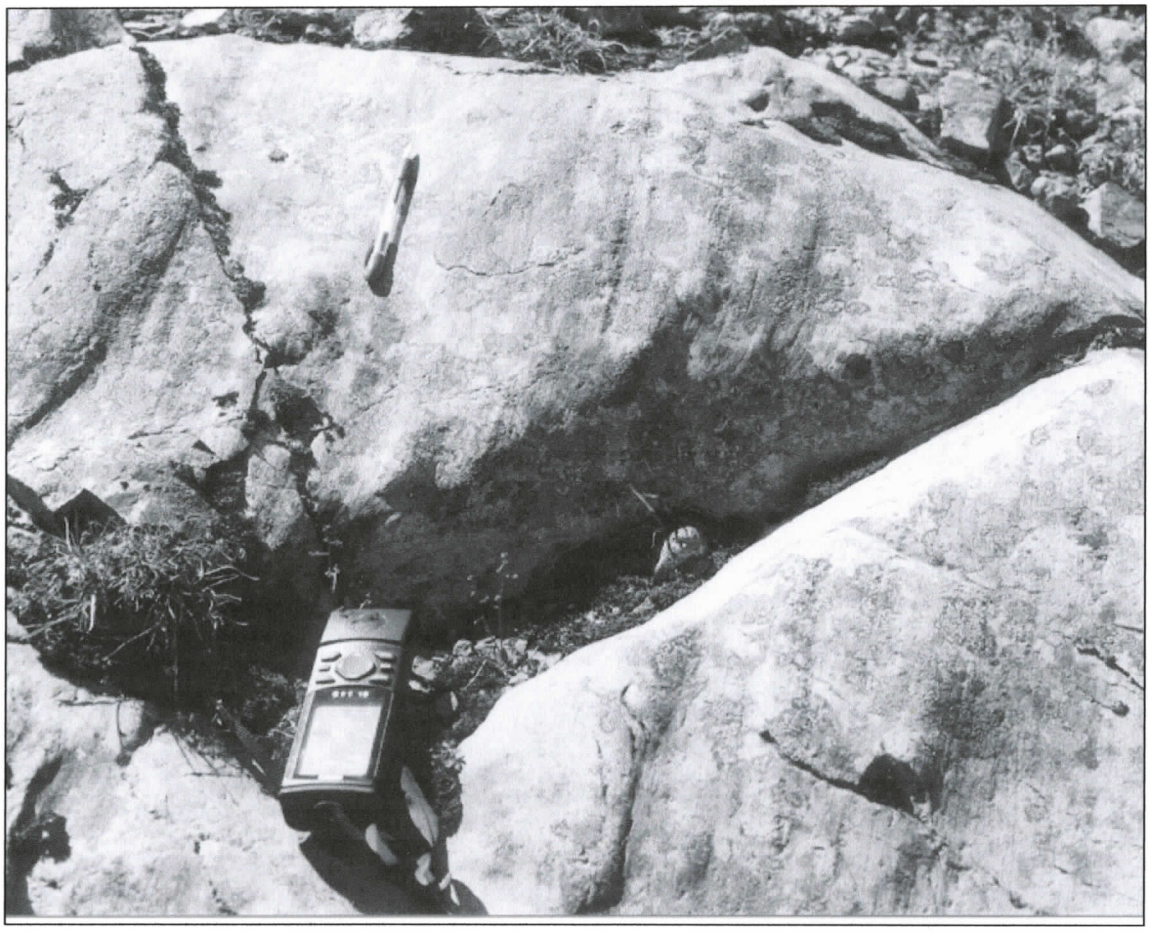

Figure 84. Rat-tails curving out of a joint that strikes nearly normal to flow, site 126. The initial rat-tail bearings appear to be inherited from the joint strike, and the final bearings parallel the main flow direction. Flow is away from the viewer.

Figure 85. Small rat-tails on vertical face at site 124. Flow was away from the viewer. GPS is about 15 cm long.

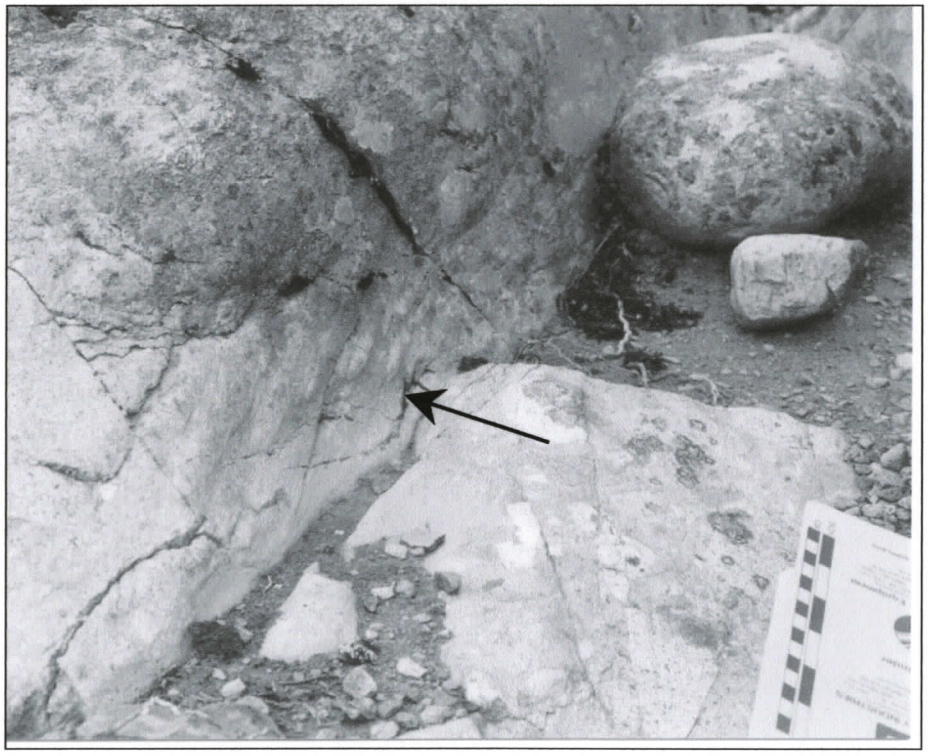

Figure 86. Arrow points to rat-tails on a near vertical rock face at site 123. The small increments on the field book are 1 cm. Flow was toward the top right of the photo.

One rat-tail at the Dome Mountain Mine study area possibly shows the susceptibility of rat-tail-forming flow to minor surface irregularity (Figure 87). The rat-tail ridge is only apparent behind the left part (looking down flow) of the initiating clast. The right, down flow part of the clast has been plucked out. There are two possible explanations for this configuration. The plucked area may have created a flow discontinuity that inhibited rat-tail formation. Even though the upstream face of the initiating clast remained complete, flow was still disrupted on the right side of the rat-tail to a degree sufficient to inhibit rat-tail development. Alternatively, a wider rat-tail could have formed, after which part of the clast was plucked out, and continuing erosion narrowed the rat-tail body. Heavy machinery could possibly have broken out the clast; however, the rat-tail tail is not existent immediately down flow of the clast cavity. If the clast was present during rat-tail formation, then a tail should have formed immediately down-flow of the clast.

5.4.3.3. Rat-tail length-to-width ratios

Lengths and widths of 115 rat-tails were measured in the field and from photographs, and their length-to-width ratios were calculated (Table 14). Width was measured perpendicular to flow at the widest part of the rat-tail and length was measured parallel to flow. The maximum rat-tail width is almost always located at the up flow end of the rat-tail. Trend analysis using power fitting indicates good correlation ($R^2 = 0.89$) between rat-tail widths and lengths, indicating that the length of the rat-tail is strongly dependent on its width (Figure 88).

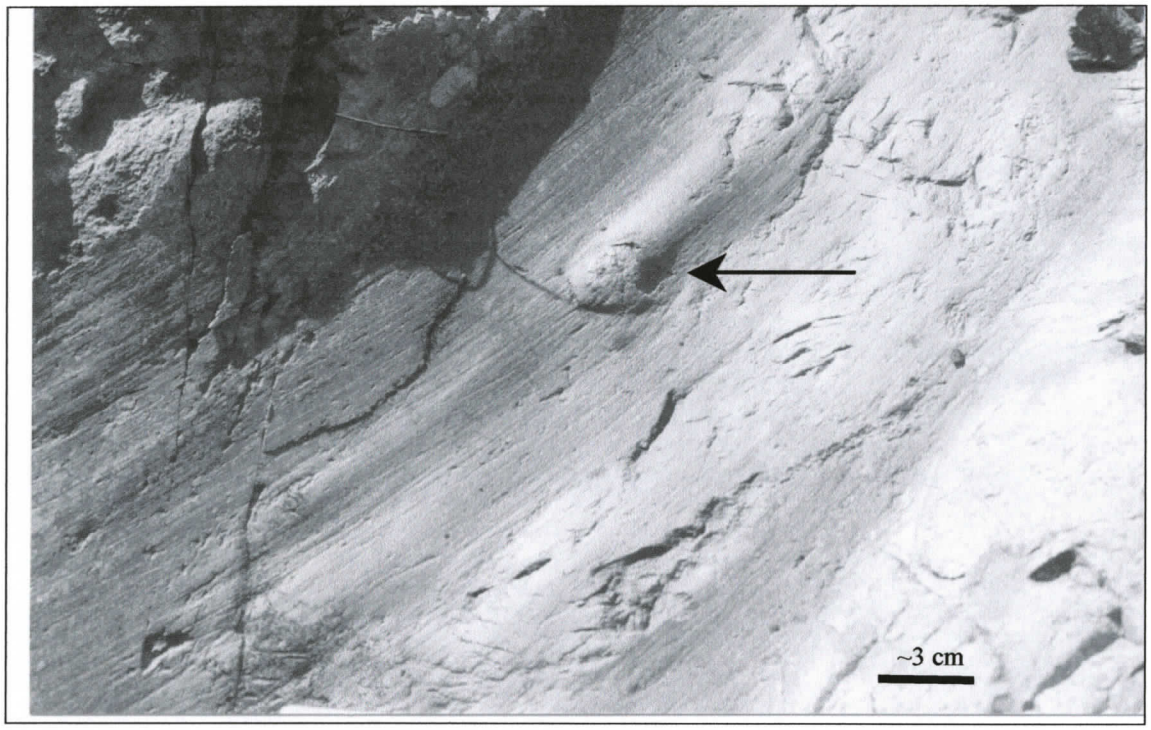

Figure 87. Rat-tails in curving furrow. Arrow points to plucked part of rat-tail clast. Flow was toward the top right of the photo.

Table 14. Rat-tail length and width statistics

	Width(cm)	*Length (cm)*	*L/W ratio*
Mean	1.7	7.2	5.4
Standard Deviation	2.3	8.1	2.2
Sample Variance	5.4	65.8	4.8
Minimum	0.1	0.6	2.0
Maximum	16.0	50.0	12.5
Count	115	115	115

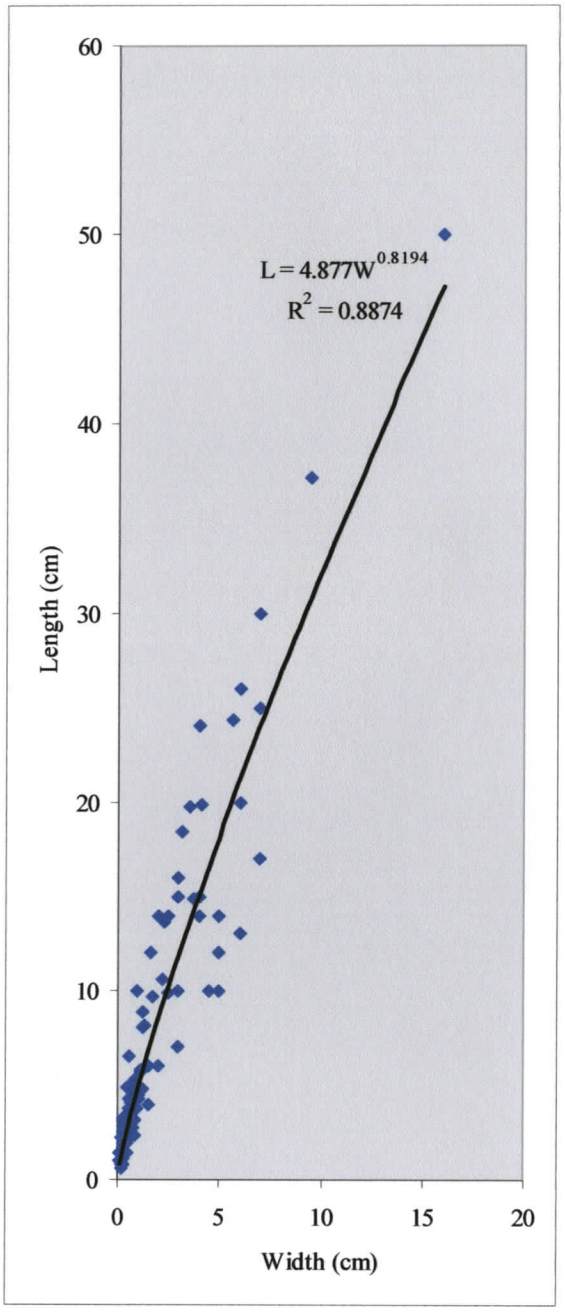

Figure 88. Power curve for lengths and widths of 115 rat-tails in the study area (see Table 14). There is a strong correlation, $R^2 = 0.89$, between length and width.

5.4.4. Striae at rat-tail sites

Striae that parallel rat-tails are present at all rat-tail sites discussed above. These parallel striae follow the same curving paths around larger rock SF or over vertical steps that are followed by the rat-tails. Striae that cross-cut rat-tails and other striae are also observed at all rat-tail sites (for example, Figure 89). Cross-cutting striae cross the axes of rat-tails or other striae at oblique angles. Striae that cross-cut rat-tails were formed after the rat-tails. Rat-tails cross-cutting other rat-tails were not observed.

A rat-tail swarm that follows a curving path around a medium-scale SF is apparently truncated by or merges with a rat-tail swarm paralleling and originating from the crest of the medium-scale SF (Figure 81). This convergence or truncation is not "cross-cutting" as used here pertaining to striae. Although the two adjacent swarms have different orientations, no evidence was found of a rat-tail that was truncating or cross-cut by either the flow path of the other swarm or by another rat-tail. The spatial arrangement of the rat-tails at the site indicates a simultaneous origin event for both swarms. Cross-cutting striae, on the other hand, indicate at least two formative events.

5.4.5. Cavettos

Cavettos are located at some rat-tail sites. Cavettos are longitudinal, sometimes sinuous grooves in bedrock cut into vertical or near vertical faces. Their presence is thought by some researchers to be indicative of meltwater erosion (Kor *et al.*, 1991; Bryant and Young, 1996; Shaw, 1996; Kor and Cowell, 1998). Cavettos were observed at the Dome Mountain Mine site (Figure 90) and at the Microwave Ridge site (Figures 91 and 92).

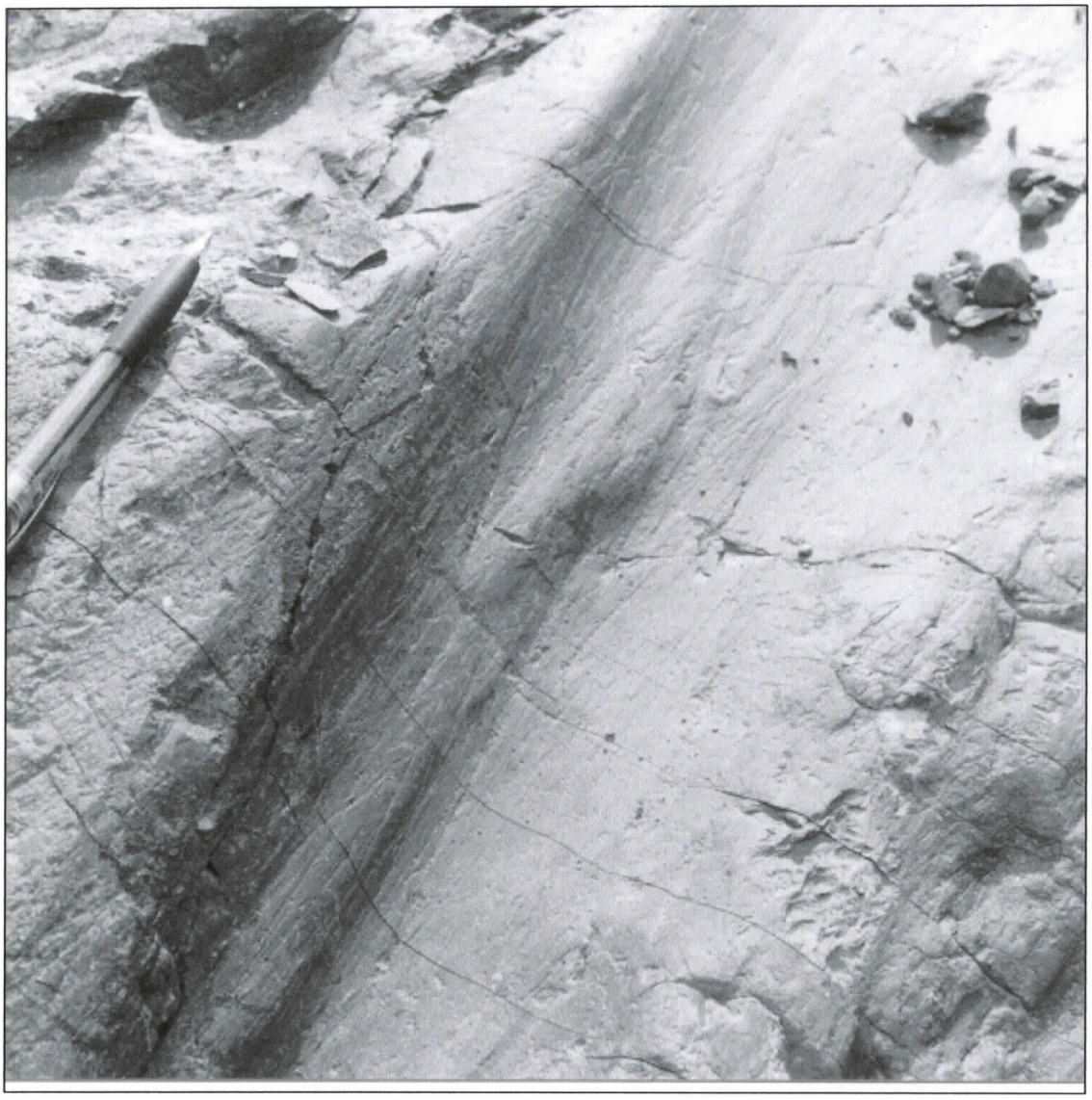

Figure 89. Striae and rat-tails in furrow at site 152p. Note parallelism of rat-tails with other rat-tails and with some striae; striae cross-cut other striae and rat-tails.

Figure 90. Straight cavetto at Dome Mountain Mine site. Flow was towards upper right. Rat-tails near cavetto overhang are those shown on Figure 89.

Figure 91. Cavetto at site 111 on Microwave ridge. Pencil is about 15 cm long. Flow is toward the upper left.

Figure 92. Cavetto at site 97, Microwave ridge. Pencil is about 15 cm long. Flow was towards the upper left.

5.5. DISCUSSION

5.5.1. Summary of streamlined forms observations

5.5.1.1. Composition of streamlined forms

More than 95% of SF observed in the field study are composed of diamicton and/or bedrock. Bedrock occurs on the up flow ends of crag-and-tails and some other SF in the lowlands. At least half of the observed upland SF are entirely bedrock. Exceptions are SF on Hazelton Peak, dominantly composed of diamicton with alpine soil upper surfaces, and SF on Nine Mile Mountain with thin soil and diamicton cover and frequent bedrock exposures. The range of diamicton deposition across the study area spans at least 1400 m of elevation. More than 95% of examined lowland SF are

composed of massive diamicton. Based on visual observations of exposed diamicton in SF sections, variations in matrix texture, clast percent, and clast size are random and not correlated with sample location within SF.

5.5.1.2. Morphology of streamlined forms

Streamlined forms in the study area have curved and linear streamlined profiles in top, side, and plan views. Streamlined forms are sometimes defined by interconnected hairpin furrows, both in upland (*e.g.* Hazelton Peak, Figures 8 and 66) and lowland areas (Chapter 2). Proximal furrows at the stoss end of lowland SF are often marked by bogs or ponds. This indicates erosion took place at the stoss end of those SF, creating an area lower than the surrounding land.

All rat-tails have streamlined shapes. The widest and highest section of a rat-tail is at the extreme up flow end of the form. Rat-tail tails taper both vertically and horizontally in a down flow direction from their up flow end. A few observed rat-tails are outlined by hairpin furrows. The hairpins are generally shallow.

5.5.1.3. Uphill and westward flow

Many upland SF examined during this field study provide evidence of uphill and westward flow at high elevations. Streamlined forms observed at alpine study sites indicate flow towards the west or southwest. West to southwest flow indicated at Hazelton Peak, Nine Mile Mountain, Hudson Bay Mountain, and Microwave Ridge is sub-parallel or parallel to SF flow directions in adjacent valleys. Westward flow directions at Dome Mountain are oblique to southeast flow indicated in the two principle valleys that flank Dome Mountain, the Babine River and Bulkley valleys.

5.5.1.4. Flow behaviour

Bedrock erosional marks record the behaviour of the eroding flow. The flow mechanism left curving, highly parallel trails of streamlined erosional forms. The curving trails followed streamlines around larger bedrock forms. The flow mechanism or mechanisms also did the following:

- eroded bedrock into streamlined shapes,
- sculpted similarly-shaped SBF across a wide size range, with dimensions from millimetres to tens of metres,
- formed hairpin furrows, less than 5 mm wide, around some small rat-tails,
- undercut the base of some rock SF beneath the stoss ends and along flanks, and
- formed rat-tails and striae on vertical rock faces.

5.5.2. Interpretations

5.5.2.1. Uphill flow

Streamlined forms at field study sites indicate that uphill flow occurred at elevations of at least 1680 m. This observation indicates that a driving ice or water surface was located at an even greater elevation somewhere in the up flow direction. If the flow mechanism was ice, then uphill flow was driven by an ice dome or ice divide that was at a greater elevation than the elevation of the site where uphill flow indicators are observed.

A driving head for uphill flow is also indicated if the SF were produced by water. If the uphill flow was the result of subglacial, confined flow, then the driving head could have been provided by either a supraglacial lake or ice overburden pressure

on a subglacial water source. Another possibility is that the driving head was provided by a deep lake impounded by glacial ice, perhaps formed during an ice sheet retreat. The flow in this case would have been unconfined. Proglacial floods up to 400 m deep are indicated by evidence in the Altay Mountains, Siberia (Rudoy and Baker, 1993).

In all cases where uphill flow in alpine areas was observed, no higher terrain is present in the adjacent areas in the up flow direction. For example, the principle landform immediately east (up flow) of Dome Mountain is the Babine River valley. The Bulkley Valley is the principle topographic feature east (up flow) of Microwave Ridge and Hudson Bay Mountain. The minimum elevation east of Dome Mountain is about 710 m, represented by the surface of Babine Lake. The minimum elevation of the floor of the Bulkley Valley east of the Hudson Bay Mountain study site is about 420 m, and about 480 m east of Microwave Ridge. Assuming similar minimum elevations during the streamlining event and given the elevations at which uphill flow indicators are found (1525-1680 m; Table 13), the driving surface must have been located more than one kilometre above the current elevations of the valley bottoms.

This inference is based on the necessity of there being an uphill-directed force acting at sites showing uphill flow. That force must have been capable of offsetting the pull of gravity acting in a downhill direction at an uphill flow site. Regardless of whether uphill flow is in an ice sheet, unconfined flood, or subglacial flood, the offsetting uphill force must be derived from the pressure created by gravity acting on an ice or water mass located above the site of uphill flow.

5.5.2.2. Parallel flows in valleys and uplands

Most of the observed upland SF in this field study are parallel or subparallel to SF in adjacent lowlands. Observations of these parallel flows were made in the Hazelton Mountains and adjacent valleys (Figure 3). Upland sediment SF on Hazelton Peak parallel the flow path of the large field of lowland SF between Hazelton Peak and the Skeena River (Figures 15 and 64). Other sites of parallel or subparallel upland and lowland SF, as determined based on field investigations, include: Nine Mile Mountain and Bulkley River, Hudson Bay Mountain and Trout Creek, and Microwave Ridge and Telkwa Valley (Figures 15 and 64). In these cases of parallel flow, it is inferred that the same flow event formed both the upland and lowland SF. Alternatively, different mechanisms and/or flow events with approximately the same flow directions could have formed the upland and lowland SF at different times. However, the simplest explanation is that, in the cases listed above, both upland and lowland SF were produced by the same event. The simplest explanation is preferred here.

Dome Mountain SF indicate west flow. Dome Mountain is flanked by the southeast-trending Babine River and Bulkley River valleys (Figures 15 and 64). Streamlined forms in these valleys, particularly the Babine valley are generally oriented towards the southeast. These relationships indicate that the southeast-trending lowland SF were produced at a different time than the west-trending upland SF.

5.5.2.3. Uniform streamlined bedrock form directions

At upland SF study sites, smaller rat-tails follow the streamlines over and around medium-scale bedrock SF. The rat-tails are always parallel to the larger forms

or are parallel to streamlines around the larger forms. No cases of cross-cutting rat-tails were observed. Such cross-cutting relationships would indicate more than one formative event. It is inferred that the same flow event formed all scales of bedrock SF at a given site.

If lowland sediment SF, upland bedrock SF, and rat-tails were formed at least in some cases by the same flow event, then there is a strong possibility that they were formed by the same flow mechanism, that is, all the subparallel forms for a given area were formed by either meltwater or by glacial ice. An alternative explanation is that both subglacial meltwater floods and glacial flow occurred simultaneously, or nearly so, and acted in the same direction. This is a valid possibility based on the likelihood of a similar gradient driving both ice and water flow.

5.5.2.4. Similar shapes at all scales

A morphological characteristic of many streamlined forms in the study area is the outlining of streamlined ridges by full or partial hairpin furrows. Interconnected hairpin furrows outline most sediment SF in the study area (*e.g.*, Figures 8, 22, and 26). Hairpin furrows also define a few rat-tails (*e.g.* Figures 78 and 87).

In cases where hairpin furrows are not evident around sediment SF, the lack of hairpins is possibly related to the stage of SF erosion at which erosive flow ceased. Shaw (1994) suggests that some types of streamlined drumlin ridges are initially developed as positive-relief forms between hairpin furrows. Further erosion removes evidence of the hairpin furrows, but leaves the drumlin ridges. In this explanation, hairpin furrows are always present at an early stage in the drumlin-forming process.

In the case of rat-tails, rat-tail location is dependent on the location of a resistant clast in less-resistant bedrock. Rat-tails do not require hairpin furrows. This could explain why more hairpin furrows are found associated with sediment SF than are found associated with rat-tails and larger rock SF in the study area. Nonetheless, some hairpin furrow features are found around a few bedrock SF, *e.g.*, concave up proximal scours and lateral furrows outline a medium-scale rock SF at Dome Mountain Mine site (Figure 82). Hairpin furrows formation around bedrock forms possibly occurred at a late stage in the formation of the bedrock SF. Allen (1982) showed that hairpin furrow formation can be initiated by bluff obstructions to water flow.

Rat-tails and upland and lowland SF are shaped similarly; they generally have broader and higher stoss ends and tapering tails. Rat-tails always have this shape. Most larger SF observed in the study area also have tapering tails. Common morphology of different types of study area SF, taken together with their parallel orientations as discussed above, supports the inference that the same mechanism produced at least some of all these different types of SF. It is noted, however, that similar morphology does not necessarily prove the same forming mechanism.

5.5.2.5. Erosional versus constructional mechanism

Although it is obvious that streamlined bedrock forms were shaped by erosion, it is not clear whether erosion, deposition, or both produced study area SF composed of sediment. Drumlin origins are attributed to both erosion and deposition (Chapter 1).

The morphology of hairpin furrows consists of a proximal scour and lateral furrow. These are negative relief features indicating that erosion was required for their

formation. Interpretation of an erosional origin for hairpin furrows is supported by their observed incision into bedrock. Since hairpin furrows define some sediment SF and crag-and-tails, then erosion is inferred to have contributed in whole or in part to the shape of those SF.

Mate (2000) suggests a dual process model for the formation of some SF. The SF may have received an initial linear shape by ice processes, after which subglacial meltwater flows further enhanced the SF shape, adding the hairpin furrow. If so, then the early SF could have been formed by glacial deposition and/or erosion, but the final streamlined form would be partially the result of subglacial water erosion. This explanation requires that later meltwater flow be in the same direction as earlier ice flow. This is possible if the subglacial meltwater flow occurred beneath the ice sheet that produced the original diamicton ridges. In that case, the same gradient would be expected to drive both ice and water flow.

Seventy out of the 72 SF examined in the field study were composed of massive diamicton. No faults or folds were detected in the SF sections, and stratified and sorted sediments were observed in only two out of 72 sections. Although no faults were observed, it is possible that they would not be easily detected in massive diamicton and so were not recognized during the field study. Folds could also be obscured if subglacial sediment deformation had completely overturned the folds and destroyed the fold noses, a possibility proposed by Boulton (1987, 1996).

If the SF were formed by till deformation beneath an ice sheet as proposed by Boulton (1987, 1998), then either sediment deformation structures would be apparent in the SF sections or sediment deformation structures would be obscured and the sections

would appear as massive diamicton. Most field study SF are composed of massive diamicton, so these SF can be fitted within Boulton's sediment deformation model.

If the SF were formed by meltwater erosion of glacially deposited diamicton with massive structure, then predicted SF composition would also be massive diamicton; hence, the meltwater model also explains study area observations. However, boulder or gravel lags in the furrows or along the crests would be possible or likely at some locations due to the sorting and winnowing actions of high energy water flows. Although several SF crests and furrows were investigated, neither definite boulder lags or other sorted sediments were found in association with the diamicton SF. However, lowland SF crests and furrows between SF are generally obscured by vegetation, fallen or cut trees, and/or colluvium. Flow deposits associated with SF formation could also be covered by later glacial melt-out deposition. If boulder lags or gravel / sand deposits exist, they may be difficult to recognize.

Although the evidence found in the field study is not conclusive with regard to the problem of SF forming processes, it is suggested here that the final shape of many study area SF is due to erosion, not constructional processes. This conclusion is primarily based on the association of study area SF with hairpin furrows and on the inferred similarity of form and process between rat-tails, which are known erosional forms, and study area SF. Observed SF composition is compatible with a meltwater erosion model, but also fits the models of SF formation by extensive subglacial sediment deformation (Boulton, 1987; 1998) and the dual process model of Mate (2000).

5.5.2.6. Parallel rat-tails and striae and cross-cutting striae

The parallelism of some striae to rat-tails observed at all rat-tail study sites has been noted. The simplest explanation of this parallelism is that the same process simultaneously formed both rat-tails and striae. An alternate explanation is that one mechanism, for example meltwater, formed rat-tails, after which another mechanism, for example glacial ice, formed striae. It is also possible that some striae are actually water-formed grooves and other striae were formed by ice.

Striae that cross-cut rat-tails and other striae occur at every rat-tail study site. Cross-cutting striae could not have formed at the same time as the striae and rat-tails on which they occur; therefore, these cross-cutting erosional marks were formed at different times by flows acting in different directions. If striae and rat-tails were formed simultaneously by the same mechanism, then it would be reasonable to expect that cross-cutting rat-tails would occur in association with cross-cutting striae. Cross-cutting rat-tails would probably be evident as smaller rat-tails oriented at oblique angles on larger rat-tails. Several examples of smaller rat-tails on larger rat-tails are shown above, but the smaller forms are always parallel to the larger forms. No cross-cutting rat-tails were observed. When the striae are parallel to the rat-tails, then it is inferred that either both feature types were formed by the same flow event or that the striae were formed by a later, parallel flow event. When striae cross-cut rat-tails, then the striae must have formed after the rat-tails. Based on this relationship and the lack of cross-cutting rat-tails, it is inferred that at least some striae were formed after rat-tails by a separate event.

5.5.2.7. Converging rat-tails in a rock cavity

Rat-tails formed by flow into a cavity are documented in Figure 80. The rat-tail orientations converge in the cavity. Rat-tail development probably requires a period of consistent flow in the same direction in order to erode the rock sufficiently to create a rat-tail form. Ice would tend to bridge the cavity, and if it did not, it seems likely that the cavity would soon fill with debris or ice. In order to maintain a consistent flow in the cavity, the ice would have to flow into the cavity at a slight angle and flow out of the cavity at a steep, almost vertical angle (Figure 80), pushing against other ice presumably flowing over the cavity. This would seem to be impossible; although, it is also difficult to conceive how water could flow in this manner. With meltwater flow, it would seem likely that turbulence would develop in the vicinity of the cavity, thereby inhibiting the formation of the parallel rat-tails that are observed. Neither a meltwater nor an ice mechanism offer a convincing solution to the problem of how these rat-tails were formed.

5.5.2.8. Relationship of rat-tail length to width

Many rat-tails consist of a stoss-end clast of some more resistant rock type embedded in a less resistant country rock matrix. The "tail" of the rat-tail usually appears to be of the same composition as the country rock in which the rat-tail clast is embedded. Rat-tail widths depend on the size of the initiating resistant clast, when such a clast is present or recognizable. The length of the rat-tail is directly dependent on its width (Figure 88). Whereas the width of many rat-tails are due to the clast size and not

due to some property of the flow mechanism, rat-tail lengths are concluded to be a function of flow mechanism.

Streamlining is caused by the minimization of resistance to flow of a form within the flow. Two components make up the resistance to flow: form drag and skin drag. Form drag is dependent on the shape of the obstacle (*e.g.*, the resistant clast of a rat-tail) and the flow separation that occurs behind the object. Skin drag is the resistance due to friction of the surface. Form drag is proportional to the cross-sectional area of the clast normal to flow, and skin drag is proportional to the surface area of the entire form. Decrease in form drag is accomplished by a lengthening tail. However, the lengthening tail increases skin friction. Streamlining is optimized when the total drag due to these two components is at a minimum.

The average aspect ratio (length to width) of 115 study area rat-tails is 5.4 with an R^2 value of 0.89 (Table 14, Figure 88). This ratio is comparable to the aspect ratio of streamlined islands in rivers. Komar (1984) measured lengths and widths of 38 streamlined islands and reported an aspect ratio of 4.3 with an R^2 value of 0.96.

5.5.3. Origins of streamlined forms

Observations, assumptions, and interpretations of the meaning of field study findings are presented in this chapter. Conclusions derived from this data are used in the following paragraphs to conclude whether glacial ice, meltwater floods, or a combination of both processes formed SF in the study area.

5.5.3.1. Summary of findings and interpretations

Uphill flow towards the west occurred at elevations up to 1680 m. This indicates a driving head, *e.g.* an ice or water surface, located more than one kilometre above the current Bulkley River and Babine River valley floors. Uphill flow formed medium-scale bedrock SF and smaller rat-tails.

Parallel lowland and upland SF occur at several locations in the Hazelton Mountains. These lowland diamicton SF and upland bedrock and diamicton SF are interpreted as forming during the same event. It is further inferred that the same mechanism formed both upland and lowland forms, though the possibility is allowed that both ice and water were active in producing SF during the same flow event.

Rat-tails at upper elevation sites maintain relative uniform directions across wide areas. Rat-tail paths follow streamlines around and over larger bedrock SF. The orientations of the rat-tails and the larger bedrock SF are parallel to lowland sediment SF at all rat-tail sites except Dome Mountain.

Almost all SF in the study area have similar morphology. Streamlined forms investigated here include sediment SF in lowlands and uplands, bedrock SF in uplands, and rat-tails in uplands. Crag-and-tails, composed of bedrock and sediment, are also common. Almost all forms consist of a larger stoss end and tapering tail. At least half of lowland SF have some degree of hairpin furrow development. A few upland SF and rat-tails show hairpin furrows. This morphological similarity of SF indicates that the same mechanism caused the final shape of study area SF.

Lowland SF have massive diamicton composition. Many are outlined by hairpin furrows. Massive diamicton composition is compatible with an erosional forming

process. It is also compatible with a constructional process if extensive deformation occurred after SF construction. Hairpin furrows are erosional features. Bedrock SF and rat-tails are erosional features. Similarity of form between lowland and upland SF indicates a common forming mechanism. Based on the above findings and inferences, study area SF are interpreted as erosional or primarily erosional features.

Cross-cutting rat-tails were not observed. Striae that cross-cuts rat-tails and other striae were observed at all rat-tail sites. If striae and rat-tails were formed by the same mechanism, then rat-tails should occur at all orientations that striae occur and rat-tails that cross-cut other rat-tails should be evident. This is not the case; hence, rat-tails and cross-cutting striae were possibly formed by different processes.

A swarm of converging rat-tails was formed by flow descending into a rock cavity. This observation is not satisfactorily explained by either meltwater or ice flow.

Rat-tail length is strongly related to the width of the stoss-end clast. This indicates rat-tail shapes are the result of the minimization of rat-tail resistance to formative flow.

5.5.3.2. Application to the origin problem

An assessment of the findings with respect to the problem of streamlined forms origins is presented in Table 15. Some findings are supportive of more than one origin mechanism.

Table 15. Streamlined forms origins indicated by field study findings									
	streamlined forms, primarily sediment			*rat-tails*			*streamlined bedrock forms, not rat-tails*		
Findings and interpretations	**ice**	**water**	**ice & water**	**ice**	**water**	**ice & water**	**ice**	**water**	**ice & water**
Uphill flow to west	x	x	x	x	x	x	x	x	x
Parallel lowland and upland SF	x	x	x				x	x	x
Rat-tails parallel to upland and lowland SF	x	x	x	x	x	x	x	x	x
Similar morphology of study area SF to known water forms		x	x		x	x		x	x
Massive diamicton in lowland SF	x	x	x						
Erosional mechanism for lowland SF	x	x	x						
Absence of cross-cutting rat-tails at sites with abundant cross-cutting striae					x	x			
Parallel striae and rat-tails				x					
Correlation of rat-tail length to width					x				

Uphill flow is possible with meltwater or ice. Parallel lowland and upland streamlined forms can also be interpreted as supporting either meltwater or glacial flows.

Absence of cross-cutting rat-tails at sites with abundant cross-cutting striae is suggestive of a meltwater origin for rat-tails. Cross-cutting striae are interpreted as ice features. Striae indicate a number of flow directions across a given area; whereas, rat-tails indicate formation by a mechanism that had a consistent flow direction across a

given area. Since rat-tails seem to show a fundamentally different type of flow than striae, then rat-tails are interpreted as meltwater forms, not as ice forms. However, the pervasive striae at these sites indicate that flow was probably subglacial and ice affected the surface after the meltwater floods.

Parallelism of rat-tails with some larger bedrock and diamicton SF indicates that the same flow event formed these different SF types. That flow event could have included meltwater and/or ice.

Study area sediment SF and rat-tails have similar morphology to forms known to be produced by water. This form similarity suggests that SF shapes studied here may have been shaped or modified by meltwater flows. Hairpin furrows are known to be formed by both water and air (Karcz, 1981; Allen, 1982) but their formation by ice has not been demonstrated. Erosion of forms similar to rat-tails and hairpin furrows has been observed in rivers (Komar, 1983; Wyrick, 2003), stream beds (Karcz, 1981), tidal flats (Allen, 1982), on tsunami headlands (Bryant and Young, 1996), and have been experimentally produced by confined acidic water flows over Plaster of Paris (Allen, 1982). It is known that water can produce shapes very similar to rat-tails and other study area SF. A combination meltwater/glacial origin is also a valid possibility, since this morphological argument is based on the final shape of the SF. Glacial ice may have formed diamicton ridges or bedrock steps that were subsequently shaped by meltwater flows.

Massive diamicton in lowland SF can be interpreted as supporting all three origin models. The conclusion that lowland SF are erosional features can also support a

water or ice origin; however, an erosive origin is only concordant with glacial erosion, not with the subglacial deformation model.

Correlation of rat-tail length to width is indicative of streamlining flow. Streamlining of river islands and other landforms by water and wind is documented (*e.g.*, Karcz, 1981; Allen, 1982; Komar, 1984). Although it is perhaps possible, it has not been shown nor explained how or why ice would produce a streamlined shape. It seems reasonable to accept a known mechanism for streamlining flow.

Based on the results of the field study, it is suggested that rat-tails in the study area were probably formed by subglacial meltwater flows. Larger upland SF may have received an initial form development from ice, but their present streamlined shape is interpreted as being probably due to meltwater flows. Lowland SF may have originally existed as subglacial drift ridges and then been subsequently streamlined.. It is suggested that streamlining of these shapes and the development of hairpin furrows were probably by meltwater floods. It is also possible that lowland and upland SF were entirely shaped by subglacial meltwater floods.

6. TOPOGRAPHIC ANALYSIS AND CLOSED CONTOURS

6.1. INTRODUCTION

One of the main questions being addressed in this thesis is whether large-scale glacially-associated floods crossed the study area. The purpose of this chapter is to investigate the geomorphologic signature of such floods and whether that signature is found in the study area. The investigation is framed by two questions: 1) Do glacially-associated floods produce characteristic landforms with consistent shape properties, and 2) if so, do study area landforms show these shape properties?

Section 6.2 reports on previous work pertaining to erosional residuals in formerly glaciated terrain. The term "erosional residuals" is used here to refer to landforms that remain after a landscape or channel has been eroded by floods, rivers or streams. The rest of the chapter is a study of whether landforms similar to flood terrain landforms are present in the study area. The investigation includes a topographic analysis designed to detect landform shapes that are similar in shape to erosional residuals produced by glacial outburst or subglacial floods.

Landform shapes are the result of a number of controls and processes. For example, landform shapes are initially controlled by lithological and structural landscape properties. Glacial, fluvial, colluvial, aeolian and other processes contribute to landform development. A main purpose of this research is to understand to what degree, if any, meltwater floods have affected the study area. Hence, this chapter is primarily focussed on attempting to detect only a particular type of landscape-forming process, fluvial erosion by glacial meltwater floods.

6.2. PREVIOUS WORK

Erosional residuals are found in inferred subglacial and proglacial flood paths and as streamlined islands in rivers. The residual shape is derived primarily from erosion, although deposition on the down flow end may contribute to the residual's final shape (Rachocki, 1981; Komar, 1983; Elfstrom and Rossbacher, 1985).

Erosional residuals can have different shapes depending on channel density. When channel density is high and residuals are closely packed, the residuals have characteristic reticulate, rhomboid, and arcuate shapes, with faceted prows and pointed tails. As channel density decreases, the erosional remnants become more streamlined, as with isolated, longitudinal river islands, and they develop rounded prows and a teardrop shape approximated by the lemniscate form (Baker, 1979; Komar, 1983, 1984; Kehew and Lord, 1986; Baker *et al.*, 1987).

Streamlined erosional residuals formed by glacial floods are documented in a number of areas. Komar (1984) quantitatively compared the lemniscate shape (Figure 93), airfoil shapes, drumlins, streamlined islands in rivers, residual "islands" in the Channelled Scabland (Baker, 1973; Baker, 1979), and streamlined forms on Mars. The streamlined islands in rivers, in the Channelled Scablands, and on Mars were similarly shaped with nearly the same length-to-width ratios, ratios that were also consistent with lemniscate shapes (Figure 93). Drumlins with tapering tails also approximate the streamlined lemniscate shape, but elliptical drumlins do not. Komar (1984) noted a reduction in the length to width ratio (L/W) of streamlined islands when they are closely packed, as in braided channels.

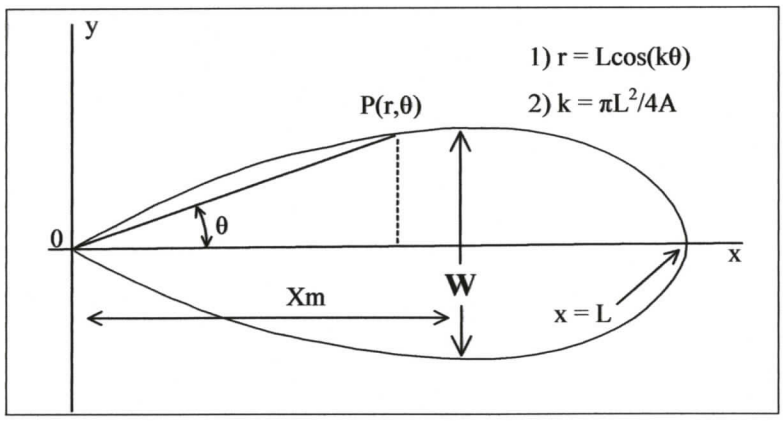

Figure 93. Lemniscate loop. Shape is generated by equation 1. Shape factor *k* is defined by equation 2. The Xm length is used in streamlined form analyses.

Progressive streamlining of erosional residuals has been documented in both glacial lake spillways and inferred subglacial settings. Kehew and Lord (1986) described several spillways in the northern Great Plains that were formed by glacial lake outburst floods. The spillways extend from northwestern Minnesota into southeastern Saskatchewan, near the inferred southwestern shore of glacial Lake Agassiz. The floods initially down cut the surface in broad, shallow anastomosed channel networks and, where a flood persisted long enough, flow became confined in deeper channels. More streamlined, isolated residuals were interpreted as indicating greater duration of the particular flood event. The most stable, basic residual dimensions of length and width were defined early in the erosional process, and were maintained as further erosion rounded and streamlined the initial shape. Strong regression equation correlations between length, width, and area were found for all northern Great Plains residuals even though only about 20 percent of the residuals had

developed into streamlined lemniscate shapes. These regression relationships are compared later in this chapter to those for study area closed contours.

Sjogren and Rains (1994) attributed the formation of the Coronation-Spondin Scablands in Alberta to progressive channelization of a subglacial sheet flood. Anastomosed channels were defined and down cut as the sheet flood progressed, producing both reticulated and streamlined erosional residuals. Greater streamlining was associated with more isolated residuals.

Other workers have interpreted elongate landforms as erosional residuals produced by glacial outburst floods. The residuals have been reported from northern Sweden (Elfstrom and Rossbacher, 1985) and Norway (Longva and Thoresen, 1991). Gore and Pickard (1998) suggested that elevated bars in modern outburst spillways in Antarctica could be erosional remnants produced by ice dam breaches and catastrophic drainage of subglacial lakes.

Residual uplands and hills in Michigan and Wisconsin that are dissected by anastomosed, reticulate networks of channels and valleys have been attributed to subglacial meltwater erosion (Johnson, 1999; Fisher and Taylor, 2002; Sjogren *et al.*, 2002). Fisher and Taylor (2002) observed that many of the interconnecting valleys are dry or hanging, indicating that they were formed by flood erosion. Subglacial meltwater networks in Antarctica have been reported (Sugden *et al.*, 1990; Sugden *et al.*, 1991; Lowe and Anderson, 2003). Lowe and Anderson (2003) detected a meltwater-produced channel network off the Antarctica coast that rivals the scale of the Washington Scablands. The channels range up to 15 km in length and 2 km in width. Recent work has detected an anastomosing channel network in the English Channel with associated

longitudinal grooves, streamlined islands, and streamlined valley margins (Gupta *et al.*, 2005). The collection of submarine landforms has been interpreted as the consequence of a glacial outburst flood.

Anastomosing channel networks in glacial terrains are frequently associated with longitudinal and transverse landforms and bedrock marks. Drumlins are found both on erosional residual uplands and within the channels (Brennand and Shaw, 1994; Sjorgren and Rains, 1995; Barnett *et al.*, 1998; Johnson, 1999; Fisher and Taylor, 2002; Sjogren *et al.*, 2002). The drumlins may be truncated by the channels (Brennand and Shaw, 1994; Barnett *et al.*, 1998). Bedrock erosional marks such as sichelwannen, comma forms, flutes, and bedrock grooves are also associated with subglacial channels networks (Booth and Hallet, 1993; Brennand and Shaw, 1994; Beaney and Shaw, 2000; Lowe and Anderson, 2003). Giant current ripples, with chord lengths (spacing) up to 160 m and heights up to 8 m, are found in glacial outburst flood paths (Baker, 1973; Baker *et al.*, 1987; Rudoy and Baker, 1993). Similarly sized and spaced transverse ridges are found in ancient tunnel channels (Brennand and Shaw, 1994; Beaney and Shaw, 2000).

Anastomosing channels are often eroded into bedrock (for example, Booth and Hallet, 1993; Brennand and Shaw, 1994; Gilbert and Shaw, 1994; Sjogren and Rains, 1995; Heritage *et al.*, 1999; Wende, 1999; Beaney and Shaw, 2000; Sjogren *et al.*, 2002). Lowe and Anderson (2003) report subglacial meltwater floods incised over 400 m into bedrock off the present coast of Antarctica. Potholes in Antarctica up to 200 m across have also been attributed to subglacial meltwater (Sugden *et al.*, 1991; Denton and Sugden, 2005). Baker (1973, 1979) discussed large-scale bedrock cavitation caused

by the formation of high-suction kolks (vertical tornado-like vortices) in deep flow from the Lake Missoula outburst flood(s).

6.3. METHODS

6.3.1. Topographic analysis

The purpose of the topographic analysis is to determine if landforms in the study area have shapes similar to shapes of streamlined erosional residuals (SER) in known or inferred flood paths. Two steps are necessary to accomplish this goal: elongated closed contours are identified as possible SER and the length to width ratios of these forms are compared to known SER located in flood paths.

The plan view shapes of possible SER are identified using contour lines generated from TRIM 1 digital elevation models (DEM) of the study area. Contours from 0 to 2000 m elevation are used with 10 m contour intervals. The TRIM 1 grid spacing is 25 m. When analyzing the entire study area, contour generation using the original grid spacing is not practical due to long processing times. Grid recalculation makes the topographic analysis possible. Recalculated DEM grids for the five study area NTS sheets are used. The recalculated grids have a tenth as many nodes as a full size TRIM 1 grid. Recalculation is done using Surfer software, and results in a diminished database size that is an accurate representation of the original data (Golden Software, Inc., 1999). At the scale of the landforms being analyzed, the recalculated grid provides contour output similar to full size DEM grids (Figures 94 and 95). Differences in output between the two grid sizes do not result in greatly different results, although differences occur (Figures 94 and 95).

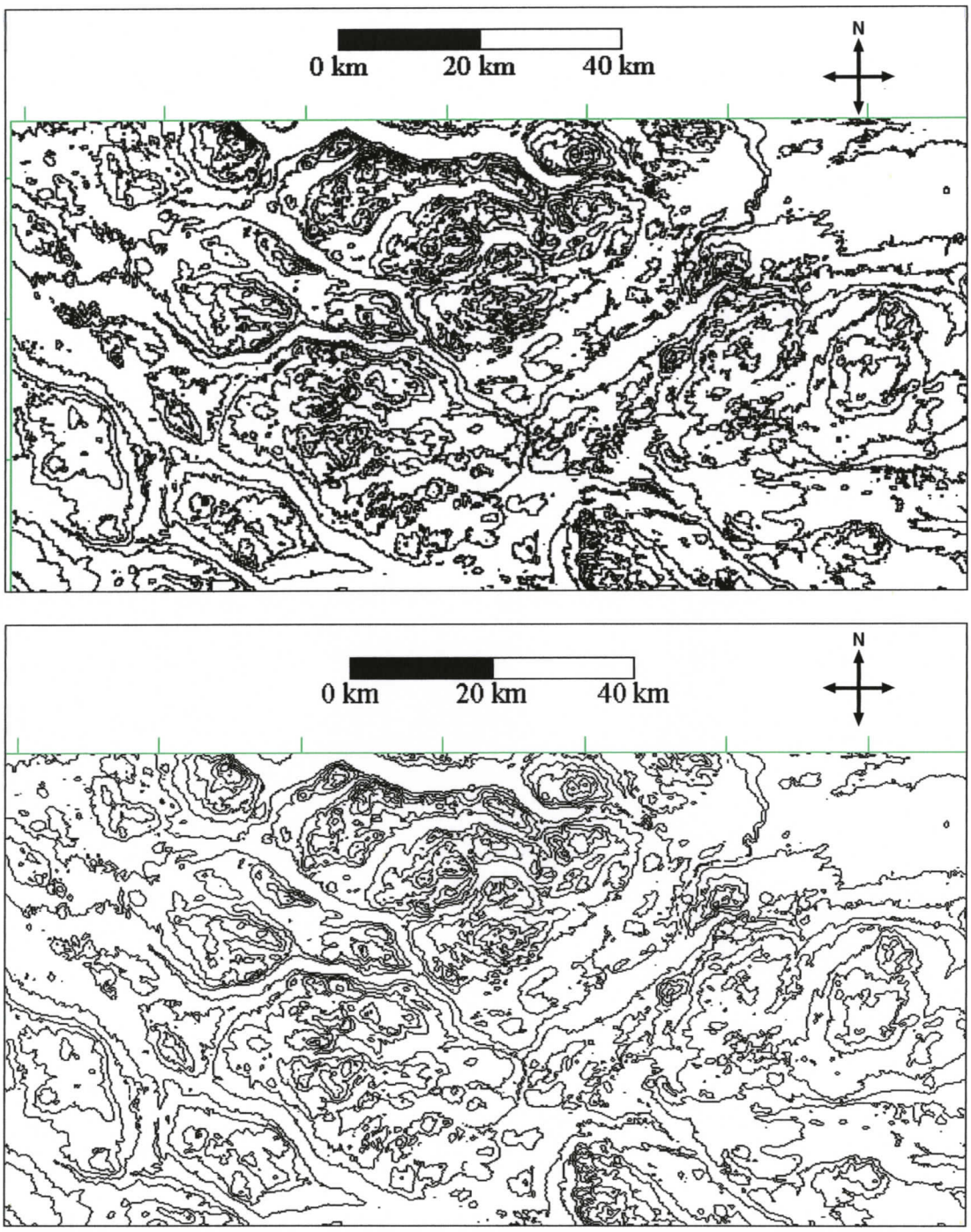

Figure 94. Contour maps of the north half of NTS 93F, 100 m contour interval. The top map is using a full-size TRIM1 DEM, and the bottom map uses the same grid recalculated to 10% of the number of nodes in the full-size grid. Upper right corner of contour maps are at about 124.01° W longitude and 54.04° N latitude.

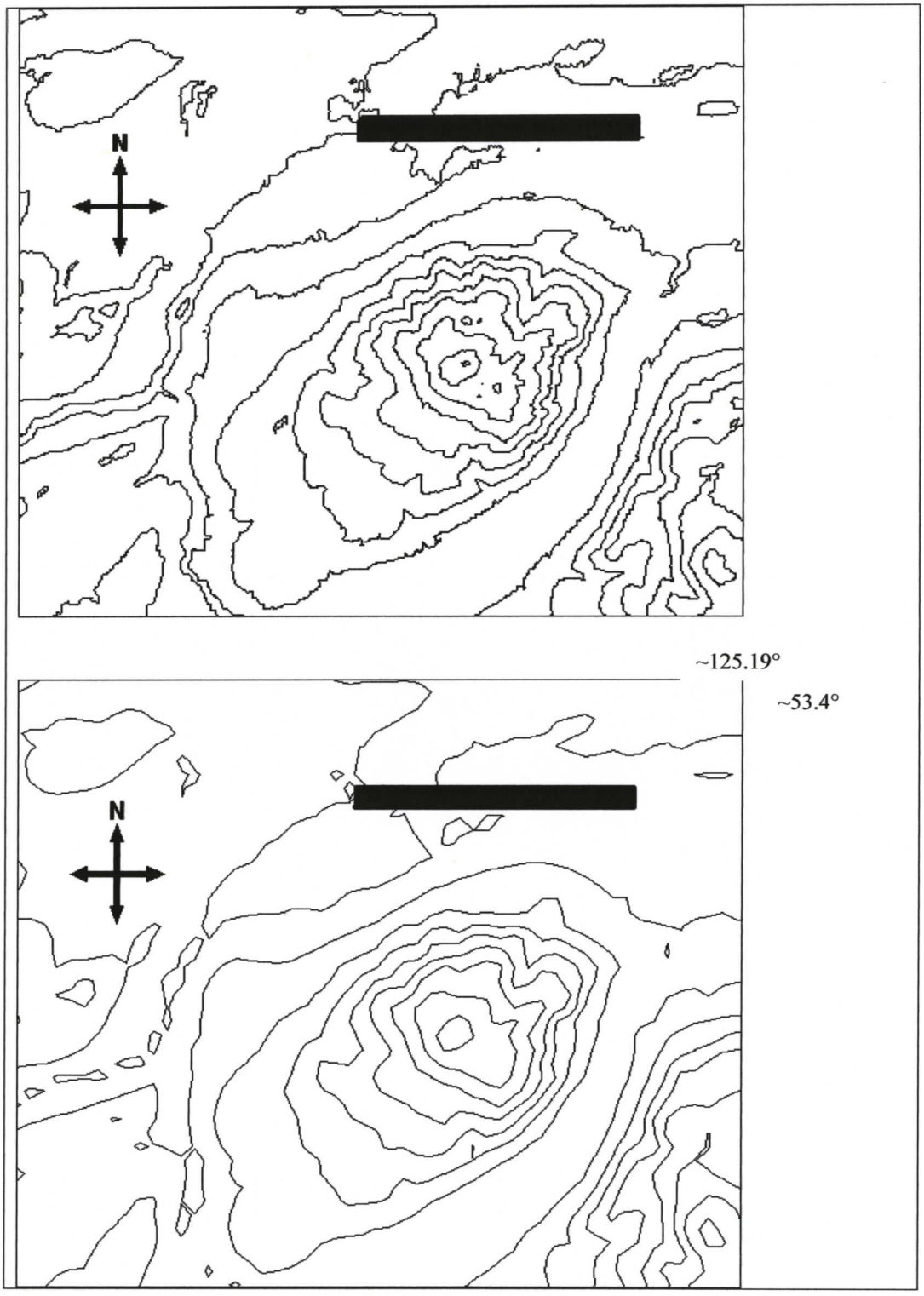

Figure 95. Contour maps at maximum zoom of contouring software. Scale bar = 5 km. Top map is using full-size grid. Bottom map uses recalculated grid. Contour interval = 100 m.

Contour lines are often used to delineate the plan view shape of drumlins in drumlin morphology studies (for example, Doornkampf and King, 1971; Jauhiainen, 1975; Mills, 1980; Evans, 1987; Harry and Trenhaile, 1987; Mills, 1987; Francek, 1991). In such studies, it is necessary to interpret which contour lines outline drumlins. This interpretation is based on a set of assumptions or criteria about drumlin shapes that may or may not be explicitly specified. For example, the drumlin mapper may select all closed contours within a particular size range that exceed a certain length to width ratio. The mapper would not choose a circular closed contour that was 10 km across, as it would not fit the known shape of a drumlin. Drumlins are, by definition, not circular in plan view nor are they 10 km across.

Observed erosional residuals and streamlined islands characteristic of flood terrains or fluvial environments are generally elongate in the direction of flow (for example, Baker and Kochel, 1978; Baker, 1979; Rachocki, 1981; Komar, 1984; Elfstrom and Rossbacher, 1985; Kehew and Lord, 1986; Longva and Thoresen, 1991; Sjogren and Rains, 1994; Lowe and Anderson, 2003). Thus, it is assumed here that most streamlined erosional residuals in flood paths will be elongated forms. The main intent of the topographic analysis is to capture into the data set all elongate closed contours in the study area greater than a minimum size. A set of topographic criteria, or rules, is used to identify possible study area SER. The use of these rules reduces the subjectivity of landform shape recognition.

The rules used in the topographic analysis for potential SER recognition follow: 1) Potential SER are defined by complete, closed contours. 2) The closed contour must be elongate, that is, it must be definable by a length and width axis; no circular or near

circular closed contours are selected as SER. Near circular is defined as having an aspect ratio (L/W) less than about 1.3. This restriction resulted in the elimination of less than 10% of closed contours that would otherwise have been mapped. 3) Only contours enclosing an area greater than 0.1 km^2 (10 hectares) are drawn. This is the practical lower limit for the scale of the study. The number of closed contours in the study area increases as the closed contour size decreases. For example, 17 closed contours are mapped with areas from 9 – 10 km^2, 41 closed contours are mapped with areas from 4 – 5 km^2, and 678 closed contours are mapped with areas from 0.1 – 1 km^2. The database becomes too large to manage at closed contour areas below 0.1 km^2. 4) When a number of adjacent closed contours are observed (for example, a 100 m high hill might be represented by ten closed contours) the largest (lowest elevation) is used. 5) If smaller, elongate contours are located at higher elevations within larger selected closed contours, then the smaller form is drawn if it represents a different orientation, is of a markedly different shape than the larger, surrounding form, or more than one smaller, adjacent form is found at the higher elevation. In these cases it is assumed that the smaller forms are potentially erosional forms in their own right, instead of just being the upper elevation expression of a larger, lower elevation form.

These rules cause a bias to be placed on closed contour selection. However, it is suggested that this bias does not negate the value of the shape analysis discussed in the following section. The shape analysis is primarily focused on closed contour aspect ratio. Only elongate forms with aspect ratios greater than about 1.3 are selected; however, no further aspect ratio restriction is enforced for closed contour selection.

6.3.2. Shape analysis

The closed contours identified as possible SER constitute the data set for shape analysis. Length and width axes for each closed contour are drawn. Length to width statistics are calculated and regression relationships determined. Length and width analysis is restricted to closed contours > 2.5 km^2 in area. This size restriction is due to the exponential increase in number of closed contours as closed contour area decreases. Since this phase of the research involves the digitizing of length and width axes for individual closed contours, a smaller size limit would increase the database to an unmanageable size.

6.4. RESULTS

The results of the topographic analysis of the study area are shown on Figure 96 (in map pocket). The map shows all closed contours found by the topographic analysis. No inferred boundaries are shown on this map; all boundaries are actual contours. Descriptive statistics of the area of the mapped closed contours are shown in Table 16. The sizes of the mapped closed contours range over four orders of magnitude, from about 0.1 km^2, the lower defined limit of the study, to 3894 km^2; 1654 closed contours are mapped.

The shapes of some of the closed contours (Figures 96 and 97) are comparable in appearance to erosional residuals produced by glacial outburst floods in the northern Great Plains (Kehew and Lord, 1986) (Figure 98) and the Channelled Scablands of eastern Washington State (Baker *et al.*, 1987) (Figure 99). Some closed contour shapes are also similar to erosional residuals believed to have been formed by subglacial

meltwater floods in the Dry Valleys in Antarctica (Denton, 1983) (Figure 100) and in northern Michigan (Johnson, 1999).

6.4.1. Fault maps and closed contour boundaries

A question being posed in this chapter is whether some closed contours in the study area represent erosional residuals defined by channel networks. If the lowland areas represent channels, then the locations of the channels would be to some degree a response to horizontal erosive flow around topographic obstacles. The locations of study area lowlands and valleys would possibly also correlate to fault locations. This possibility is examined by overlaying closed contours with known study area faults (Figures 101 and 102) (faults from MacIntyre, 1996).

It can be seen that in a number of cases, parts of the boundaries of the closed contours, particularly in the mountainous parts of the study area, are coincident with or paralleled by faults. The shapes of many closed contours are apparently influenced by fault locations.

Table 16. Descriptive statistics of the area (km^2) of closed contours	
Count	1654
Minimum	0.1
Maximum	3893.8
Range	3893.7
Mean	21.0
Standard Error	3.4
Median	1.3
Standard Deviation	153.0
Sample Variance	23422.1

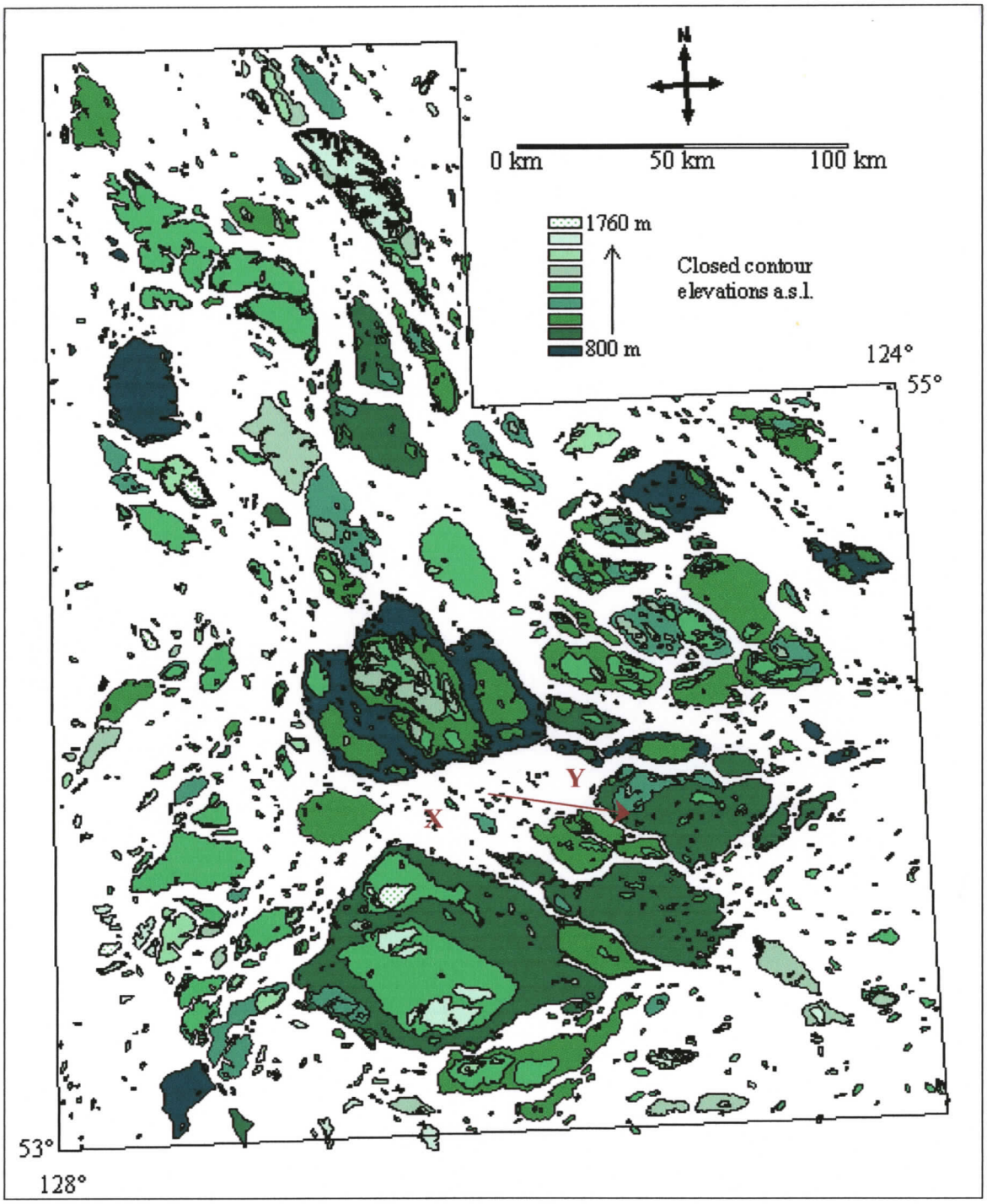

Figure 97. Small-scale duplicate of Figure 96, the main closed contour map found in the map pocket. See Figure 96 for complete legend. X shows an area lacking large landforms. Direction of increasing size of CC is indicated by the arrow at Y.

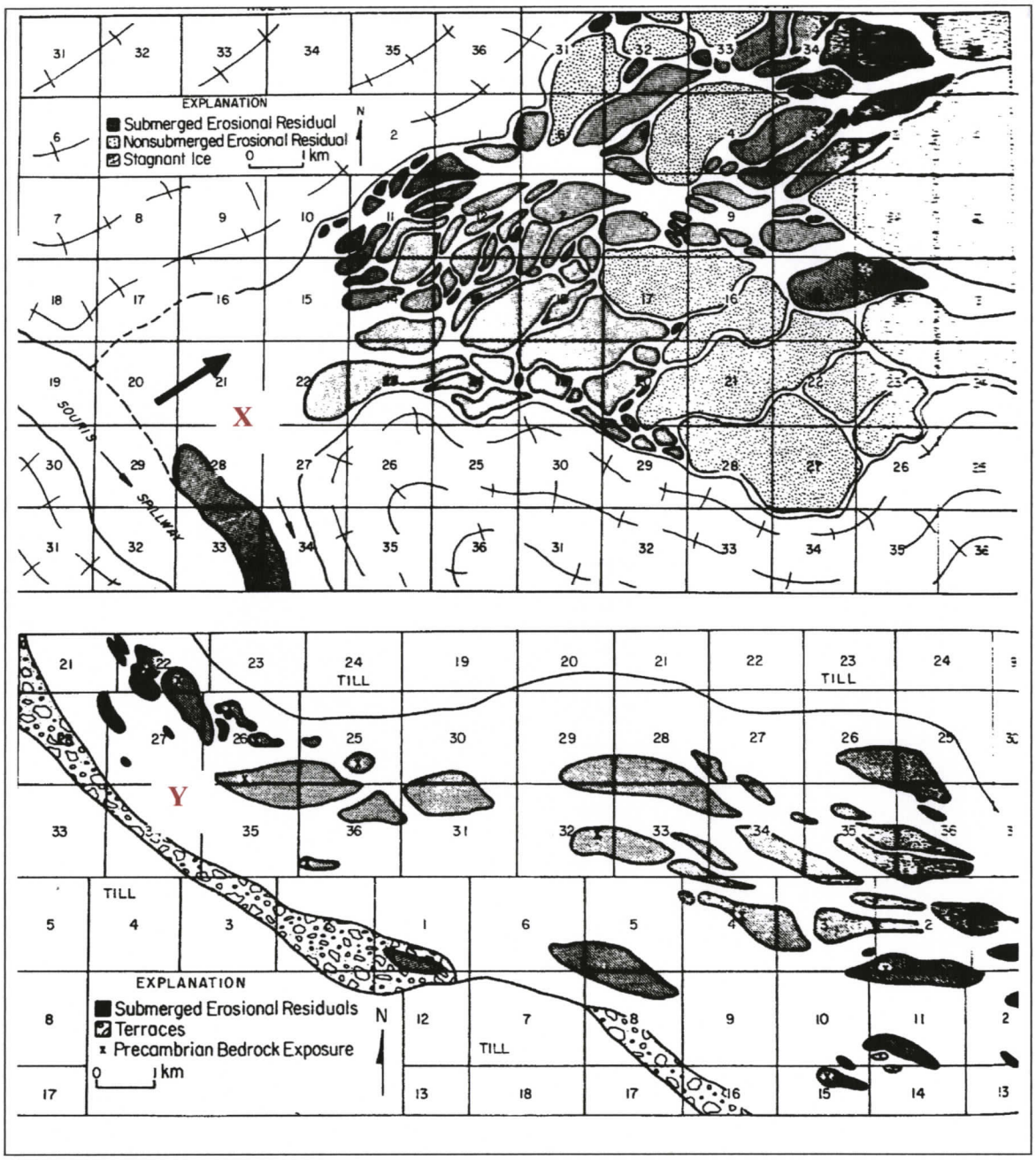

Figure 98. Erosional residuals in glacial outburst flood channels in Minnesota (bottom) and in area of anastomosed channels near Minot, North Dakota (top). Residuals are formed in sediment although bedrock is exposed between residuals in the Minnesota spillway. Flow directions are towards the east. Maps from Kehew and Lord, 1986, with permission from the Geological Society of America.

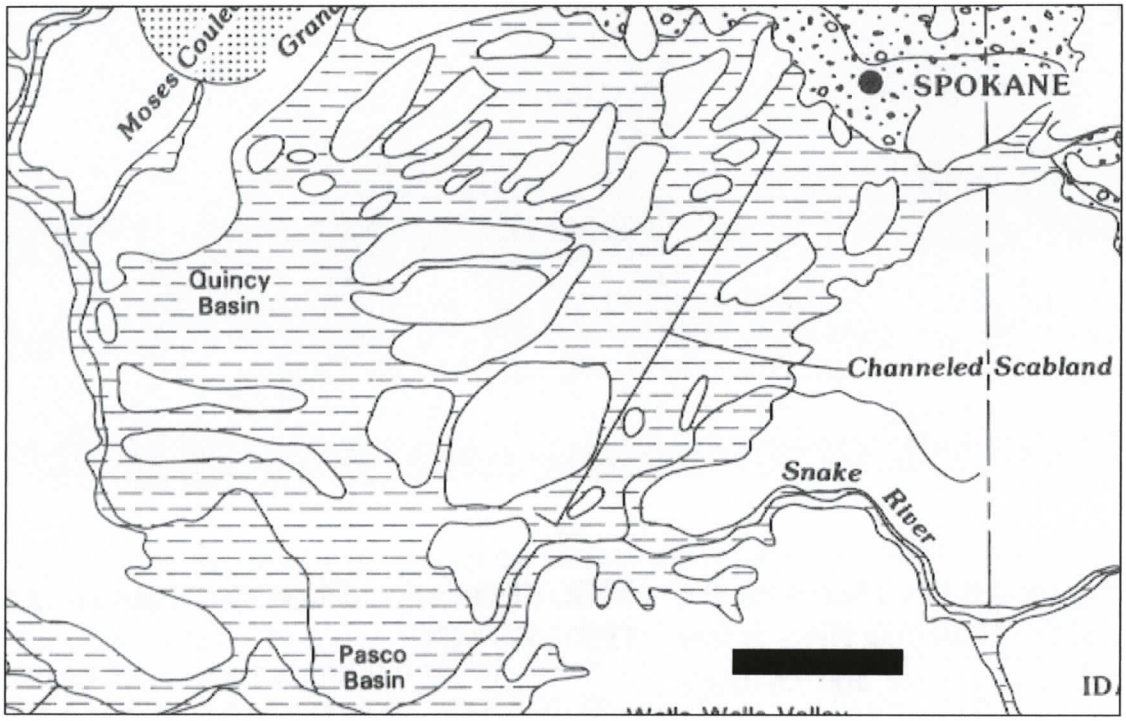

Figure 99. Erosional residuals of the Channelled Scabland in Washington, products of the Lake Missoula outburst flood(s) (Baker, 1973; Baker *et al.*, 1987). Flow is generally towards the southwest. North is towards the top of the figure, and scale bar represents approximately 30 km. From Baker *et al.*, 1987; reprinted with permission from the Geological Society of America.

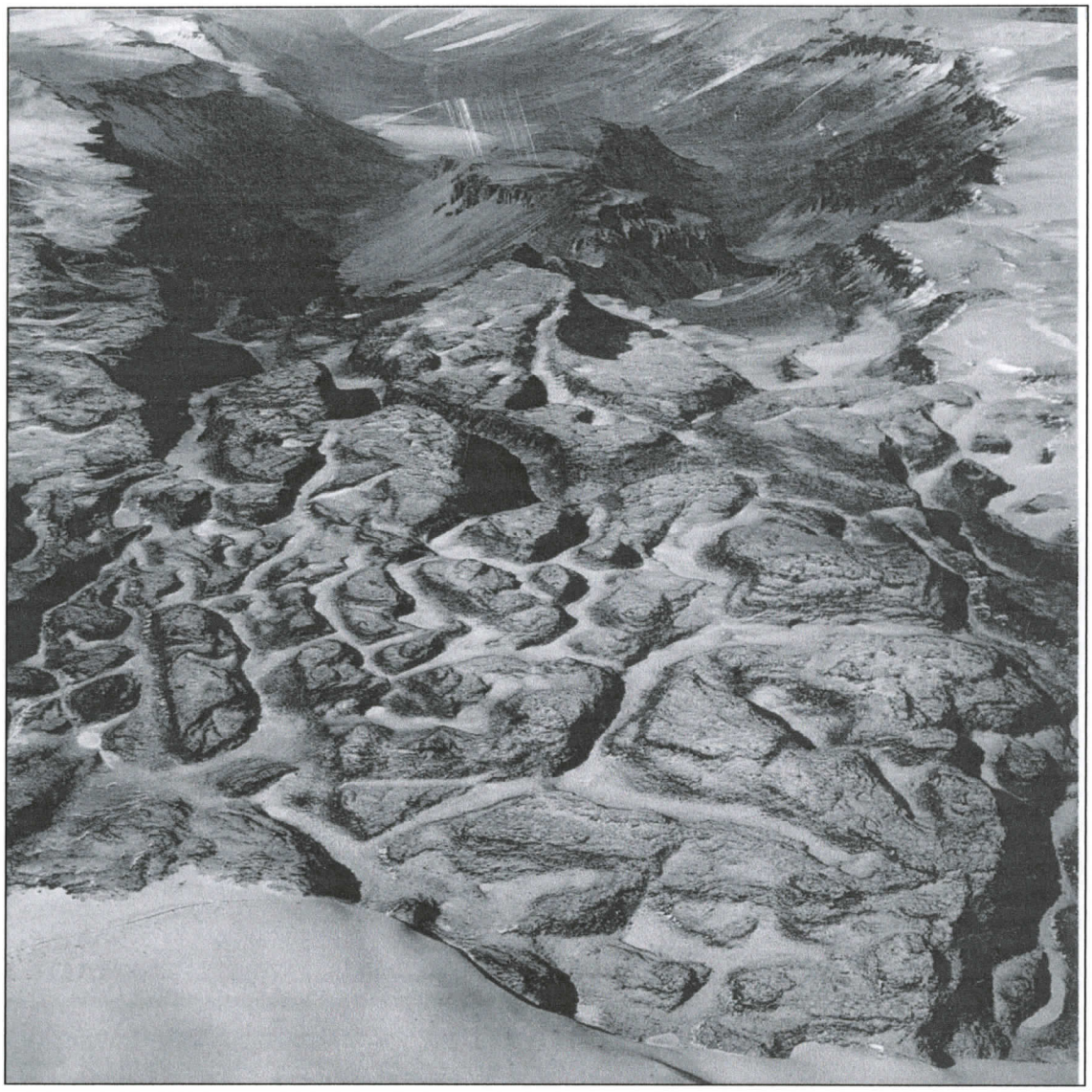

Figure 100. "The Labyrinth", interpreted as a subglacial meltwater channel system at Dry Valleys, Antarctica (Sugden *et al.*, 1991; Benn and Evans, 1998). Oblique aerial photograph from the cover of December 1983 issue of Geology (Denton, 1983). Reprinted with permission from George H. Denton. The distance across the channel in the vicinity of the butte in the background is about 600 m.

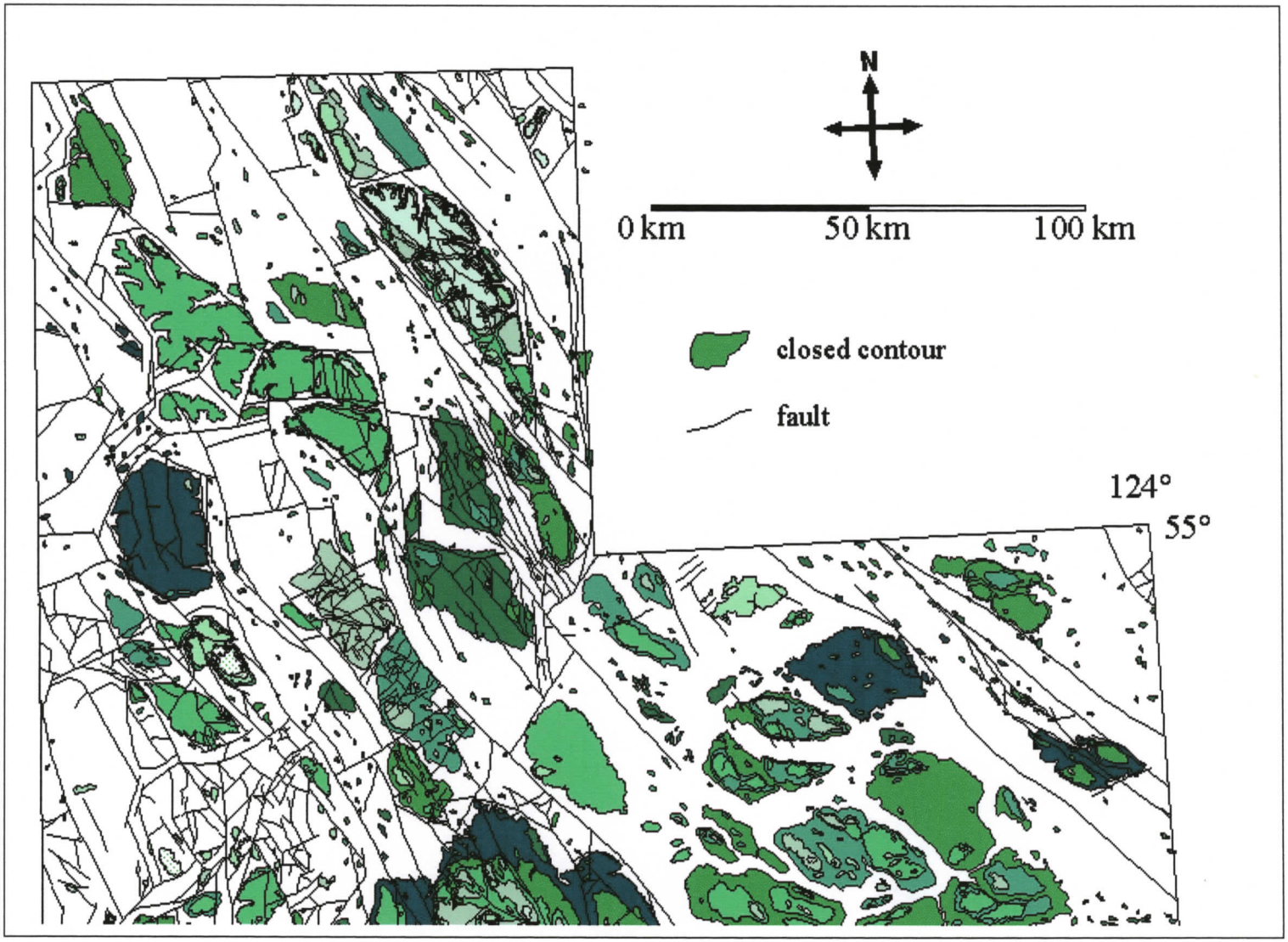

Figure 101. Faults over closed contours, north half of study area. Only closed contours greater than 10 km^2 are shown.

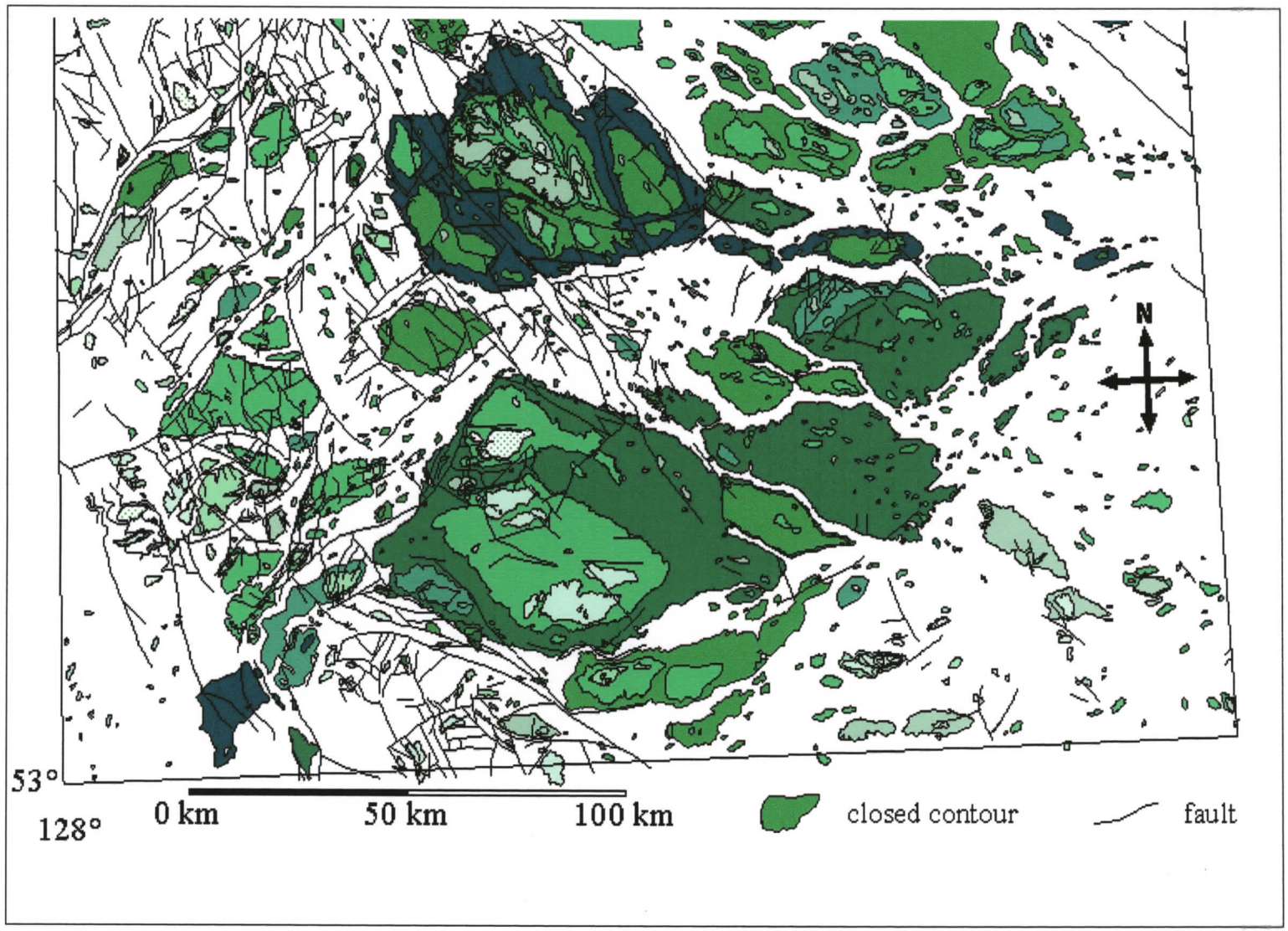

Figure 102. Faults over closed contours, south half of study area. Only closed contours greater than 10 km^2 are shown.

6.4.2. Shape analysis

Numerical shape analysis is conducted on the mapped study area closed contours that exceed 2.5 km^2 in area. The purpose of the shape analysis is: 1) to determine if the lengths of study area closed contours correlate to their widths; and, 2) to determine if the length to width ratios of the closed contours are similar to those of erosional residuals known or believed to have been formed by fluvial processes, including glacial outburst floods.

It is noted above that closed contour selection rules restrict the data set, including only forms with aspect ratios greater than about 1.3. However, this restriction is only a lower limit and still allows a theoretically infinite range of closed contour aspect ratios. It is suggested here that the bias introduced into the topographic analysis by this restriction does not prohibit the collection of useful data using the topographic analysis methodology.

One purpose of analyzing study area aspect ratios is to determine if forces that were instrumental in the final shaping of landforms were acting in the horizontal plane, and if so, at what orientations those forces were directed. Closed contour lengths and widths are measured with respect to the horizontal plane. If lengths correlate to widths, then the length of a form is dependent on its width. If so, then it is inferred that a process acting in the same plane as the length and width axes was responsible for the correlated dimensions of the form; forms elongated systematically with respect to the

horizontal and with constant length to width ratios would not be due to a process acting normal to the surface.

However, it is noted that correlated length to width ratios could also derive from structural controls. For example, it is clear that joints and faults observed in bedrock are often regularly spaced. Such fault spacing could result in bedrock forms with consistent aspect ratios. In such a case, correlation would not be related to a unidirectional erosive process.

The constructed length and width axes of study area closed contours greater than 100 km^2 in area are shown in Figures 103, 104, and 105. Length and width axes of closed contours from 2.5 to 100 km^2 in area are shown in Appendix D. The lengths of the depicted axes are used in the numerical shape analysis. Similar erosional residual axes construction was used by Kehew and Lord (1986) (Figure 106). Analyzed lengths range from 2.5 to 102.3 km (Table 17); however, the aspect ratios (L/W) are remarkably consistent across all closed contour size ranges (Table 18). Aspect ratios for closed contours in three different size categories are almost identical. Also note the small standard deviations and sample variances. These observations indicate that aspect ratio is controlled by some property and/or process that is effective across a wide size range of landforms.

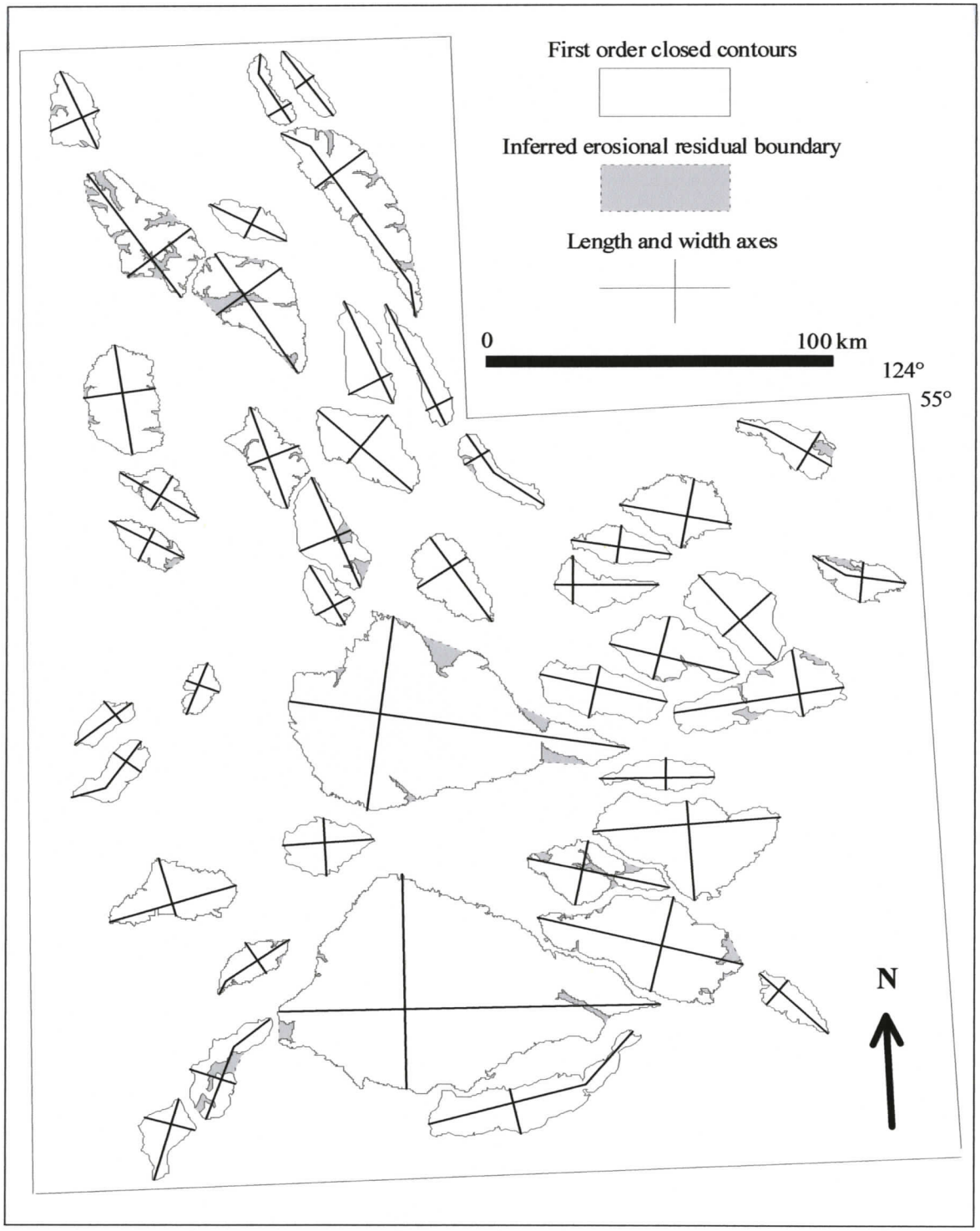

Figure 103. First order closed contours showing length and width axes. Only closed contours with areas greater than 100 km^2 are shown.

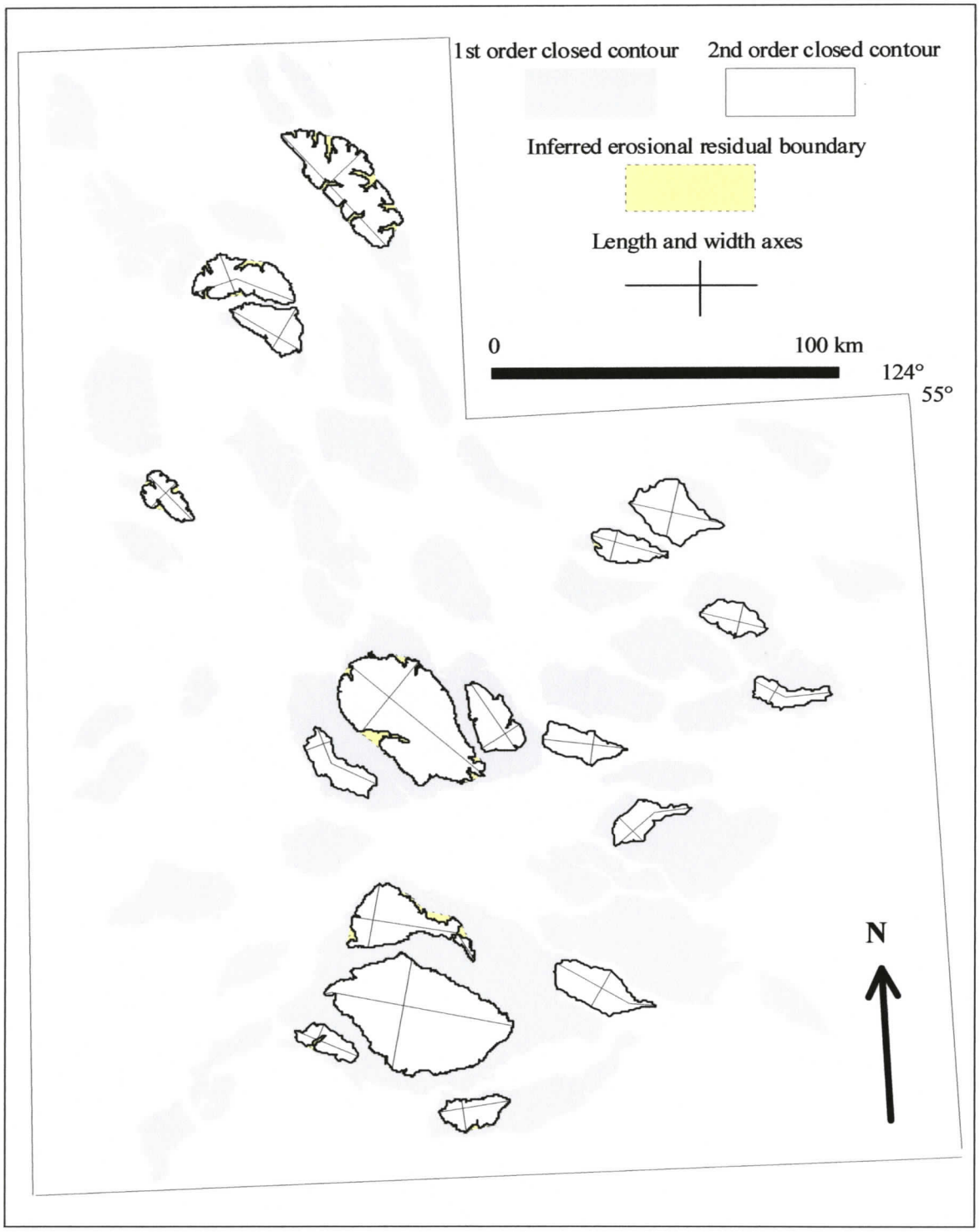

Figure 104. Second order closed contours showing length and width axes. Closed contour areas are greater than 100 km^2. Second order forms are at higher elevations than first order forms (see Figure 96, map pocket).

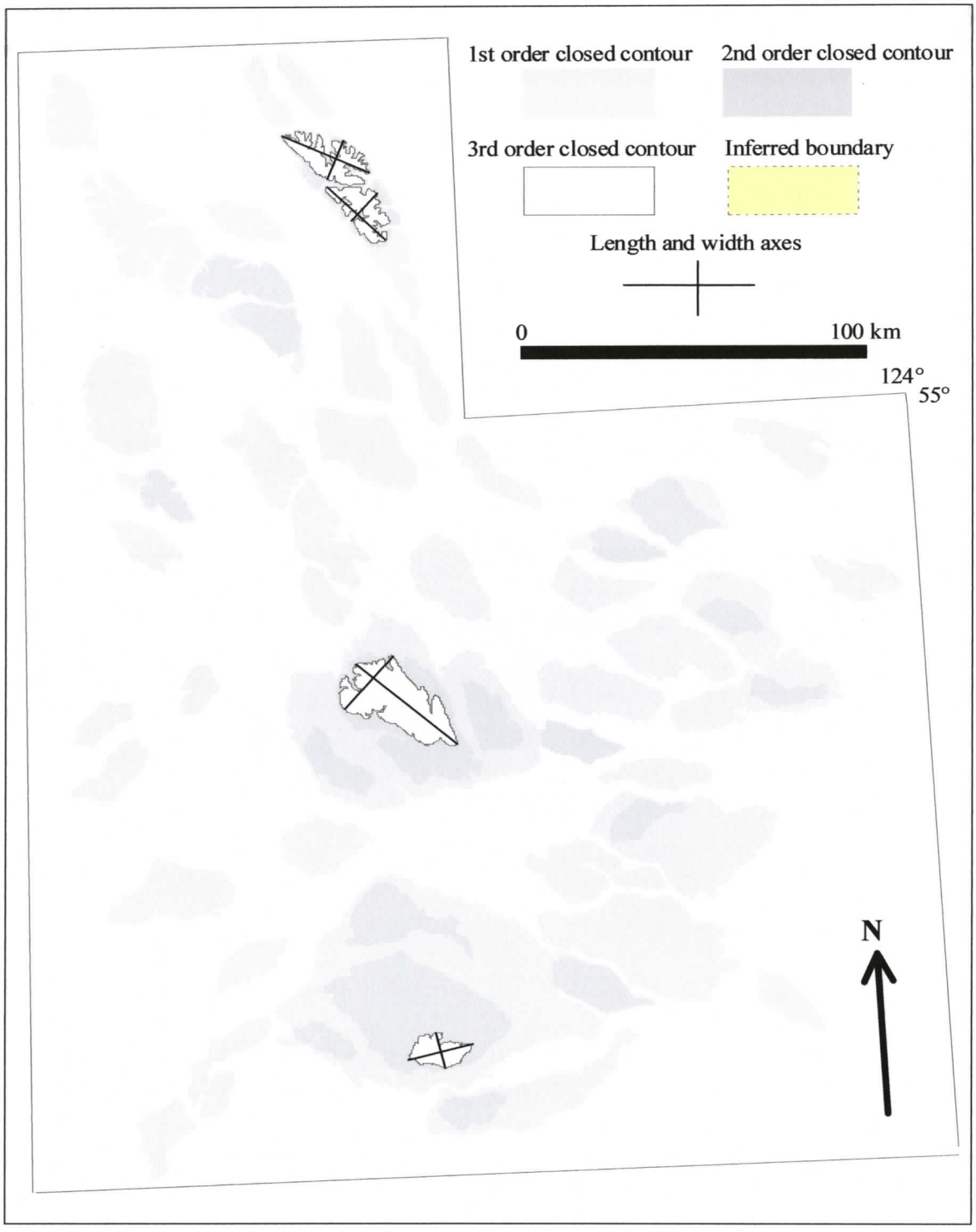

Figure 105. Third order closed contours showing length and width axes. Closed contour areas are greater than 100 km^2. Third order forms are at higher elevations than first and second order forms (see Figure 96, map pocket).

Figure 106. Streamlined erosional residuals formed in glacial lake spillways, taken from Kehew and Lord (1986). Upper figure is derived from Minot spillway residuals in North Dakota; lower figure is from Minnesota spillway. Scale bars are 1 km long. Length and width axes used by Kehew and Lord in numerical shape analysis are shown. Reprinted by permission of Geological Society of America.

Table 17. Length, width, and aspect ratio (L/W) of study area closed contours < 2.5 km^2 in area			
	Length	*Width*	*L/W*
Mean	9.9	4.4	2.38
Standard Deviation	11.5	5.7	0.67
Sample Variance	133.3	32.1	0.48
Minimum	2.5	0.9	1.33
Maximum	102.3	62.3	5.12
Count	527	527	527

Table 18. Aspect ratios for different size ranges of study area closed contours			
	2.5-10 km^2	*10-100 km^2*	*>100 km^2*
Mean	**2.39**	**2.38**	**2.36**
Standard Deviation	0.69	0.61	0.73
Sample Variance	0.48	0.37	0.54
Range	3.74	2.77	3.55
Minimum	1.38	1.33	1.56
Maximum	5.12	4.11	5.11
Count	283	179	65

Study area aspect ratios are at the low end of the range but comparable to aspect ratios of erosional residuals in northern Great Plains glacial lake spillways (Kehew and Lord, 1986), the Channelled Scablands of eastern Washington state (Baker, 1979), glacial outburst flood paths in Sweden (Elfstrom and Roffsbacher, 1985), and man-made alluvial fan and active glacial outwash braid bars (Rachocki, 1981) (Table 19). Regression analysis and power fitting of aspect ratios of study area closed contours

demonstrates a strong correlation between length and width, with an R^2 value of 0.89 (Figure 107). The lengths of closed contour shapes are strongly dependent on their widths. Similar strong correlations and power equations relating length to width are reported for erosional residuals in glacial lake spillways (Baker, 1979; Kehew and Lord, 1986) and for streamlined river islands (Komar, 1984) (Table 20). The study area values indicate less elongation than the erosional residuals in the Channelled Scabland and the Great Plains. This discrepancy is discussed later in this chapter.

Table 19. Shape statistics for erosional residuals

	Count	*Area (km^2), avg.*	*Length, avg. or range (km)*	*Width, avg. or range (km)*	*L/W, avg.*
1. Study area closed contours	527	23.8	9.9	4.4	2.38
2. Glacial-lake spillway (Kehew and Lord, 1986)	168	0.6	1.39	0.42	3.39
3. Channelled Scablands (Baker, 1979)	135	nd	0.6 – 25[1]	0.2-9[1]	3.15
4. Streamlined river islands (Komar, 1984)	38	nd	0.3 – 5[2]	0.06 – 1.3[2]	4.3
5. Erosional remnants in Sweden (Elfstrom and Roffsbacher, 1985)	9	nd	0.2 – 1.0	nd	2.5
6. Man-made braid bars (Rachocki, 1981)	82	nd	0.0004 – 0.006[3]	0.0002 – 0.003[3]	2.44
7. Active glacial outwash braid bars (Rachocki, 1981)	42	nd	nd	nd	2.35

[1]approximate range, from Figure 3 of Baker (1979)

[2]approximate range, from Figure 6 of Komar (1984)

[3]approximate range, Figure 51 of Rachocki (1981)

nd = no data

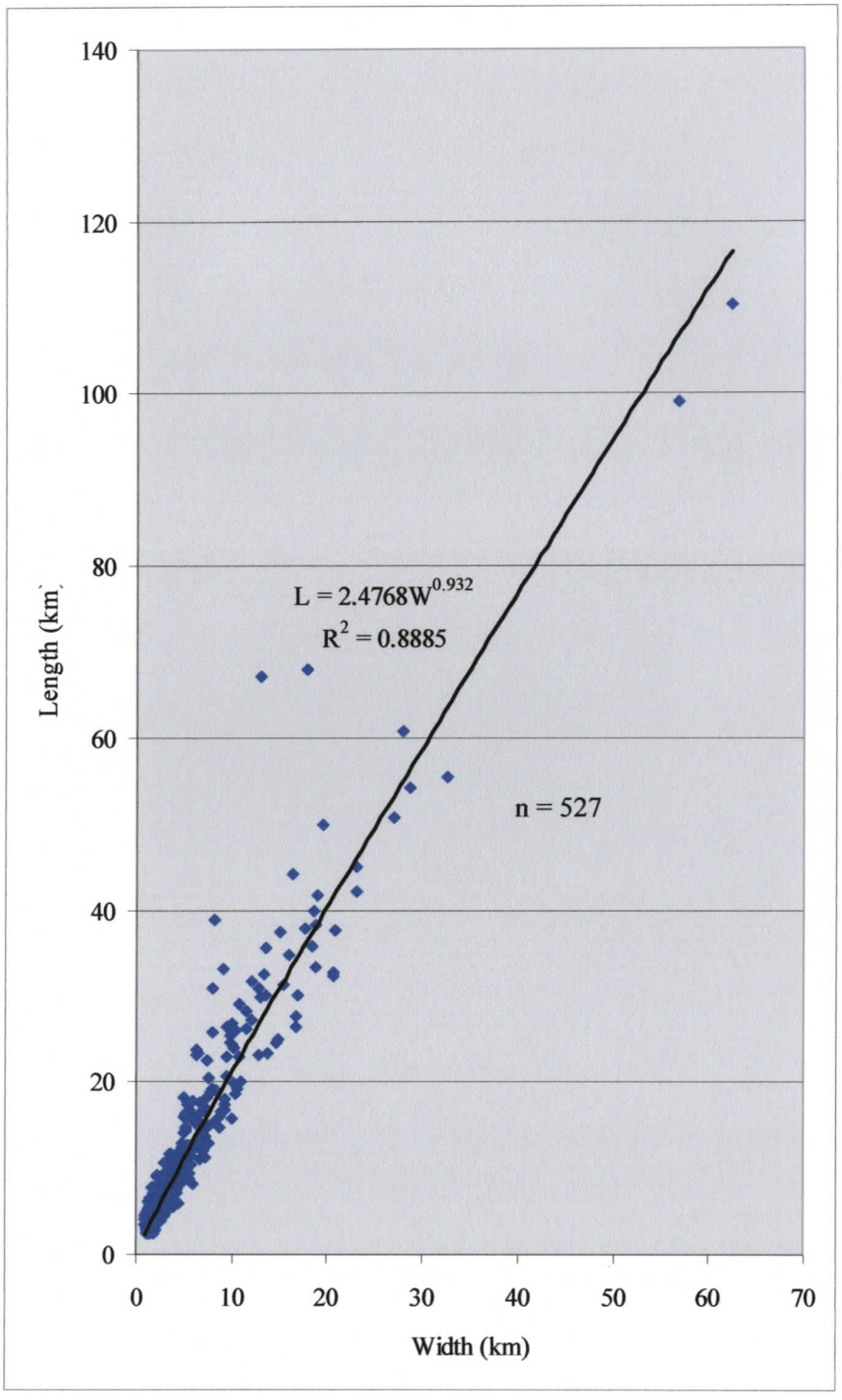

Figure 107. Plot of width versus length for study area closed contours.

Table 20. Regression equations for closed contours, erosional residuals, and river islands	
Study area closed contours	$L = 2.48W^{0.932}$
	$R^2 = 0.89$
Glacial-lake spillway (Kehew and Lord, 1986)	$L = 3.06W^{0.97}$
	$R^2 = 0.73$
Streamlined river islands (Komar, 1984)	$L = 4.01W^{0.958}$
	$R^2 = 0.96$
Channelled Scablands (Baker, 1979)	$L = 3.01W^{1.02}$
	$R^2 = 0.87$

6.5. DISCUSSION

Landform shapes are the result of several controls and processes. Some controls on landscape morphology include lithological and sediment composition, variations in composition across the landscape, and locations and orientations of folds and faults. Glacial, fluvial, colluvial, and aeolian erosion and deposition contribute to landform development. Erosional patterns are often superimposed on erosional forms from earlier events, *i.e.*, glacial topography would be expected to often reflect preglacial topography. A main purpose of the research presented here is to understand to what degree, if any, meltwater floods have affected the study area. The effect of floods and rivers on the shape development of landforms has been measured and these data are available. Topographic analysis discussed in this chapter focuses on determining if study area landform shapes can be related to fluvially-shaped landforms.

Although definition of a glaciological mechanism for closed contour aspect ratio correlation is not attempted here, a summary of possible glacial landscape elements is included in the interpretations. The lowland/upland configuration found across much of the study area could be described by these landscape elements.

6.5.1. Similarity of closed contour shapes to erosional residuals

The shapes of the closed contours are compared qualitatively and quantitatively to the shapes of erosional residuals known or thought to have been formed by fluvial agents. Isolated islands streamlined by rivers or floods generally develop the characteristic shape approximated by the mathematically derived lemniscate loop (Figure 97) (Komar, 1984). When islands are more closely packed, then the channel and associated islands/bars develop a braided appearance. Islands and bars are cut by channels and develop faceted rhomboid, or diamond, shapes. Close packing can also result in lemniscate islands with the pointed end directed upstream (Kehew and Lord, 1986). Experiments with initially elongated islands indicated that the shapes tend to remain elongated when subjected to erosive flow (Komar, 1983). Thus, characteristic island and erosional residual shapes in high velocity flows include rhomboid, reverse lemniscate, lemniscate, and elongated forms.

Examples of these forms can be seen in northern Great Plains glacial outburst flood spillways (Figures 98 and 106); in the Channelled Scablands formed by the catastrophic drainage of glacial lake Missoula (Figure 99); in inferred subglacial meltwater flood channels in Antarctica (Figure 100); and in countless modern braided

channels. Many closed contours are interpreted as shapes that approximate erosional residuals and streamlined islands (Figures 96, 103-105, and Appendix D).

Strong length to width correlation indicates a shape derived by a unidirectional process, with respect to a given form, acting horizontally. Both ice and fluvial erosion can be unidirectional formative processes acting along the earth's surface. The aspect ratios of the closed contours are consistent at all size ranges, from 2.5 km^2 to 3893 km^2.

Closed contour aspect ratio values and regression equations are quite similar to aspect ratios and regression equations of erosional residuals interpreted as products of glacial floods or other fluvial processes (Tables 19 and 20). The aspect ratio is related to the development of a surface of least resistance to eroding flow. This does not mean that SER development can not include a depositional element. Nonetheless, deposits that make up the tails of streamlined islands, for example, persist because they are in a non-eroding area in the lee of a flow obstruction (Komar, 1983).

The resistance of an island to the force of a stream is made up of two components, the form drag and skin drag, as described by Wyrick (2003, p 289):

> Drag force is the combination of form drag and skin drag. The form drag is dependent upon the shape of the object and arises from flow separation behind the object. The shape controls the wake size and the amount of momentum and energy dissipated in the turbulence. Streamlining will reduce the wake zone and hence the form drag. The skin drag is proportional to the surface area of the object that is subjected to the flow conditions.

Streamlined forms develop less drag force than non-streamlined forms. Streamlining results in the development of a tail down flow of a flow obstruction. The flow obstruction may be a resistant clast in bedrock, in the case of a rat-tail, or a vegetated bar in the case of a river island. The tail can develop by both depositional and erosional

processes. As streamlining continues, form drag is reduced, but surface area, and consequently skin drag, increases. For a given set of flow conditions, a shape exists that minimizes the total drag force. This streamlined shape presents the least resistance to flow. The most important flow condition is the Reynolds (Re) number, which is proportional to fluid velocity and inversely proportional to fluid viscosity.

The Reynolds number is a dimensionless number expressing the ratio of inertial force to viscous force, and is expressed by:

$$\frac{\rho V l}{\mu}$$

where ρ = density, V = velocity, l = length and μ = viscosity. The upper term represents inertial forces and the lower term represents viscous forces. At low Reynolds numbers, viscous forces predominate; at high Reynolds numbers inertial forces predominate (Binder, 1962). Flowing ice has Re numbers estimated variously as on the order of 10^{-13} (Fowler and Larson, 1978) or 10^{-16} (Shaw, 1994). Meltwater floods are estimated to have had Re numbers on the order of 10^{8} (Shaw, 1994), and Re numbers that produced streamlined islands and Channelled Scablands residuals were estimated to be between 10^{4} and 10^{5} (Komar, 1983).

Based on measurements of erosional residuals in the Channelled Scablands, Baker and Kochel (1978) and Baker (1979) postulated that an aspect ratio in the range of 3 to 4 was developed in "equilibrium" forms and corresponded to a streamlined, minimal drag form. Komar (1983) confirmed this hypothesis by measuring experimentally produced streamlined islands and by investigating minimal drag airfoil dimensions.

The average aspect ratios of the erosional residuals in the northern Great Plains spillways and Channelled Scablands are within the 3-4 range and the aspect ratio for streamlined river islands is 4.3 (Table 19). However, study area closed contours, erosional remnants in Sweden composed of boulder-rich till, active glacial outwash braid bars, and alluvial fan braid bars show aspect ratios between 2.35 and 2.5 (Table 19). Higher channel densities, that is, close packing of residuals, inhibits streamlining (Komar, 1984; Kehew and Lord, 1986). Baker (1979) hypothesized that higher Re numbers tend to result in more elongated islands. Lower Re numbers could be due to lower velocities and/or higher fluid viscosities. Wyrick (2003) reported preliminary results indicating that hyperconcentrated flows produce streamlined islands with lower aspect ratios. Subglacial floods may have been hyperconcentrated with eroded sediments. This hyperconcentration would increase the viscosity of the water or slurry, and lower the Re, thus possibly reducing the aspect ratio.

6.5.2. Spatial arrangement of closed contours

Determination of precise flow directions from the orientations of individual erosional residuals is sometimes not possible. The orientation of the long axes of an erosional residual that is part of a braided or anastamosed channel is often not exactly parallel to the main flow direction; however, large bars generally parallel flow. Rachoki (1981) measured 84 braid bars in an alluvial fan and constructed a "statistical braid bar" (Figure 108). The average braid bar distal angle was about 50°. Since the distal angle of a braid bar also serves as the side of a channel, the distal angle represents typical deviation of braid bar channels from the main flow direction.

The spatial arrangement of long axes of closed contours greater than 100 km^2 in area indicates a non-random arrangement (Figure 109). Southeast-trending long axes are most common in NTS 93M and 93L and correspond to the structural and tectonic grain across the study area. Generally east-west-trending long axes characterize most of NTS 93E, 93F, and 93K. East-northeast (west-southwest) long axes are found in the Coast Mountains along the western parts of NTS 93E and 93L.

Although some long axes orientations shown in Figure 109 correspond to general flow directions indicated by SF mapping (Figure 27), differences are apparent. Extensive fields of ENE-trending SF are present in NTS 93F and 93K in the eastern part of the study area; whereas, only three of the long axes shown on Figure 109 strike north of east. Spatial patterns are more difficult to identify on plots of long axes of closed contours less than 100 km^2 (Figure 110). More variation in orientation is apparent among the long axes of closed contours less than 100 km^2 than among the long axes of the larger closed contours.

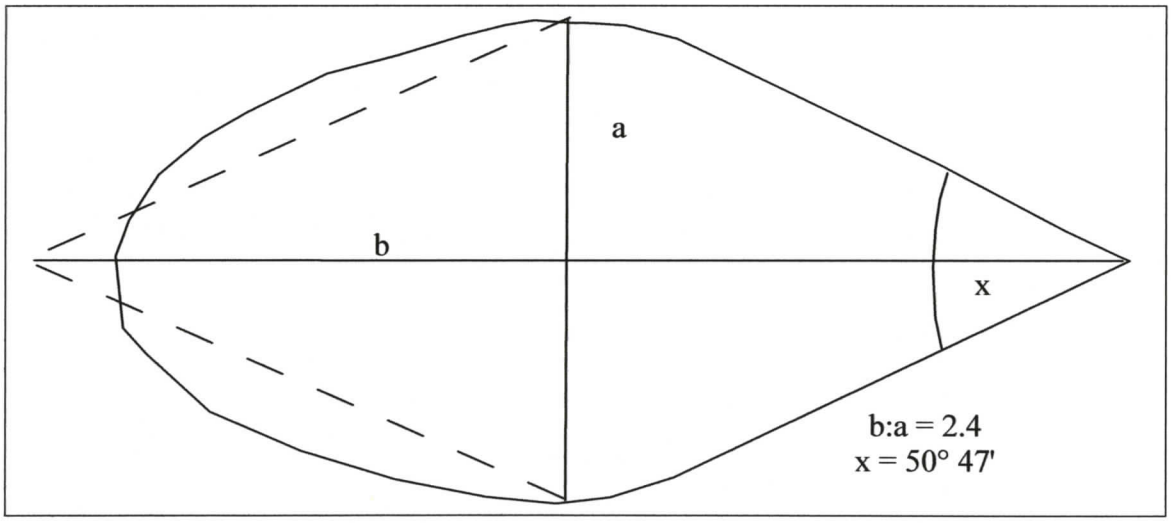

Figure 108. "Statistical braid bar", re-drawn from Rachoki (1981). Flow is towards the right. The distal angle is represented by x.

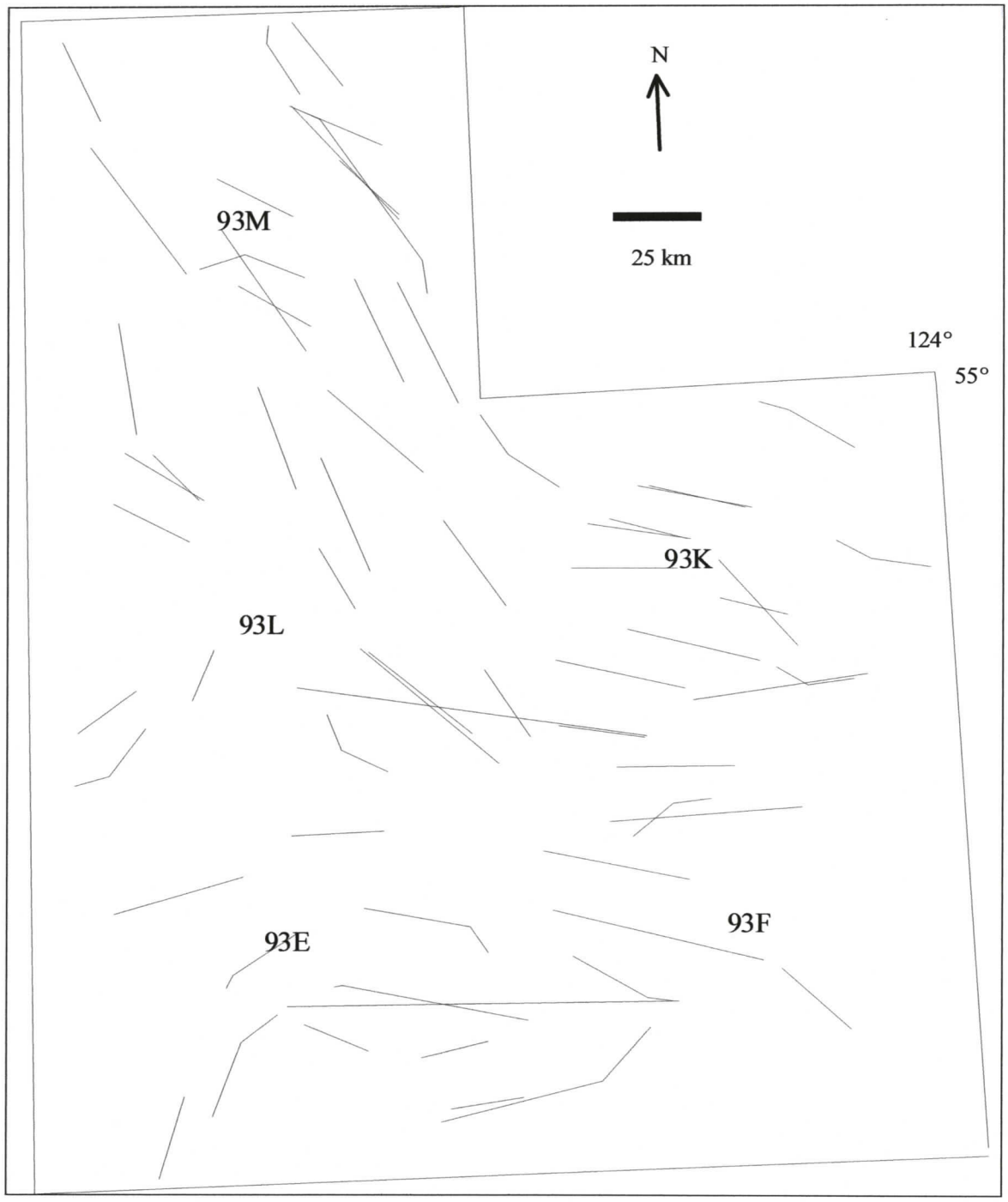

Figure 109. Long axes of closed contours greater than 100 km^2 in area.

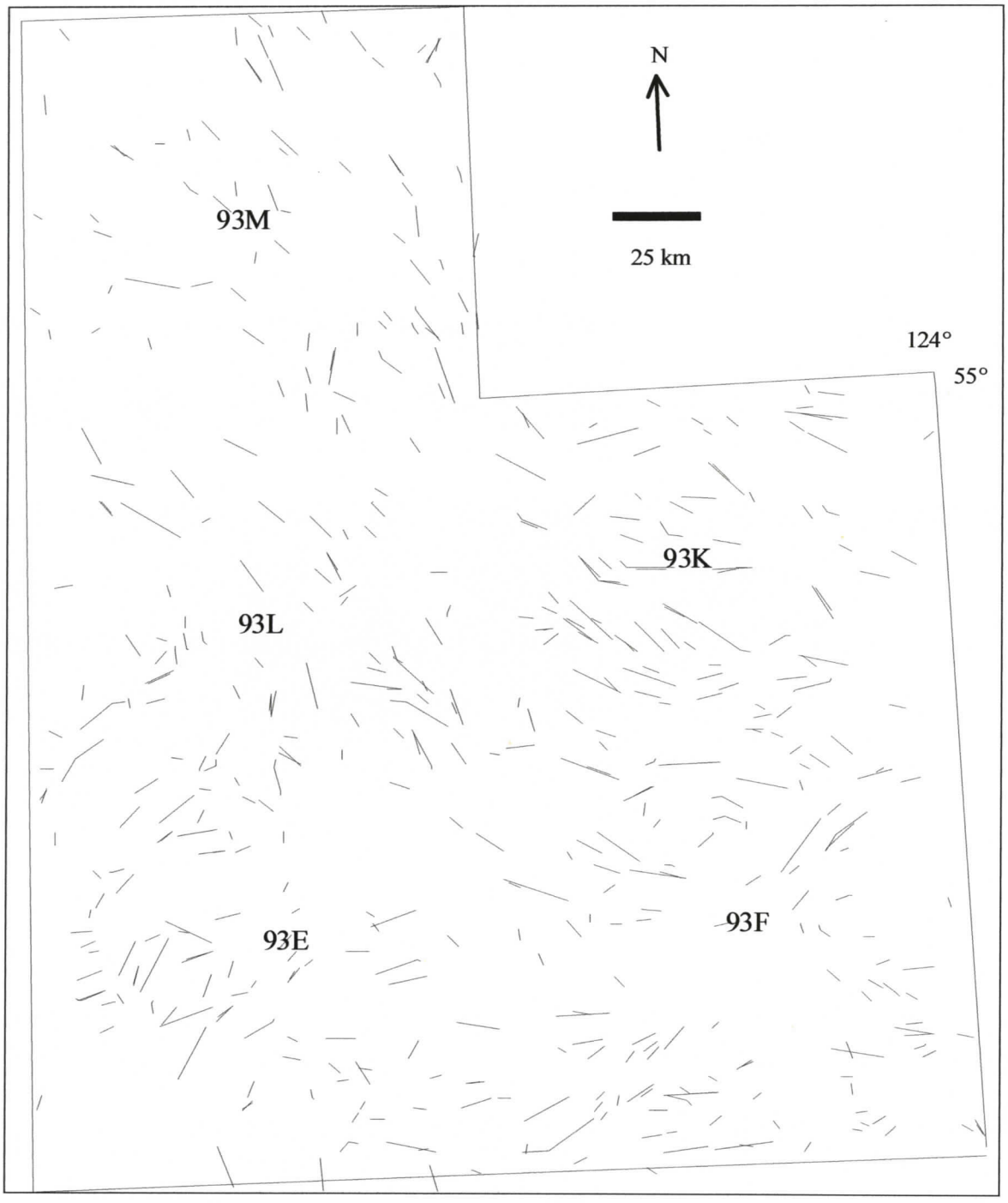

Figure 110. Long axes of closed contours less than 100 km^2 in area.

The inferred northern Great Plains glacial lake spillways channels discussed by Kehew and Lord (1986) are comparable in some respects to study area "channels". An area of flow constriction in the Minot channel (Figure 98, top figure, denoted by letter x) has no erosional residuals. This is somewhat similar to a zone of possible flow constriction in the study area (Figure 97, denoted by letter x); the zone of constriction in the study area is characterized by closed contours that are much smaller than closed contours in the surrounding area. These areas of flow constriction, both in the northern Great Plains and in the study area, could represent areas of increased velocity and greater erosion. A progressive increase in erosional residual size is apparent in the Minnesota spillway in the northern Great Plains channel system where channel width increases (Figure 98, letter y). In this case, larger residuals were formed as flow widened and velocity slowed. Similarly, larger residuals in one part of the study area correspond to widening flow (Figure 97, letter y and arrow indicating flow direction).

6.5.3. Orientations of streamlined forms and closed contour long axes

Strikes of SF are compared to strikes of closed contour long axes using a frequency histogram (Figure 111). Streamlined forms show a peak in occurrence at azimuths representing east-northeast strikes. The high percentage of SF found with these strikes is due to the large number of ENE –trending SF found in NTS 93F and 93K (Figure 15). The greatest percentages of closed contour long axes are found between about 90° and 160° azimuth, representing southeast strikes (Figure 111). These strikes correspond to the dominant southeast structural and tectonic trend in the area, indicating a strong correlation between study area landform orientations and structure.

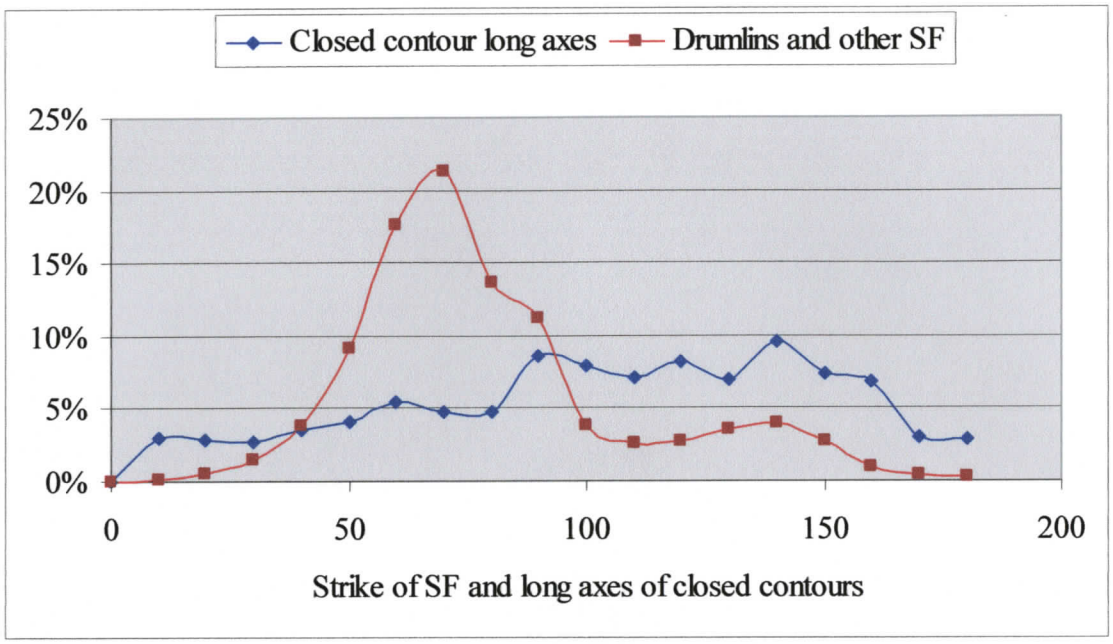

Figure 111. Frequency histograms of streamlined landforms (drumlins, crag-and-tails, etc.) and closed contour strikes.

6.5.4. Interpretation

6.5.4.1. Shape analysis

It is suggested here that some streamlined landform shapes in the study area are the result, at least in part, of glacial outburst or subglacial meltwater floods. Other controls have also affected landform development. Faults appear to have been instrumental in defining the location and preliminary shapes of many closed contours. Lithological controls and preglacial erosion undoubtedly affected landscape development. Glacial processes have also altered the landscape.

It is suggested here that the shapes in the horizontal plane of many of the closed contours represent a response to erosion by one or more glacial floods. Strong length-to-width regression relationships imply a horizontally acting erosive process. It is possible that this correlation could be due to pre-existing characteristics of the landforms. However, the length-to-width relationship is consistent across about three orders of magnitude of landform area (Tables 16 and 18). This correlation across a large size range indicates that the controls responsible for the correlation must be operative at both regional and smaller scales. It is unlikely that pre-existing lithologic controls would show this type of correlation but some pre-existing structural controls might. Closed contours are similar in appearance to erosional residuals in braided channel networks. Closed contours demonstrate an average aspect ratio of 2.38, near the low end of but still within the range of aspect ratios for erosional residuals, from 2.35 to 4.3, in other areas (Table 19). Closed contours also demonstrate R^2 values of 0.89 for length to width correlation; other reported R^2 values for known erosional residuals range from 0.73 to 0.96 (Table 20).

Braid bar geometry in braided channels is stable with respect to the shapes of bars. Channels may migrate or dissect existing bars, but the characteristic shapes of the residuals are retained (Rachocki, 1981). This stability is related to the principle of least work. The shape and configuration of the braided channel changes until it presents the least resistance to flow. It is then in a stable configuration unless the flow changes.

Kehew and Lord (1986) determined that the aspect ratio of erosional residuals in braided channels is obtained early in the streamlining process. The stabilization of aspect ratio is among the first stages of morphological equilibrium of landforms in

braided channel development. In braided channels with higher channel density, and corresponding high density of erosional residuals, stable aspect ratios may be the only quantitatively detectable signature of morphological equilibrium. In channel segments where the density of erosional residuals is small, isolated erosional residuals show the same aspect ratios as more densely packed erosional residuals that are located in the same channel. However, the isolated islands obtain a higher level of streamlining morphology, as indicated by the development of a lemniscate form (Figure 93). The development of more streamlined forms in more isolated locations is also noted in the study area (*e.g.*, see numbered locations on Figure 112).

If some study area landforms received their present shape by fluvial processes, then these landforms should show a strong length to width regression relationship and have aspect ratios similar to known erosional residuals in other fluvial settings. Both these predictions are verified by the shape analysis (Tables 19 and 20).

6.5.4.2. Closed contour long axes

Strikes of closed contour long axes occur from 0 - 180° azimuth (Figure 111). The most noticeable peak in frequency corresponds to the southeast structural and tectonic grain of the study area. This finding does not support a process control on closed contour shapes, but indicates that landform shapes are derived from pre-glacial or pre-meltwater flow controls.

6.5.4.3. Requirements of a meltwater origin hypothesis

If many study area closed contours received their current shape by subglacial meltwater floods, then the volumes of flow would have exceeded the Lake

Missoula flood(s). This inference is based on the relative size of the Lake Missoula flood path compared to the study area. Flood depths would possibly have exceeded 1000 m and flow widths would have been over 100 km.

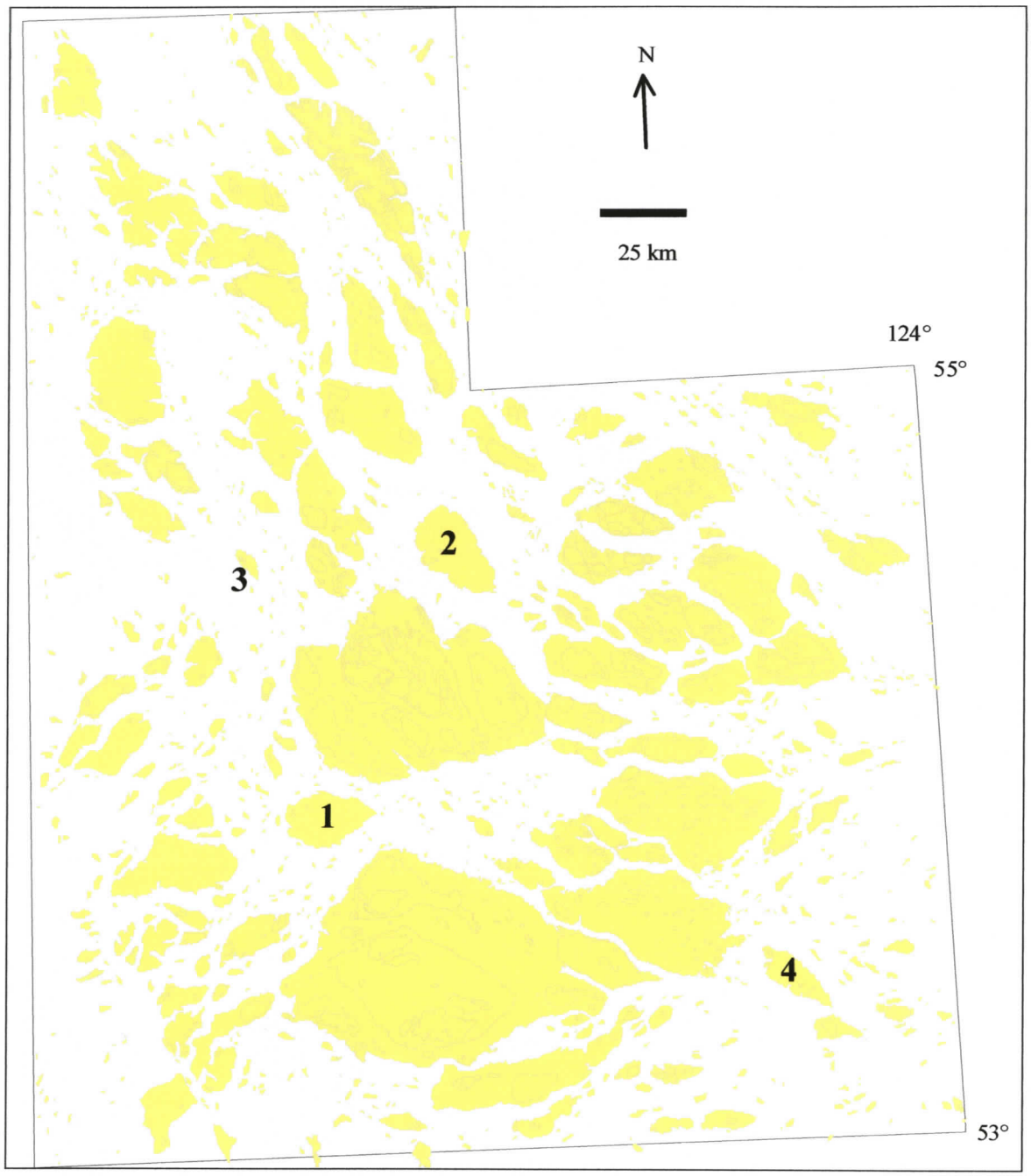

Figure 112. A few large-scale closed contours in more isolated locations that have possibly more lemniscate shapes (see numbered locations).

A possible triggering mechanism for large-scale floods is subglacial volcanic eruptions. Subglacial volcanic eruptions have been suggested as sources of subglacial floods in Antarctica (Denton and Sugden, 2005) and have been associated with recent glacial outburst floods in Iceland (Gudmundsson, 2001; Gudmundsson *et al.*, 2004). However, significant Quaternary volcanic deposits have not been mapped immediately west and north of the study area; minor Quaternary volcanics (only a few square kilometres in outcrop) have been noted northwest of the study area (Massey *et al.*, 2003a). Evidence of volcanic activity that could have triggered large-scale meltwater floods is not apparent.

6.5.4.4. Alternate explanation of closed contour morphology

Flowing ice is a possible alternative mechanism producing study area closed contour morphology. Study area upland/lowland landform patterns can be explained by conventional glacial theory. Large-scale erosional forms in glacial terrains are thought to be cumulative across more than one glacial cycle; whereas, the depositional record is often found to only show evidence of the most recent glaciation. The following discussion is related primarily to erosional landscape elements. It is assumed here that erosion was the dominant process producing the large-scale upland/lowland pattern defined by the topographic analysis.

Erosion style and degree of erosion are related to several factors. First, lithology and structure of bedrock clearly influence erosion patterns. Some lithologies are more resistant to erosion than others. Fault and joint orientations and spacing direct both

interglacial fluvial and glacial ice flows. Areas of higher joint density may be more susceptible to erosion. Structural and lithological controls would have provided more resistant or more elevated areas that were subsequently modified by preglacial fluvial erosion. The location of some study area uplands would correspond to strata that is more resistant to erosion than surrounding bedrock and sediment. Similarly, up thrust intrusives probably mark some upland locations.

There is some correlation between closed contour locations and bedrock intrusives. For example, intrusive outcrops along the Quanchas Range appear to correlate with closed contour landforms along that range (Figures 5 and 15).

It is also apparent that fault location is highly correlated with the location of many study area valleys and lowlands, and the location of many study area uplands are partially or completely bounded by faults (Figures 101 and 102). Preglacial, fluvial erosion may have produced a dendritic drainage system with topographic features derived from these lithological and structural controls.

During glacial advance, the lowlands of this preglacial topography would have acted as conduits for the development of glacial troughs and valleys. Subsequent glacial activity would deepen and extend this lowland network. Upland areas would also have been modified by more slowly moving ice. Up thrust blocks would be rounded by ice flow. Breaching by ice across topographic divides could have transformed an initially dendritic valley network into an anastomosing network.

Landscapes of selective linear erosion, consisting of deep troughs separated by plateaus, are common in glacial terrains. The troughs are thought to mark faster-moving ice streams. Trough locations can be developed by a combination of preferential

streaming of ice along pre-existing valleys; by ice flow that exploited tectonic, structural, and lithological weaknesses and trends; and/or by glacial flow that was unrelated to underlying topography. Final trough configurations may form dendritic or anastamosed patterns. Patterns of lowland occurrence in the study area can be described as anastomosing and perhaps dendritic. Thus, the study area lowland/upland configuration fits a glacial landscape of selective linear erosion.

Some of the major lowlands in the study area that would be identified as troughs include the Babine River valley, Bulkley Valley, Kispiox/Skeena Valley, Stewart Lake/Stuart River lowland, Francois Lake, Ootsa Lake, and Eutsuk/Tetachuck Lakes (Figure 15). The Babine River valley and Babine Lake are about 200 km long and about 5 km wide. The Bulkley River valley is also about 200 km long and 10 km wide through its widest section. Elevation differences between major lowlands and upland ridges in the study area are around 1 km. The longest troughs currently recognized on earth are located in Antarctica, and are about 1000 km long, more than 50 km wide, and up to 3.4 km deep. Study area valleys are somewhat smaller than these Antarctica troughs.

It is also possible that some study area lowlands were tunnel valleys formed during late glacial stages. The origins of tunnel valleys are not satisfactorily explained, although meltwater is generally presumed to have a major role in their development (O' Cafaigh, 1996). Tunnel valleys can be up to 100 km in length and 4 km wide. They can exist in isolation or as part of dendritic or anastomosing channel networks. Tunnel valleys frequently have undulatory long profiles. Like glacial troughs, they commonly have overdeepened basins along their floors, are often occupied by lakes, and have

hanging tributary valleys. Tunnel valleys often have wide flat bottoms and steep sides. They may be filled by thick sedimentary sequences and detectable only by geophysical techniques or boring logs. Larger study area valleys such as the Bulkley and Babine river valleys exceed the upper size limits of most recognized tunnel valleys. However, segments of Francois Lake, which is a natural lake, or the chain of lakes including Ootsa Lake, Eutsuk Lake, and Euchu Reach, lakes created by Kinney Dam, could possibly represent tunnel valleys.

The interconnecting pattern of lowlands defined by the topographic analysis could have received their current configuration during the development of glacial troughs and/or tunnel valleys. Correlated aspect ratios of uplands could be related to fault patterns. Based on a cursory examination, many study area fault blocks in the western half of the study area, defined by intersecting SE- and shorter NE-striking faults, are elongated in plan view (Figures 101 and 102). A detailed numerical analysis of the aspect ratios of these fault blocks could reveal an alternate cause for closed contour aspect ratio correlation. However, such an investigation is not included in this research but is recommended for future work.

6.5.4.5. Aspect ratio correlation

There is a remarkable correlation between length and width of mapped closed contours. This correlation implies some type of control and/or process consistently resulted in final landform shapes with similar aspect ratios. This pattern of shape development was apparently effective across a large landform size range. An explanation for the development of aspect ratios in fluvial landforms has been tested by

observation and experiment. That explanation is based on the minimization of form and skin drag relationships in high Re number flows as discussed earlier. The aspect ratios and regression relationships of these known or inferred fluvial forms are similar to those of the study area closed contours. Hence, the explanation for form development of fluvial forms is easily extended to study area landforms.

If the alternative, more conventional explanation for closed contour morphology presented above is correct, then two possibilities are suggested to account for the highly correlated aspect ratios of study area landforms. First, the aspect ratios could be inherited from fault block patterns. Second, an ice mechanism for producing correlated aspect ratios must exist. A hypothesis for an ice mechanism that would produce study area aspect ratio correlation was not attempted in this study and was not found in the literature.

Ice does not obtain the Re numbers of flowing water due to its much slower velocities and higher viscosities. The Re numbers of flowing ice are on the order of 17-24 orders of magnitude less than Re numbers of flowing water (Fowler and Larson, 1978; Komar, 1983; Shaw, 1994); hence, form drag due to flow separation would be minimal. Therefore, the explanation used to explain fluvial landform streamlining can not be readily extended to ice flow. A different mechanism is necessary to explain how or why ice would create a suite of different-sized streamlined landforms with highly correlated aspect ratios.

Topographic analysis data indicate high correlation of closed contour aspect ratios across a wide range of sizes. The consistency of the length to width ratio across a wide size range indicates that the correlation is primarily due to process, not to pre-

existing structural or lithological controls. Structure and lithology undoubtedly affected initial landform locations, sizes, and shapes, but final shapes are most likely derived from process, *i.e.*, water and/or ice flow. This inference is supported by recent findings on braid bar shapes in 15 rivers. Aspect ratios of braid bars covering four orders of magnitude in size were found to be scale invariant (Smith *et al.*, 2005).

The correlated aspect ratios of study area landforms are similar to known or inferred fluvial forms and can be explained by drag minimization in water flows. That mechanism is not readily applicable to ice flow because low ice flow velocities would not result in flow separation or form drag. Whereas it is clear that a meltwater mechanism can explain high correlation of closed contour aspect ratios, it is not clear whether an ice mechanism would produce aspect ratio correlation across a wide range of landform sizes. The simplest explanation is that many study area closed contours were streamlined by water, possibly subglacial meltwater or outburst floods.

The most difficult problem for a meltwater flood mechanism is the definition of a flood source or sources. Huge amounts of water are necessary to form even the smaller closed contours, and a source for that water is not apparent. The absence of a readily identifiable flood source weakens the argument for a meltwater mechanism for closed contour shapes.

As mentioned previously, a number of controls affect landform shapes. Catastrophic meltwater floods are just one, relatively rare process affecting the landscape. Although topographic analysis indicates a fluvial origin for many study area closed contours, a source for the meltwater floods that would have shaped these forms is not apparent. Furthermore, structural controls on landform shapes are apparent and

other controls, *e.g.* lithological, are likely. The preliminary data presented here indicates major fluvial shaping of many study area landforms; however, further work is necessary to verify this interpretation. Recommendations for future work are given in Chapter 7. If later work shows that closed contour shapes are not primarily the result of meltwater floods, then it can be inferred that flowing ice can create erosional residuals very similar to landforms known to be developed by flowing water.

7. SUMMARY AND CONCLUSIONS

The principle focus of this thesis is to provide a better understanding of the origin of streamlined forms in glaciated terrain. Several approaches are used to gain that understanding. Results and discussion of research approaches are presented and discussed in Chapters 2 through 6. Summaries of the main findings and interpretations from this research are presented in the section 7.1. In section 7.2, summaries from each chapter are related, and conclusions drawn.

The main research objectives, as set forward in Chapter 1, are met as follows: 1) a methodology is developed for digital mapping of streamlined forms across a large regional (more than 67,000 km^2); 2) computer methods for statistically analyzing the collected data are developed and applied; 3) relationships between streamlined form characteristics and terrain attributes, found using these statistical analyses methods, are presented; 4) a computer analysis that simulates glacial erosion at a local scale is developed and applied to the problem of SF origins; 5) field studies of drumlins and streamlined bedrock forms are conducted and findings applied to advancing the understanding of SF origins and glacial history of the study area; and, 6) a method for topographic analysis is developed and applied to study area landforms. A relationship between closed contour lengths and widths that is similar to fluvially produced landforms is found.

7.1. SUMMARY

7.1.1. Study area and streamlined form origin theories

The study area is located in central British Columbia and includes a region where the Coast, Hazelton, and Skeena Mountains on the west and north adjoin the Interior Plateau to the east (Figure 1). Major mountain ranges are often separated by broad valleys, for example the Bulkley River and Babine River valleys (Figure 15). The plateau region is characterized by rounded and rolling uplands separated by a network of longitudinal lowlands, lakes, and broad valleys (Figures 2 and 3). Extensive deposits of diamicton are found across most of the study area on the plateau and in the broad valleys between the mountain ranges in the west and north (Fulton, 1995) (Figure 4).

About half the bedrock that underlies the study area is volcanic (Massey *et al.*, 2003a; Massey *et al.*, 2003b) (Figure 5). Faults express the generally southeast tectonic trend common to the Cordillera, with numerous other generally east and northeast striking faults (MacIntyre, 1996) (Figure 6). Few faults are mapped on the plateau, presumably due to the glacial drift cover.

Streamlined form origin theories invoke glacial ice, meltwater floods, or combinations of both as forming mechanisms. Glacial ice is hypothesized to have preferentially deformed subglacial sediment into streamlined shapes in the sediment deformation model (Boulton, 1987; Boulton, 1996). A glacial abrasion model proposes that streamlined bedrock forms were formed by glacial ice erosion (Boulton, 1974; Boulton, 1979). Meltwater flows are also thought to have created both streamlined sediment and bedrock forms, *e.g.*, drumlins and rat-tails (Kor *et al.*, 1991; Shaw, 1996;

Shaw, 2002). The "dual process" model suggests that subglacial drumlins and crag-and-tails were created by ice and subsequently enhanced by subglacial meltwater (Mate, 2000; Knight, 2002).

7.1.2. Streamlined forms map

Figure 15 is a large map of streamlined forms (SF) located in the map pocket. The map is produced using satellite and DEM images. The greatest advantage of the mapping methodology used here is that an extensive SF map of a large region can be developed relatively rapidly compared to more traditional mapping efforts using air photo interpretation and field investigations.

Based on SF orientations, three principle flow direction ranges are evident in the study area: south-southeast to southeast, northeast to east-northeast, and west-southwest to west (Figure 27). The source of ice or water that formed the southeast-trending forms was located north of the study area. The Skeena Mountains are located immediately north of the study area and are a probable location for that source (Ryder and Maynard, 1991; Stumpf *et al.*, 2000; this study). Ryder and Maynard (1991) show glacial flow out from the Skeena Mountains in almost all compass directions, including flow towards the southeast and southwest. Most southeast SF flow indications occur in SE-trending lowlands or valleys.

The southeast part of the study area is dominated by east-northeast flow. The Coast Mountains or an ice divide oriented north-south along the Quanchas Range (Stumpf *et al.*, 2000) are possible sources for this flow (Figures 3, 15, and 27).

West flow up valleys that drain the Coast Mountains and Hazelton Mountains (Figure 3) is indicated by remote imaging. Field studies (Chapter 5) also document west flow at upper elevations in the Hazelton Mountains and Babine Range. A possible source is an ice divide exceeding 1680 m elevation located to the east of the Babine Range (Stumpf *et al.,* 2000). This minimum elevation is based on the presence of uphill-trending streamlined bedrock forms (SBF) on Dome Mountain in the Babine Range (Chapter 5).

Streamlined forms in east-trending flow paths in NTS 93K are deflected northward by northerly flow from the Cariboo Mountains located southeast of the study area (Plouffe, 2000). This deflection indicates that east flow across 93K and the north flow from the Cariboo were simultaneous during some time interval. Also, southeast-trending SF swarms in 93K are possibly deflected towards the east and/or cross-cut by ENE-trending flow sourced in the Coast Mountains. This relationship suggests that SE and ENE flows across the western and southern parts of 93K were also simultaneous at some point in time.

Groups of SF follow curving paths both up and down valleys. Uphill-oriented curving paths are interesting in the context of an ice origin hypotheses, since dome-driven ice sheets are often described as advancing regardless of topography. However, ice could still be deflected by topography beneath an uphill advancing ice sheet since contrary flow directions at different vertical levels in a glacier have been observed (Rea and Whalley, 1994). Groups of SF also cross valleys.

If NTS 93K is divided into two diagonal halves separated by a line drawn from the northwest to the southeast corner of the map sheet, lower SF densities occur in the

southwest half than occur in the northeast half of the map sheet area (Figure 43). Similarly, lower SF densities occur in the southeast "diagonal" half of NTS 93F than occur in the northwest "diagonal" half (Figure 43). Both of these low SF density areas have greater elevation (Figure 39) than the respective adjacent diagonal halves with relatively higher SF density. Most of the area represented by these map sheets is located on the Nechako Plateau and northern extremity of the Fraser Plateau (Figure 3). It is probable that the lower elevation areas in these two map sheets have thicker diamicton deposits than the higher elevation areas, favouring the development of relatively more SF.

7.1.3. Statistical analyses

Cross-cutting SF flow groups characterize the northeast part of the study area (Chapter 2). This area is also cut by many interconnected SE- and NE-trending valleys and lowlands. Elevation data indicate that the northeast quadrant is topographically lower than the rest of the study area. The northeast quadrant is interpreted as a zone of converging ENE and SE flows. The flows may have been contemporaneous at some point in time.

Streamlined form length is statistically related to slope. The more level the slope, the greater the SF length; that is, as uphill or downhill surface inclination increases, shorter SF are formed. This finding may be related to the relative availability and thickness of sediment on level surfaces versus sediment availability on more inclined slopes. Sloping surfaces probably accumulate less sediment than level surfaces due to erosion. Thick areas of sediment also tend to occur in low depositional basins

that are relatively level compared to areas with shallow bedrock that are typically characterized by steep, higher relief terrain. Longer SF would possibly form on surfaces with thicker till, since flow would not be disrupted by bedrock outcrops as frequently as it might on surfaces with thinner till cover. Thus , longer SF on more level surfaces may be mainly a result of increased till availability.

At a local scale (sample squares 2 – 30 km on a side), elevation has no statistically significant effect on SF length. When considering larger areas (sample squares 40 – 60 km on a side), greater SF lengths are found at lower elevations. It is suggested that this result is related to thicker and more widespread till occurring at lower elevations. Till is generally more easily eroded than most bedrock in the study area. Vertically and laterally continuous till deposits would allow the progressive development of longer SF. In higher elevation areas where till deposits are thinner and discontinuous, SF length development would possibly be disrupted by bedrock outcrops.

7.1.4. Glacial erosion analysis

Two types of surfaces are "eroded" in this study using the two-dimensional incremental glacial erosion model developed during this research. Erosion of a flat surface with an inner core of more resistant material and erosion of a rock drumlin shape are analyzed. Erosion of the flat surface with the resistant core first results in a roche moutonnée form. This form is replaced by an equilibrium form consisting of two slope-parallel surfaces separated by an inclined plane at the location of the resistant core.

Erosion of the rock drumlin shape results in a level surface at the original location of the rock drumlin. However, a modified form of the drumlin shape is propagated up-ice during successive iterations of the analysis tool. At a given location, the drumlin shape is reduced to a plane. As the "tail" of the form is planed down, a ridge is propagated in the up-ice direction. During this propagation, the slope of the up-ice face of the ridge changes from a "typical" drumlin shape, convex upwards, to a slightly concave upwards surface somewhat resembling the up-ice surface of a roche moutonnée form (Figure 58). At that point, no further modification to the ridge form occurs, but the up-ice propagation continues. A similar up-ice form propagation was noted by Boulton (1974) in his theoretical glacial erosion/deposition model.

Two surface types found in glacial terrains are produced by the analysis: the roche moutonnée and the flat surface. The roche moutonnée form is an intermediate erosional form and does not persist. A drumlin shape does not form, neither does an existent drumlin form persist at a single location. However, a ridge form, initiated by the drumlin shape, propagates in the up-ice direction. Streamlined tails are not produced down flow of a resistant core. Since both rock drumlins and rat-tails are common in glaciated terrains, it may be significant that neither is produced. However, a modified version of the analysis tool, *e.g.* a version that permitted ice bridging, could quite conceivably produce different results. Nonetheless, the ice erosion model as configured does not preserve rock drumlins nor produce rat-tails.

The results also indicate that roche moutonnée forms could be produced by ice flow. The up-ice propagation of a ridge form indicates that stress conditions beneath an ice sheet, if triggered by an existing ridge, could favour the development of subglacial

ridges, though these ridges do not have a typical drumlin shape. Both the roche moutonnée forms and the propagating ridge are temporary forms beneath the ice sheet, but could still be preserved if ice flow ceased before the forms were "planed" down.

7.1.5. Field studies

Some bedrock drumlins and rat-tails at high elevation sites indicate that uphill westward flow occurred at elevations up to 1680 m, confirming uphill flow indicated by the SF map. This observation indicates that an ice dome or ice divide surface was located to the east of the uphill flow sites at an even greater elevation. Valleys are located in the up flow direction at these alpine sites. Elevation differences between valley floors and sites with streamlined bedrock forms (SBF) indicate that the surface driving the SF-producing flow must have been located more than one kilometre above the current elevations of the valley bottoms.

The SF-producing flow could have been ice, unconfined meltwater floods, or confined subglacial flows. Possible sources are an ice divide, ice dome, supraglacial lake(s), and/or subglacial lake(s).

Rat-tails at alpine SF sites do not cross-cut other rat-tails; all rat-tails appear to have been formed by the same flow event. Rat-tails occur on rock drumlins, roche moutonnées, and on larger rat-tails, but in every case the superimposed rat-tail is parallel to the larger form or parallel to the flow path around or along the larger form. There is no indication that rat-tails and rock drumlins at a given site were formed by more than one flow event.

This indication of singular flow does not hold with striae. Many striae cross-cut SBF; however, some striae parallel rat-tails, rock drumlins, and flow paths around streamlined bedrock forms. In the first case, it is known that at least some striae were formed after SBF by a separate event; although, the cross-cutting striae event could have occurred shortly after the SBF event. The erosion style of the flow event or events that formed the cross-cutting striae was different than the erosion style of the flow that formed the rat-tails; this inference is based on the absence of cross-cutting rat-tails where cross-cutting striae are common. In the second case, it seems that the same mechanism that formed the rat-tails may have formed some of the striae. This is inferred because rat-tails and some striae are parallel. However, striae that are parallel to rat-tails occur on rat-tails and along the lateral furrows along the sides of rat-tails (*e.g.*, Figures 75 and 87). This shows that at least some parallel striae formed after rat-tails formed.

The simplest and most direct explanation for parallel striae and rat-tails is that both features were formed by ice. Striae are almost always interpreted as ice features. Another possibility is that rat-tails may have formed by water in subglacial floods, and striae were formed as moving ice re-attached to the ground surface.

The presence of cross-cutting striae is explained most simply by an initial water event forming rat-tails, and a subsequent ice event creating striae. If ice formed both rat-tails and striae, then there should be cross-cutting rat-tails since there are cross-cutting striae. The lack of cross-cutting rat-tails indicates that at least some striae were formed by a different mechanism than that which formed rat-tails. Another possibility

is that rat-tails were formed by more viscously flowing ice, and, after a change in ice conditions, cross-cutting striae were formed by more rigid ice.

Hairpin furrows are interpreted here as features created by erosion. This interpretation is supported by the presence of hairpin furrows outlining some rock drumlins and rat-tails. Many drumlins and crag-and-tails that are primarily composed of sediment are also outlined by hairpin furrows. Since SBF hairpin furrows are due to erosion, then the hairpin furrows around these SF indicates shaping by erosion. The morphological similarity of lowland SF to upland rock drumlins and rat-tails suggests that the same type of process shaped both features. It is possible, however, that the lowland SF may have initially been subglacial ridges that were subsequently eroded and shaped by water.

Uphill, west flow is shown by rat-tail and rock drumlin orientations at high elevations in the Hazelton Mountains and Babine Range. Uphill west flow is also indicated by SF in valleys of the Coast and Hazelton Mountains. These valleys are adjacent to the upland rat-tail and rock drumlin sites. Since both the lowland and upland forms show similar flow direction, then it is likely that the same flow event formed both the upland SBF and the adjacent lowland SF.

The sediment deformation model (Boulton, 1987) includes sediment deposition and re-organization along with folding and faulting of sediment beds in the drumlin forming process. No evidence of faulting or folding of drumlin sediments is observed in the field study (Chapter 5). This finding does not support the sediment deformation model. However, Boulton (1987) states that initial folds in drumlins are rapidly destroyed, leaving no evidence of deformation. This seems possible; however, the

explanation preferred here is that study area drumlins were most likely shaped by streamlining erosional flow.

7.1.6. Topographic analysis and closed contours

A method of topographic analysis is developed and results in a map of closed contours that represent study area landforms (Figure 96). Closed contour lengths are statistically correlated to their widths. The correlation is interpreted as largely being due to the process that formed the landforms. The most likely processes that caused the correlated lengths and widths are glacial ice and/or meltwater floods.

Closed contour aspect ratios and regression relationships are similar to those reported for streamlined islands in rivers (Komar, 1984), braid bars (Rachocki, 1981), and streamlined erosional residuals thought to have been formed by proglacial outburst floods (Baker, 1979; Elfstrom and Roffsbacher, 1985; Kehew and Lord, 1986). The similarity of some study area closed contour shapes and dimension relationships to fluvial landforms suggests that large-scale fluvial processes may have shaped some study area landforms.

7.2. CONCLUSIONS

7.2.1. Origins of streamlined forms

The main question that this thesis attempts to answer is whether glacial ice, meltwater floods, or both mechanisms formed study area streamlined forms. Many of the results and associated interpretations presented here indicate that subglacial meltwater floods may have been instrumental in shaping both medium- to large-scale

landscape SF and small-scale streamlined bedrock forms. Some results indicate action by glacial ice. Neither process is ruled out by research results.

7.2.1.1. Findings supporting a water origin

Field studies of rat-tails and rock drumlins indicate a water origin for these types of SF. Forms like rat-tails are known to be formed by water and by wind (Chapter 1), both of which can attain Reynolds numbers that initiate flow separation behind an obstacle. Striae are usually attributed to ice. The mechanism that formed some striae at field study sites was probably different than the mechanism that formed rat-tails. This conclusion is drawn because there are cross-cutting striae but there are no cross-cutting rat-tails. The glacial erosion model indicates that rat-tails are not formed by glacial erosion; basal shear stresses as modeled do not produce a tail down flow of a resistant clast. These results do not support ice as a forming mechanism for SBF; therefore, a water origin for SBF is suggested by default. The glacial erosion model also indicates that a streamlined rock drumlin shape does not persist in a given location when subjected to shear stresses at the base of an ice sheet. However, since a ridge is propagated up-ice by the model, this result can be interpreted for both a water and ice origin.

Lowland streamlined forms are interpreted as being formed and/or shaped by water as an erosive agent because they are frequently outlined by hairpin furrows. Hairpin furrows are known to be formed by water. Streamlined forms have shapes similar to SBF. Since SBF are interpreted as water features, then this similar morphology also supports a water origin for lowland SF.

Greater SF lengths are associated with more horizontal surfaces and, at a sub-regional scale, with lower elevations. These findings suggest that the length of sediment-dominated SF may be related mainly to the availability of till and possibly also to the absence of flow obstructions such as outcrops.

Drumlins and crag-and-tails investigated in this study are interpreted as receiving their streamlined shape by erosional processes based on the outlining of many SF by hairpin furrows. Hairpin furrows are clearly erosional features. An erosional origin for SF is not required for either a meltwater or ice model; however, the sediment deformation model relies largely on deposition, sediment re-organization, and deformation processes to explain drumlin formation (Boulton, 1987).

Correlated lengths and widths of closed contours and shape similarity to fluvial landforms indicate that fluvial processes shaped some study area landforms. Subglacial meltwater floods are a possible explanation of the shapes and aspect ratio correlation of these landforms.

7.2.1.2. Alternative interpretations of findings for water

Streamlined bedrock forms may have formed by glacial abrasion. It is known that water flow can erode shapes similar to rock drumlins and rat-tails. Both a water and an ice mechanism are accepted here as plausible explanations of SBF formation. However, since water has a proven capability to form SBF, a water origin for SBF is preferred.

Study area drumlins may have originated as ridges beneath ice sheets. Massive diamicton composition could be the result of extensive sediment deformation or the

drumlin ridges may be the result of glacial erosion. Streamlined shapes may have been subsequently developed by meltwater flows. This dual process explanation for SF origins is accepted as an alternate to SF being formed entirely by water. It is supported by the up-ice propagation of a ridge in the erosion model.

Correlations between closed contour lengths and widths could have been due to a number of processes. Some possible controls on landform shapes include faults, lithology, and lateral variation in sediment composition. Glacial ice could conceivably have produced closed contour shapes.

7.2.1.3. Findings supporting an ice origin

Parallelism of some striae with SBF at field study sites supports an ice origin for SBF. Striae are generally attributed to glacial abrasion. The simplest explanation of these parallel forms is that both striae and SBF were created by the same process.

A relationship between slope mode and SF length is reported in Chapter 3. For a given degree of slope, longer SF are found on downhill slopes. For example, SF are somewhat longer on downhill slopes than on uphill slopes in the 0 – 3° slope range (Table 5). The differences in lengths between the uphill and downhill SF are not as great as differences arising from the steepness of the slope. Slope steepness has a greater influence on SF length than does slope mode (section 3.4.5.3). Nonetheless, a secondary, lesser relationship between slope mode and length is indicated. Glacial ice would be expected to have higher velocities on downhill slopes, possibly resulting in longer SF relative to those formed by uphill-flowing ice. Hence, the statistical analysis

results can be interpreted as indicating lengthening due to gravity, possibly concordant with an ice origin for SF.

7.2.1.4. Alternative interpretations of findings for ice

Two alternative explanations for striae and SBF parallelism are presented here. The explanations are concurrent with the water origin hypothesis. Some parallel striae at SBF sites may be water grooves formed by small scale vortices and/or corrasion. Secondly, if SBF formed by subglacial meltwater floods, then some SBF-parallel striae may have formed as the glacial roof re-attached to the ground surface.

This alternate explanation is more complex than the inference that ice created both SBF and striae. When considered independent of other thesis findings, the simpler explanation that ice created both SBF and striae is preferred. However, other thesis findings support meltwater floods across the study area, namely, hairpin furrows that outline many SF and closed contour landforms that may be streamlined erosional residuals. Furthermore, cross-cutting striae occur along with parallel striae, but the same is not true for rat-tails. Therefore, the alternate explanation of a meltwater origin for rat-tails is allowed.

The statistical effect of longer SF being present on downhill slopes is discussed in Chapter 3. It is concluded in that discussion that the amount of slope (*i.e.*, how close the slope is to horizontal) has a greater influence on SF length than the slope "mode" (*i.e.*, uphill or downhill). Streamlined forms on more level surfaces are longer than those on steeper downhill slopes. The interpretation that is adopted here is that the tendency for downhill SF to be longer is valid, but is secondary to the tendency for SF

on more level surfaces to be longer than those on steeper surfaces. The "downhill effect" can be explained as a result of initial development of longer ridges on downhill slopes by glacial ice. Subsequent subglacial meltwater floods could have significantly altered this pattern, and preferentially developed longer SF on more level surfaces. The observed secondary effect of longer SF on downhill slopes could be a relic of earlier ice flow.

7.2.2. Conclusions

Findings indicate that subglacial meltwater floods may have had a widespread effect on the study area landscape. The field study and erosion model suggest that rat-tails and rock drumlins investigated here were formed by high elevation subglacial meltwater floods. Hairpin furrows are commonly found around lowland drumlins and are interpreted as the result of subglacial meltwater floods. This observation indicates that many lowland drumlins and crag-and-tails may have been formed by subglacial meltwater floods. A possible alternate explanation for these landforms is discussed in the following paragraph. Some closed contours are possibly streamlined erosional residuals shaped by meltwater floods.

Parallel and cross-cutting striae on rat-tails and rock drumlins indicate ice activity after the meltwater floods. This activity was possibly of short duration since streamlined bedrock forms persisted through the striating event; the erosion model also suggests that streamlined forms do not persist beneath an ice sheet. However, lowland sediment SF may have been initiated as glacially-formed till ridges. This possibility is

supported by the glacial erosion model. However, it is suggested that the final streamlined shapes of SF are due to subglacial meltwater floods.

7.2.3. Implications of meltwater floods

Two problems arise from a subglacial meltwater hypothesis for SF formation: no sources for extremely large meltwater flows are readily apparent and sedimentary records of those flows have not been clearly identified. Although largely conjectural, possible solutions to these two problems are discussed below.

The three main flow directions indicated in the study area are west, southeast, and east-northeast. A subglacial meltwater reservoir in the Interior Plateau region is a possible source for the westward flow event. Striae and west-trending rat-tails in the Babine Range and Hazelton Mountains occur at elevations up to 1680 m and indicate a driving head located at an even higher elevation somewhere east of the Babine Range. An ice divide or ice dome could provide that elevated surface. During ice sheet retreat and down wasting, a subglacial lake may have formed beneath the ice sheet. Pressurized flow from beneath the ice sheet towards the west may have been triggered by relatively rapid ice thinning at the western margin of the ice sheet. One of the problems associated with this hypothetical scenario is the difficulty in maintaining an elevated surface in the interior during ice down wasting that would be high enough to force water westward across the Coast Mountains.

Both southeast and ENE SF flow paths are many kilometres across and are apparently formed by flow emanating from the Stikine Mountains, to the north, and from the Coast Mountains to the west. The southeast flow may have, at times, been

simultaneous with the ENE flow based on the apparent eastward deflection of southeast flow by ENE flow and by northerly flow from the Cariboo Mountains. It also appears, based on cross-cutting flow relationships in NTS 93K, that ENE flow cross-cuts southeast-trending SF swarms.

Likely locations for large subglacial or supraglacial meltwater reservoirs in the Stikine and Coast Mountains are not apparent. It is conceivable that smaller water reservoirs could have formed behind ice dams in east-facing or south-facing valleys or in supraglacial lakes dammed up against the east or southeast sides of the mountains. These lakes might then have been released subglacially towards the Nechako Plateau. However, these possible source areas appear to be too small and isolated to be capable of generating the large volumes of water necessary to produce the extremely broad and continuous SF fields that occur in the lowlands and on the plateau. The main problem is that the source areas for the southeast and ENE SF-producing flow are located in mountainous regions that appear to preclude the development of significant meltwater reservoirs. It is possible that multiple reservoirs existed in different areas but they would have to drain simultaneously from these different source regions to explain the observed converging and parallel SF fields. However, mountainous source areas are entirely concordant with an ice theory for SF formation.

The second implication for the meltwater hypothesis is that the floods would have eroded an extremely large amount of sediment in order to produce the high number of SF present in the study area. The greatest number of SF were formed by ENE and southeast flows that converge spatially, and possibly temporally as well, in the eastern part of the study area. The flow that produced these forms exited the study

area to the east. Based on regional flow indicators, there are at least two possible paths for the flow: eastward over the Rocky Mountains to the Peace River area in northern Alberta and southward down the Rocky Mountain Trench (Natural Resources Canada, 2005). There is also indication of northward deflection of east flow due to flow emanating from the Cariboo Mountains (Plouffe, 2000).

Rapidly flowing water generally results in the deposition of sorted sedimentary deposits. Some sedimentary record of SF-producing flow should be detectable down flow of the Nechako Plateau. No report of significant fluvial deposits that could be linked to high volume meltwater flows from the study area was found in this study. Either the discovery of such deposits or a convincing explanation of why such deposits are not found is needed in order to satisfy the implications of the meltwater flood theory.

7.2.4. Future work

Further research is suggested based on these findings and conclusions. More understanding of possible streamlined erosional residuals in the study area could be obtained by field studies and computer analysis. Field studies could focus on the inferred down flow ends of possible erosional residuals. Deposition of boulders on the lee ends of erosional remnants in Sweden has been observed (Elfstrom and Rossbacher, 1985) and Komar (1983) noted that down flow deposition contributed to the form of some streamlined islands. Computer analysis could be directed towards constructing vertical profiles along flow of potential streamlined erosional residuals. If the residuals

were fully submerged by streamlining flow, then streamlining should be evident in vertical profile.

A field study of high elevation sites in the Quanchas Range, the Fawnie Range, the Nechako Range, and the Kitimat Ranges could provide data on SBF and striae occurrences that would help to further define the extents and directions of SBF- and striae-forming flow.

More research and regional surficial geology mapping is required to look for evidence of subglacial or supraglacial lakes, both in possible high mountain source areas and in the Interior Plateau. In addition, more work is required to calculate the volumes of material that were removed during the formation of SF in the study area and to look for potential depositional sinks for these sediments.

Finally, the SF map presented in this thesis provides a wealth of information over a large, topographically and geologically diverse region that can be used to evaluate the local glacial history of many different areas throughout the region. The details of flow patterns in most local areas have not been investigated in this study. In addition, the implications of this work for applied glacial geology studies such as drift prospecting have not been investigated to any great detail. For example, if SF record meltwater flow directions and the diamicton deposits were laid down by earlier glacial flow, then there should be areas where flow directions indicated by the SF would be significantly different from glacial dispersal directions indicated by till geochemistry. An evaluation of the glacial dispersal data available in numerous mineral industry exploration reports and elsewhere would be of interest in this regard and would provide an additional physical test of the theories discussed in this dissertation.

REFERENCES

Aalto, K.R., Aalto, R., Garrison-Laney, C.E., and Abramson, H.F. 1999. Tsunami sculpturing of the Pebble Beach wave-cut platform, Crescent City area, California. Journal of Geology, 107, 607-622.

Aario, R. 1987. Drumlins of Kuusamo and Rogen-ridges of Ranua, northeast Finland. In Drumlin Symposium. Eds. J. Menzies and J. Rose. Balkema, Rotterdam. 87-101.

Allen, J.R.L. 1970. Principles of Physical Sedimentology. Allen and Unwin, London.

Allen, J.R.L. 1982. Sedimentary Structures. Developments in Sedimentology 30B. Elsevier, Amsterdam, vol. 2, 663 pages.

Allen, P.A. 1997. Earth Surface Processes. Blackwell Science Ltd., Oxford.

American Geological Institute 1976. Dictionary of Geological Terms. Anchor Books, Garden City, NY. 472 p.

Armstrong, J.E. and Tipper, H.W. 1948. Glaciation in north central British Columbia. American Journal of Science, 246, 283-210.

Ash, C.H., Macdonald, R.W.J., and Paterson, I.A. 1993. Geology of the Stuart-Pinchi Lake area, Central British Columbia. B.C. Ministry of Energy, Mines and Petroleum Resources, Open File 1993-9.

Baker, V.R. 1973. Erosional forms and processes for the catastrophic Pleistocene Missoula floods in Eastern Washington. In Fluvial Geomorphology, ed. M. Morisawa. George Allen and Unwin, London, 123-148.

Baker, V.R. 1979. Erosional processes in channelized water flows on Mars. Journal of Geophysical Research, 84(B14), 7985-7993.

Baker, V.R. and Komar, P.D. 1987. Cataclysmic flood processes and landforms, *In* Centennial Special Volume 2, Geological Society of America, 423-443.

Baker, V.R. and Kochel, R.C. 1978. Morphometry of streamlined forms in terrestrial and martian channels. Proceedings of the 9th Lunar and Planetary Science Conference, 3193-3203.

Baker, V.R., Greeley, R., Komar, P.D., Swanson, D.A. and Waitt, R.B. 1987. Columbia and Snake River Plains. In Geomorphic systems of North America: Boulder, Colorado, Geological Society of America, Centennial Special Volume 2. 403-467.

Baker, V.R., Benito, G., and Rudoy, A.N. 1993. Paleohydrology of Late Pleistocene superflooding, Altay Mountains, Siberia. Science, 259, 348-350.

Barnett, P.J., Sharpe, D.R., Russell, H.A.J., Brennand, T.A., Gorrell, G., Kenny, F., and Pugin, A. 1998. On the origin of the Oak Ridges Moraine. Canadian Journal of Earth Science, 35, 1152-1167.

Beaney, C. and Shaw, J. 2000. The subglacial geomorphology of southeast Alberta: evidence for subglacial meltwater erosion. Canadian Journal of Earth Sciences 37, 51-61.

Beaney, C.L. 2002. Tunnel channels in southeast Alberta, Canada: evidence for catastrophic channelized drainage. Quaternary International, 90, 67-74.

Bellefontaine, K., Legun, A., Massey, N. W,D, and Desjardins, P.J., 1995: Mineral Potential Project, Digital Geological Compilation NEBC South half, (83D, E; 93F, G, H, I, J, K, N, O, P), Ministry of Energy, Mines and Petroleum Resources, Open File 1995-24.

Benn, D.I. and Evans, D.J.A. 1998. Glaciers and Glaciation. Arnold, London. 734 pages.

Binder, R.C. 1962. Fluid Mechanics, 4th edition. Prentice-Hall, Inc., Englewood Cliffs, N.J.. 453 pages.

Booth, D.B. and Hallet, B. 1993. Channel networks carved by subglacial water: Observations and reconstruction in the eastern Puget Lowland of Washington. Geological Society of America Bulletin, 105, 671-683.

Boulton, G.S. 1974. Processes and patterns of glacial erosion. In Coates, D.R., ed. Glacial geomorphology. Binghampton, State University of New York, 41-87.

Boulton, G.S. 1979. Processes of glacial erosion on different substrata. Journal of Glaciology, 23, 15-38.

Boulton, G.S. 1987. A theory of drumlin formation by subglacial sediment deformation. In Drumlin Symposium. Eds. J. Menzies and J. Rose. Balkema, Rotterdam. 25-80.

Boulton, G.S. 1996. Theory of glacial erosion, transport and deposition as a consequence of subglacial sediment deformation. Journal of Glaciology, 42, 75-84.

Boulton, G.S. and Hindmarsh, R.C.A. 1987. Sediment deformation beneath glaciers: rheology and geological consequences. Journal of Geophysical Research, 92 (B9), 9059-9082.

Boulton, G.S. and Vivian, R. 1973. Underneath the glaciers. Geographical Magazine, 45, 311-319.

Boyce, J.I. and Eyles, N. 1991. Drumlins carved by deforming till streams below the Laurentide ice sheet. Geology, 19, 787-790.

Brennand, T.A. and Shaw, J. 1994. Tunnel channels and associated landforms, south-central Ontario: their implications for ice-sheet hydrology. Canadian Journal of Earth Science, 31, 505-522.

Bryan, R.B., Campbell, I.A., and Yair, Aaron 1987. Postglacial geomorphic development of the Dinosaur Provincial Park badlands, Alberta. Canadian Journal of Earth Science, 24, 135-146.

Bryant, E.A. and Young, R.W. 1996. Bedrock-Sculpturing by Tsunami, South Coast New South Wales, Australia. Journal of Geology, 104, 565-582.

Clague, J.J. 1984. Quaternary geology and geomorphology, Smithers-Terrace-Prince Rupert area, British Columbia. Geological Survey of Canada, Memoir 413, 71 pages.

Clague, J.J. 1989. Cordilleran ice sheet. in Chapter 1 of Quaternary Geology of Canada and Greenland, ed. R.J. Fulton, Geological Survey of Canada, Geology of Canada, no. 1, 40-42.

Clark, C.D. 1993. Mega-scale glacial lineations and cross-cutting ice-flow landforms. Earth Surface Processes and Landforms, 18, 1-29.

Clark, C.D. 1994. Large scale ice-molded landforms and their glaciological significance. Sedimentary Geology, 91, 253-268.

Clark, C.D. and Wilson, C. 1994. Spatial analysis of lineaments. Computers and Geosciences, 20, 1237-1258.

Dahl, R. 1965. Plastically sculptured detail forms on rock surfaces in northern Nordland, Norway. Geografiska Annaler, Series A, 47, 3-140.

Dardis, G.F. 1987. Sedimentology of late-Pleistocene drumlins in south-central Ulster, Northern Ireland. In Drumlin Symposium. Eds. J. Menzies and J. Rose. Balkema, Rotterdam. 215-224.

Dardis, G.F. and McCabe, A.M. 1987. Subglacial sheetwash and debris flow deposits in late-Pleistocene drumlins, Northern Ireland. In Drumlin Symposium. Eds. J. Menzies and J. Rose. Balkema, Rotterdam. 225-240.

Dargahi, B. 1990. Controlling mechanism of local scouring. Journal of Hydraulic Engineering, 116, 1197-1214.

Davis, N.F.G. and Mathews, W.H. 1944. Four phases of glaciation with illustrations from southwestern British Columbia. Journal of Geology, 52, 403-413.

Denton, G.H. 1983. Geology, 11:12, front cover.

Denton, G.H. and Sugden, D.E. 2005. Meltwater features that suggest Miocene ice-sheet overriding of the Transantarctic Mountains in Victoria Land, Antarctica.

Diakow, L.J. and Koyanagi, V. 1988. Geology of the East Half Whitesail Reach and Northeast Half Chikamin Mountain Map Sheets. B.C. Ministry of Energy, Mines and Petroleum Resources, Open File 1988-2, 2 sheets

Diakow, L.J. and Timmerman, J. 1990. Geology of the Nanika Lake Map Area. B.C. Ministry of Energy, Mines and Petroleum Resources, Open File 1990-15.

Diakow, L.J., and Levson, V.M. 1997. Bedrock and Surficial Geology of the Southern Nechako Plateau, Central British Columbia (NTS 93F/2,3,6,7); B.C. Ministry of Energy, Mines and Petroleum Resources, Geoscience Map 1997-2 1:100 000 scale map.

Diakow, L.J., Drobe, J.R., and Poulton, T.P. 1994. Geology Between Eutsuk Lake and Morice Lake, Whitesail Lake Map Area, West-central British Columbia. B.C. Ministry of Energy, Mines and Petroleum Resources, Bulletin 90.

Diakow, L.J., Webster, I.C.L., Whittles, J.A., Richards, T.A., Giles, T.R., Levson, V.M., and Weary, G.F. 1995. Bedrock and surficial geology of the Chedakuz Creek map area. B.C. Ministry of Energy, Mines and Petroleum Resources, Open File 1995-17.

Dionne, J.C. 1987. Tadpole rock (rocdrumlin): A glacial streamline molded form. In Drumlin Symposium. Eds. J. Menzies and J. Rose. Balkema, Rotterdam. 149-159.

Doornkampf, J.C. and King, C.A.M. 1971. Numerical Analysis in Geomorphology. Arnold, London. 372 pages.

Dowdeswell, J.A. and Siegert, M.J. 1999. The dimensions and topographic setting of Antarctic subglacial lakes and implications for large-scale water storage beneath continental ice sheets. GSA Bulletin, 111, 254-263.

Dreimanis, A. 1993. Water-eroded crescentic scours and furrows associated with subglacial flutes at Breidamerkurjokull, Iceland. Boreas, 22, 110-112.

Dury, G.H. 1971. Relation of morphometry to runoff frequency. In Introduction to Fluvial Processes, ed. R.J. Chorley, Methuen and Co Ltd, 177-188.

Elfstrom, A. and Rossbacher, L. 1985. Erosional remnants in the Baldakatj Area, Lapland, Northern Sweden. A terrestrial analog for Martian landforms. Geografiska Annaler. Series A, Physical Geography, 67, 167-176.

Evans, D.J.A. 2001. Glaciers. Progress in Physical Geography 25 (3), 428-439.

Evans, I.S. 1987. A new approach to drumlin morphometry. In Drumlin Symposium. Eds. J. Menzies and J. Rose. Balkema, Rotterdam. 119-130.

Evans, I.S. 1996. Abraded rock landforms (whalebacks) developed under ice streams in mountain areas. Annals of Glaciology, 22, 9-16.

Fahnestock, R.K. and Bradley, W.C. 1973. Knik and Matanuska Rivers, Alaska: A contrast in braiding. In Fluvial Geomorphology, ed. M. Morisawa. George Allen and Unwin, London, 220-250.

Ferbey, T. 2004. Quaternary geology, ice-flow history and till geochemistry of the Huckleberry Mine Region, west-central British Columbia, unpublished MSc Thesis. University of Victoria. 301 pages.

Ferbey, T. and Levson, V.M. 2001. Ice flow history of Tahtsa Lake - Ootsa Lake region (NTS 93 E/10, 11,14,15, & 16). British Columbia Ministry of Energy and Mines, Energy and Minerals Division, Open File 2001-8, 1 sheet.

Fisher, T.G. and Taylor, L.D. 2002. Sedimentary and stratigraphic evidence for subglacial flooding, south-central Michigan, USA. Quaternary International, 90, 87-115.

Flint, R.F. 1957. Glacial and Pleistocene Geology. John Wiley and Sons, New York.. 553 pages.

Forbes, D.L. and Syvitski, J.P.M. 1994. Paraglacial coasts. In Coastal Evolution. Eds. R.W.G. Carter and C.D. Woodroffe. Cambridge University Press, Cambridge. 373-424.

Francek, M.A. 1991. A spatial perspective on the New York drumlin field. Physical Geography, 12, 1-18.

Fulton, R.J. 1991. A conceptual model for growth and decay of the Cordilleran Ice Sheet. Geographie Physique et Quaternaire, 45, 281-286.

Fulton, R.J., compiler 1995. Surficial materials of Canada, Geological Survey of Canada, Map 1880A, scale 1:5 000 000.

Gaba, R.G 1992. Geology and mineral resources of the Babine Mountains Recreation Area. B.C. Ministry of Energy, Mines and Petroleum Resources, Paper 1992-5.

Gabrielse, H., Monger, J.W.H., Wheeler, J.O., and Yorath, C.J. 1991. Part A. Morphogeological belts, tectonic assemblages, and terranes: *in* Chapter 2 of Geology of the Cordilleran Orogen in Canada. Eds. H.Gabrielse and C.J. Yorath. Geological Survey of Canada, Geology of Canada, no. 4. 15-28.

Gilbert, R. and Shaw, J. 1994. Inferred subglacial meltwater origin of lakes on the southern border of the Canadian Shield. Canadian Journal of Earth Sciences, 31, 1630-1637.

Geological Survey Branch 2003. Terrain and soil maps, Ministry of Energy and Mines web site URL: http://www.em.gov.bc.ca/Mining/Geolsurv/Terrain&Soils/Default.htm

Giles, T.R. and Levson, V.M. 1995. Surficial geology and Quaternary stratigraphy of the Tsacha Lake Area, B.C. Ministry of Energy, Mines and Petroleum Resources, Open File 1995-10.

Glasser, N.F. and Nicholson, F.H. 1998. Subglacial meltwater erosion at Loch Treig. Scottish Journal of Geology, 34, 7-13.

Glasser, N.F., Crawford, K.R., Hambrey, M.J., Bennett, M.R. and Huddart, D. 1998. Lithological and structural controls on the surface wear characteristics of glaciated metamorphic bedrock surfaces: Ossian Sarsfjellet, Svalbard. The Journal of Geology, 106, 319-329.

Golden Software, Inc. 1999. Surfer Version 7 help files, topic: Gridding | Smoothing Grids | Recalculating a Grid.

Goldstein, B. 1994. Drumlins of the Puget Lowland, Washington State, USA. Sedimentary Geology, 91, 299-311.

Gore, D.B. and Pickard, J. 1998. Proglacial hydrology and drainage, southeastern Vestfold Hills, East Antarctica. Proceedings of the Linnean Society of New South Wales, 119, 181-196.

Gupta, S., Collier, J., Potter, G., and Palmer-Felgate, A. 2005. Catastrophic flood geomorphology in the English Channel compared with Martian outflow channels. Geophysical Research Abstracts, 7, 10803.

Gray, J.M. 1982. Unweathered, glaciated bedrock on an exposed lake bed in Wales. Journal of Glaciology, 28, 483-497.

Gudmundsson, M.T. 2001. Volcanism and glaciers - processes and environmental impact. In Earth system processes, programs with abstracts, Geological Society of America and Geological Society of London, International. 45.

Gudmundsson, M.T., Sigmundsson, F, Björnsson, H, and Högnadóttir, T. 2004. The 1996 eruption at Gjálp, Vatnajökull icecap, Iceland: efficiency of heat transfer, ice deformation and subglacial water pressures. Bulletin of Volcanology, 66, 46-65.

Hanvey, P.M. 1987. Sedimentology of lee-side stratification sequences in late-Pleistocene drumlins, north-west Ireland. In Drumlin Symposium. Eds. J. Menzies and J. Rose. Balkema, Rotterdam. 241-253.

Harbor, Jonathan M. 1988. Numerical modeling of the development of U-shaped valleys by glacial erosion. Geological Society of America Bulletin, 104, 1364-1375.

Harry, D.G. and Trenhaile, A.S. 1987. The morphology of the Arran drumlin field, southern Ontario, Canada. In Drumlin Symposium. Eds. J. Menzies and J. Rose. Balkema, Rotterdam. 161-173.

Hart, J.K. 1995. Recent drumlins, flutes and lineations at Vestari-HagafellsJokull, Iceland. Journal of Glaciology, 41, 596-606.

Hart, J.K. and Smith, B. 1997. Subglacial deformation associated with fast ice flow, from Columbia Glacier, Alaska. Sedimentary Geology, 111, 177-197.

Hattestrand, C., Goodwillie, D., and Kleman, J. 1999. Size distribution of two cross-cutting drumlin systems in northern Sweden: a measure of selective erosion and formation time length. Annals of Glaciology, 28, 146-152.

Herget, J. 2005. Reconstruction of Pleistocene ice-dammed lake outburst floods in the Altai Mountains, Siberia. Geological Society of America, Special Paper 386, 118 pp.

Heritage, G.L., van Niekerk, A.W., and Moon, B.P. 1999. Geomorphology of the Sabie River, South Africa: an incised bedrock-influenced channel. In Varieties of Fluvial Form, eds. A.J. Miller and A. Gupta. John Wiley and Sons, Ltd., Chichester, Great Britain. 53-79.

Hindmarsh, R.C.A. 2004. A numerical comparison of approximations to the Stokes equations used in ice sheet and glacier modeling. Journal of Geophysical Research, 109.

Holland, S.S. 1964. Landforms of British Columbia, a physiographic outline. British Columbia Department of Mines and Petroleum Resources, Bulletin 48, 138 pages.

Jansson, K.N. and Kleman, J. 1999. The horned crag-and-tails of the Ungava Bay landform swarm, Quebec - Labrador, Canada. annals of Glaciology, 28, 168-174.

Jansson, K.N., Kleman, J. and Marchant, D.R. 2002. The succession of ice-flow patterns in north-central Quebec-Labrador, Canada. Quaternary Science Reviews, 21, 503-523.

Jansson, K.N., Stroeven, A.P. and Kleman, J. 2003. Configuration and timing of Ungava Bay ice streams, Labrador-Ungava, Canada. Boreas, 32, 256-262.

Jauhiainen, E. 1975. Morphometric analysis of drumlin fields in northern Central Europe. Boreas, 4, 219-230.

Johnson, M.D. 1999. Spooner Hills, northwest Wisconsin: High-relief hills carved by subglacial meltwater of the Superior Lobe. in Mickelson, D.M. and Attig, J.W., eds., Glacial Processes Past and Present: Boulder, Colorado, Geological Society of America Special Paper 337. 83-92.

Jorgensen, F. and Piotrowski, J.A. 2003. Signature of the Baltic Ice Stream on Funen Island, Denmark during the Weischselian glaciation. Boreas, 32, 242-255.

Karcz, I. 1981. Reflections on the origin of small scale longitudinal stream-bed scours. In Fluvial Geomorphology, ed. M. Morisawa. George Allen and Unwin, London, 149-173.

Karczewski, A. 1987. Lithofacies variability of a drumlin in Pomerania, Poland. In Drumlin Symposium. Eds. J. Menzies and J. Rose. Balkema, Rotterdam. 177-183.

Kehew, A.E. and Lord, M.L. 1986. Origin and large-scale erosional features of glacial-lake spillways in the northern Great Plains. Geological Society of America Bulletin, 97, 162-177.

Keller, E.A. and Melhorn, W.N. 1981. Bedforms and fluvial processes in alluvial stream channels: selected observations. In Fluvial Geomorphology, ed. M. Morisawa. George Allen and Unwin, London, 253-283.

Kerr, F.A. 1934. Glaciation in northern British Columbia. Royal Society of Canada, Transactions, Ser. 3, 28, 17-31.

Knight, J. 2002. Bedform patterns, subglacial meltwater events, and Late Devensian ice sheet dynamics in north-central Ireland. Global and Planetary Change, 35, 237-253.

Komar, P.D. 1983. Shapes of streamlined islands on Earth and Mars: Experiments and analyses of the minimum-drag form. Geology, 11, 651-654.

Komar, P.D. 1984. The lemniscate loop - comparisons with the shapes of streamlined landforms. Journal of Geology, 92, 133-145.

Kor, P.S.G. and Cowell, D.W. 1998. Evidence for catastrophic subglacial meltwater sheetflood events on the Bruce Peninsula, Ontario. Canadian Journal of Earth Science, 35, 1180-1202.

Kor, P.S.G., Shaw, J., and Sharpe, D.R. 1991. Erosion of bedrock by subglacial meltwater, Georgian Bay, Ontario: a regional view. Canadian Journal of Earth Science, 28, 623-642.

Levson, V.M. 2001. Quaternary geology of the Babine porphyry copper district: implications for geochemical exploration. Canadian Journal of Earth Sciences, 38, 733-749.

Levson, V.M. 2002. Quaternary geology and till geochemistry of the Babine porphyry copper belt, B.C. (NTS 093L/9, 16; M/1, 2, 7 & 8). Ministry of Energy and Mines, Energy and Minerals Division, Bulletin 110, 278 pages.

Levson, V.M. and Giles, T.R. 1994. Surficial geology and Quaternary stratigraphy of the Fawnie Creek Area, B.C. Ministry of Energy, Mines and Petroleum Resources, Open File 1994-9.

Levson, V.M. and Giles, T.R. 1997. Quaternary geology and till geochemistry studies in the Nechako and Fraser Plateaus, Central British Columbia (NTS 93 C/1, 8, 9, 10; F/2, 3, 7; L/16; M/1). Ministry of Employment and Investment, Geological Survey Branch, Paper 1997-2, 121-145.

Levson, V.M. and Mate, D.J. 2002. Till geochemistry of the Tetachuck Lake and Marilla map areas (NTS 93 F/5 and F/12). British Columbia Geological Survey, Open File 2002-11, 180 pages.

Levson, V.M., Stumpf, A.J., and Stuart, A.J. 1998. Quaternary geology and ice-flow studies in the Smithers and Hazelton map areas (93L and M): implications for exploration. in Geological Fieldwork 1997, British Columbia Geological Survey, Paper 1998-1, pages 5-1 to 5-8.

Longva, O. and Thoresen, M.K. 1991. Iceberg scours, iceberg gravity craters and current erosion marks from a gigantic Preboreal flood in southeastern Norway. Boreas, 20, 47-62.

Lowe, C., Levson, V.M., Struik, L.C., Plouffe, A., Anderson, R.G., and Mate, D. 2001. Digital elevation model, Nechako River map area, British Columbia. Geological Survey of Canada, Open File 4027, scale 1:250 000.

Lowe, A.L. and Anderson, J.B. 2003. Evidence for abundant subglacial meltwater beneath the paleo-ice sheet in Pine Island Bay, Antarctica. Journal of Glaciology, 49, 125-138.

MacIntyre, D.G. 1985. Geology and mineral deposits of the Tahtsa Lake District west central British Columbia. B.C. Ministry of Energy, Mines and Petroleum Resources, Bulletin 75.

MacIntryre, D.G. 1996. faults_bc_dd. B.C. Ministry of Energy & Mines, Geological Survey Branch, Victoria. Unpublished. Online link: http://www.em.gov.bc.ca/DL/BC_maps/shp/faults_bc_dd.zip.

MacIntyre, D.G. 2001. Geological compilation map Babine Porphyry Copper District Central British Columbia. B.C. Ministry of Energy, Mines and Petroleum Resources, Open File 2001-3.

MacIntyre, D. and Schiarizza, P. 1999. Bedrock geology Cunningham Lake. B.C. Ministry of Energy, Mines and Petroleum Resources, Open File 1999-11.

MacIntyre, D.G., Brown, D., Desjardins, P. and Mallett, P. 1987. Geology of Dome Mountain Area. B.C. Ministry of Energy, Mines and Petroleum Resources, Open File 1987-1.

MacIntyre, D.G., Desjardins, P., Tercier, P. and Koo, J. 1989. Geology of the Telkwa River Area. B.C. Ministry of Energy, Mines and Petroleum Resources, Open File 1989-16.

MacIntyre, D.G., Ash, C.H. and Britton J.M. 1994a. Geological compilation, Skeena-Nass Area, West-Central British Columbia, (NTS 93E, L, M; 94D; 103G, H, I, J, O, P; 104A, B); B.C. Ministry of Energy, Mines and Petroleum Resources, Open File 1994-14, Scale 1:250,000.

MacIntyre, D. G., Ash C. and Britton, J., 1994b: Nass-Skeena (93/E, L, M; 94/D; 103/G, H, I, J, P; 104/A, B), Ministry of Energy, Mines and Petroleum Resources, Open File 1994-14.

MacIntyre, D.G., Webster, I. and Bellefontaine, K. 1996. Bedrock geology of the Fulton Lake Map Area, North Central B.C. B.C. Ministry of Energy, Mines and Petroleum Resources, Open File 1996-29.

McIntyre, D., Webster I., and Desjardins, P. 1998. Bedrock geology of the Old Fort Mountain map area, North-Central B.C. B.C. Ministry of Energy, Mines and Petroleum Resources, Open File 1997-10.

Massey, N.W.D., MacIntyre, D.G. and Desjardins, P.J. 2003a. Digital geology map of British Columbia: Tile NN9 North Coast, B.C. Ministry of Energy and Mines, Geofile 2003-13 (version), scale 1:250,000.

Massey, N.W.D., MacIntyre, D.G. and Desjardins, P.J., 2003b: Digital Map of British Columbia: Tile NN10 Southwest B.C., B.C. Ministry of Energy and Mines, Geofile 2003-21 (version 2), scale 1:250,000.

Mate, D.J. 2000. Quaternary geology, stratigraphy and applied geomorphology in southern Nechako Plateau, central British Columbia, unpublished MSc Thesis. University of Victoria. 253 pages.

Mate, D.J. and Levson, V.M. 2001. Quaternary stratigraphy and history of the Ootsa Lake - Cheslatta River area, Nechako Plateau, Central British Columbia. Canadian Journal of Earth Sciences. 38. 751-765

Menzies, J. 1987. Towards a general hypothesis on the formation of drumlins. In Drumlin Symposium. Eds. J. Menzies and J. Rose. Balkema, Rotterdam. 9-24.

Menzies, J. and Rose, J. 1987. In Introduction: Drumlin Symposium. Eds. J. Menzies and J. Rose. Balkema, Rotterdam. 1-5.

Mills, H. 1980. An analysis of drumlin form in the northeastern and north-central United States: Summary. Geological Society of America Bulletin, Part 1, 91, 637-639.

Mills, H. 1987. Morphometry of drumlins in the northeastern and north-central USA. In Drumlin Symposium. Eds. J. Menzies and J. Rose. Balkema, Rotterdam. 131-147.

Munro, M. and Shaw, J. 1997. Erosional origin of hummocky terrain in south-central Alberta, Canada. Geology, 25, 1027-1030.

Munro-Stasiuk, M.J. and Shaw, J. 2002. The Blackspring Ridge Flute Field, south-central Alberta, Canada: evidence for subglacial sheetflow erosion. Quaternary International, 90, 75-86.

Munro-Stasiuk, M.J. and Sjogren, D.B. 2002. Evidence for province-wide water storage and catastrophic drainage beneath the Laurentide Ice Sheet, Alberta, Canada. In The Extremes of the Extremes: Extraordinary Floods, eds. A. Snorrason, H.P. Finnsdottir, and M.E. Moss, IAHS Publication no. 271, 113-119.

Neville, A.M. and Kennedy, J.B. 1968. Basic Statistical Methods for Engineers and Scientists. International Textbook Company, Scranton, Pennsylvania. 325 p.

National Resources Canada – accessed 2005. The Atlas of Canada – Surficial Materials. http://atlas.gc.ca/site/english/maps/environment/land/surficialmaterials

Newman, W.A. and Mickelson, D.M. 1994. Genesis of Boston Harbor drumlins, Massachusetts. Sedimentary Geology, 91, 33-343.

Nye, J.F. 1969. The effect of longitudinal stress on the shear stress at the base of an ice sheet. Journal of Glaciology, 8, 207-213.

Nye, J.F. 1970. Glacier sliding without cavitation in a linear viscous approximation. Proceedings of the Royal Society of London, 315a, 381-403.

O' Cafaigh, C. 1996. Tunnel valley genesis. Progress in Physical Geography, 20, 1-19.

Pair, D.L. 1997. Thin film, channelized drainage, or sheetfloods beneath a portion of the Laurentide Ice Sheet: an examination of glacial erosion forms, northern New York State, USA. Sedimentary Geology, 111, 199-215.

Panton, R.L. 1996. Incompressible flow. John Wiley and Sons, Inc., New York.

Paterson, W.S.B. 1994. The Physics of Glaciers, 3rd edition. Pergamon, Oxford. 480 p.

Plouffe, A. 1994. Surficial geology, Tezzeron Lake, British Columbia. Geological Survey of Canada, Open File 2846, 1:100 000 scale map.

Plouffe, A. 1996a. Surficial geology, Burns Lake, British Columbia, Geological Survey of Canada, Open File 3184, 1:100 000 scale map.

Plouffe, A. 1996b. Surficial geology, Cunningham Lake, British Columbia (93K/NW), Geological Survey of Canada, Open File 3183, 1:100 000 scale map.

Plouffe, A. 1996c. Surficial geology, Fraser Lake, British Columbia (93 K/SE), Geological Survey of Canada, Open File 3182, 1:100 000 scale map.

Plouffe, A. 1998a. Surficial geology, Tahultzu Lake, British Columbia (93 F/NE), Geological Survey of Canada, Open File 3620, 1:100 000 scale map.

Plouffe, A. 1998b. Surficial geology, Tahultzu Lake, British Columbia (93 F/NE), Geological Survey of Canada, Open File 3620, 1:100 000 scale map.

Plouffe, A. 2000. Quaternary geology of the Fort Fraser and Manson River map areas, central British Columbia. Geological Survey of Canada, Bulletin 554, 62 pages.

Plouffe, A. and Levson, V.M. 2004a. Surficial geology, Entiako Lake, British Columbia. Geological Survey of Canada, Open File 4157, 2004.

Plouffe, A. and Levson, V.M. 2004b. Surficial geology, Tatelkuz Lake, British Columbia. Geological Survey of Canada, Open File 4001.

Plouffe, A., Levson, V.M., and Mate, D.J. 2004. Surficial geology, Nechako River, British Columbia. Geological Survey of Canada, Map 2067A, scale 1:250 000.

Rachocki, A. 1981. Alluvial Fans. John Wiley and Sons, Ltd., Chichester, Great Britain. 161 pages.

Rains, B., Shaw, J., Skoye, R., Sjogren, D., and Kvill, D. 1993. Late Wisconsin subglacial megaflood paths in Alberta. Geology, 21, 323-326.

Rains, R.B., Shaw, J., Sjogren, D.B., Munro-Stasiuk, M.J., Skoye, K.R., Yound, R.R., and Thompson, R.T. 2002. Subglacial tunnel channels, Porcupine Hills, southwest Alberta, Canada. Quaternary International, 90, 57-65.

Rampton, V.N. 2000. Large-scale effects of subglacial meltwater flow in the southern Slave Province, Northwest Territories, Canada. Canadian Journal of Earth Science, 37, 81-93.

Rattas, M. and Piotrowski, J.A. 2003. Influence of bedrock permeability and till grain size on the formation of the Saadjarve drumlin field, Estonia, under an east-Baltic Weichselian ice stream. Boreas, 32, 167-177.

Rea, B.R. and Whalley, W.B. 1994. Subglacial observations from Øksfjordjøkelen, North Norway. Earth Surface Processes and Landforms, 19, 659-673.

Rea, B.R., Evans, D.J.A., Dixon, T.S., and Whalley, W.B. 2000. Contemporaneous, localized, basal ice-flow variations: implications for bedrock erosion and the origin of p-forms. Journal of Glaciology, 46, 154, 470-476.

Richards, K. 1982. Rivers. Methuen, London, 358 p.

Richardson, P.D. 1968. The generation of scour marks near obstacles. Journal of Sedimentary Petrology, 38, 965-970.

Rose, J. 1987. Drumlins as part of a glacier bedform continuum. In Drumlin Symposium. Eds. J. Menzies and J. Rose. Balkema, Rotterdam. 103-116.

Rudoy, A.N. and Baker, V.R. 1993. Sedimentary effects of cataclysmic late Pleistocene glacial outburst flooding, Altay Mountains, Siberia. In Current Research in Fluvial Sedimentology, ed. C.R. Fielding. Sedimentary Geology, 85, 53-62.

Ryder, J.M. and Maynard, D. 1991. The Cordilleran ice sheet in northern British Columbia. Géographie physique et Quaternaire, 35, 355-363.

Sawagaki, T. and Hirakawa, K. 1997. Erosion of bedrock by subglacial meltwater, Soya Coast, East Antarctica. Geografiska Annaler, Series A, Physical Geography, 79, 223-238.

Scheepers, A.C.T. and Rust, I.C. 1999. The Uniab River Fan: an unusual alluvial fan on the hyper-arid Skeleton Coast, Namibia. In Varieties of Fluvial Form, eds. A.J. Miller and A. Gupta. John Wiley and Sons, Ltd., Chichester, Great Britain. 273-294.

Schiarizza, P., Panteleyev, A., Gaba, R.G., Glover, J.K., Desjardins, P.J. and Cunningham, J., 1994: Cariboo - Chilcotin Area (92J, K, N, O, P; 93A, B, C, F, G, H), Ministry of Energy, Mines and Petroleum Resources, Open File 1994-7.

Schumm, S.A., Mosley, M.P., and Weaver, W.E. 1987. Experimental Fluvial Geomorphology, John Wiley and Sons, Toronto, 413 pages.

Selby, M.J. 1985. Earth's Changing Surface. Clarendon Press, Oxford. 606 pages.

Sharp, M., Dowdeswell, J.A., and Gemmell, J.C. 1989. Reconstructing past glacier dynamics and erosion from glacial geomorphic evidence: Snowdon, North Wales. Journal of Quaternary Science, 4, 115-130.

Sharpe, D.R. 1987. The stratified nature of drumlins from Victoria Island and Southern Ontario, Canada. In Drumlin Symposium. Eds. J. Menzies and J. Rose. Balkema, Rotterdam. 185-214.

Shaw, J. 1983. Drumlin formation related to inverted melt-water erosional marks. Journal of Glaciology, 29, 461-479.

Shaw, J. 1994. Hairpin erosional marks, horseshoe vortices and subglacial erosion. Sedimentary Geology, 91, 269-283.

Shaw, J. 1996. A meltwater model for Laurentide subglacial landscapes. In Geomorphology Sans Frontieres. Eds. B.S. McCann and D.C. Ford. John Wiley and Sons, New York. 181-236.

Shaw, J. 2001. Sedimentary evidence favoring the formation of Rogen landscapes by outburst floods. http://www.sentex.net/~tcc/rogen/main.html

Shaw, J. 2002. The meltwater hypothesis for subglacial bedforms. Quaternary International, 90, 5-22.

Shaw, J. and Freshauf, R.C. 1973. A kinematic discussion of the formation of glacial flutings. Canadian Geographer 17, 19-35.

Shaw, J. and Kvill, D. 1984. A glaciofluvial origin for drumlins of the Livingstone Lake area, Saskatchewan. Canadian Journal of Earth Sciences, 21, 1442-1459.

Shaw, J. and Sharpe, D. 1987. Drumlin formation by subglacial meltwater erosion. Canadian Journal of Earth Sciences, 24, 2316-2322.

Shaw, J., Faragini, D.M., Kvill, D.R., and Rains, R.B. 2000. The Athabasca fluting field, Alberta, Canada: implications for the formation of large-scale fluting (erosional lineations). Quaternary Science Reviews, 19, 959-980.

Shaw, J., Munro-Stasiuk, M., Sawyer, B., Beaney, C., Lesemann, J., Musacchio, A., Rains, B, and Young, R.R. 1999. The Channeled Scabland: back to Bretz? Geology, 27, 605-608.

Shaw, J., Rains, B., Eyton, R., and Weissling, L. 1996. Laurentide subglacial outburst floods: landform evidence from digital elevation models. Canadian Journal of Earth Sciences, 33, 1154-1168.

Shoemaker, E.M. 1991. On the formation of large subglacial lakes. Canadian Journal of Earth Sciences, 28, 1975-1981.

Shoemaker, E.M. 1992. Water sheet outburst floods from the Laurentide Ice Sheet. Canadian Journal of Earth Science, 29, 1250-1264.

Shoemaker, E.M. 1995. On the meltwater genesis of drumlins. Boreas, 24, 3-10.

Sjogren, D.B., Fisher, T.G., Taylor, L.D., Jol, H.M., and Munro-Stasiuk, M.J. 2002. Incipient tunnel channels. Quaternary International, 90, 41-56

Sjorgren, D.B. and Rains, R.B. 1995. Glaciofluvial erosional morphology and sediments of the Coronation - Spondin Scabland, east-central Alberta. Canadian Journal of Earth Sciences, 32, 565-578.

Smalley, I.J. 1966. Drumlin formation: a rheological model. Science, 151, 1379-1380.

Smalley, I.J. and Piotrowski, J.A. 1987. Critical strength/stress ratios at the ice-bed interface in the drumlin forming process: From 'dilatancy' to 'cross-over'. In Drumlin Symposium. Eds. J. Menzies and J. Rose. Balkema, Rotterdam. 81-86.

Smalley, I.J. and Unwin, D.J. 1968. The formation and shape of drumlins and their distribution and orientation in drumlin fields. Journal of Glaciology, 31, 220-228.

Smith, D.G. 1973. Aggradation of the Alexandra - North Saskatchewan River, Banff Park, Alberta. In Fluvial Geomorphology, ed. M. Morisawa. George Allen and Unwin, London, 211-219.

Smith, H.T.U. 1948. Giant glacial grooves in Northwest Canada. American Journal of Science, 246, 503-514.

Smith, G.H.S., Ashworth, P.J., Best, J.L., Woodward, J., and Simpson, C.J. 2005. The morphology and facies of sandy braided rivers: some considerations of scale invariance. Abstract at University of Birmingham web site, <http://www.gees.bham.ac.uk/research/ees/GSS/abstracts.htm>.

Springer, G.S. and Wohl, E.E. 2002. Empirical and theoretical investigations of sculpted forms in Buckeye Creek Cave, West Virginia. The Journal of Geology, 110, 469-481.

Stalsberg, K., Larsen, E., Ottesen, D. and Sejrup, H.P. 2003. Middle to Late Weichselian Norwegian Channel Ice Stream deposits and morphology on Jaeren, southwestern Norway and the eastern North Sea area. Boreas, 32, 149-166.

Stokes, C.R. and Clark, C.D. 2002. Are long subglacial bedforms indicative of fast ice flow? Boreas, 31, 239-249.

Stuart, R.A. 1960. Geology of the Kemano - Tahtsa Area. B.C. Ministry of Energy, Mines and Petroleum Resources, Bulletin 42.

Struik, L.C. 1998a. Bedrock geology of the Fraser Lake map area, central British Columbia; Geological Survey of Canada, Open File 3339, 1:100 000 scale coloured map.

Struik, L.C. 1998b. Bedrock geology, Tezzeron map area, central British Columbia (93KNW); Geological Survey of Canada, Open File 3624, 1:100 000 scale colour map.

Struik, L.C. and Whalen, J.B. 1998. Bedrock geology, Endako, central British Columbia (93K/03); Geological Survey of Canada, Open File 3630, 1:100 000 scale colour map.

Struik, L. C., Fallas, K., Hrudey, M. G., and Whalen, J. B. 2000. Bedrock geology, Burns Lake, British Columbia. Geological Survey of Canada, Open File 3840, 1 sheet.

Stumpf, A.J., Broster, B.E., and Levson, V.M. 2000. Multiphase flow of the late Wisconsinan Cordilleran ice sheet in western Canada. Geological Society of America Bulletin 112, 1850-1863.

Sugden, D.E. and John, B.S. 1976. Glaciers and Landscape. Edward Arnold, London, 374 pages.

Sugden, D.E., Denton, G.H., and Marchant, D.R. 1991. Subglacial meltwater channel systems and ice sheet overriding, Asgard Range, Antarctica. Geografiska Annaler. Series A, Physical Geography, 73, 109-121.

Sugden, D.E., Marchant, D.R., and Denton, G.H. 1990. Subglacial meltwater system, Sessrumir Valley, western Asgard Range, Antarctica. Antarctic Journal of the United States. 56-58.

Theakstone, W.H. 1979. Observations within cavities at the bed of the glacier Østerdalsisen, Norway. Journal of Glaciology, 23, 273-281.

Tinkler, K.J. 1993. Fluvially sculpted rock bedforms in Twenty Mile Creek, Niagara Peninsula, Ontario. Canadian Journal of Earth Science, 30, 945-953.

Tipper, H.W. 1971a. Glacial geomorphology and Pleistocene history of central British Columbia. Department of Energy, Mines and Resources, Geological Survey of Canada, Bulletin 196, 89 pages.

Tipper, H.W. 1971b. Multiple glaciation in central British Columbia. Canadian Journal of Earth Sciences, 8, 743-752.

Tipper, H.W. 1994. Preliminary interpretations of glacial and geomorphic features of Smithers map area (93 L), British Columbia. Geological Survey of Canada, Open File 2837, 7 p. and map.

van Niekerk, A.W., Heritage, G.L., Broadhurst, L.J. and Moon, B.P. 1999. Bedrock anastomosing channel systems: morphology and dynamics in the Sabie River, Mpumalanga Province, South Africa. In Varieties of Fluvial Form, eds. A.J. Miller and A. Gupta. John Wiley and Sons, Ltd., Chichester, Great Britain. 34-51.

Webb, J.A. and Fielding, C.R. 1999. Debris flow and sheetflood fans of the northern Prince Charles Mountains, East Antarctica. In Varieties of Fluvial Form, eds. A.J. Miller and A. Gupta. John Wiley and Sons, Ltd., Chichester, Great Britain. 317-341.

Wende, R. 1999. Boulder bedforms in jointed-bedrock channels. In Varieties of Fluvial Form, eds. A.J. Miller and A. Gupta. John Wiley and Sons, Ltd., Chichester, Great Britain. 190-216.

Wetherup, S. 1998. Bedrock geology, Nulki Hills, British Columbia (93F/09, 16); Geological Survey of Canada, Open File 3631, 1:100 000 scale colour map.

Wilchinsky, A.V. and Chugunov, V.A. 2000. Ice-stream-ice-shelf transition: theoretical analysis of two-dimensional flow. Annals of Glaciology, 30, 153-162.

Williams, P.F. and Rust, B.R. 1969. The sedimentology at a braided river. Journal of Sedimentary Petrology, 39, 649-679.

Williams, S.P. 1997. Geological compilation, Nechako River, British Columbia (93F); Geological Survey of Canada, Open File 3429, 1:250 000 scale coloured map.

Wyrick, J. 2003. Fluvial indicators of hyperconcentrated flows – with application to the floods on Mars. Hydrological Science and Technology 2002 AIH Annual Meeting, 19:1-4, 287-292.

APPENDIX A. STREAMLINED FORMS ON SHADED RELIEF IMAGES

The following pages consist of 20 maps, representing mapped streamlined forms for each quarter (northeast (NE), northwest (NW), southeast (SE), and southwest (SW)) of NTS 93E, 93F, 93K, 93L, and 93M.

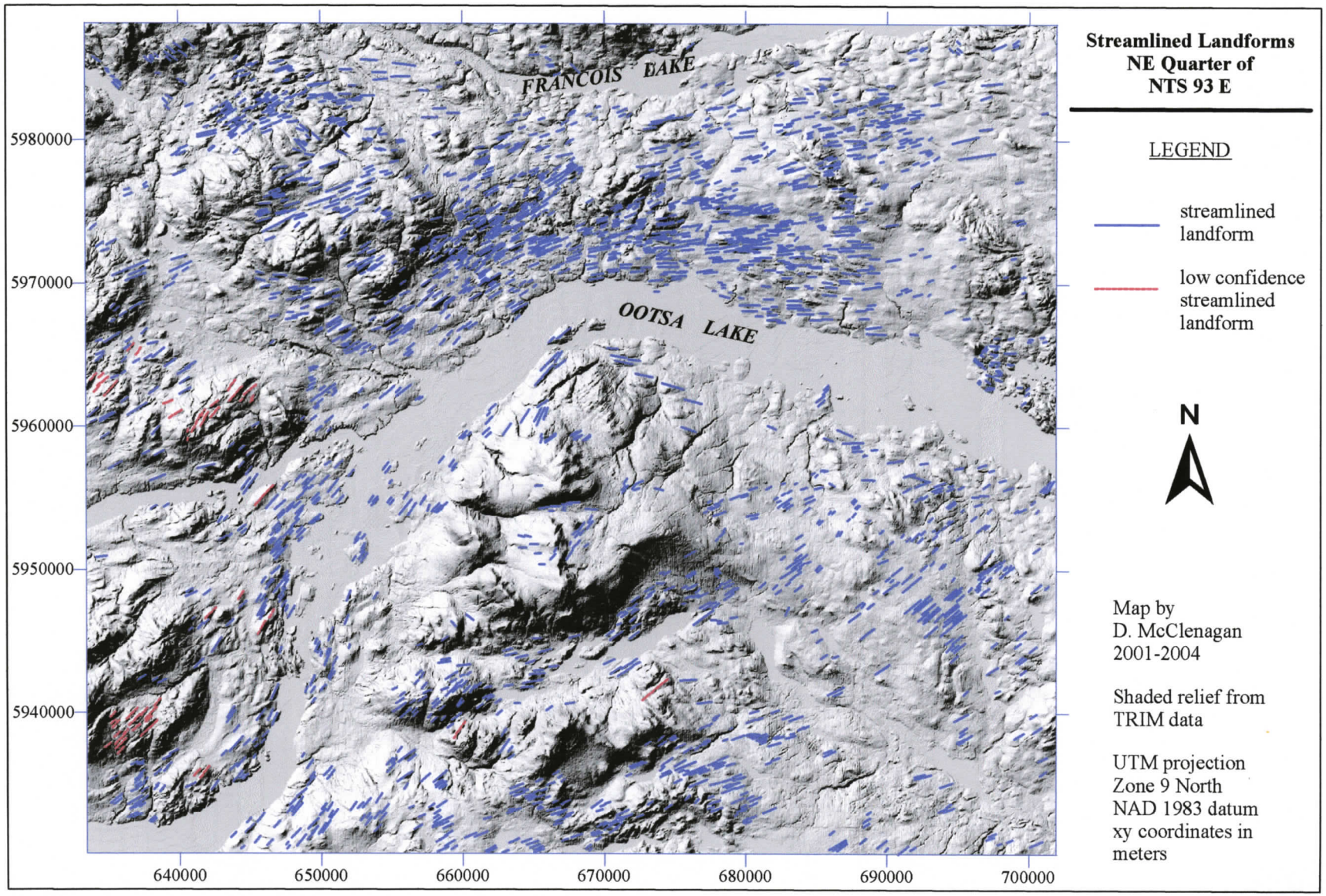
FRANCOIS LAKE
OOTSA LAKE
5980000
5970000
5960000
5950000
5940000
640000
650000
660000
670000
680000
690000
700000
Streamlined Landforms
NE Quarter of
NTS 93 E
LEGEND
streamlined landform
low confidence streamlined landform
N
Map by
D. McClenagan
2001-2004
Shaded relief from TRIM data
UTM projection
Zone 9 North
NAD 1983 datum
xy coordinates in meters

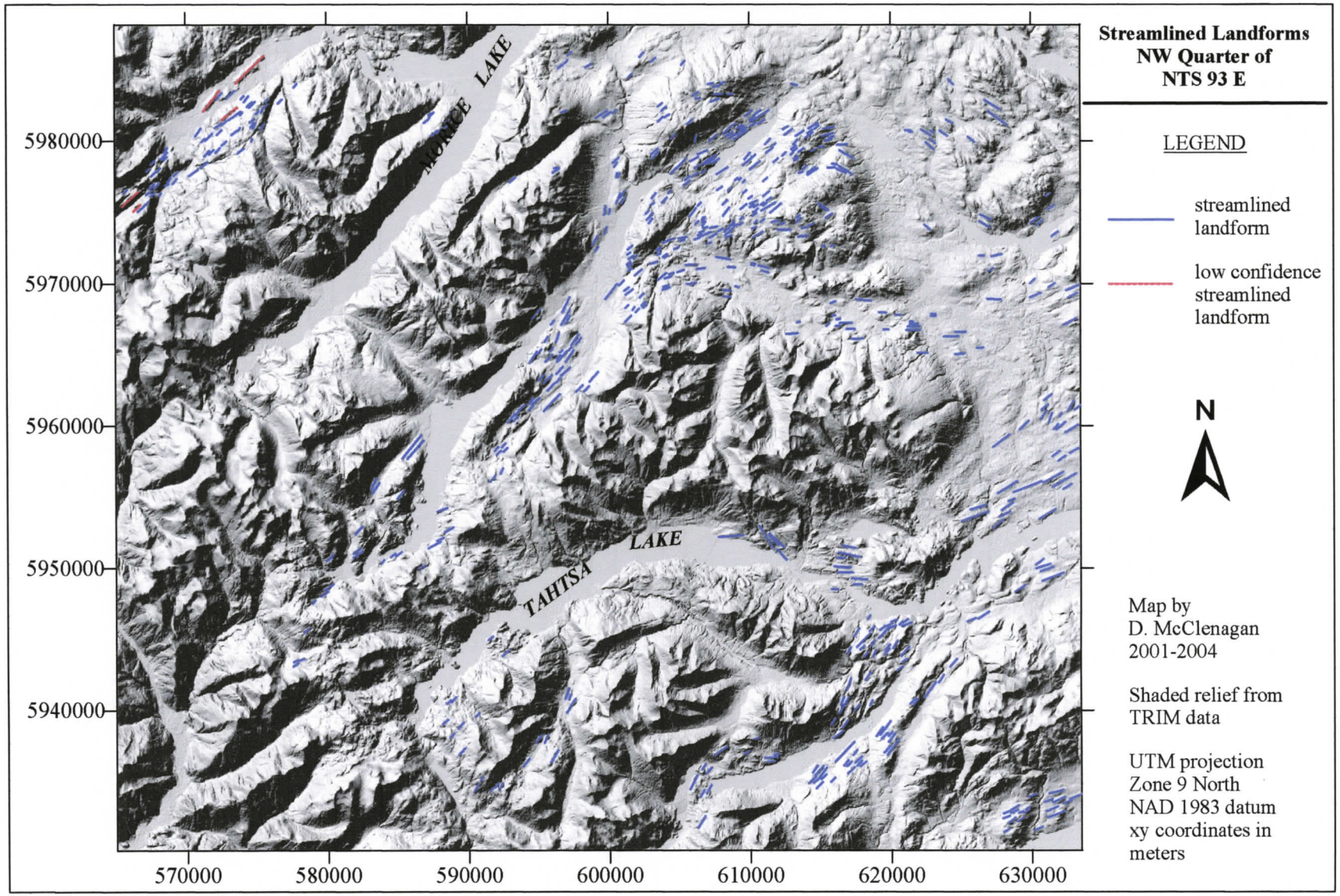
MORICE LAKE
TAHTSA LAKE
5980000
5970000
5960000
5950000
5940000
570000
580000
590000
600000
610000
620000
630000
Streamlined Landforms
NW Quarter of
NTS 93 E
LEGEND
streamlined landform
low confidence streamlined landform
N
Map by
D. McClenagan
2001-2004
Shaded relief from TRIM data
UTM projection
Zone 9 North
NAD 1983 datum
xy coordinates in meters

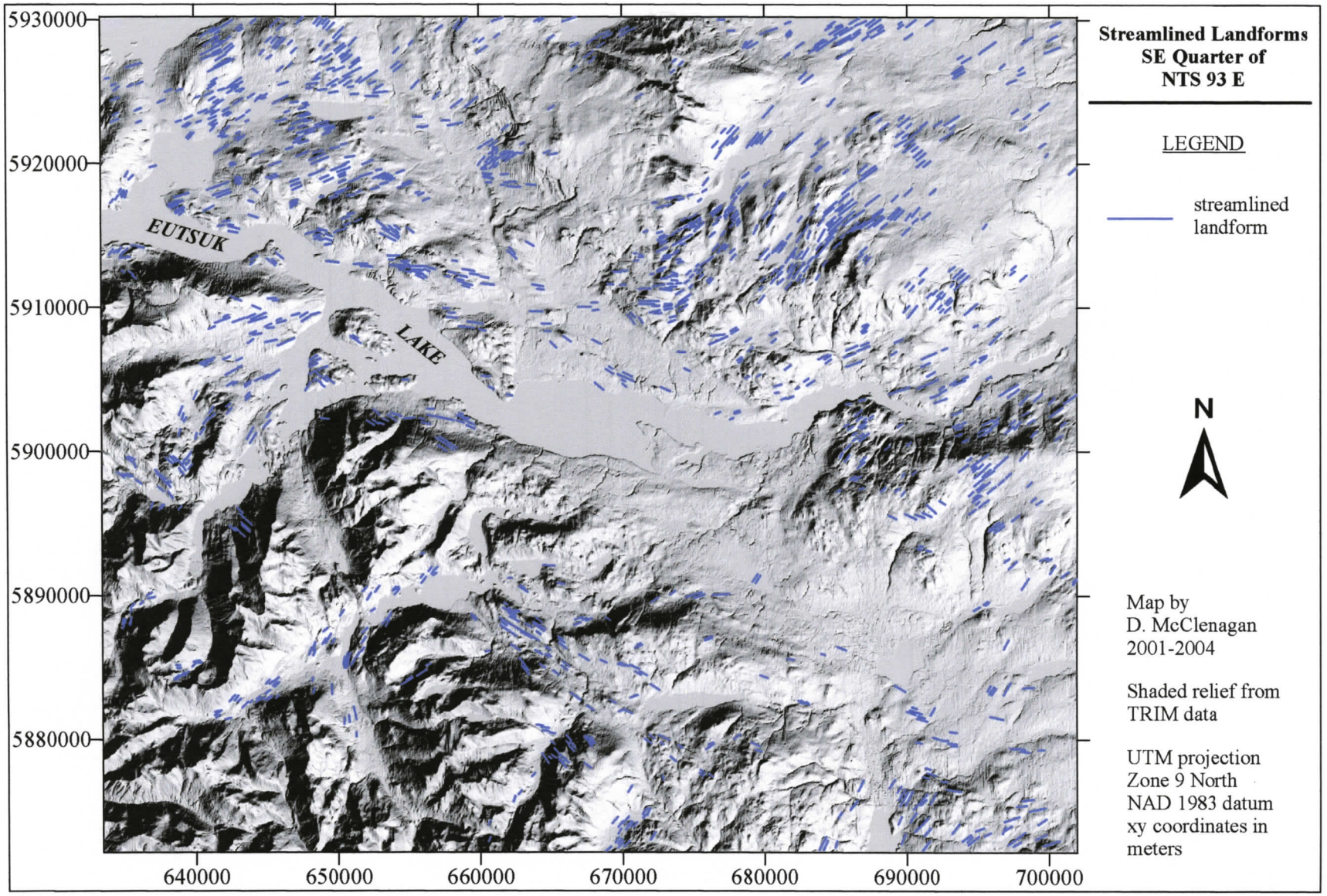
5930000
5920000
5910000
5900000
5890000
5880000
640000
650000
660000
670000
680000
690000
700000
EUTSUK
LAKE
Streamlined Landforms
SE Quarter of
NTS 93 E
LEGEND
streamlined
landform
N
Map by
D. McClenagan
2001-2004
Shaded relief from
TRIM data
UTM projection
Zone 9 North
NAD 1983 datum
xy coordinates in
meters

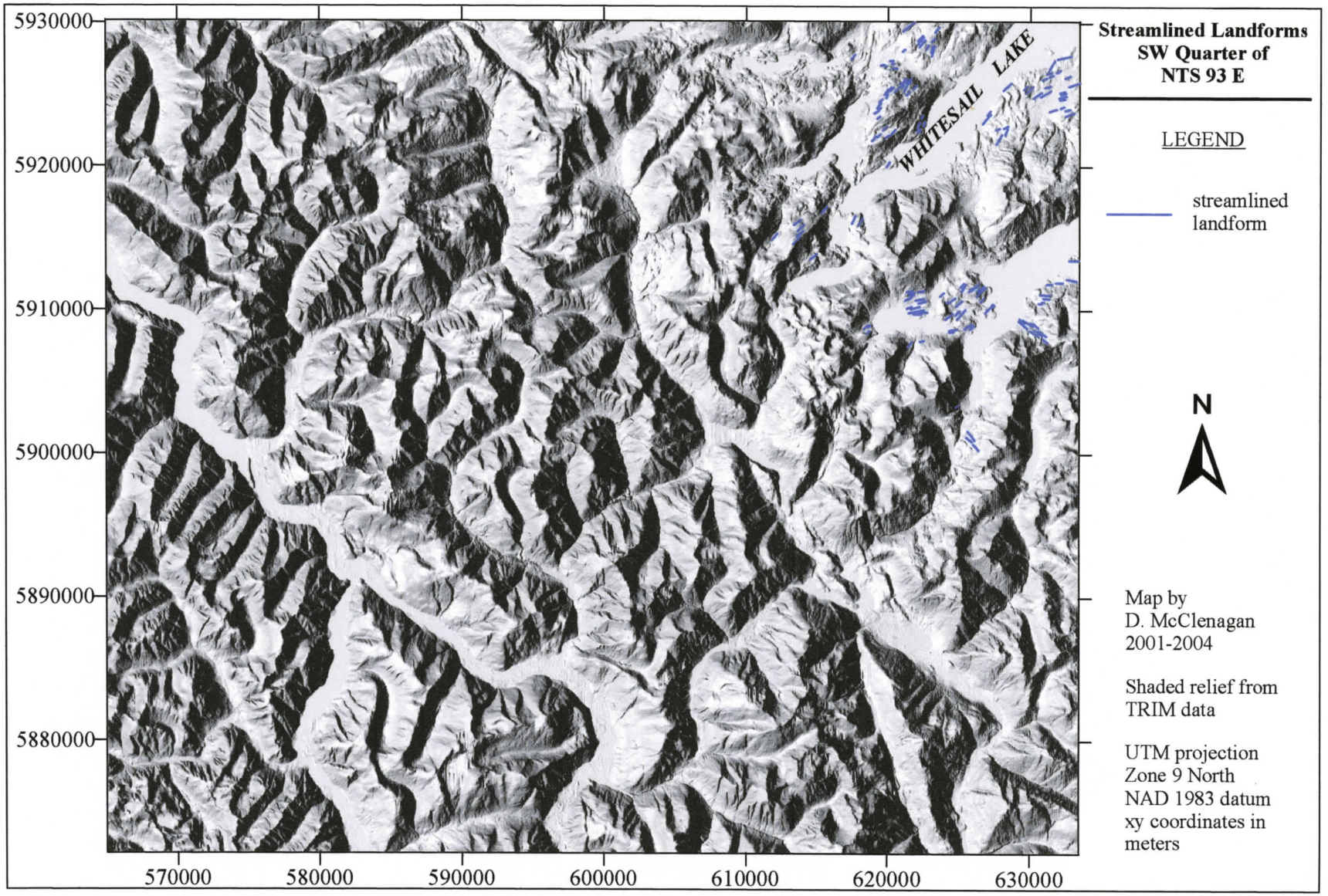
5930000
5920000
5910000
5900000
5890000
5880000
570000
580000
590000
600000
610000
620000
630000
WHITESAIL LAKE
Streamlined Landforms
SW Quarter of
NTS 93 E
LEGEND
streamlined landform
N
Map by
D. McClenagan
2001-2004
Shaded relief from TRIM data
UTM projection
Zone 9 North
NAD 1983 datum
xy coordinates in meters

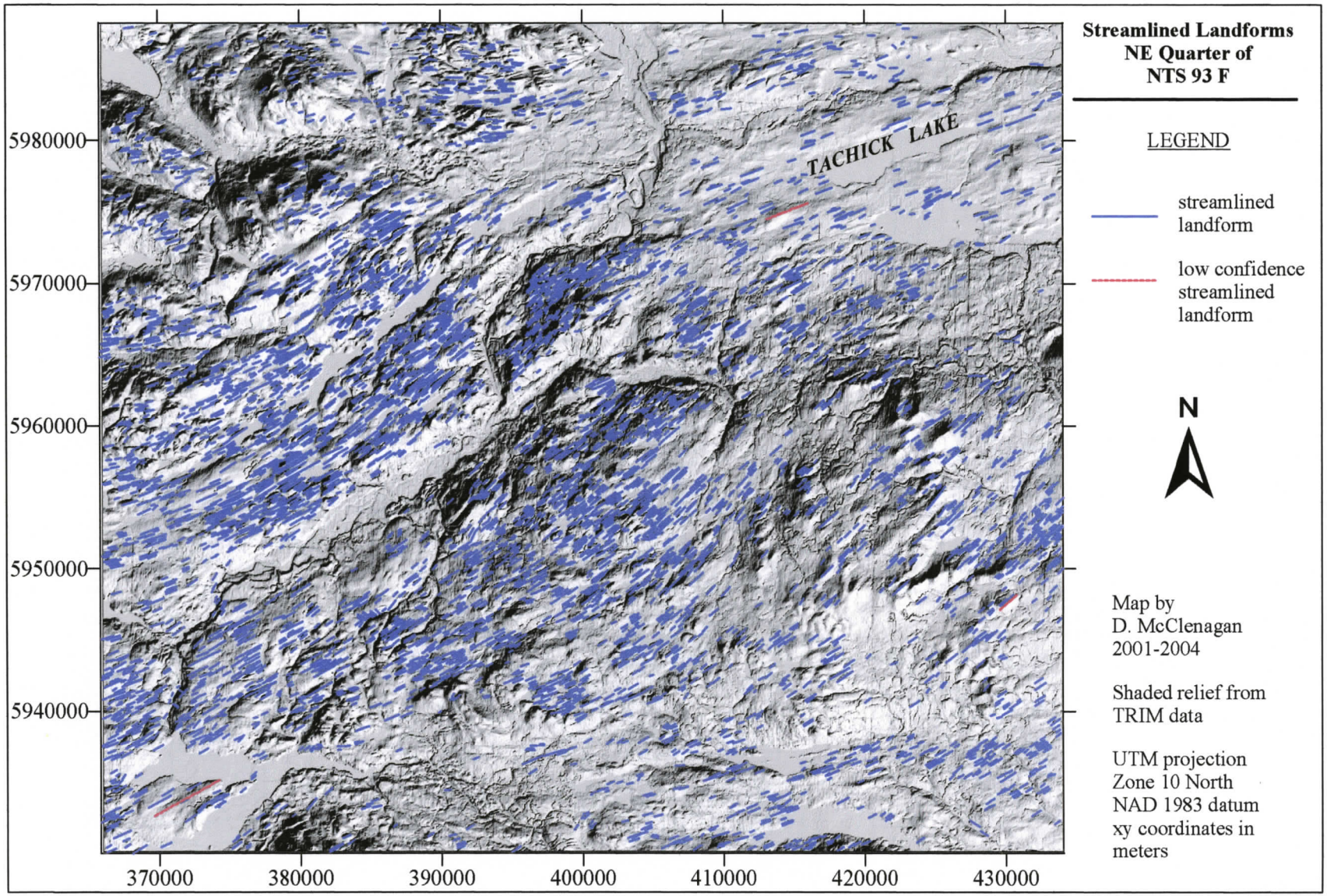
Streamlined Landforms
NE Quarter of
NTS 93 F
LEGEND
streamlined landform
low confidence streamlined landform
N
TACHICK LAKE
5980000
5970000
5960000
5950000
5940000
370000
380000
390000
400000
410000
420000
430000
Map by
D. McClenagan
2001-2004
Shaded relief from TRIM data
UTM projection
Zone 10 North
NAD 1983 datum
xy coordinates in meters

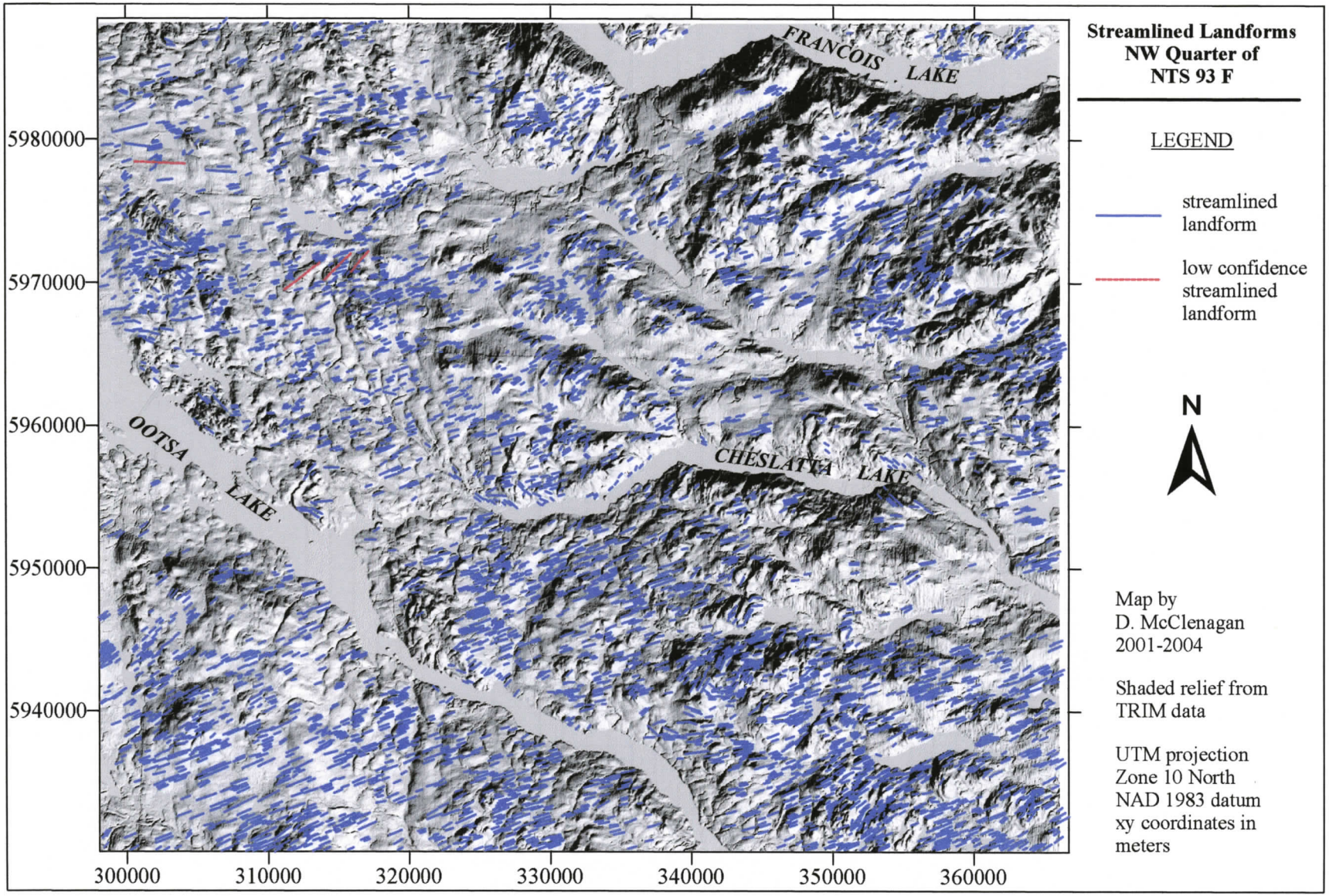
FRANCOIS LAKE
OOTSA LAKE
CHESLATTA LAKE
5980000
5970000
5960000
5950000
5940000
300000
310000
320000
330000
340000
350000
360000
Streamlined Landforms
NW Quarter of
NTS 93 F
LEGEND
streamlined landform
low confidence streamlined landform
N
Map by
D. McClenagan
2001-2004
Shaded relief from TRIM data
UTM projection
Zone 10 North
NAD 1983 datum
xy coordinates in meters

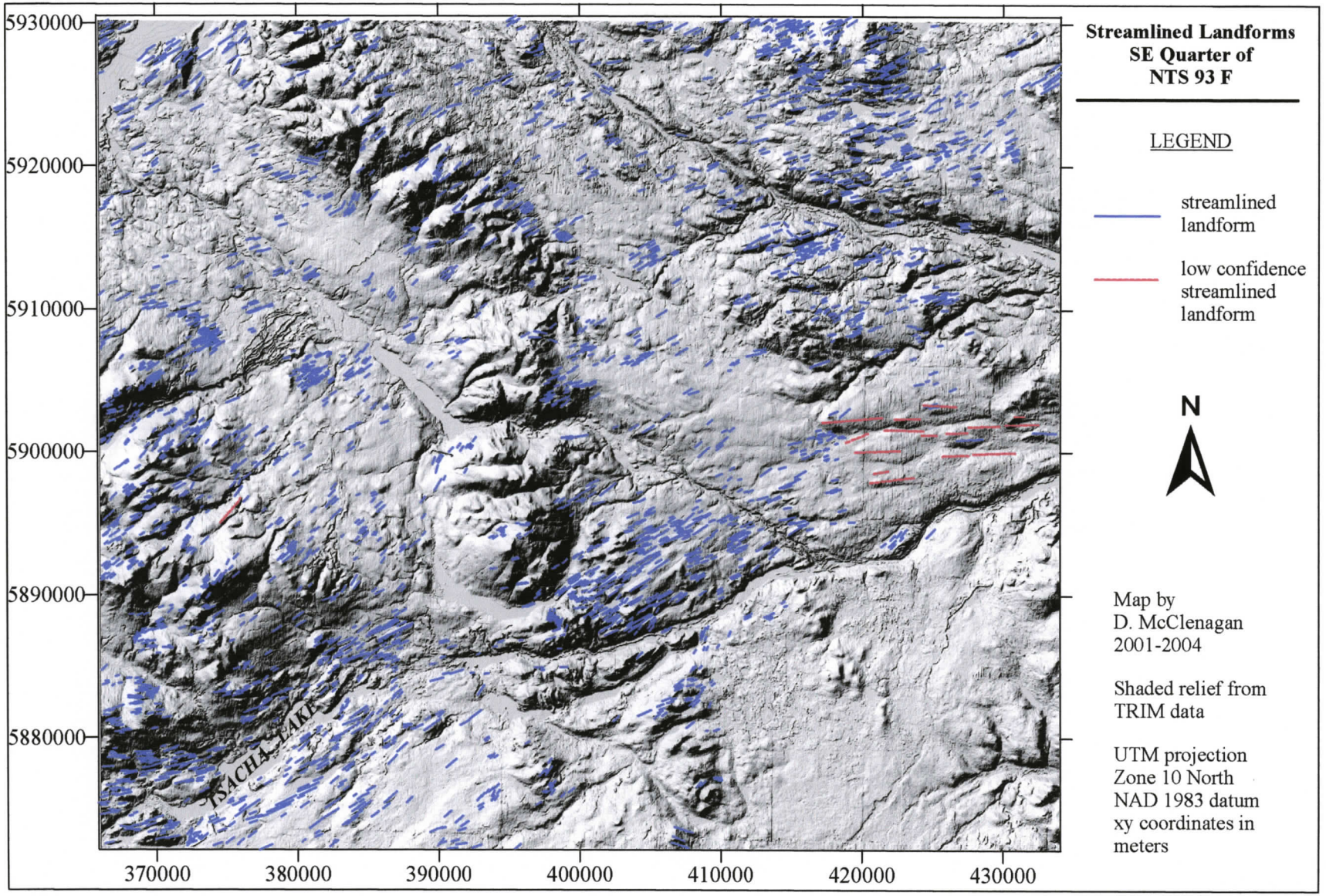
5930000
5920000
5910000
5900000
5890000
5880000
370000
380000
390000
400000
410000
420000
430000
TSACHA LAKE
Streamlined Landforms
SE Quarter of
NTS 93 F
LEGEND
streamlined landform
low confidence streamlined landform
N
Map by
D. McClenagan
2001-2004
Shaded relief from TRIM data
UTM projection
Zone 10 North
NAD 1983 datum
xy coordinates in meters

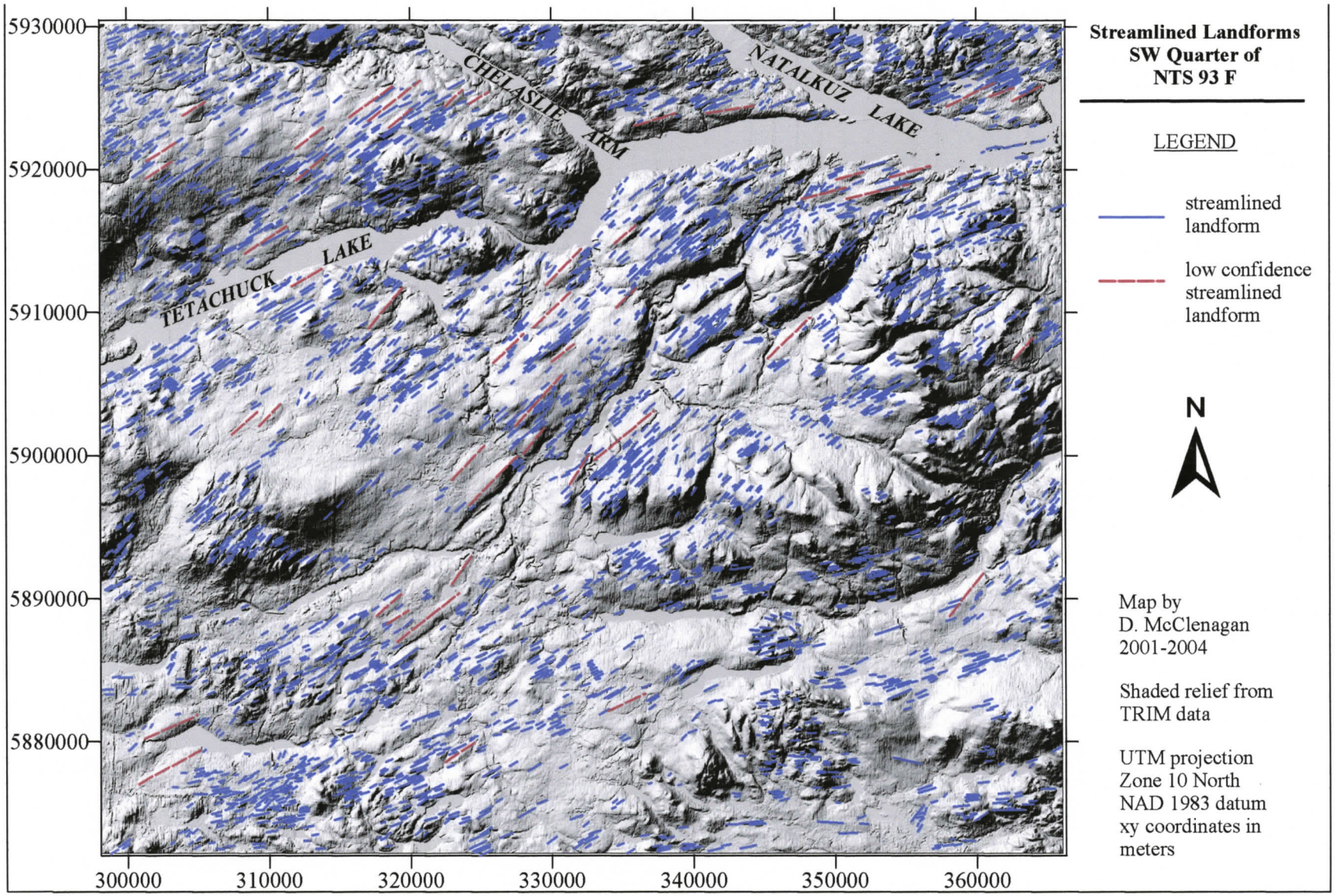
5930000
5920000
5910000
5900000
5890000
5880000
300000
310000
320000
330000
340000
350000
360000
CHELASLIE ARM
NATALKUZ LAKE
TETACHUCK LAKE
Streamlined Landforms
SW Quarter of
NTS 93 F
LEGEND
streamlined landform
low confidence streamlined landform
N
Map by
D. McClenagan
2001-2004
Shaded relief from
TRIM data
UTM projection
Zone 10 North
NAD 1983 datum
xy coordinates in
meters

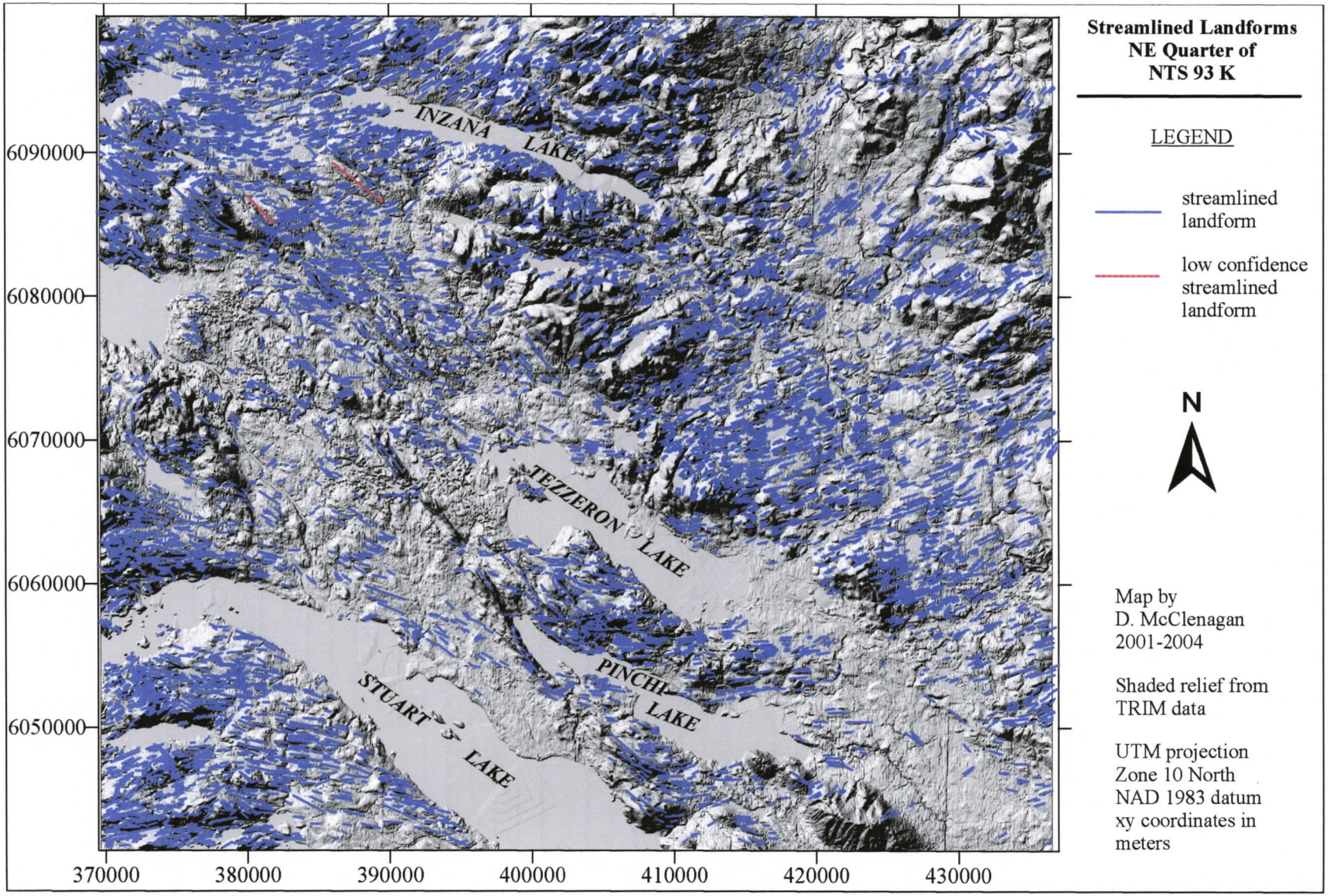
INZANA LAKE
TEZZERON LAKE
PINCHI LAKE
STUART LAKE
6090000
6080000
6070000
6060000
6050000
370000
380000
390000
400000
410000
420000
430000
Streamlined Landforms
NE Quarter of
NTS 93 K
LEGEND
streamlined landform
low confidence streamlined landform
N
Map by
D. McClenagan
2001-2004
Shaded relief from TRIM data
UTM projection
Zone 10 North
NAD 1983 datum
xy coordinates in meters

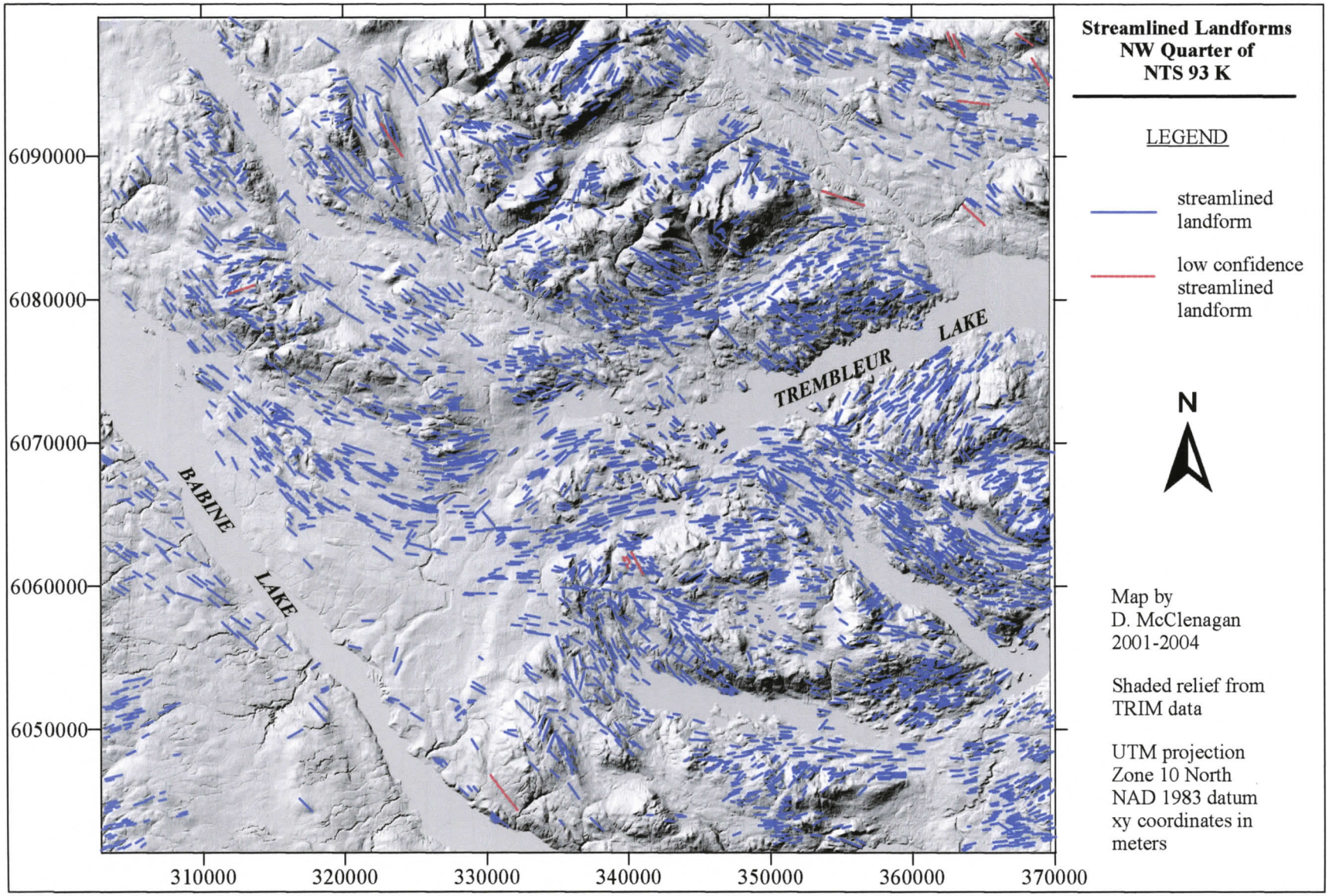
Streamlined Landforms
NW Quarter of
NTS 93 K
LEGEND
streamlined landform
low confidence streamlined landform
N
TREMBLEUR LAKE
BABINE LAKE
6090000
6080000
6070000
6060000
6050000
310000
320000
330000
340000
350000
360000
370000
Map by
D. McClenagan
2001-2004
Shaded relief from
TRIM data
UTM projection
Zone 10 North
NAD 1983 datum
xy coordinates in
meters

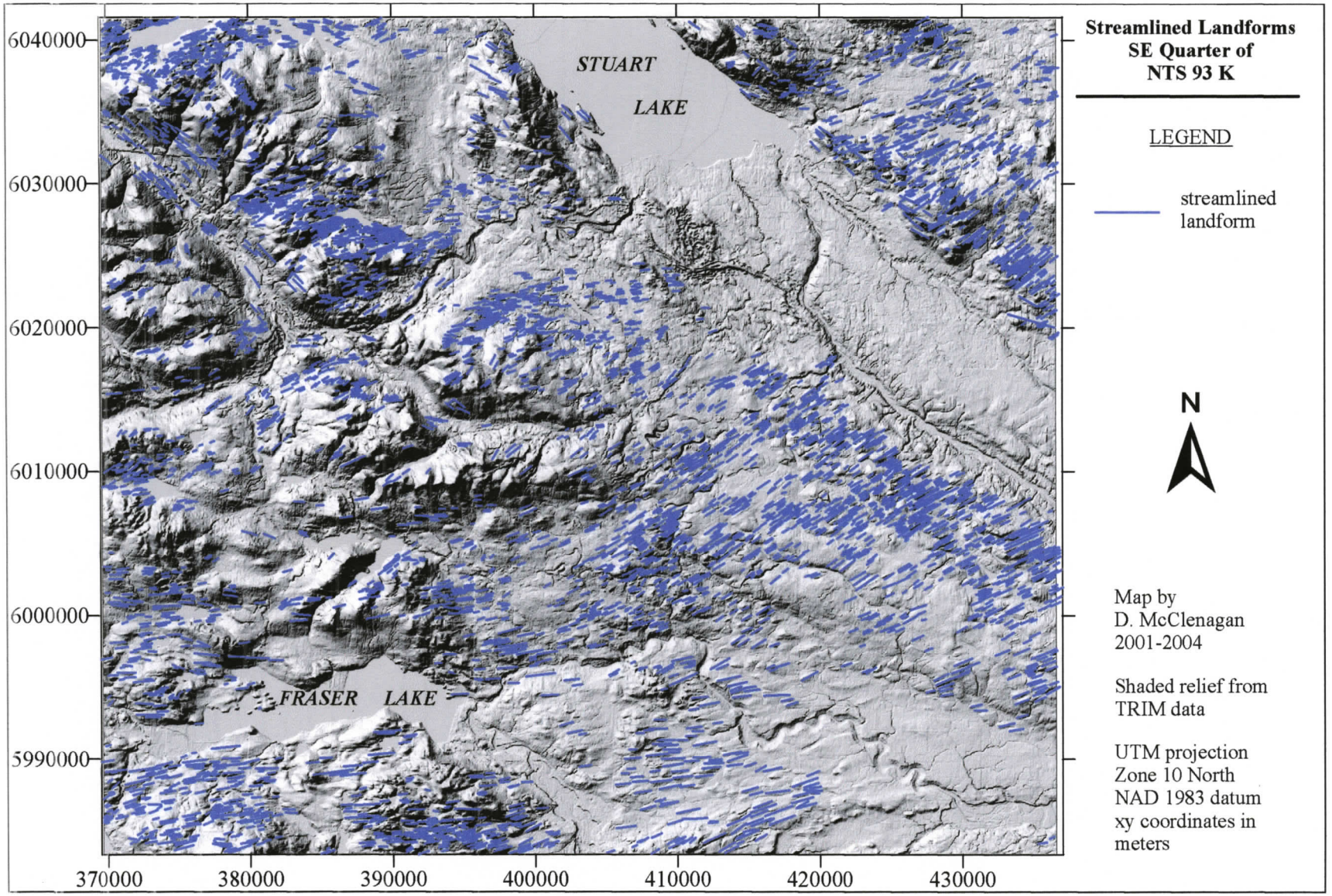
STUART
LAKE
FRASER LAKE
6040000
6030000
6020000
6010000
6000000
5990000
370000
380000
390000
400000
410000
420000
430000
Streamlined Landforms
SE Quarter of
NTS 93 K
LEGEND
streamlined
landform
N
Map by
D. McClenagan
2001-2004
Shaded relief from
TRIM data
UTM projection
Zone 10 North
NAD 1983 datum
xy coordinates in
meters

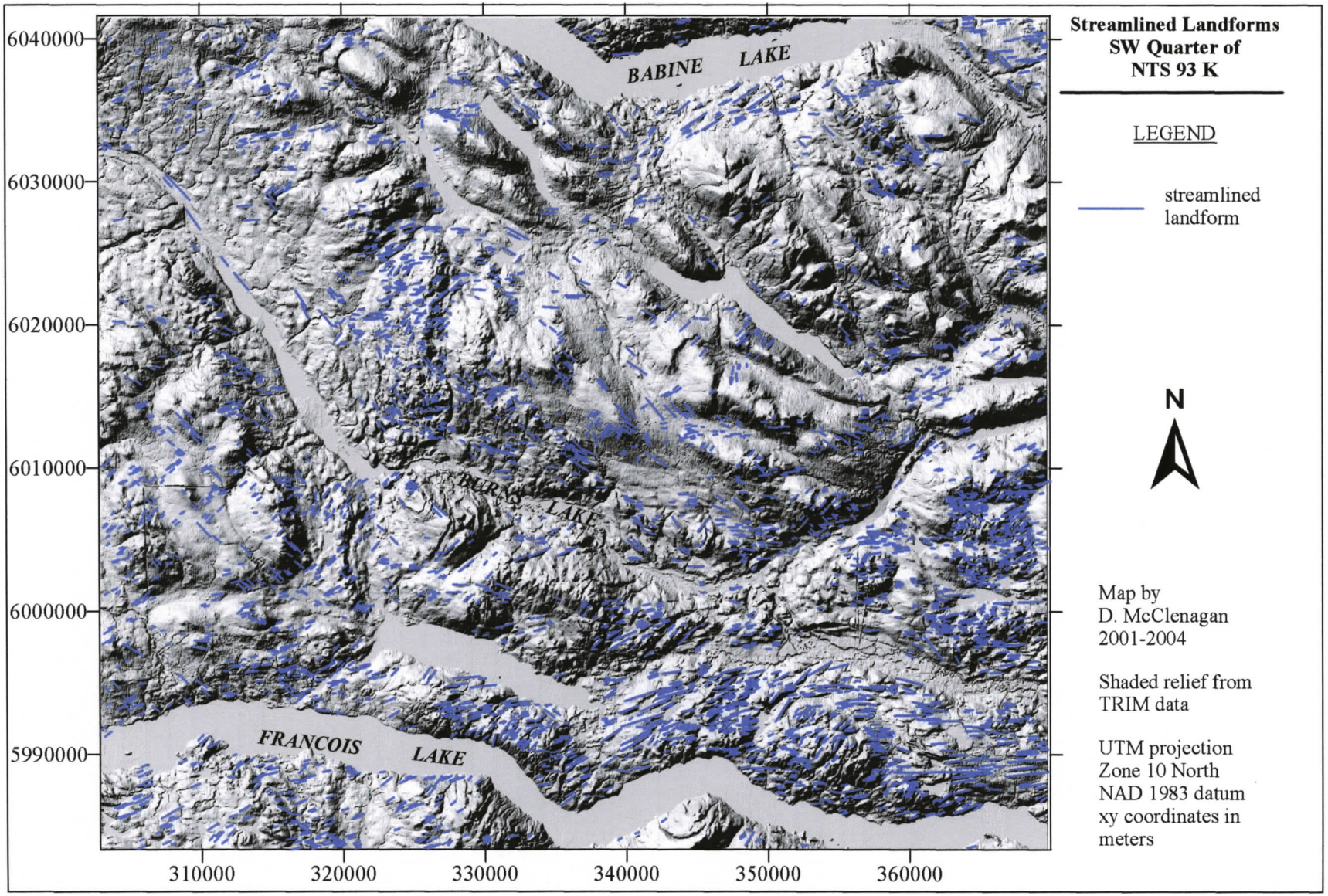
6040000
6030000
6020000
6010000
6000000
5990000
310000
320000
330000
340000
350000
360000
BABINE LAKE
BURNT LAKE
FRANCOIS LAKE
Streamlined Landforms
SW Quarter of
NTS 93 K
LEGEND
streamlined landform
N
Map by
D. McClenagan
2001-2004
Shaded relief from
TRIM data
UTM projection
Zone 10 North
NAD 1983 datum
xy coordinates in
meters

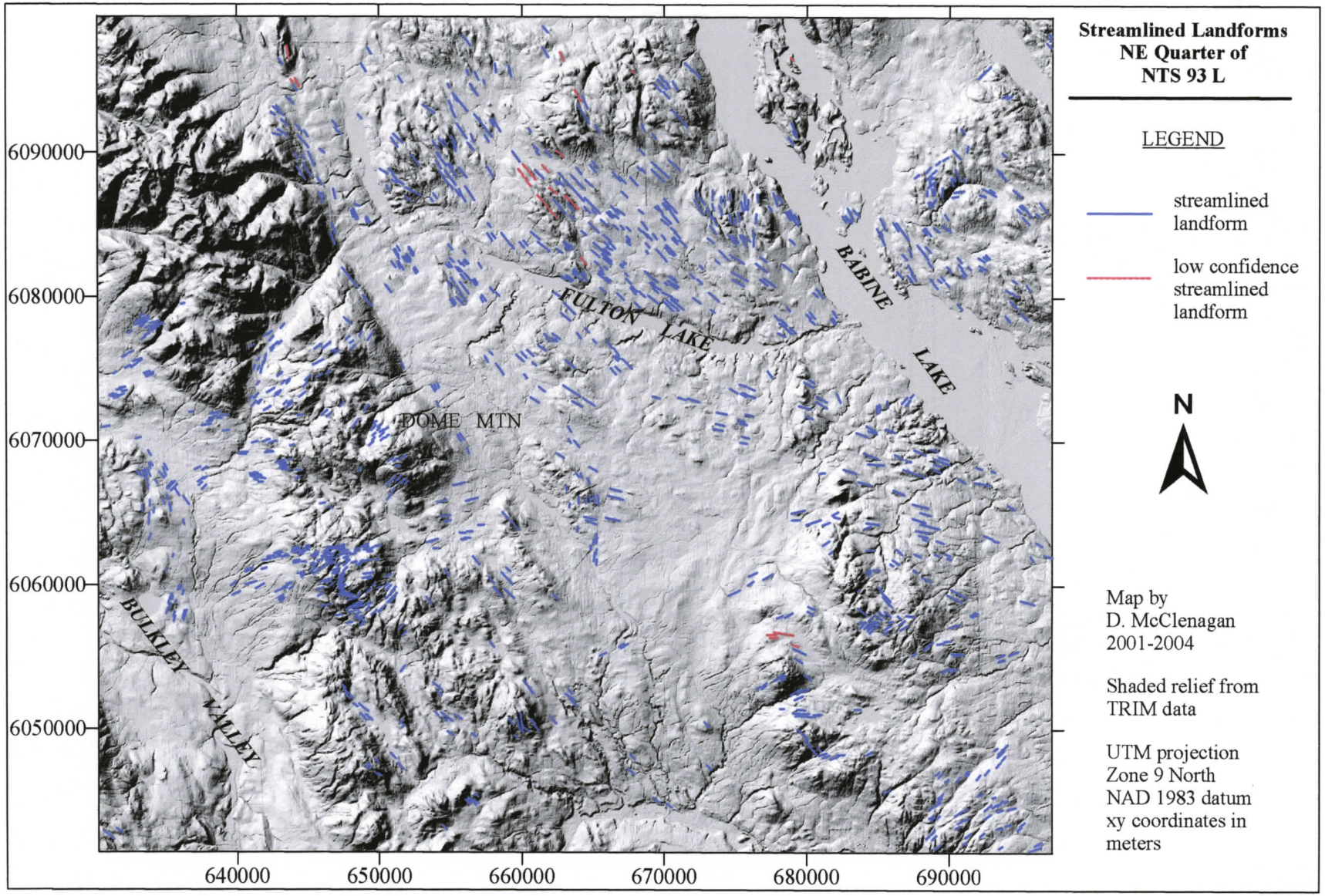
Streamlined Landforms
NE Quarter of
NTS 93 L
LEGEND
streamlined landform
low confidence streamlined landform
N
Map by
D. McClenagan
2001-2004
Shaded relief from TRIM data
UTM projection
Zone 9 North
NAD 1983 datum
xy coordinates in meters
DOME MTN
FULTON LAKE
BABINE LAKE
BULKLEY VALLEY
6090000
6080000
6070000
6060000
6050000
640000
650000
660000
670000
680000
690000

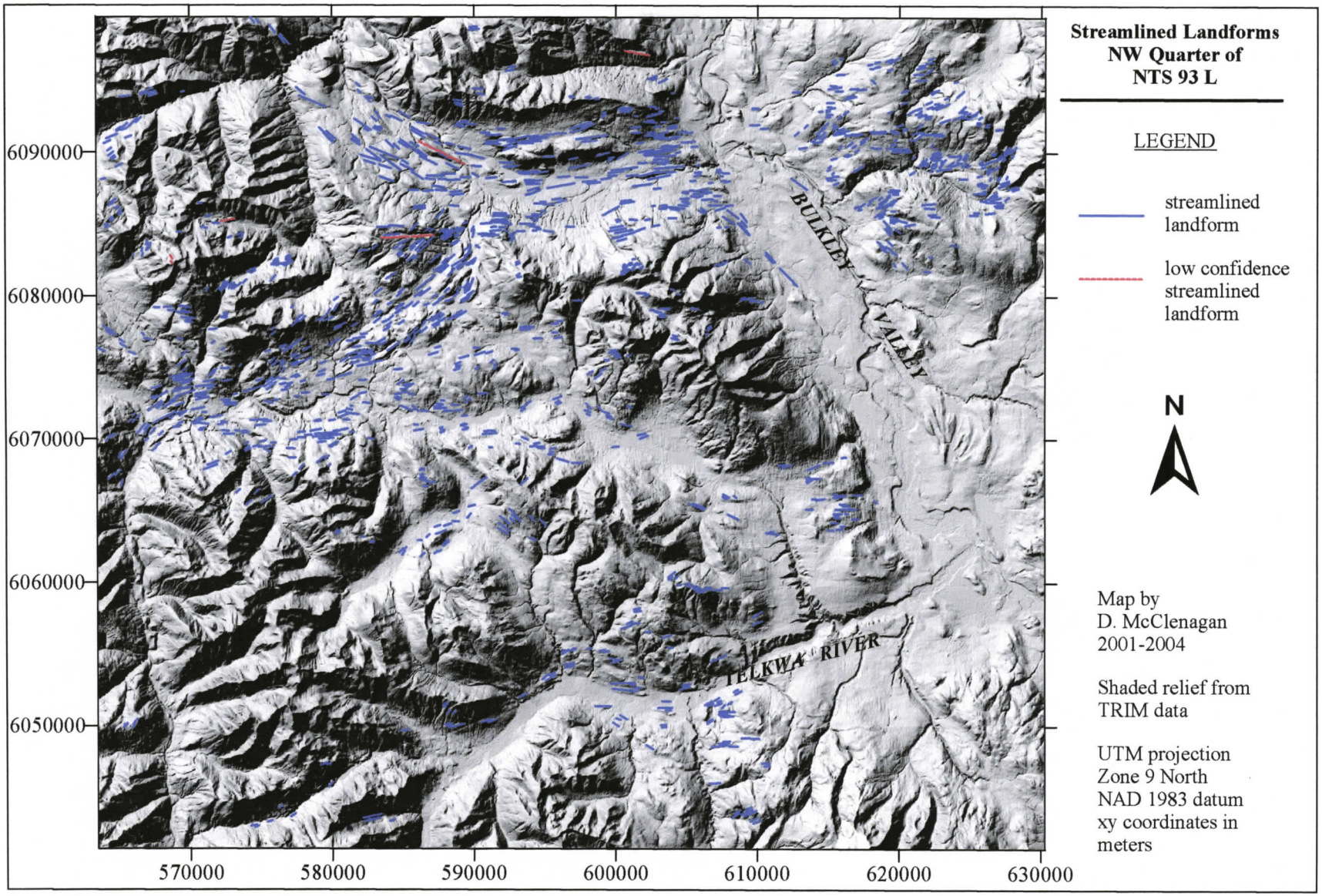
Streamlined Landforms
NW Quarter of
NTS 93 L
LEGEND
streamlined landform
low confidence streamlined landform
N
BULKLEY VALLEY
TELKWA RIVER
6090000
6080000
6070000
6060000
6050000
570000
580000
590000
600000
610000
620000
630000
Map by
D. McClenagan
2001-2004
Shaded relief from
TRIM data
UTM projection
Zone 9 North
NAD 1983 datum
xy coordinates in
meters

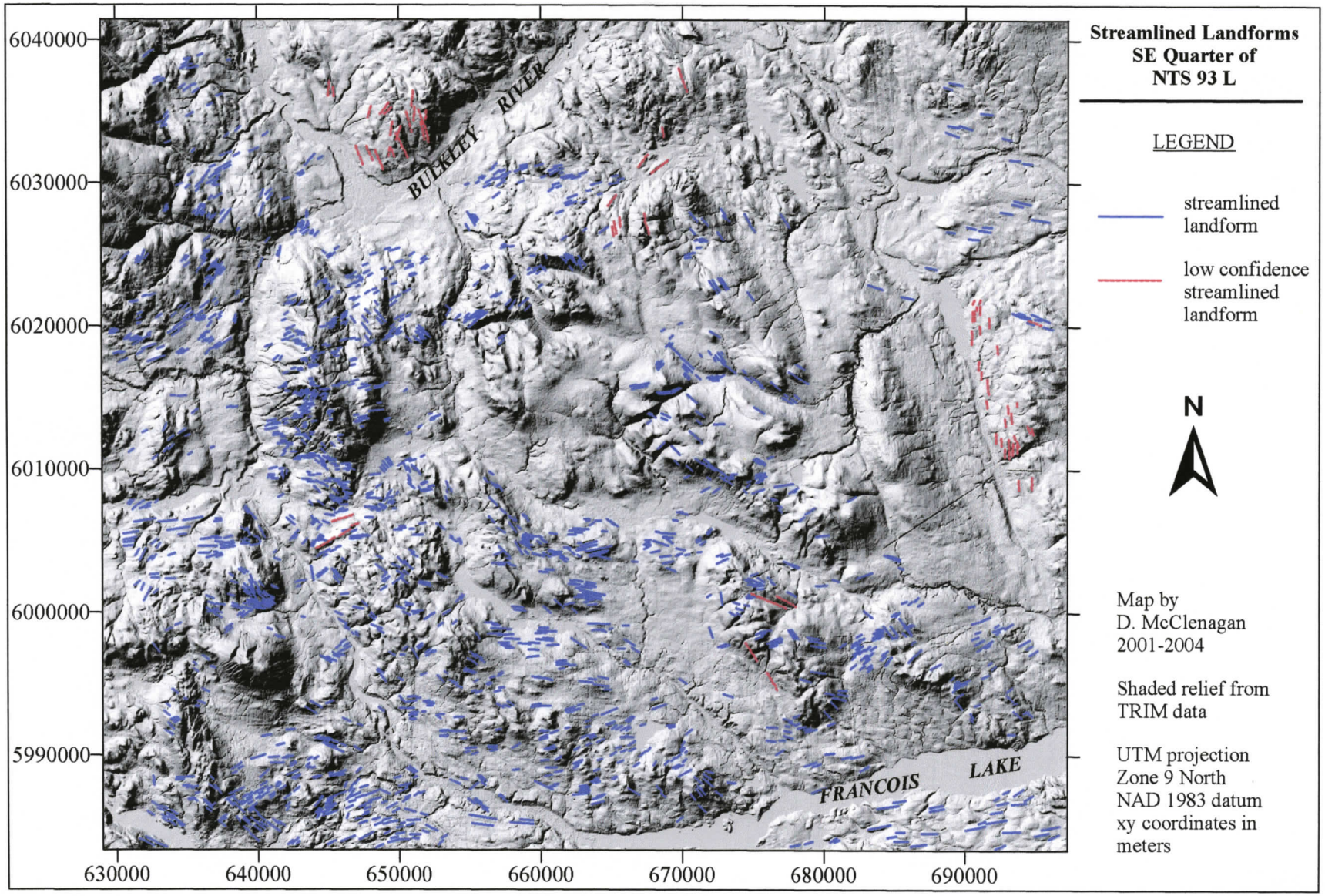
6040000
6030000
6020000
6010000
6000000
5990000
630000
640000
650000
660000
670000
680000
690000
BULKLEY RIVER
FRANCOIS LAKE
Streamlined Landforms
SE Quarter of
NTS 93 L
LEGEND
streamlined landform
low confidence streamlined landform
N
Map by
D. McClenagan
2001-2004
Shaded relief from TRIM data
UTM projection
Zone 9 North
NAD 1983 datum
xy coordinates in meters

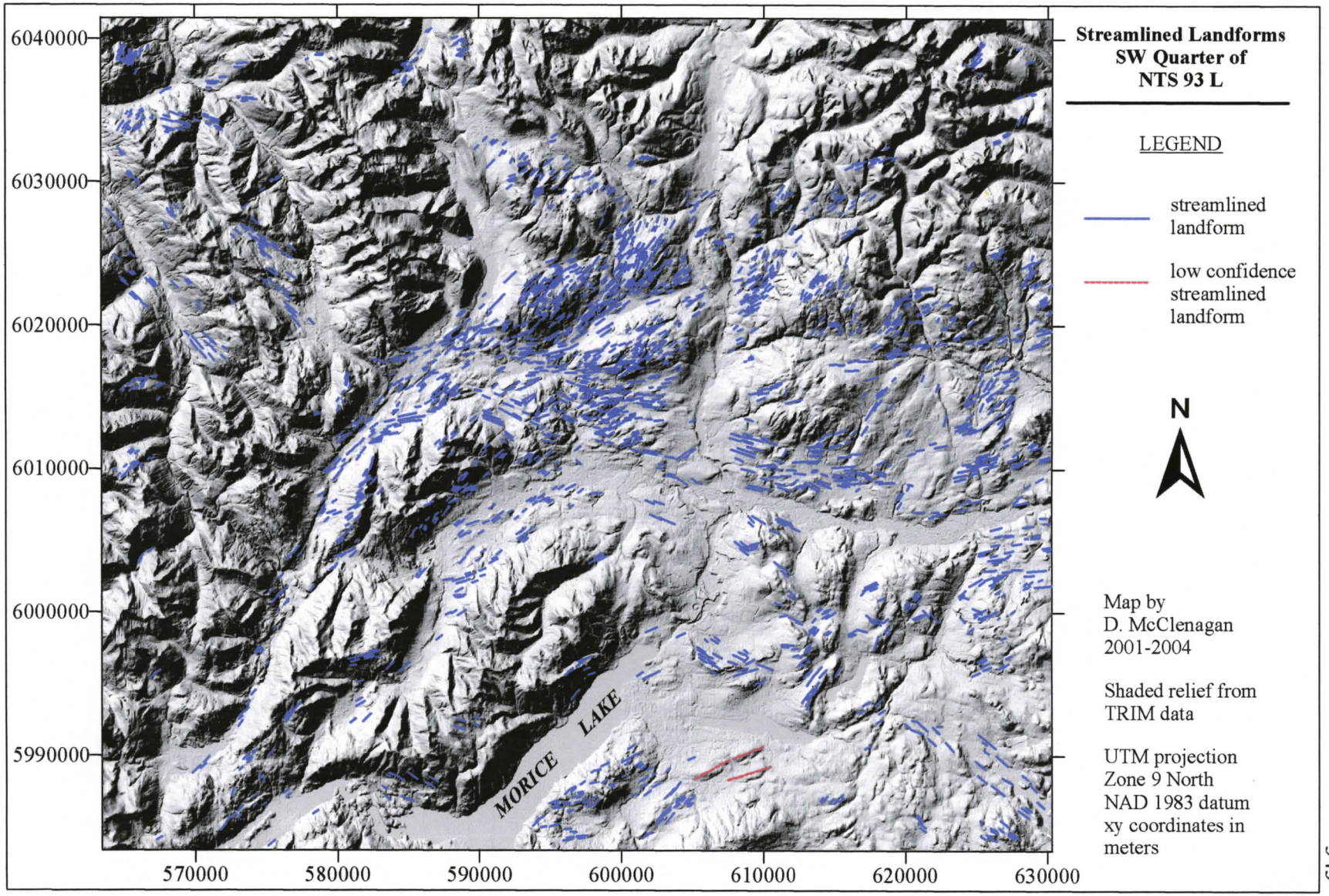
6040000
6030000
6020000
6010000
6000000
5990000
570000
580000
590000
600000
610000
620000
630000
MORICE LAKE
Streamlined Landforms
SW Quarter of
NTS 93 L
LEGEND
streamlined landform
low confidence streamlined landform
N
Map by
D. McClenagan
2001-2004
Shaded relief from TRIM data
UTM projection
Zone 9 North
NAD 1983 datum
xy coordinates in meters

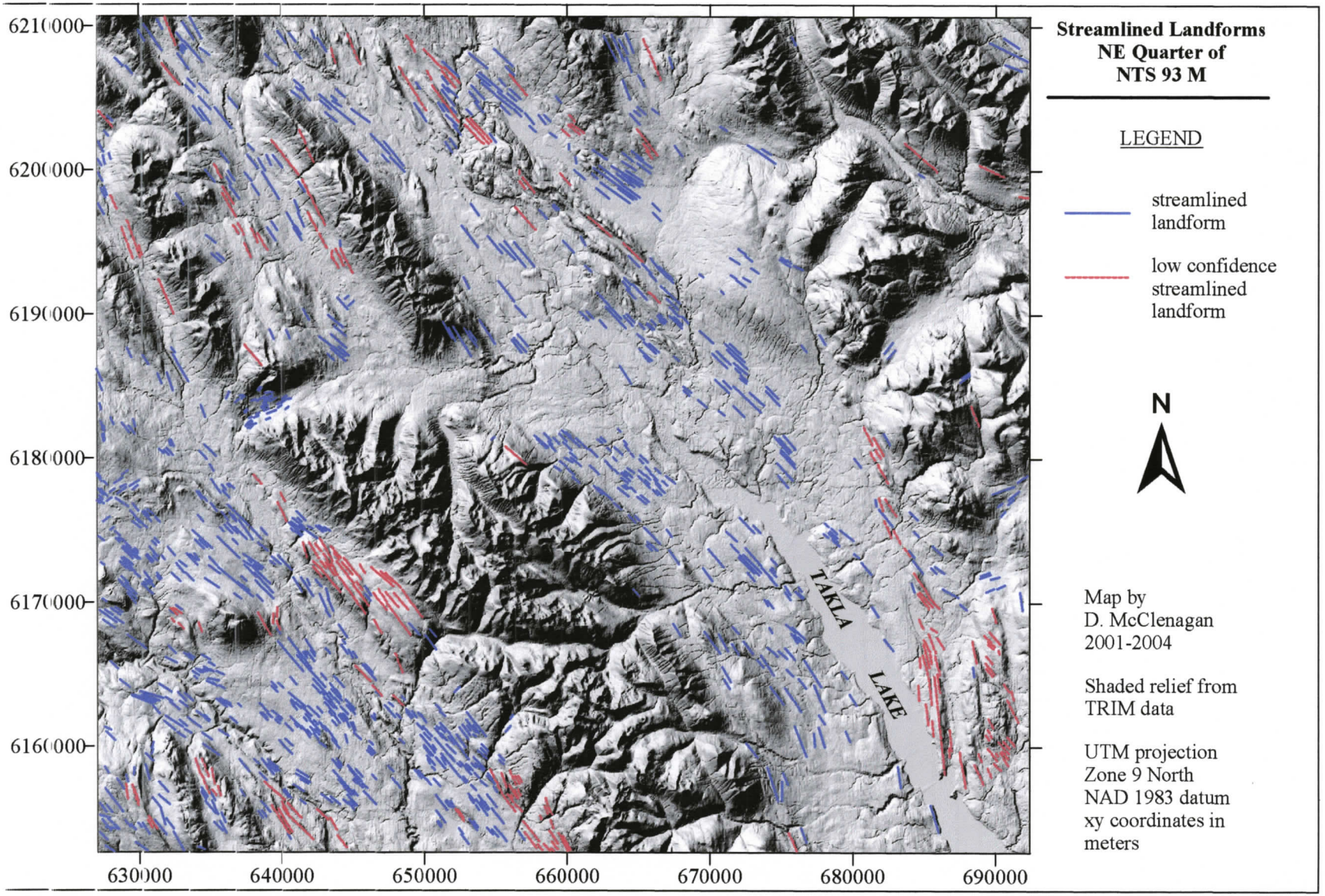
6210000
6200000
6190000
6180000
6170000
6160000
630000
640000
650000
660000
670000
680000
690000
TAKLA
LAKE
Streamlined Landforms
NE Quarter of
NTS 93 M
LEGEND
streamlined landform
low confidence streamlined landform
N
Map by
D. McClenagan
2001-2004
Shaded relief from
TRIM data
UTM projection
Zone 9 North
NAD 1983 datum
xy coordinates in
meters

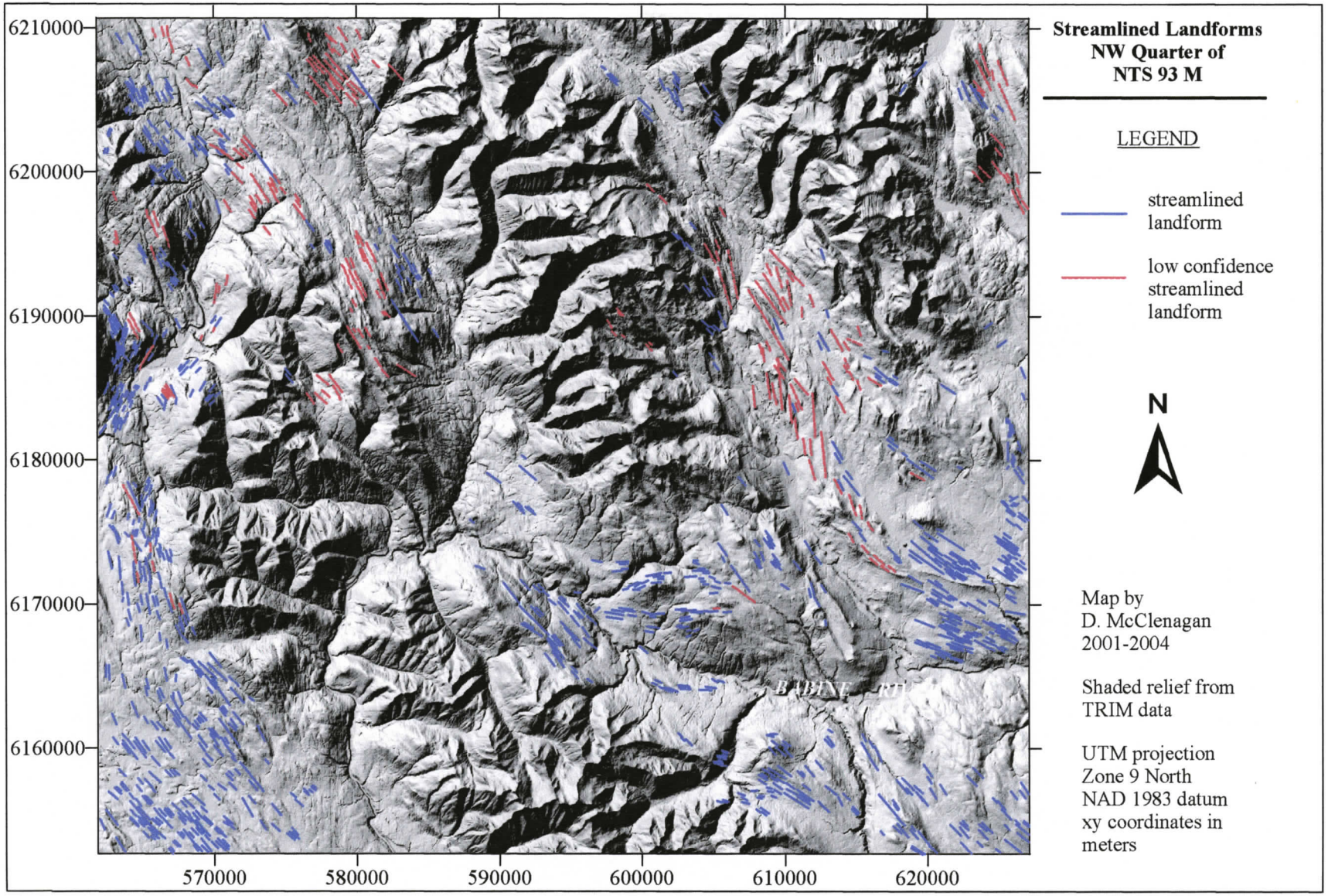
6210000
6200000
6190000
6180000
6170000
6160000
570000
580000
590000
600000
610000
620000
Streamlined Landforms
NW Quarter of
NTS 93 M
LEGEND
streamlined landform
low confidence streamlined landform
N
Map by
D. McClenagan
2001-2004
Shaded relief from
TRIM data
UTM projection
Zone 9 North
NAD 1983 datum
xy coordinates in
meters

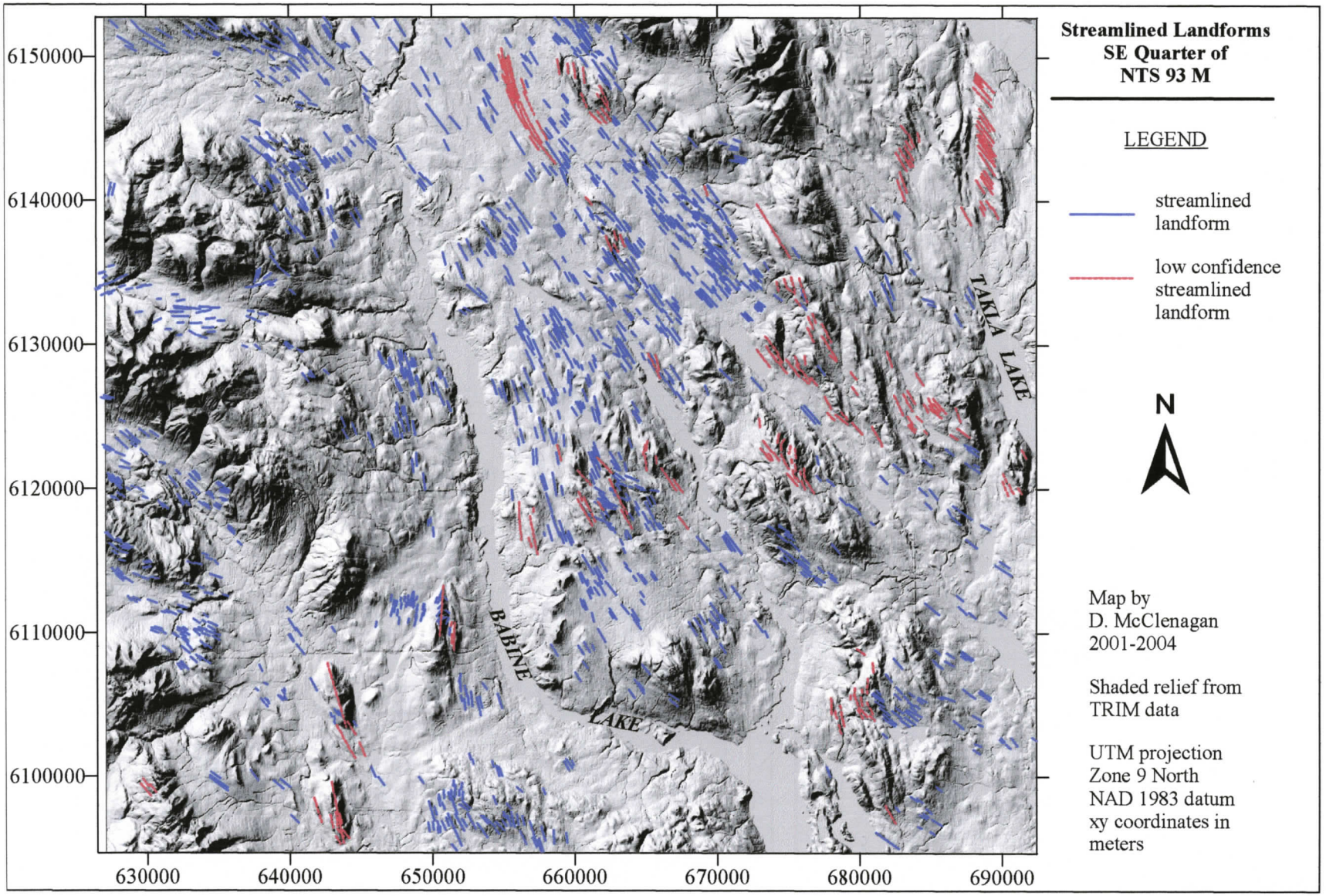
Streamlined Landforms
SE Quarter of
NTS 93 M
LEGEND
streamlined landform
low confidence streamlined landform
N
TAKLA LAKE
BABINE LAKE
Map by
D. McClenagan
2001-2004
Shaded relief from
TRIM data
UTM projection
Zone 9 North
NAD 1983 datum
xy coordinates in
meters
6150000
6140000
6130000
6120000
6110000
6100000
630000
640000
650000
660000
670000
680000
690000

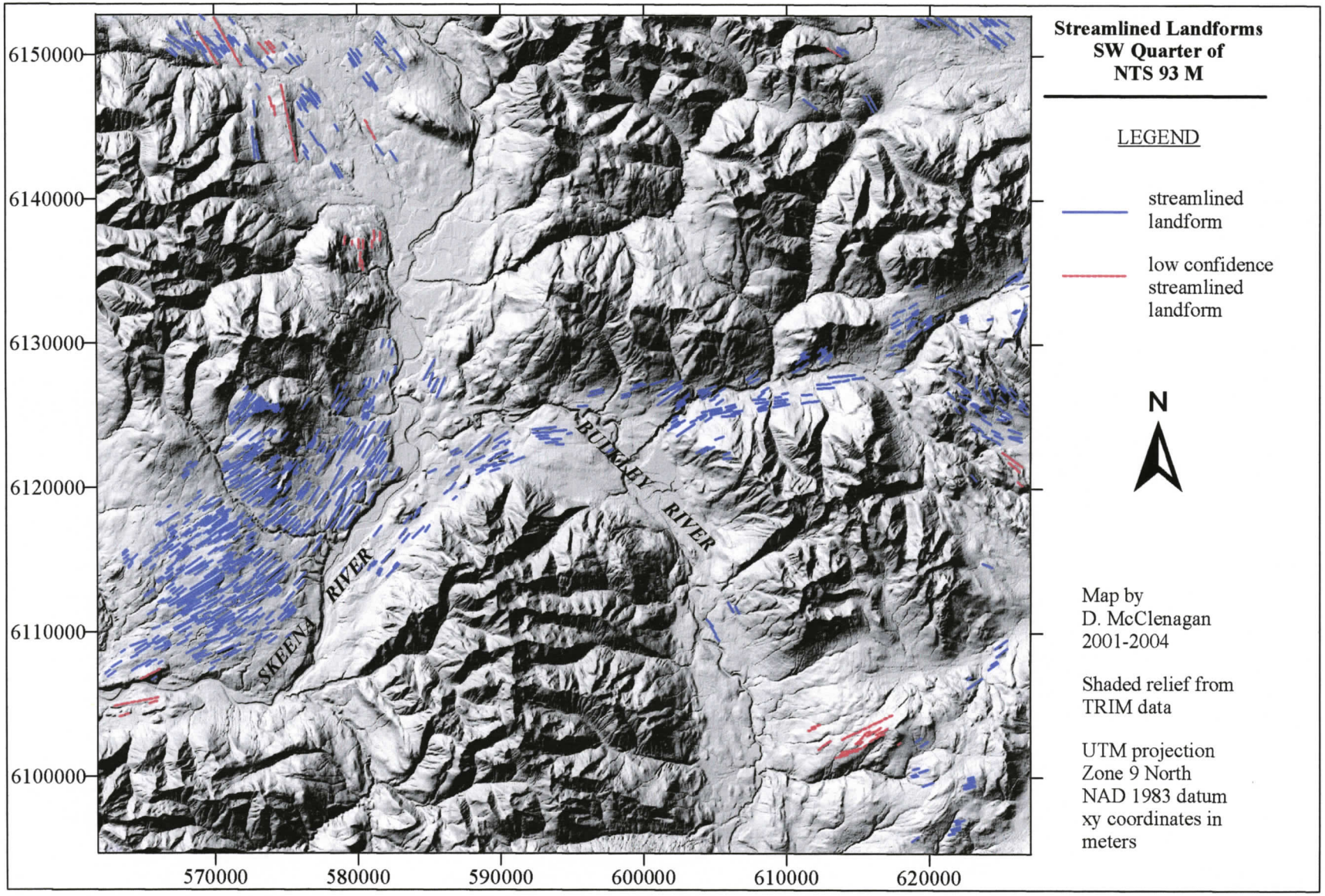
6150000
6140000
6130000
6120000
6110000
6100000
570000
580000
590000
600000
610000
620000
SKEENA RIVER
BULKLEY RIVER
Streamlined Landforms
SW Quarter of
NTS 93 M
LEGEND
streamlined landform
low confidence streamlined landform
N
Map by
D. McClenagan
2001-2004
Shaded relief from TRIM data
UTM projection
Zone 9 North
NAD 1983 datum
xy coordinates in meters

APPENDIX B. LOCATIONS OF STREAMLINED FORMS COMPOSED PRIMARILY OF DIAMICTON

UTM Zone 9			
ID	**Site Name**	**Easting**	**Northing**
44	Hazelton Field	573991	6125452
45	Hazelton Field	570505	6111878
49	Hazelton Field	577272	6116988
50	Hazelton Field	575287	6116861
51	Hazelton Field	574598	6117112
52	Hazelton Field	574517	6117112
53	Hazelton Field	573933	6117647
54	Hazelton Field	573802	6117844
55	Hazelton Field	571230	6113101
56	Hazelton Field	574398	6119770
57	Hazelton Field	574398	6119770
58	Hazelton Field	571514	6119362
59	Hazelton Field	571179	6123492
61	Hazelton Field	571069	6123349
62	Hazelton Field	571087	6123024
63	Hazelton Field	571007	6122576
64	Hazelton Field	571062	6122767
65	Hazelton Field	570948	6122754
66	Hazelton Field	570989	6122228
67	Hazelton Field	571121	6121821
69	Hazelton Field	571347	6121349
70	Hazelton Field	571301	6121140
71	Hazelton Field	571271	6120789
72	Hazelton Field	571414	6120055
73	Hazelton Field	568222	6117009
74	Hazelton Field	568451	6116771
80	Hazelton Field	566809	6116919
81	Hazelton Field	566065	6115118
82	Hazelton Field	565350	6112965
83	Hazelton Field	567052	6109430
84	Hazelton Field	568420	6110210
85	Hazelton Field	569251	6111110
86	Hazelton Field	570877	6112473
87	Hazelton Field	572911	6113842
84b	Hazelton Field	568997	6110742

UTM Zone 9, cont.			
44	Hazelton Peak	573393	6125917
140	Nine Mile Mountain	593815	6132441
141	Nine Mile Mountain	593759	6132368
97	Ootsa Lake	696757	5962565
102	Ootsa Lake	668794	5972630
103	Ootsa Lake	655850	5963294
14	Telkwa Valley	594811	6053297
24	Telkwa Valley	607363	6054376
3	Trout Creek	590515	6085101
7	Trout Creek	593886	6091144
12	Trout Creek	590256	6089609
17	Trout Creek	582544	6074840
18	Trout Creek	582227	6075242
19	Trout Creek	582693	6075400
20	Trout Creek	582900	6078112
22	Trout Creek	587576	6082248
10, 11	Trout Creek	591528	6090655

UTM Zone 10			
ID	**Site Name**	**Easting**	**Northing**
26	Endako	342260	5999631
29	Endako	341011	5995903
30	Endako	341427	5996352
31	Holy Cross Road	385800	5990584
32	Holy Cross Road	385528	5988956
33	Holy Cross Road	385935	5987211
34	Holy Cross Road	385969	5985130
35	Holy Cross Road	386067	5984486
36	Holy Cross Road	386025	5983767
37	Holy Cross Road	386773	5979153
38	Holy Cross Road	386946	5979865
39	Holy Cross Road	386315	5980998
40	Holy Cross Road	385863	5982176
41	Holy Cross Road	385917	5981870
42	Holy Cross Road	385861	5982638
43	Holy Cross Road	385890	5982980
94	Ootsa Lake	306851	5986519

APPENDIX C. STREAMLINED BEDROCK FORMS

Slope mode: u = uphill, d = downhill, l = level, nd = no data

ID	Location	Type of erosional mark	Orien-tation (deg.)	Elevation (m)	Slope mode	UTM zone	Easting	Northing
97	Ootsa Lake	medium small SBF	105	853	nd	9	696757	5962565
98	Ootsa Lake	medium small SBF	100	853	nd	9	696721	5962589
100	Ootsa Lake	medium small SBF	107	944	nd	9	672963	5973038
94	Ootsa Lake	furrow	78	817	nd	10	306851	5986519
95	Ootsa Lake	SBF	75	937	nd	10	311803	5958706
28	Endako	medium SBF	60	811	nd	10	342398	5991917
89	Microwave Rdg.	medium SBF	263	1484	nd	9	603358	6058298
90	Microwave Rdg.	furrows	243, 260	1487	nd	9	603485	6058875
91	Microwave Rdg.	furrow	288	1720	u	9	599186	6063364
92	Microwave Rdg.	rat-tails	265	1647	u,d	9	600055	6062064
92	Microwave Rdg.	medium SBF	270	1647	u	9	600055	6062064
93	Microwave Rdg.	rat-tails	264	1588	nd	9	600090	6061410
107	Microwave Rdg.	furrows	285	1751	u	9	599033	6063518
108	Microwave Rdg.	furrow	283	1745	u	9	599063	6063506
110	Microwave Rdg.	small SBF	270	1643	u	9	600161	6062129
111	Microwave Rdg.	medium small SBF	276	1638	u	9	600160	6062059
112	Microwave Rdg.	medium SBF	270	1639	u	9	600064	6061969
112	Microwave Rdg.	rat-tails	270	1639	u	9	600064	6061969
115	Microwave Rdg.	rat-tails	265-275	1644	u	9	599895	6062133
116	Microwave Rdg.	rat-tails	275-305	1638	u	9	599898	6062083
117	Microwave Rdg.	rat-tails	270	1614	u	9	599498	6061679
118	Dome Mt. Peak	rat-tails	265-253	1693	u	9	650979	6069139
119	Dome Mt. Peak	grooves	270	1714	u	9	650883	6069123
120	Dome Mt. Peak	small SBF	253	1745	d	9	650805	6069033
123	Dome Mt. Peak	rat-tails	300-268	1705	u	9	650877	6069272
124	Dome Mt. Peak	rat-tails	248	1705	u	9	650881	6069273
125	Dome Mt. Peak	rat-tails	275-253	1704	u	9	650889	6069269
126	Dome Mt. Peak	rat-tails	263-253	1704	u	9	650903	6069253
128	Dome Mt. Peak	rat-tails	280-260	1684	u	9	651047	6068934
129	Dome Mt. Peak	small SBF	245	1679	u	9	651076	6068829
130	Dome Mt. Peak	rat-tails	255	1678	u	9	651083	6068843
131	Dome Mt. Peak	medium SBF	253	1677	u	9	651120	6068858
131	Dome Mt. Peak	rat-tails	278	1677	n	9	651120	6068858
132	Dome Mt. Peak	rat-tails	263	1671	u	9	651114	6068893
133	Dome Mt. Peak	rat-tails	253	1670	u	9	651104	6068908
134	Dome Mt. Peak	medium SBF	253	1672	u	9	651194	6068866
135	Dome Mt. Peak	rat-tails	259	1674	u	9	651210	6068843

ID	Location	Type of erosional mark	Orien-tation (deg.)	Elevation (m)	Slope mode	UTM zone	Easting	Northing
152a	Dome Mt. Mine	medium SBF	245	1369	u	9	653128	6068868
152a	Dome Mt. Mine	rat-tails	248	1369	u	9	653128	6068868
152b	Dome Mt. Mine	rat-tails	275-258	1365	u	9	653129	6068795
152d	Dome Mt. Mine	rat-tails	253	1369	u	9	653121	6068803
152e	Dome Mt. Mine	rat-tails	258	1369	u	9	653122	6068806
152f	Dome Mt. Mine	rat-tails	255	1369	u	9	653117	6068802
152h	Dome Mt. Mine	rat-tails	265	1368	u	9	653126	6068810
152i	Dome Mt. Mine	rat-tails	245	1370	u	9	653122	6068825
152j	Dome Mt. Mine	rat-tails	238-245	1372	u	9	653117	6068843
152k	Dome Mt. Mine	medium SBF	255	1371	u	9	653120	6068843
152k	Dome Mt. Mine	rat-tails	235-252	1371	u	9	653120	6068843
152l	Dome Mt. Mine	rat-tails	245-233	1367	u	9	653137	6068850
152o	Dome Mt. Mine	rat-tails	208	1367	u	9	653134	6068850
152o	Dome Mt. Mine	rat-tails	245-255	1367	u	9	653134	6068850
152t	Dome Mt. Mine	rat-tails	235-243	1364	u	9	653145	6068860
147	Hudson Bay Mt.	small SBF	262	1715	u	9	610141	6072015
148	Hudson Bay Mt.	medium SBF	253	1692	u	9	610383	6071818
148	Hudson Bay Mt.	small SBF	253	1692	u	9	610383	6071818
151	Hudson Bay Mt.	rat-tails	263	1177	l	9	612806	6069111
154	Hudson Bay Mt.	small SBF	270	1732	u	9	604744	6077826
155	Hudson Bay Mt.	miniature SBF	285-265	1859	l	9	605053	6077648
162	Hudson Bay Mt.	medium small SBF	210	1983	u	9	605210	6077153
162	Hudson Bay Mt.	miniature SBF	210	1983	u	9	605210	6077153
164	Hudson Bay Mt.	miniature SBF	300	1942	d	9	605165	6077273
165	Hudson Bay Mt.	miniature SBF	355	1875	u	9	605133	6077519
167	Hudson Bay Mt.	medium SBF	270	1563	u	9	604796	6078499
23	Trout Creek	medium SBF	240	862	u	9	588880	6083663
143	Nine Mile Mt.	furrows	240	1610	l	9	594316	6131209
47	Hazelton Field	small SBF	223	603	l	9	568611	6115874

APPENDIX D. CLOSED CONTOURS LESS THAN 100 KM^2 WITH LENGTH AND WIDTH AXES

The following pages comprise 20 maps of closed contours between 2.5 km^2 and 100 km^2 in area, shown with constructed length and width axes. The maps are numbered 1 – 20, starting at the northwest corner of the study area and proceeding west to east, north to south. The map areas overlap so that the entire outline of every closed contour between 2.5-100 km^2 is visible on at least one map. Please refer to Figure 96 (map pocket) to see all closed contours on one map. North is always towards the top of the page.

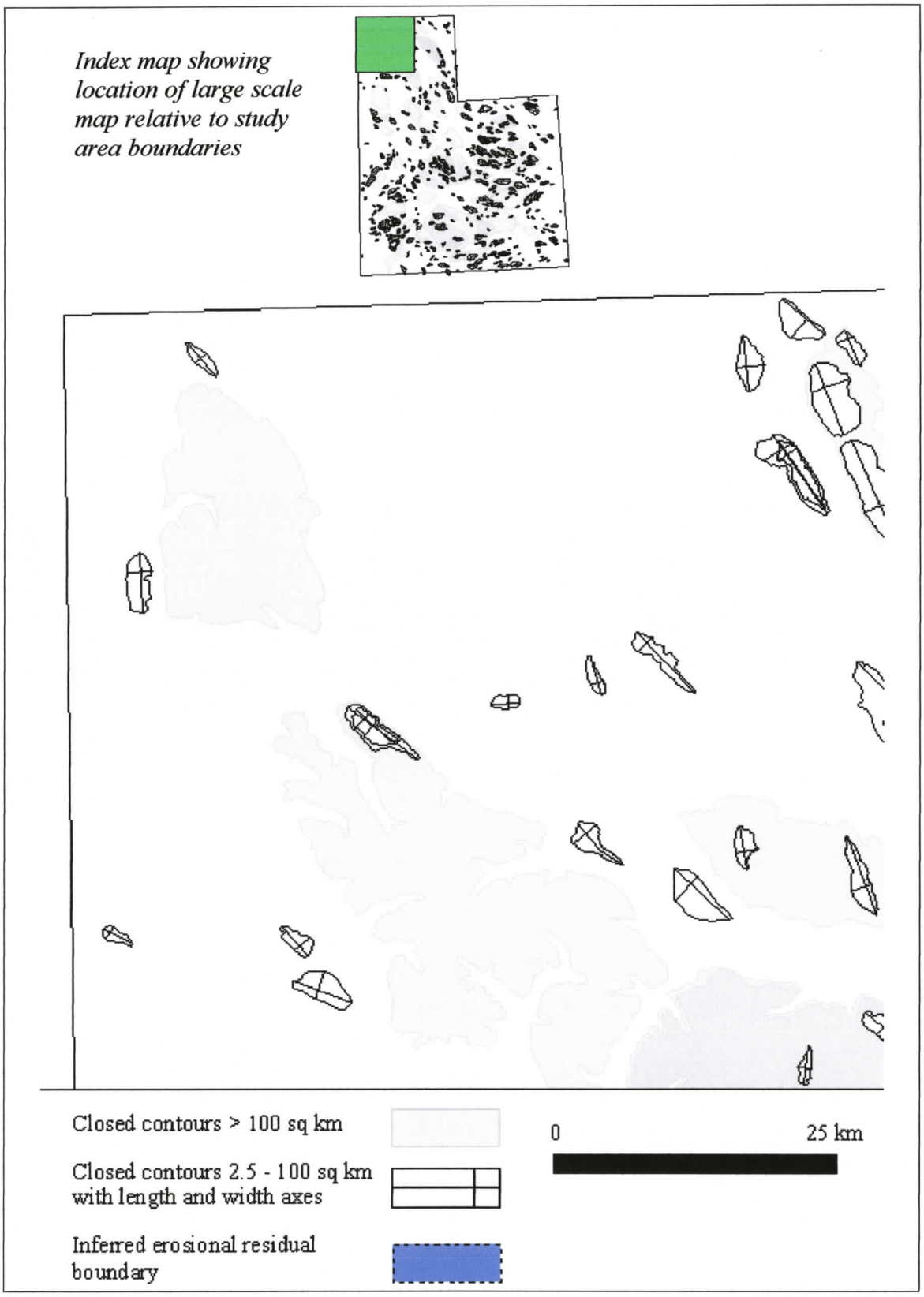
Index map showing location of large scale map relative to study area boundaries
Closed contours > 100 sq km
Closed contours 2.5 - 100 sq km with length and width axes
Inferred erosional residual boundary
0
25 km

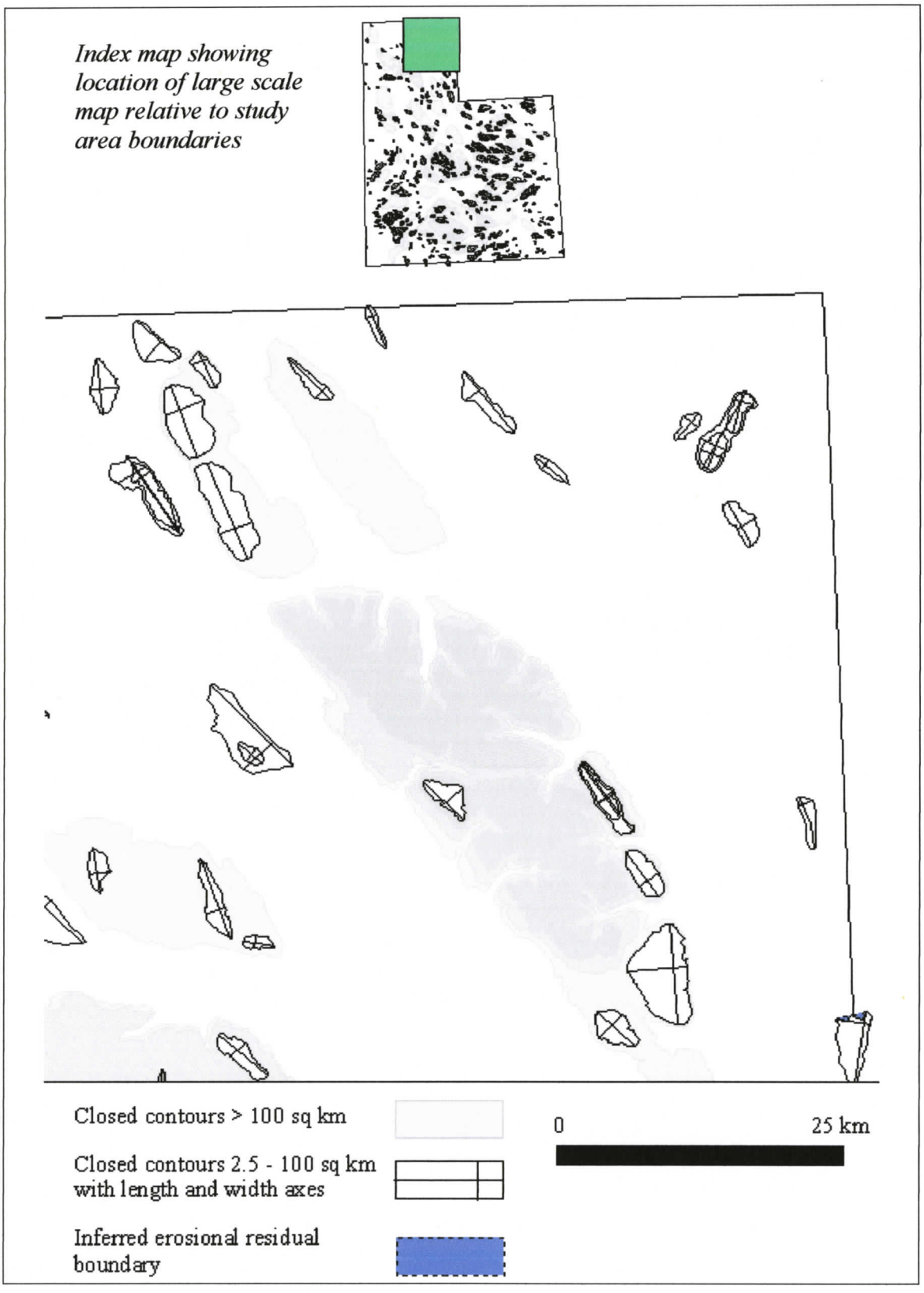
Index map showing location of large scale map relative to study area boundaries
Closed contours > 100 sq km
Closed contours 2.5 - 100 sq km with length and width axes
Inferred erosional residual boundary
0
25 km

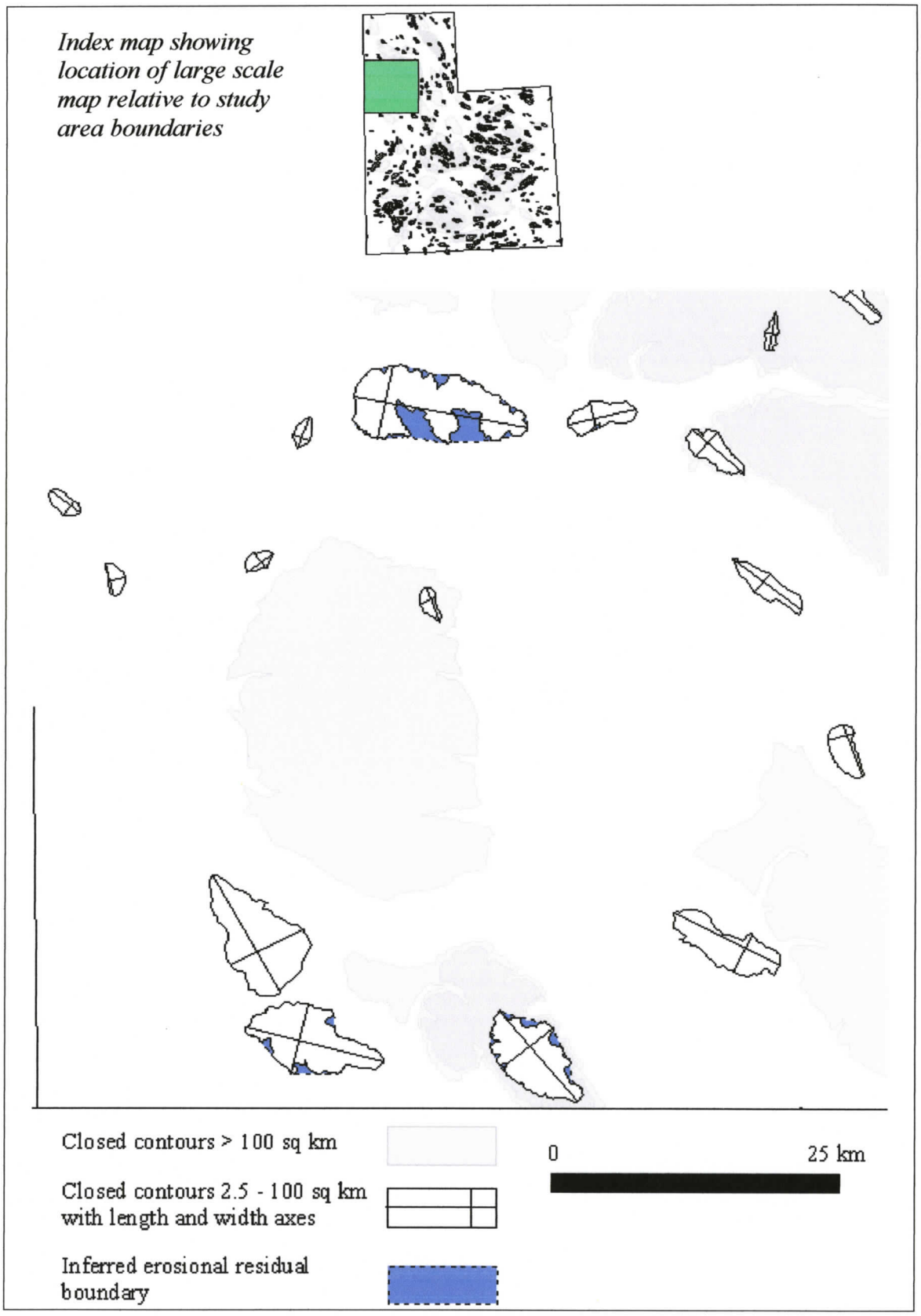
Index map showing location of large scale map relative to study area boundaries
Closed contours > 100 sq km
Closed contours 2.5 - 100 sq km with length and width axes
Inferred erosional residual boundary
0
25 km


Index map showing location of large scale map relative to study area boundaries
Closed contours > 100 sq km
Closed contours 2.5 - 100 sq km with length and width axes
Inferred erosional residual boundary
0
25 km

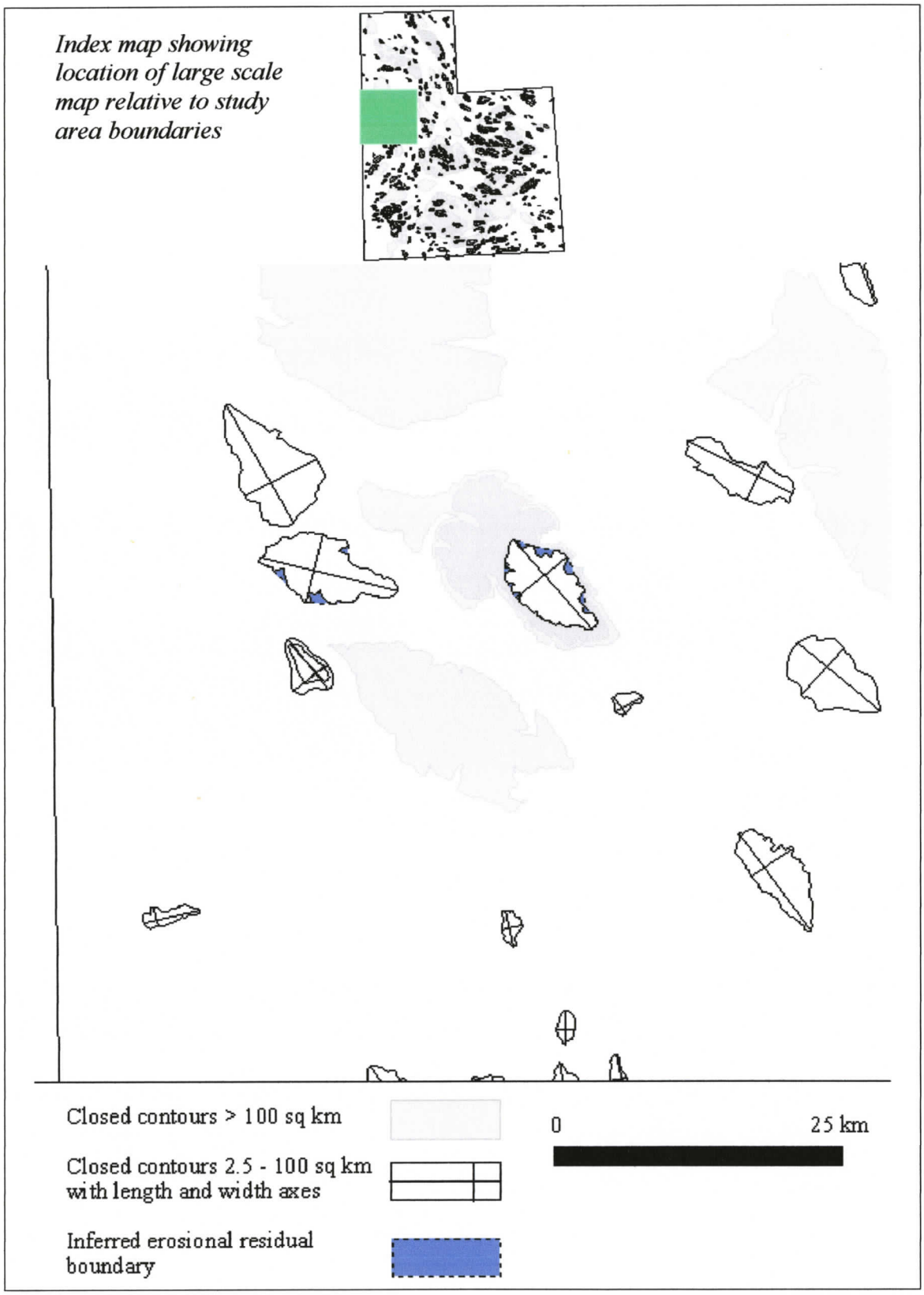
Index map showing location of large scale map relative to study area boundaries
Closed contours > 100 sq km
Closed contours 2.5 - 100 sq km with length and width axes
Inferred erosional residual boundary
0
25 km


Index map showing location of large scale map relative to study area boundaries
Closed contours > 100 sq km
Closed contours 2.5 - 100 sq km with length and width axes
Inferred erosional residual boundary
0
25 km

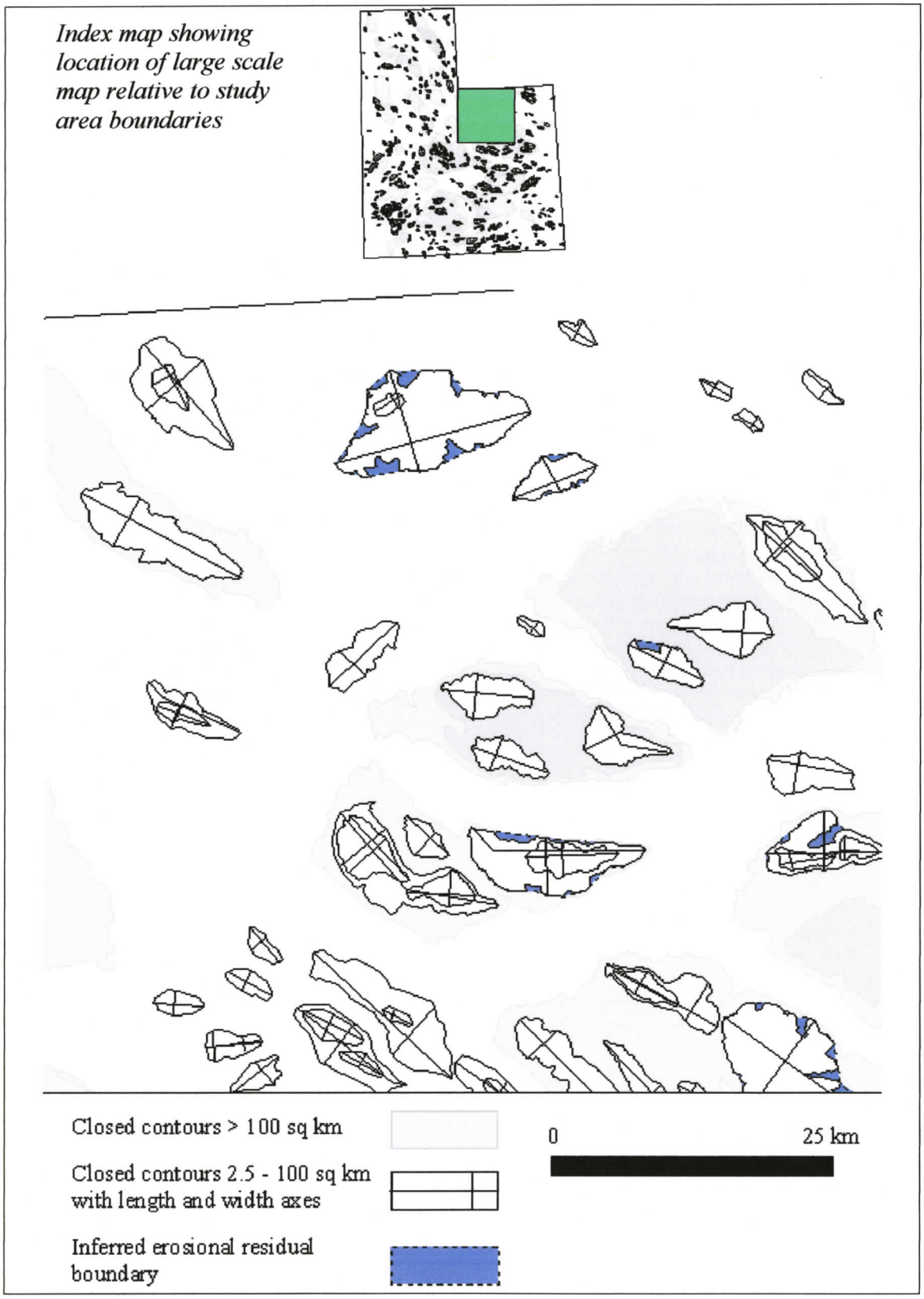
Index map showing location of large scale map relative to study area boundaries
Closed contours > 100 sq km
Closed contours 2.5 - 100 sq km with length and width axes
Inferred erosional residual boundary
0
25 km


Index map showing location of large scale map relative to study area boundaries
Closed contours > 100 sq km
Closed contours 2.5 - 100 sq km with length and width axes
Inferred erosional residual boundary
0
25 km

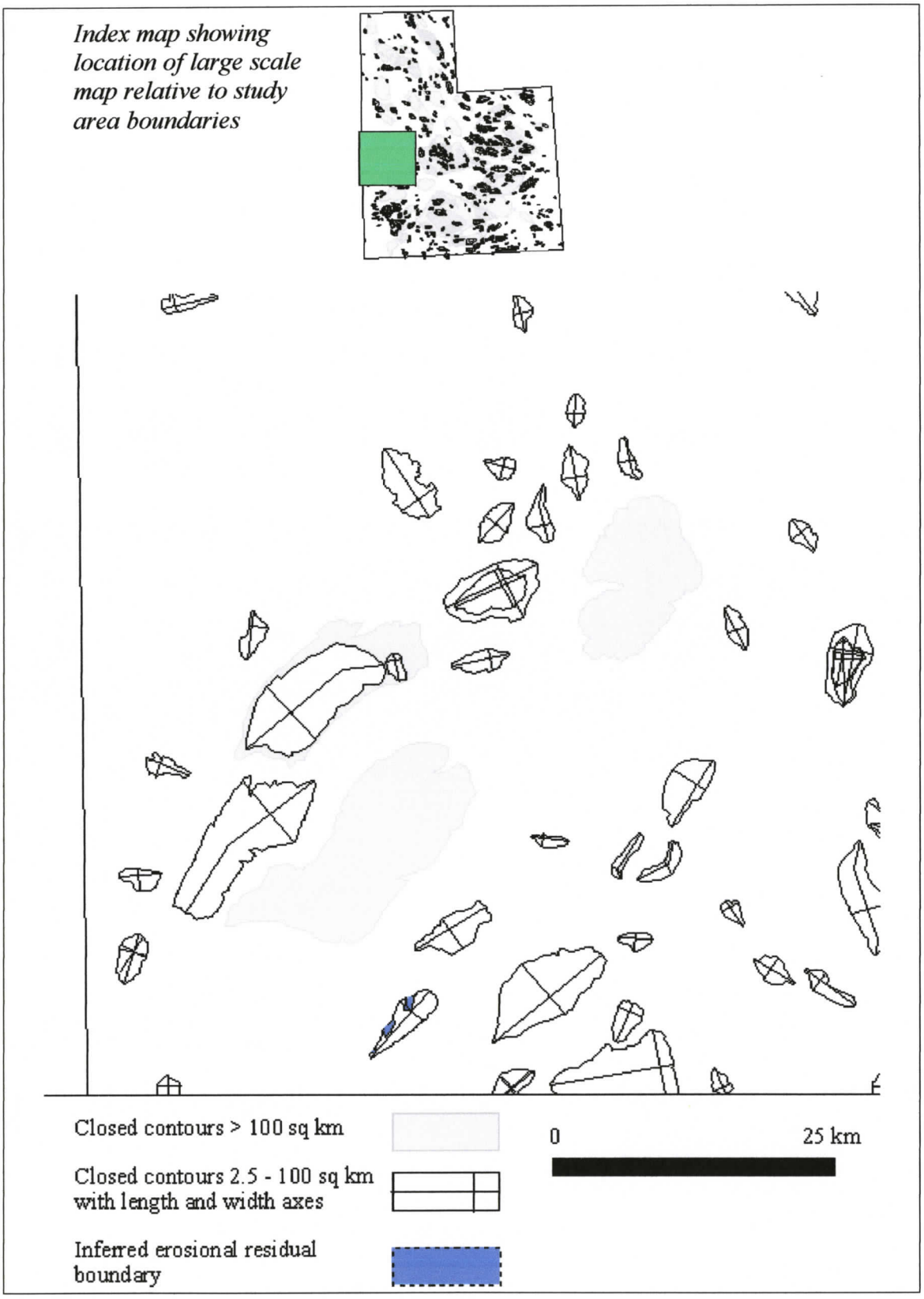
Index map showing location of large scale map relative to study area boundaries
Closed contours > 100 sq km
Closed contours 2.5 - 100 sq km with length and width axes
Inferred erosional residual boundary
0
25 km


Index map showing location of large scale map relative to study area boundaries
Closed contours > 100 sq km
Closed contours 2.5 - 100 sq km with length and width axes
Inferred erosional residual boundary
0
25 km

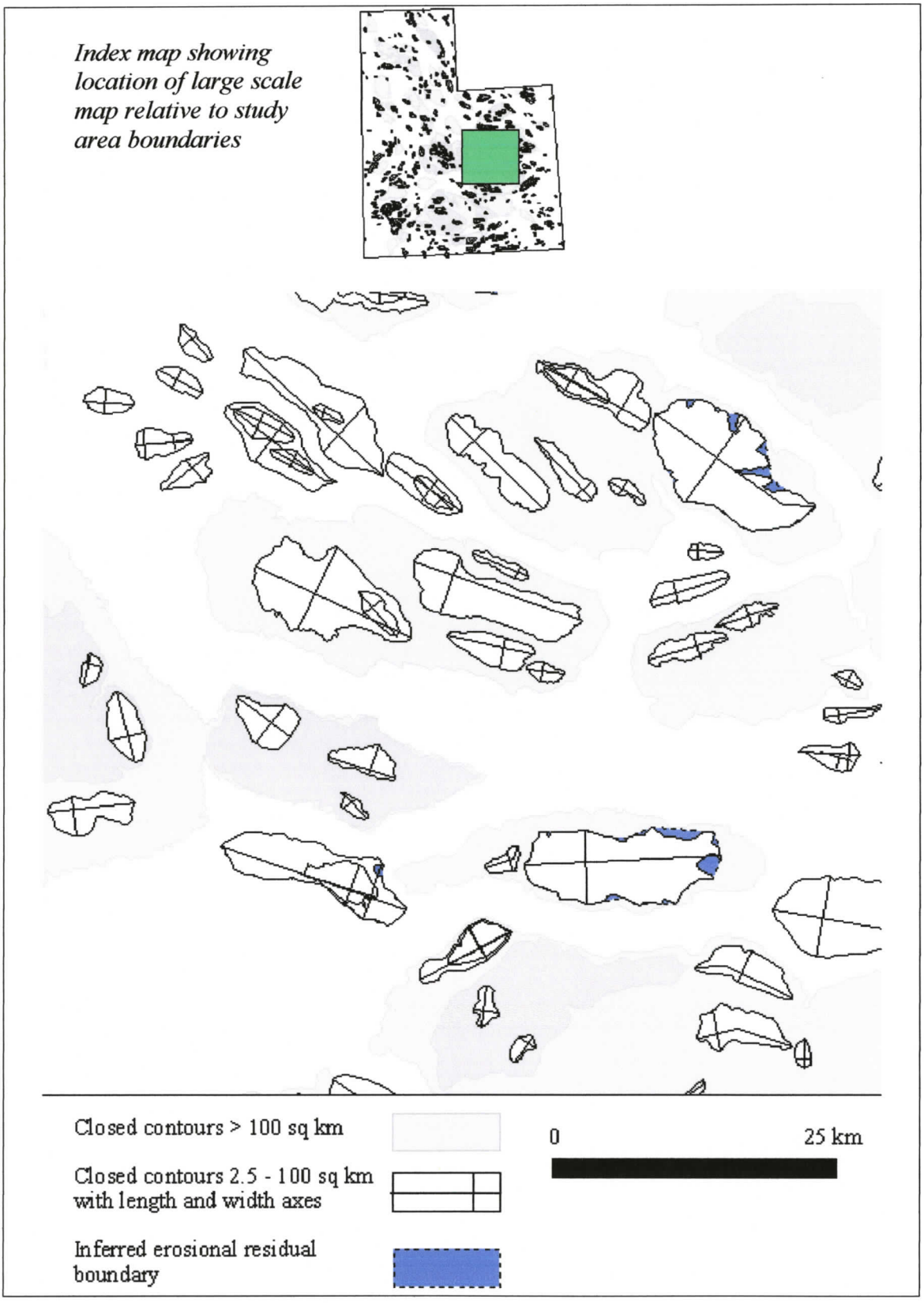
Index map showing location of large scale map relative to study area boundaries
Closed contours > 100 sq km
Closed contours 2.5 - 100 sq km with length and width axes
Inferred erosional residual boundary
0
25 km

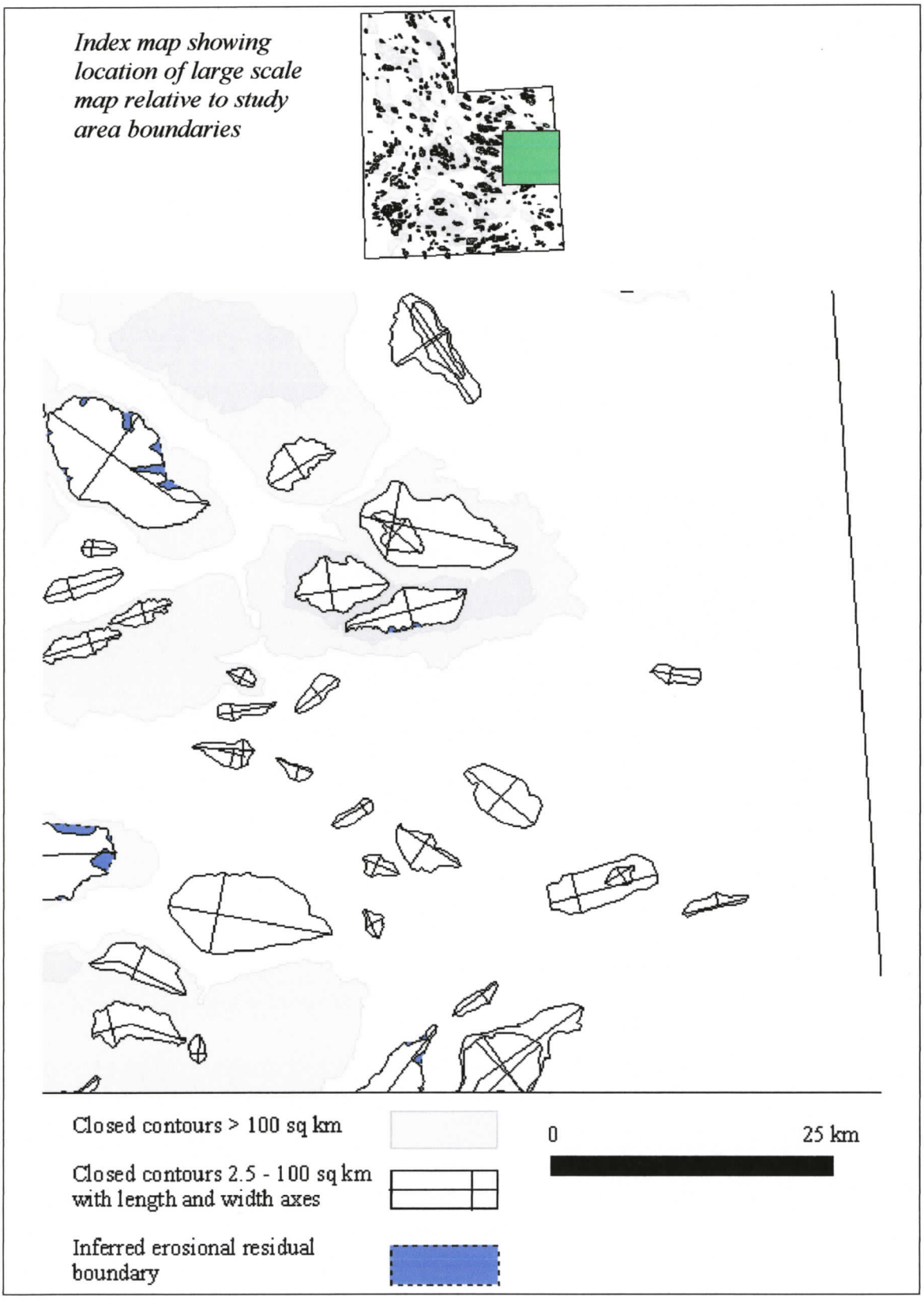
Index map showing location of large scale map relative to study area boundaries
Closed contours > 100 sq km
Closed contours 2.5 - 100 sq km with length and width axes
Inferred erosional residual boundary
0
25 km

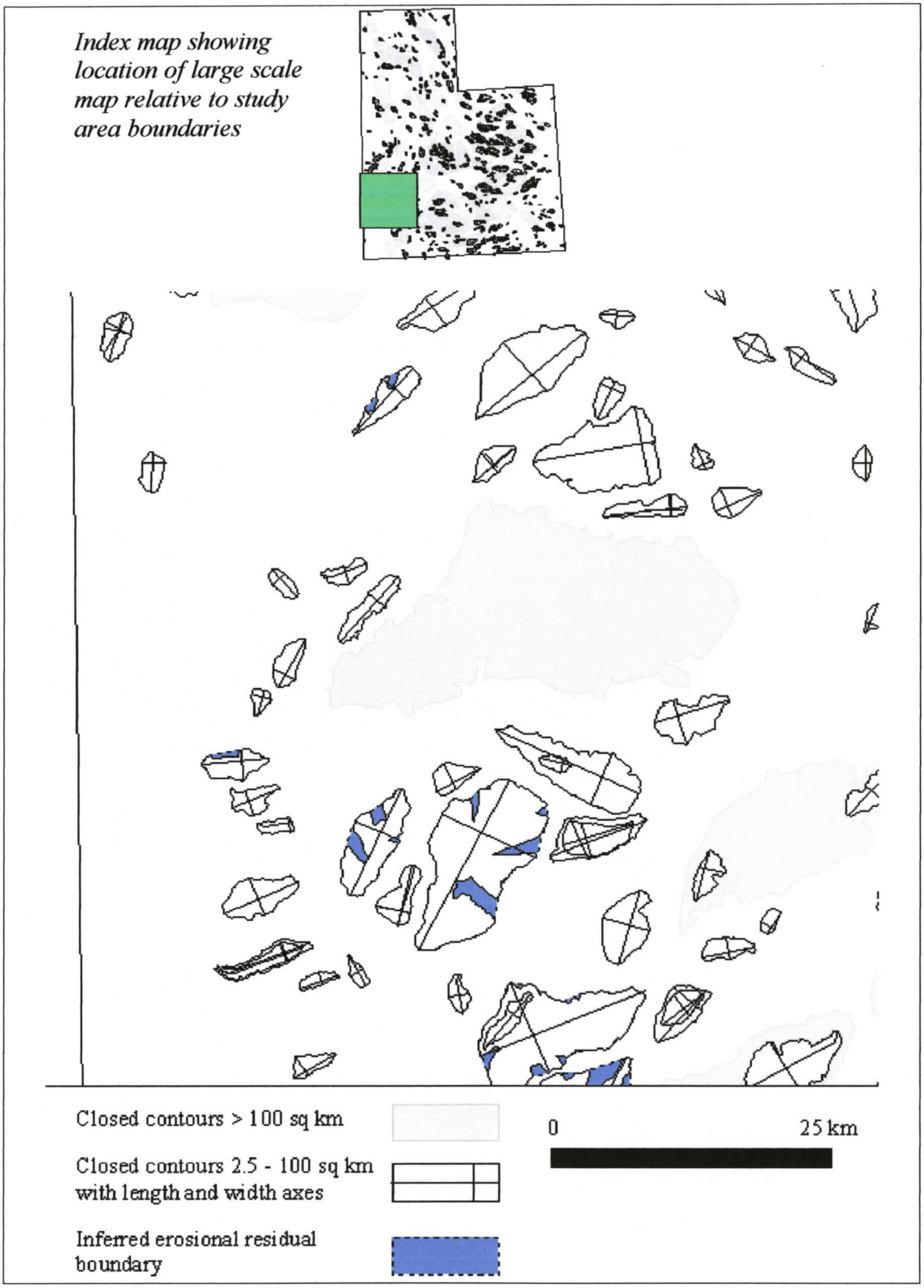
Index map showing location of large scale map relative to study area boundaries
Closed contours > 100 sq km
Closed contours 2.5 - 100 sq km with length and width axes
Inferred erosional residual boundary
0
25 km


Index map showing location of large scale map relative to study area boundaries
Closed contours > 100 sq km
Closed contours 2.5 - 100 sq km with length and width axes
Inferred erosional residual boundary
0
25 km

Index map showing location of large scale map relative to study area boundaries

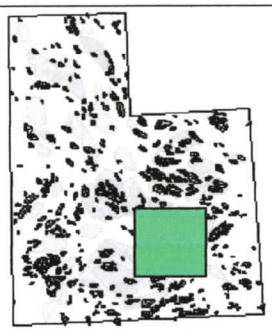

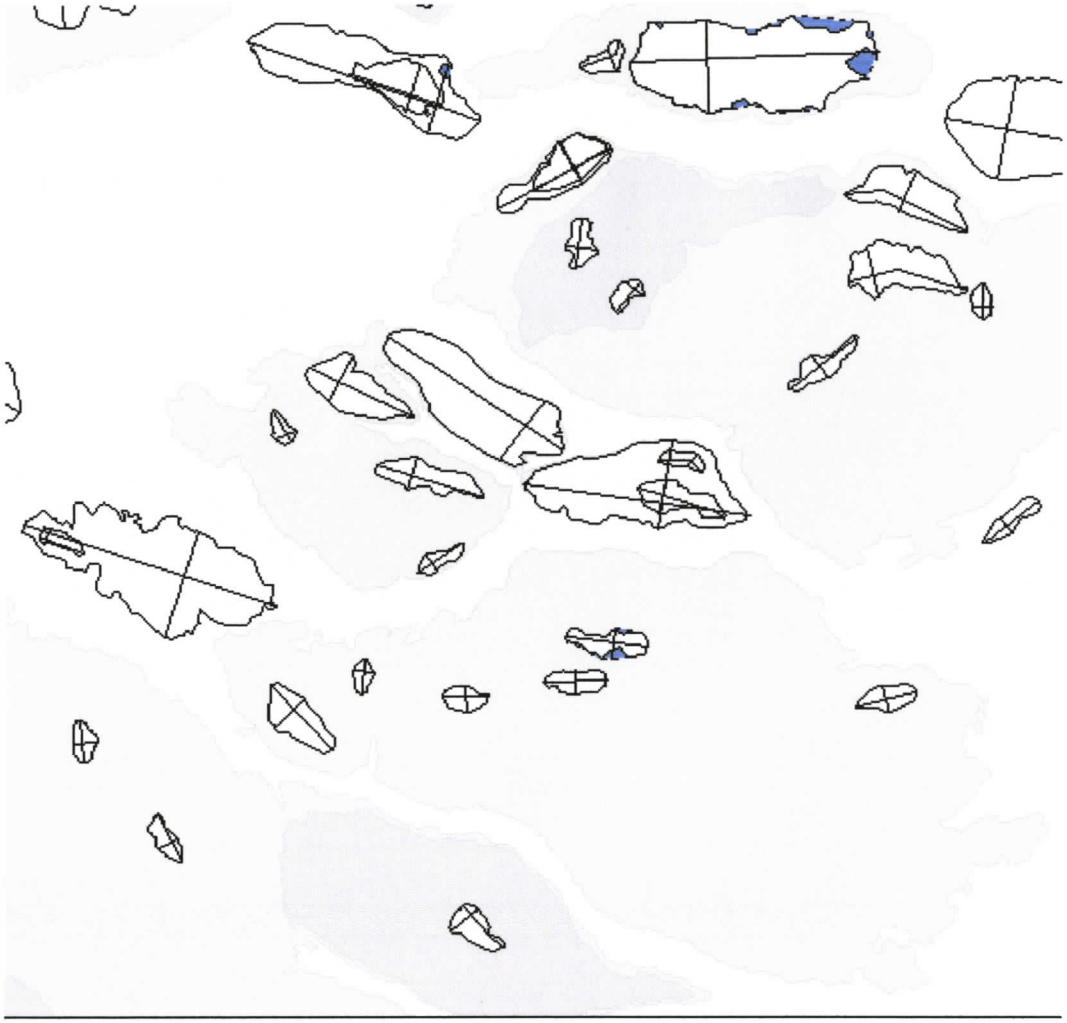

Closed contours > 100 sq km

Closed contours 2.5 - 100 sq km with length and width axes

Inferred erosional residual boundary

0 25 km

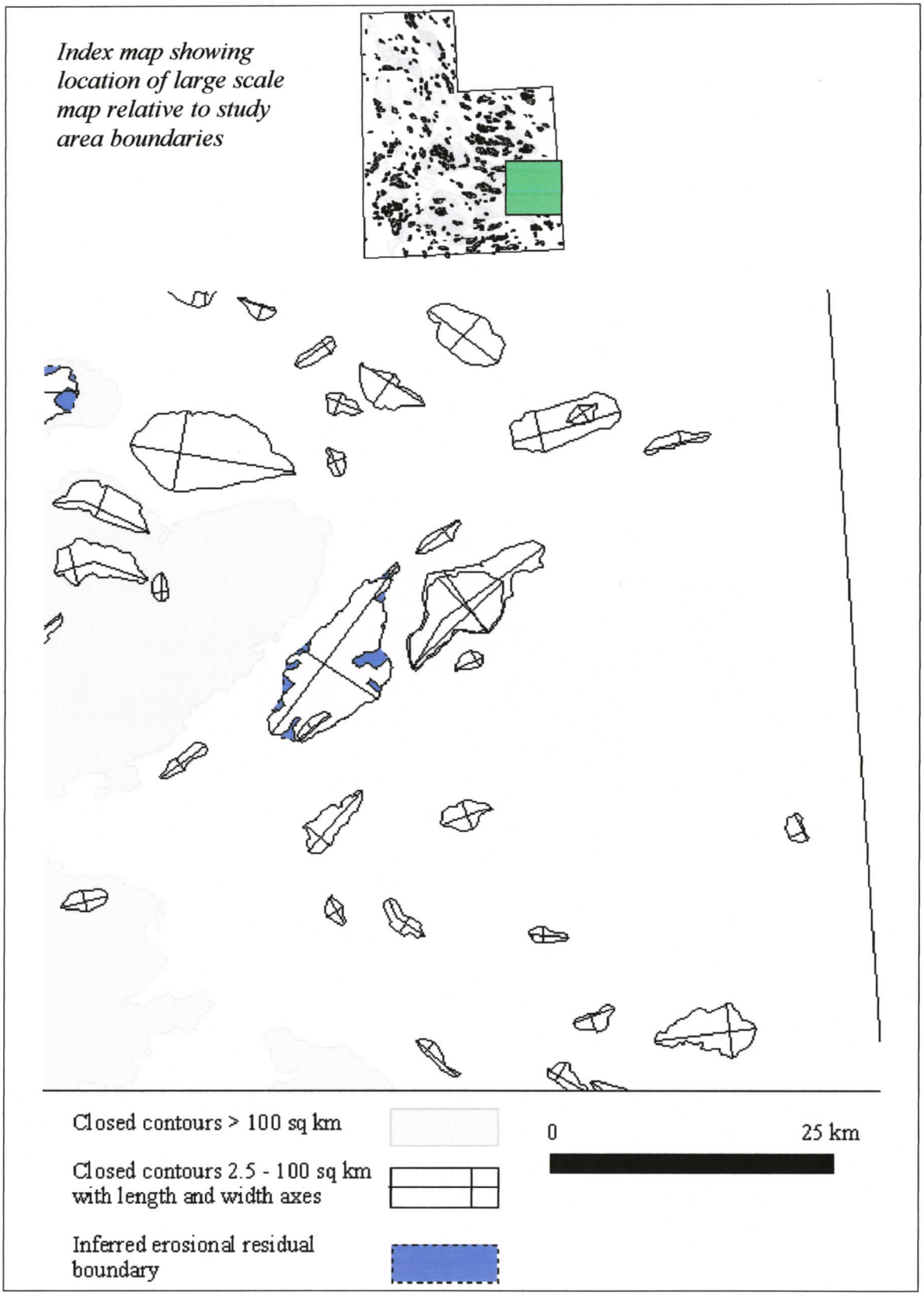
Index map showing location of large scale map relative to study area boundaries
Closed contours > 100 sq km
Closed contours 2.5 - 100 sq km with length and width axes
Inferred erosional residual boundary
0
25 km

Index map showing location of large scale map relative to study area boundaries

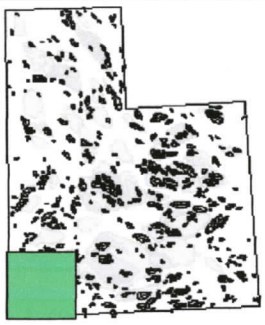

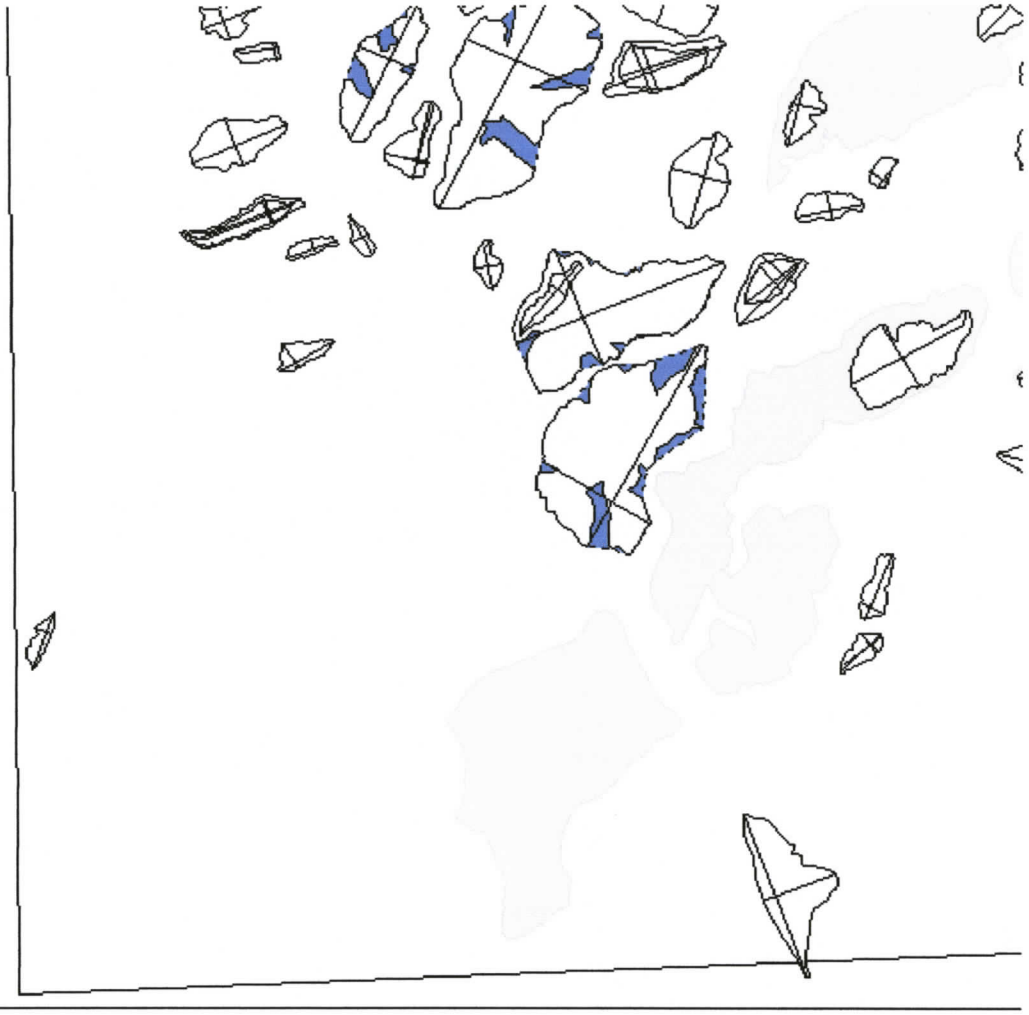

Closed contours > 100 sq km

Closed contours 2.5 - 100 sq km with length and width axes

Inferred erosional residual boundary

0 25 km

Index map showing location of large scale map relative to study area boundaries

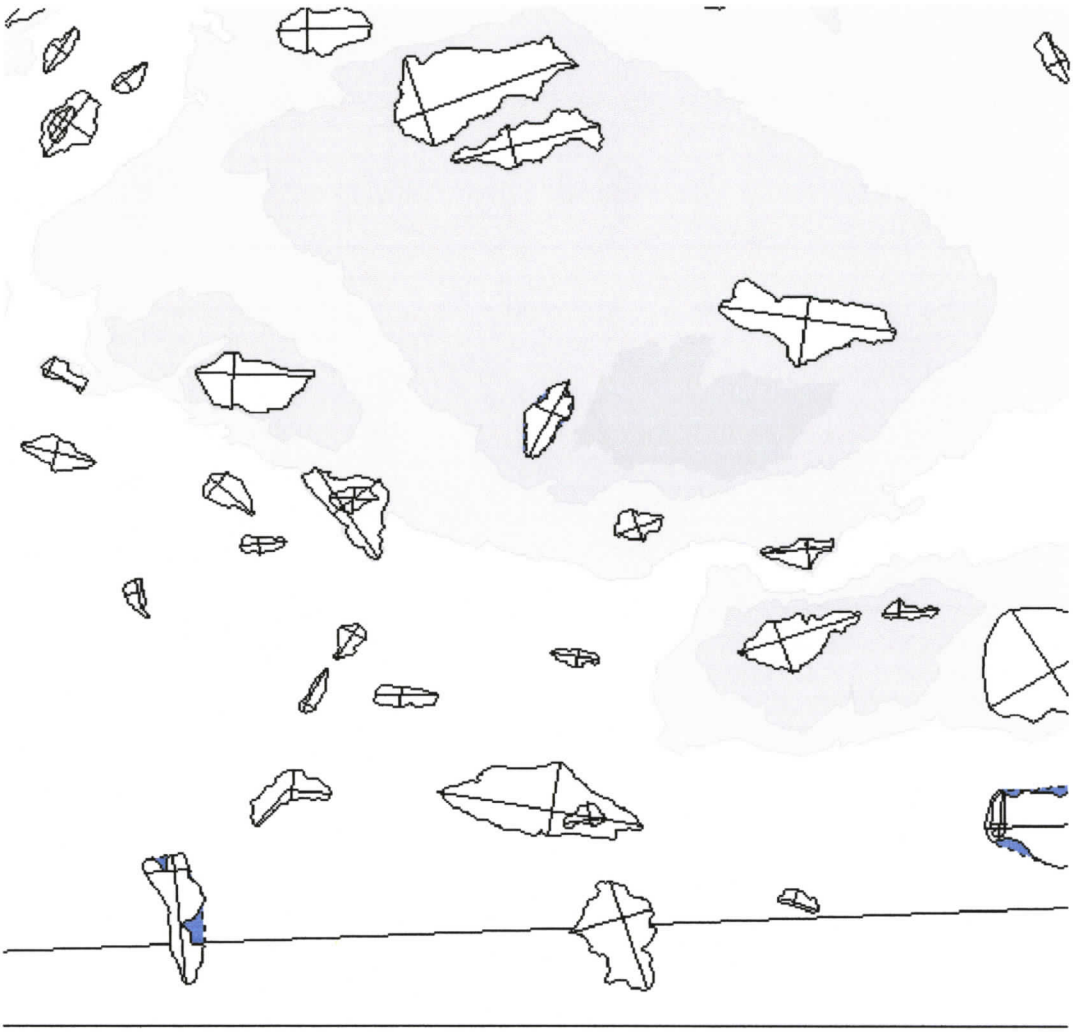

Closed contours > 100 sq km

Closed contours 2.5 - 100 sq km with length and width axes

Inferred erosional residual boundary

0 25 km

Index map showing location of large scale map relative to study area boundaries

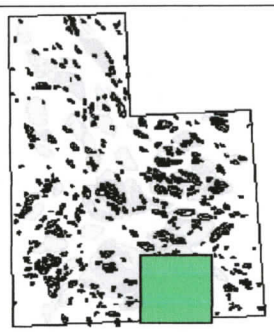

Closed contours > 100 sq km

Closed contours 2.5 - 100 sq km with length and width axes

Inferred erosional residual boundary

0 25 km

Index map showing location of large scale map relative to study area boundaries

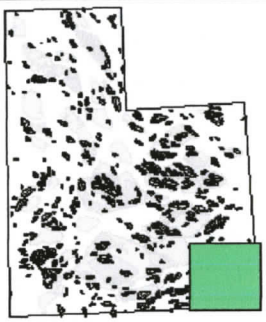

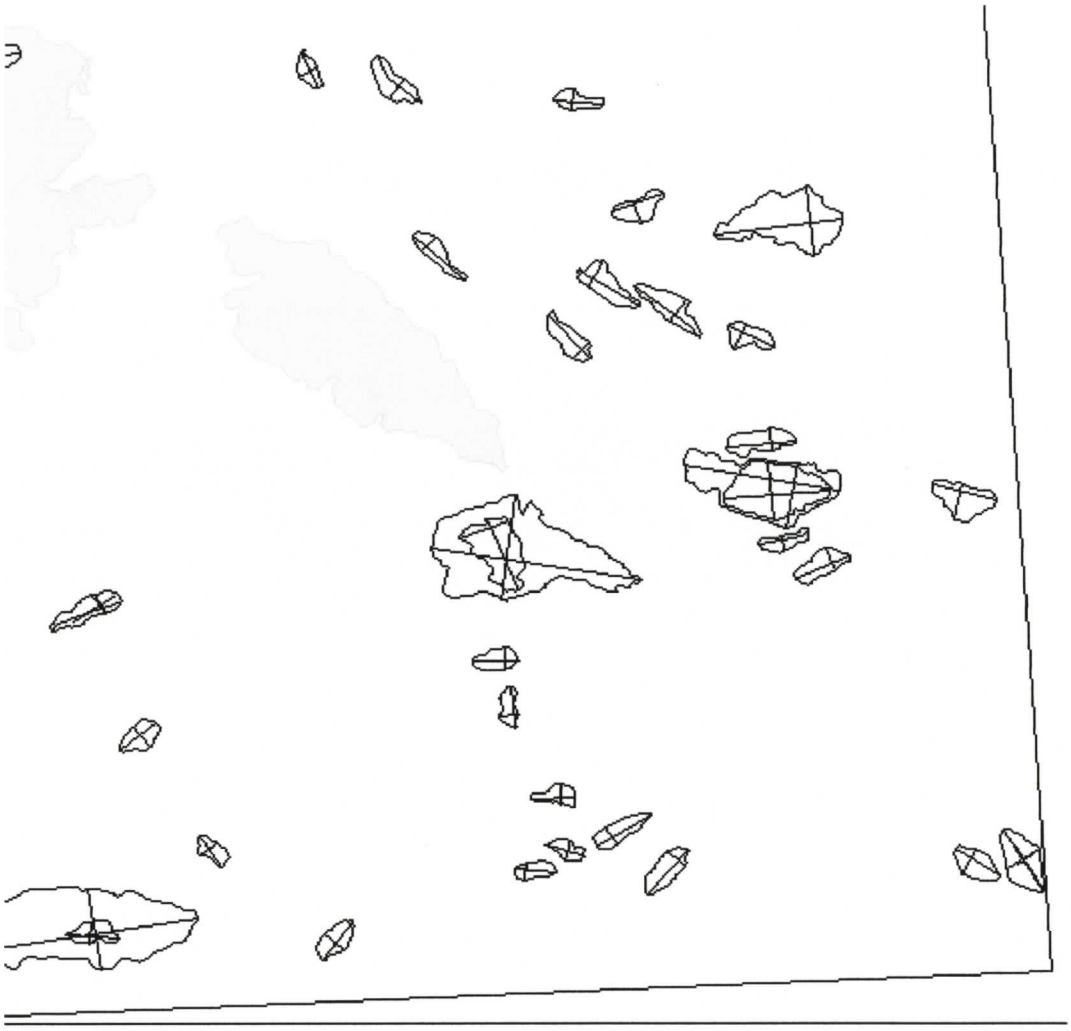

Closed contours > 100 sq km

Closed contours 2.5 - 100 sq km with length and width axes

Inferred erosional residual boundary

0 25 km

Figure 15

STREAMLINED LANDFORMS IN CENTRAL BRITISH COLUMBIA

(NTS 93E, 93F, 93K, 93L, 93M)

Map by J. Donald McClenagan (2001-2005)

kilometres

0 20 40 60 80

Digital base map from British Columbia Ministry of Environment, Lands, and Parks.
Modified from 1:20,000 TRIM digital data
North American Datum 1983
Universal Transverse Mercator, Grid Zones 9 & 10

Contours shown: 800 - 1300 m (green to white) and 1300 - 2000 m (white to blue)
Altitudes in meters above sea level, 100 m interval

1996 declination at the center of the west border of 93 K was 23° 15' easterly, mean annual decrease of 8.9'.

LEGEND

streamlined landform, variable length

128° 00'
126° 00'
124° 00'
56° 00'
55° 00'
53° 00'
N

KISPIOX RIVER
SKEENA RIVER
BULKLEY RIVER
DRIFTWOOD RIVER
BABINE RIVER
TAKLA LAKE
TROUT CREEK
HUDSON BAY MTN
TELKWA RIVER
GROUSE MTN
CHINA NOSE MTN
MORICE RIVER
MORICE LAKE
MANIKA LAKE
TAHTSA LAKE
TAHTSA REACH
WHITESAIL REACH
WHITESAIL LAKE
QUANCHAS RANGE
EUTSUK LAKE
OOTSA LAKE
BABINE LAKE
DECKER LAKE
BURNS LAKE
FRANCOIS LAKE
INZANA LAKE
TREMBLEUR LAKE
TEZZERON LAKE
PINCHI LAKE
STUART LAKE
STUART RIVER
ENDAKO RIVER
FRASER LAKE
NECHAKO RIVER
CHESLATTA LAKE
INTATA REACH
CHESLASLIE ARM
EUCHU REACH
NATALKUZ LAKE
TETACHUCK LAKE
ISACHA LAKE
BLACKWATER RIVER

Figure 96

CLOSED CONTOURS IN CENTRAL BRITISH COLUMBIA

(NTS 93E, 93F, 93K, 93L, 93M)

Map by J. Donald McClenagan (2001-2005)

0 km 20 km 40 km 60 km 80 km

Closed Contour Elevations a.s.l.

- 1510-1760 m
- 1410-1500 m
- 1310-1400 m
- 1210-1300 m
- 1110-1200 m
- 1010-1100 m
- 910-1000 m
- 810-900 m
- 0-800 m

Data source from
British Columbia Ministry of Environment, Lands, and Parks
1:20,000 TRIM I digital data
North American Datum 1983
Universal Transverse Mercator, Grid Zones 9 & 10

Data grid re-calculated to 10% of total available nodes using Golden Software Surfer 7.0.

1996 declination at the center of the west border of 93 K was 23° 15' easterly, mean annual decrease of 8.9'.

N

128° 00'
126° 00'
124° 00'
56° 00'
55° 00'
53° 00'